

UNIVERSITÄT  
BAYREUTH

Dissertation

---

**The Sternheimer Approach to  
Linear Response Time-Dependent  
Density Functional Theory**

---

**Fabian Hofmann**



---

# **The Sternheimer Approach to Linear Response Time-Dependent Density Functional Theory**

---

Von der Universität Bayreuth  
zur Erlangung des Grades eines  
Doktors der Naturwissenschaften (Dr. rer. nat.)  
genehmigte Abhandlung

von

**Fabian Hofmann**

aus Bayreuth

1. Gutachter: Prof. Dr. Stephan Kümmel
2. Gutachter: Prof. Dr. Miguel A. L. Marques

Tag der Einreichung: 04. August 2020

Tag des Kolloquiums: 04. Dezember 2020



# Abstract

As natural light-harvesting mechanisms are more efficient and robust than artificial solar technology, a deeper understanding of the energy absorption and conversion processes in plants and bacteria is at the center of a lot of current research. The theoretical prediction and interpretation of these phenomena requires methods that facilitate a quantum mechanical description of systems made from several thousands of electrons. Density functional theory in its Kohn-Sham formulation is by far the most popular method for the study of molecules, clusters and solids due to its beneficial ratio of accuracy to computational cost, and its time-dependent extension (TDDFT) is commonly used for the description of dynamical properties of molecular and nanostructures. The reliability and efficiency of Kohn-Sham density functional theory is determined by the approximation to the exchange-correlation energy (or potential) employed in practical applications.

For the study of electronic excitations one usually resorts to TDDFT in the linear regime. Linear response calculations in the Casida formulation are routinely done with most quantum chemistry codes. While the Casida approach is technically highly developed and quite efficient for medium-sized systems, it involves virtual orbitals, which leads to an unfavorable scaling with the system size. Additionally, as an eigenvalue problem with a dense matrix, it is not suited for a high degree of parallelization. Therefore, the Casida scheme is not optimal for the study of the larger systems occurring in natural light-harvesting complexes, which prompts the development of alternative linear response methods.

The investigation of the relevant processes in these systems through TDDFT is further complicated by the fact that they involve certain types of electronic excitations that most commonly used exchange-correlation approximations cannot predict reliably. This includes, among others, charge-transfer excitations, which play an important role in, e. g., photosynthetic reaction centers. More involved approximations that give a qualitatively correct description of charge-transfer exist, but are too expensive for applications in larger systems. This has motivated the development of various cheaper approximations that aim at mimicking the decisive features of, e. g., expensive exact-exchange based range-separated hybrid functionals. Meta-generalized gradient approximations seem to particularly well-suited for this task, but like most other approximations that might improve the description of charge transfer and other difficult excitations, they are orbital dependent approximations, which makes their application in time-dependent Kohn-Sham calculations highly nontrivial.

In order to address these problems, this thesis is focused on advancing an alternative, lesser-known linear response scheme, the Sternheimer method. While only relatively few applications of the scheme have been reported so far, it is particularly promising for the study of large systems since it only involves occupied orbitals, scales favorably with the system size, and can be parallelized massively, most notably because different frequencies can be treated completely independently.

In the first part of the thesis the scheme is developed further, regarding both formal and technical aspects. Among other things, a new derivation is presented, it is extended to the treatment of triplet excitations, and novel strategies for the efficient evaluation of excitation energies are put forward. Then the scheme is employed to study an orbital independent exchange-correlation approximation designed to mimic properties of exact exchange, the Armiento-Kümmel generalized gradient approximation. To be able to study more flexible approximations, a new and efficient way of treating orbital dependent exchange-correlation potentials in the Sternheimer approach is developed, which suggests that the Sternheimer method might be better suited for the application for orbital functionals than linear response schemes based on Casida's equations or on real-time propagation. Finally, this method is applied to the recently developed TASK meta-generalized gradient approximation, and TASK's performance in the description of charge transfer in a donor-acceptor-donor system of experimentally relevant size is studied.

# Kurzdarstellung

Da natürliche Lichtsammelmechanismen effizienter und robuster als künstliche Solartechnologie sind, ist ein tieferes Verständnis der Energieabsorptions- und -umwandlungsprozesse in Pflanzen und Bakterien Gegenstand vieler aktueller Studien. Die theoretische Vorhersage und Interpretation dieser Phänomene erfordert Methoden, die die quantenmechanische Beschreibung von Systemen aus mehreren tausend Elektronen ermöglichen. Die Dichtefunktionaltheorie, insbesondere in der Formulierung nach Kohn und Sham, ist bei Weitem der beliebteste Ansatz zur Untersuchung von Molekülen, Clustern und Festkörpern, hauptsächlich aufgrund ihres vorteilhaften Verhältnisses von Genauigkeit zu Rechenaufwand. In ihrer zeitabhängigen Version (TDDFT) ist sie die gängige Methode zur Beschreibung dynamischer Eigenschaften von Molekülen und Nanostrukturen. Zuverlässigkeit und Effizienz der Kohn-Sham-Dichtefunktionaltheorie wird durch die Näherung bestimmt, die in praktischen Anwendungen für die Austauschkorrelationsenergie (oder das entsprechende Potential) gebraucht wird.

Für die Untersuchung elektronischer Anregungen wird üblicherweise auf TDDFT im linearen Regime zurückgegriffen. Lineare Antwortberechnungen in der Casida-Formulierung werden routinemäßig mit den meisten Quantenchemie-Codes durchgeführt. Während der Casida-Ansatz auf einem hohen technischen Entwicklungsstand und für mittelgroße Systeme durchaus effizient ist, greift er auf unbesetzte Orbitale zurück, was zu einem ungünstigen Skalierungsverhalten mit der Systemgröße führt. Als Eigenwertproblem mit einer dicht besetzten Matrix ist er außerdem nicht für ein hohes Maß an Parallelisierung geeignet. Daher ist das Casida-Schema nicht optimal für das Studium größerer Systeme, wie sie in natürlichen Lichtsammelkomplexen vorkommen, wodurch die Entwicklung alternativer linearer Antwortmethoden angeregt wird.

Die Untersuchung der relevanten Prozesse in solchen Systemen mittels TDDFT wird weiter erschwert durch die Tatsache, dass sie bestimmte Arten von elektronischen Anregungen beinhalten, welche von den meisten gängigen Austauschkorrelationsnäherungen nicht zuverlässig vorhergesagt werden können. Dazu zählen unter anderem Ladungstransferanregungen, die eine wichtige Rolle z. B. in photosynthetischen Reaktionszentren spielen. Komplexere Näherungen, die prinzipiell eine qualitativ korrekte Beschreibung von Ladungstransfer ermöglichen, existieren, sind aber für Anwendungen in größeren Systemen zu teuer. Das hat die Entwicklung verschiedener weniger aufwendiger Näherungen motiviert, welche darauf abzielen, die entscheidenden Merkmale beispielsweise von teuren, auf exaktem Austausch basierenden, reichweitenseparierten Hybridfunktionalen nachzuahmen. Meta-generalisierte Gradientennäherungen scheinen für diese Aufgabe besonders gut geeignet zu sein, aber wie bei den meisten Näherungen, die die Beschreibung von Ladungstransfer und anderen schwierigen Anregungen verbessern könnten, handelt es sich hierbei um orbitalabhängige Näherungen, deren Verwendung in zeitabhängigen Kohn-Sham-Rechnungen äußerst schwierig ist.

Um diese Probleme anzugehen, konzentriert sich diese Arbeit auf die Weiterentwicklung eines alternativen, weniger bekannten linearen Antwortschemas, der Sternheimer-Methode. Obwohl

dieses Schema bisher nur relativ wenig Anwendung findet, ist es besonders vielversprechend für die Untersuchung großer Systeme, da es nur besetzte Orbitale benötigt, günstig mit der Systemgröße skaliert und massive Parallelisierung erlaubt, insbesondere weil verschiedene Frequenzen vollständig unabhängig voneinander behandelt werden können.

Im ersten Teil der Arbeit wird das Schema sowohl formal als auch technisch weiterentwickelt. Unter anderem wird eine neue Herleitung vorgestellt, das Schema wird auf die Beschreibung von Triplettanregungen erweitert und neuartige Strategien zur effizienten Auswertung von Anregungsenergien werden vorgeschlagen. Dann wird das Schema verwendet, um eine orbitalunabhängige Austauschkorrelationsnäherung zu untersuchen, welche zu dem Zweck entwickelt worden ist, Eigenschaften des exakten Austauschs nachzuahmen: Die verallgemeinerte Gradientennäherung von Armiento und Kümmel. Um flexiblere Approximationen studieren zu können, wird als nächstes eine neue und effiziente Methode zum Einsatz orbitalabhängiger Austauschkorrelationspotentiale im Rahmen des Sternheimer-Ansatzes entwickelt, was nahe legt, dass die Sternheimer-Methode für die Anwendung von Orbitalfunktionalen besser geeignet sein könnte als auf Casidas Gleichungen oder auf Echtzeit-Propagation basierende lineare Antwortschemata. Schließlich wird diese Methode auf die kürzlich entwickelte meta-generalisierte Gradientennäherung TASK angewandt, und TASKs Abschneiden in der Beschreibung von Ladungstransfer in einem Donor-Akzeptor-Donor-System von experimentell relevanter Größe wird untersucht.

# Contents

<b>Abstract</b>	<b>v</b>
<b>Kurzdarstellung</b>	<b>vii</b>
<b>I Theory and Outline of Results</b>	<b>1</b>
<b>1 Introduction</b>	<b>3</b>
<b>2 Density Functional Theory</b>	<b>5</b>
2.1 Ground-State Theory: The Hohenberg-Kohn Theorems and the Kohn-Sham Approach . . . . .	5
2.2 Fundamentals of Time-Dependent Density Functional Theory . . . . .	7
2.3 Construction of the Time-Dependent Exchange-Correlation Potential . . . . .	8
2.4 Time-Dependent Linear Response Theory . . . . .	9
<b>3 Orbital Functionals</b>	<b>11</b>
3.1 Beyond Explicit Density Dependence . . . . .	11
3.2 Problems of Standard Functionals . . . . .	12
3.3 The (Time-Dependent) Optimized Effective Potential . . . . .	13
3.4 Approximations to the Optimized Effective Potential . . . . .	15
3.5 The Generalized Kohn-Sham Scheme . . . . .	16
<b>4 Practical Approaches to Computational Spectroscopy within Density Functional Theory</b>	<b>19</b>
4.1 Established Methods . . . . .	19
4.1.1 Excitation Energies as Eigenvalues: The Casida Scheme . . . . .	19
4.1.2 Simulating Electron Dynamics in Real Time . . . . .	20
4.2 The Sternheimer Approach as an Efficient Alternative . . . . .	21
<b>5 Developing the Sternheimer Method into an Efficient Linear Response Scheme</b>	<b>25</b>
5.1 Formal Insights on the Sternheimer Approach from a New Derivation . . . . .	26
5.2 Technical Developments . . . . .	27
5.3 Orbital Functionals in the Sternheimer Scheme . . . . .	29
5.4 Studying Different Approaches to the Charge-Transfer Problem . . . . .	31
5.5 The Sternheimer Scheme as a Functional Analysis Tool . . . . .	33

<b>List of Abbreviations</b>	<b>36</b>
<b>Bibliography</b>	<b>37</b>
<b>List of Publications</b>	<b>51</b>
<b>II Publications</b>	<b>53</b>
<b>Publication 1</b>	
Linear response time-dependent density functional theory without unoccupied states: The Kohn-Sham-Sternheimer scheme revisited	<b>55</b>
<b>Publication 2</b>	
On the challenge to improve the density response with unusual gradient approximations	<b>73</b>
<b>Publication 3</b>	
Efficiently evaluating the Krieger-Li-Iafrate and common-energy-denominator approximations in the frequency-dependent Sternheimer scheme	<b>89</b>
<b>Publication 4</b>	
Molecular excitations from meta-generalized gradient approximations in the Kohn-Sham scheme	<b>107</b>
<b>Acknowledgments</b>	<b>121</b>
<b>Eidesstattliche Versicherung</b>	<b>123</b>

# **Part I**

---

## **Theory and Outline of Results**



# CHAPTER 1

## Introduction

Despite the growing public acceptance of the idea that the world needs a “green new deal” [Fri07], i. e., a large scale move away from traditional to renewable, clean energy sources, we are still lacking the technology to fully replace, e. g., fossil fuels. Among the different routes towards alternative energy sources, the efforts to harness solar energy seem to be particularly promising, as nature has already found and realized quite efficient ways to do so in plants or bacteria. However, current man-made solar technology is far from the efficiency and robustness that natural light-harvesting systems achieve. Therefore, gaining a deeper understanding of the intricate mechanisms at work in, e. g., chlorophyll, is of vital importance for the further development of industrial solutions to the energy problem.

Meaningful insights on this complex subject can only be gained if experiments are accompanied and illuminated by a theoretical description of the involved processes. This, however, requires a theoretical framework that can take into account the quantum mechanical phenomena that play an important role in the absorption and processing of photons, but can also cope with the size and complexity of natural light harvesting systems. The wave-function based formulation of quantum mechanics quickly reaches its limits for these systems because of its exponential scaling with the system size. The most popular alternative for the description of the electronic properties of molecules, nanostructures and solids is density functional theory (DFT) [HK64], an (in principle exact) reformulation of quantum mechanics in terms of a simpler quantity (the density) that relies on efficient approximations to the exchange-correlation (xc) part of the energy (cf. Sec. 2.1) in practical applications. It is typically applied within the Kohn-Sham scheme [KS65], which introduces the concept of molecular orbitals to DFT. The main reason for its popularity is its favorable ratio of accuracy to numerical costs.

For the description of absorption, excitation, and transport processes, time-dependent DFT (TDDFT) [RG84] in the linear regime is of particular interest. While not as firmly established as its ground-state counterpart, linear response TDDFT also has become one of the most frequently employed techniques to compute optical properties at least in finite systems (molecules and nanoparticles), and the most common formulation of the linear response equations, the Casida scheme [Cas95], is part of most modern quantum chemistry codes.

There are, however, different unsolved problems, especially regarding the application of TDDFT in the context mentioned above, i. e., the study of light-harvesting processes in systems of experimentally relevant size: first, the Casida approach, combined with sufficiently large atom-centered Gaussian basis sets, can be quite efficient for treating small- to medium-sized systems,

but it scales unfavorably with the system size, making it rather inefficient for the description of, e. g., large chlorophyll complexes. This is mostly due to its dependence on unoccupied orbitals and to its formulation as a dense eigenvalue problem that does not parallelize well (cf. Subsec. 4.1.1). Second, the description of light converting processes relies on the correct prediction of several types of excitations, like charge-transfer or double excitations, for which most commonly used xc approximations yield qualitatively wrong results (Sec. 3.2). While, in principle, approximations are known that can improve on the prediction of, e. g., charge-transfer excitations, these typically involve exact Fock exchange or self-interaction correction terms that require the calculation of a large number of Coulomb integrals between orbitals, making them too expensive for a practical application in large systems. Therefore, cheaper xc approximations are needed that can capture the relevant features of these known, yet expensive solutions. A promising class of approximations that might achieve this are so-called meta-generalized gradient approximations (meta-GGAs).

This thesis addresses these two issues. To this purpose, Chapter 2 first recapitulates the basic concepts behind TDDFT, and then Chapter 3 gives an overview of the important class of orbital dependent xc approximations, which contains virtually all candidates for an improved description of difficult excitations. Chapter 4 discusses and compares different formulations of linear response TDDFT, with a focus on pointing out some advantages of a so far relatively underused and underdeveloped approach, the Sternheimer scheme. The progress made in the course of this thesis on advancing the Sternheimer method, finding new ways to include orbital dependent xc approximations in Sternheimer-based linear response calculations, and studying the performance of two recently developed approximations, as presented in detail in the four publications that constitute Part II of this dissertation, is summarized in Chapter 5: [Publication 1](#) is concerned with the theoretical and practical framework of the Sternheimer scheme. It solidifies its formal foundations by presenting a rigorous, self-contained derivation of the relevant equations, extends it to a spin-dependent formulation that can treat triplet excitations, clarifies some open formal questions, and develops new and efficient techniques to solve the scheme and to extract excitation energies from its solutions. After [Pub. 2](#) tackles the question whether the charge-transfer problem might be solved with unusual, yet orbital independent xc approximations by studying the response properties of the AK13 functional [[AK13](#)], [Pub. 3](#) presents a scheme that facilitates linear response calculations with orbital dependent xc approximations (within the Kohn-Sham scheme) using the Sternheimer approach. This scheme finally allows [Pub. 4](#) to study the time-dependent linear response performance of TASK [[AK19](#)], a recently developed meta-GGA that was specifically designed to mimic the static response behavior of established, more expensive approximations.

## CHAPTER 2

# Density Functional Theory

Since this thesis is mostly concerned with time-dependent (TD) problems, in this Chapter the ground-state (GS) version of DFT will be reviewed briefly and only as far as necessary for the subsequent discussion of TDDFT. The reader is referred to the vast variety of literature on this topic, e. g., [PY89, PK03, DG90, ED11]. A more comprehensive overview of TDDFT can be found, e. g., in [vL01, MMN<sup>+</sup>12].

The basic idea behind both versions of the theory is to replace the complicated many-body wave function  $\Psi(\mathbf{r}_1\sigma_1, \mathbf{r}_2\sigma_2, \dots, \mathbf{r}_{N_e}\sigma_{N_e})$  of a system of  $N_e$  electrons by a function of only one coordinate, the density  $n(\mathbf{r})$  or  $n(\mathbf{r}, t)$ , in order to avoid the exponential scaling of wavefunction based descriptions of quantum mechanics. For open-shell systems or systems under the influence of a magnetic field coupling to the electron spins, DFT can be generalized to a spin-dependent formulation which will be used throughout this thesis and in which the total density is replaced by the spin-densities  $\{n_\sigma\}_{\sigma=\uparrow,\downarrow}$ , with  $n = n_\uparrow + n_\downarrow$ .

### 2.1 Ground-State Theory: The Hohenberg-Kohn Theorems and the Kohn-Sham Approach

GS DFT is based on two main premises: All GS properties of a many-body system can in principle be calculated from its GS density, and minimizing the system's energy as a functional of  $n_\sigma$  yields the true GS density. Both properties have been proven in a seminal paper by Hohenberg and Kohn [HK64] and are called the Hohenberg-Kohn theorems.

In practice, DFT is usually employed in the Kohn-Sham (KS) scheme [KS65]. There, one introduces an artificial non-interacting system with a local, multiplicative potential  $v_{s\sigma}(\mathbf{r})$  that is fixed by the constraint that both the auxiliary and the true, interacting system have the same density. The GS of this system is then simply the Slater determinant constructed from its  $N_e = N_\uparrow + N_\downarrow$  energetically lowest orbitals. Provided such a potential exists, it is a unique (up to an additive constant) functional of the density by virtue of the Hohenberg-Kohn theorem. This in turn guarantees that the orbitals  $\varphi_{j\sigma}$  and the kinetic energy

$$T_s = \sum_{\sigma \in \{\uparrow, \downarrow\}} \sum_{j=1}^{N_\sigma} \left\langle \varphi_{j\sigma} \left| -\frac{\hbar^2}{2m} \nabla^2 \right| \varphi_{j\sigma} \right\rangle \quad (2.1)$$

of the non-interacting system (with electron mass  $m$  and reduced Planck constant  $\hbar$ ) are density

functionals as well,  $T_s[\{n_\sigma\}] = T_s[\{\phi_{j\tau}[\{n_\sigma\}]\}]$ . Thus,  $T_s$  can be used to partition the energy of the *interacting* system with density  $n_\sigma$  according to

$$E[\{n_\sigma\}] = T_s[\{n_\sigma\}] + \sum_\sigma \int v_\sigma(\mathbf{r}) n_\sigma(\mathbf{r}) d^3r + E_H[n] + E_x[\{n_\sigma\}] + E_c[\{n_\sigma\}]. \quad (2.2)$$

Here,  $v_\sigma$  is the external potential of the true interacting system (possibly containing spin-dependent contributions from a magnetic field  $B$ ),

$$E_H = \frac{e^2}{2} \int \int \frac{n(\mathbf{r})n(\mathbf{r}')}{|\mathbf{r}-\mathbf{r}'|} d^3r d^3r' \quad (2.3)$$

(with the elementary charge  $e$ ) is the classical electrostatic repulsion energy of the electrons or *Hartree energy*,

$$E_x = -\frac{e^2}{2} \sum_\sigma \sum_{i,j=1}^{N_\sigma} \int \int \frac{\phi_{i\sigma}^*(\mathbf{r}) \phi_{i\sigma}(\mathbf{r}') \phi_{j\sigma}^*(\mathbf{r}') \phi_{j\sigma}(\mathbf{r})}{|\mathbf{r}-\mathbf{r}'|} d^3r d^3r', \quad (2.4)$$

like  $T_s$ , is an implicit density functional and is called the exact-exchange energy (EXX), and  $E_c$  collects correlation contributions to the kinetic and interaction energy. In practical calculations, at least  $E_c$  needs to be approximated, and one typically approximates the sum  $E_{xc} = E_x + E_c$ . The choice of a density functional approximation (DFA) for  $E_{xc}$  determines both cost and accuracy of a DFT calculation.

From (2.2) one can show that the KS potential is given by

$$v_{s\sigma}[\{n_\tau\}](\mathbf{r}) = v_\sigma(\mathbf{r}) + v_H[n](\mathbf{r}) + v_{xc\sigma}[\{n_\tau\}](\mathbf{r}), \quad (2.5)$$

with the Hartree potential

$$v_H[n](\mathbf{r}) = e^2 \int \frac{n(\mathbf{r}')}{|\mathbf{r}-\mathbf{r}'|} d^3r' \quad (2.6)$$

and the xc potential

$$v_{xc\sigma}[\{n_\tau\}](\mathbf{r}) = \frac{\delta E_{xc}}{\delta n_\sigma(\mathbf{r})}. \quad (2.7)$$

With this density-dependent expression for  $v_{s\sigma}$ , the density of an interacting system can be found by self-consistently finding the lowest energy solutions to the single-particle Schrödinger equation

$$\hat{h}_\sigma \phi_{j\sigma}(\mathbf{r}) = \left[ -\frac{\hbar^2}{2m} \nabla^2 + v_{s\sigma}[\{n_\tau\}](\mathbf{r}) \right] \phi_{j\sigma}(\mathbf{r}) = \epsilon_{j\sigma} \phi_{j\sigma}(\mathbf{r}) \quad (2.8)$$

of the corresponding non-interacting KS system, with  $n_\sigma(\mathbf{r}) = \sum_{j=1}^{N_\sigma} |\phi_{j\sigma}(\mathbf{r})|^2$ .

## 2.2 Fundamentals of Time-Dependent Density Functional Theory

In principle, the GS density should give access to all properties of the many-body system, including its excited state energies. However, finding suitable density functionals for these is a nontrivial task, and in practice one rather resorts to determining excitation energies by simulating time-dependent spectroscopy experiments, e. g., photoabsorption, in the linear regime. The framework for this is the TD extension of DFT. It is based on the theorems by Runge, Gross [RG84] and Van Leeuwen [vL99] which, in a nutshell, make the following two statements: Every property of a TD many-body system with a fixed interaction  $w$  (e. g.,  $w = e^2/|\mathbf{r} - \mathbf{r}'|$ ) propagating from an initial state  $|\Psi_0\rangle$  under the influence of an external potential  $v_\sigma(\mathbf{r}, t)$  is a unique functional of  $|\Psi_0\rangle$  and the TD density  $n_\sigma(\mathbf{r}, t)$ ; and this density can be reproduced in a system with a different interaction  $w'$ , a suitable initial state  $|\Phi_0\rangle$ , and an effective potential  $v_{s\sigma}(\mathbf{r}, t)$ .

Choosing  $|\Phi_0\rangle$  to be a determinant and  $w' = 0$  allows to find the density of the interacting system by propagating the orbitals  $\varphi_{j\sigma}(\mathbf{r}, t)$  of a non-interacting time-dependent Kohn-Sham (TDKS) system according to

$$\hat{h}_\sigma(t) \varphi_{j\sigma}(\mathbf{r}, t) = \left[ -\frac{\hbar^2}{2m} \nabla^2 + v_{s\sigma}(\mathbf{r}, t) \right] \varphi_{j\sigma}(\mathbf{r}, t) = i\hbar \partial_t \varphi_{j\sigma}(\mathbf{r}, t), \quad (2.9)$$

and then evaluating the density as

$$n_\sigma(\mathbf{r}, t) = \sum_{j=1}^{N_\sigma} |\varphi_{j\sigma}(\mathbf{r}, t)|^2. \quad (2.10)$$

Applying the Runge-Gross theorem to the non-interacting system shows that  $v_{s\sigma}(\mathbf{r}, t)$  and the orbitals  $\varphi_{j\sigma}(\mathbf{r}, t)$  are functionals of the density and the initial determinant.

While TDDFT is mostly used for linear response (LR) calculations, it is not restricted to the linear regime and can in principle describe nonlinear dynamics as well. This becomes relevant, e. g., in the description of systems exposed to high-intensity laser beams, as it is done in photoemission experiments [Bau97, LvL98, PG99, BC01, LK05, DGS<sup>+</sup>16, DK16]. The initial-state dependence of  $v_{s\sigma}(\mathbf{r}, t)$  becomes particularly important in the description of the dynamics of a system initially prepared in a non-equilibrium state [FLSM15, LFM16].

In this thesis, however, only the response to an external perturbation of systems initially in their GS is considered. The initial state of the TDKS system is then simply chosen to be the determinant found in a GS KS calculation. As the Hohenberg-Kohn theorem guarantees that both the many-body wave function and the KS determinant of the GS are functionals of the GS density, which in this situation is obviously the TD density at the initial time, the KS potential, orbitals, as well as all observables become unique functionals of the TD density alone:

$$v_{s\sigma}(\mathbf{r}, t) = v_{s\sigma}[\{n_\tau\}](\mathbf{r}, t) \quad \text{and} \quad \varphi_{j\sigma}(\mathbf{r}, t) = \varphi_{j\sigma}[\{n_\tau\}](\mathbf{r}, t). \quad (2.11)$$

The TDKS potential is usually partitioned according to

$$v_{s\sigma}[\{n_\tau\}](\mathbf{r},t) = v_\sigma(\mathbf{r},t) + v_H[n](\mathbf{r},t) + v_{xc\sigma}[\{n_\tau\}](\mathbf{r},t), \quad (2.12)$$

paralleling the partitioning of the GS potential. Here,  $v_H[n](\mathbf{r},t) = v_H[n(t)](\mathbf{r})$  is simply the GS expression for the Hartree potential but evaluated at the TD density, and the TD xc potential  $v_{xc\sigma}(\mathbf{r},t)$  is defined by Equation (2.12), encompasses all nontrivial interaction effects, and has to be approximated in practical calculations. While both  $v_{s\sigma}(\mathbf{r},t)$  and  $v_{xc\sigma}(\mathbf{r},t)$  are local, multiplicative potentials (i. e., simple functions of  $\mathbf{r}$  and  $t$  and not, e. g., integral or differential operators), as a functional of the density,  $v_{xc\sigma}(\mathbf{r},t)$  is generally non-local in time and space. Particularly, this means that it contains memory effects.

### 2.3 Construction of the Time-Dependent Exchange-Correlation Potential

A straightforward generalization of the GS approach to approximate  $E_{xc}$  and then calculate  $v_{xc\sigma}(\mathbf{r})$  as the functional derivative to the TD case by defining the potential  $v_{xc\sigma}(\mathbf{r},t)$  as the (standard) derivative of some action functional with respect to  $n_\sigma(\mathbf{r},t)$ , as originally proposed by Runge and Gross [RG84], is problematic, since this would in general lead to causality issues in the resulting response functions related to the memory of  $v_{xc\sigma}[\{n_\tau\}](\mathbf{r},t)$  [vL98, vL01].

Therefore, alternative ways to construct the potential have to be found in the TDKS approach. One could, for instance, use a TD generalization of Görling-Levy perturbation theory [GL93, GL94] to construct a perturbation series for the potential without having to refer to any action or energy functional [Gör97].

The most widely used class of DFAs to  $v_{xc\sigma}(\mathbf{r},t)$  is based on the *adiabatic approximation*. Here, one simply inserts the TD density into an explicitly density-dependent expression for the GS xc potential:

$$v_{xc\sigma}(\mathbf{r},t) \approx \left[ \frac{\delta E_{xc}}{\delta n_\sigma(\mathbf{r})} \right]_{\{n_\tau(t)\}}. \quad (2.13)$$

The fact that such a potential can be written as the derivative of the action functional  $A_{xc} = \int E_{xc}[\{n_\sigma(t)\}] dt$  does not lead to causality problems since in the adiabatic approximation, the potential is an instantaneous functional of the density, i. e., it has no memory.

In a formally similar way, one can construct approximations to  $v_{xc\sigma}(\mathbf{r},t)$  from orbital-dependent expressions for the GS potential by evaluating them at the TDKS orbitals. These constructions are in principle density functionals since the KS orbitals are density functionals. However, the TDKS orbitals at time  $t$  gain their density dependence through propagation under the influence of the density-dependent KS potential, starting from the GS at some initial time  $t_0 < t$ , which makes them functionals of the density at all times  $t'$  between  $t_0$  and  $t$ . Therefore, such an *orbital-adiabatic* potential is a non-adiabatic functional of the density and generally exhibits a memory effect. The question of how this type of xc potentials can be used in TD LR

calculations is discussed in [Pub. 3](#).

In principle, there is also a more involved way of introducing the functional derivative concept into TDDFT: In the *Keldysh formalism* [[vL98](#), [vL01](#)], one defines action functionals on an extended space of densities that depend not on physical time but on a pseudo-time contour, which represents a noninvertible parametrization of physical time. Then the xc potential can be defined as the functional derivative of an xc action functional with respect to this more general class of pseudo-densities, but evaluated at the physical density. This leads to potentials which can have memory but still have causal response functions.

## 2.4 Time-Dependent Linear Response Theory

The performance of a particular DFA for the xc potential in predicting LR properties is usually discussed in terms of the time or frequency-dependent xc kernel [[vL01](#)],

$$\begin{aligned} f_{\text{xc}\sigma\tau}(\mathbf{r}, \mathbf{r}', t - t') &= \left. \frac{\delta v_{\text{xc}\sigma}(\mathbf{r}, t)}{\delta n_{\tau}(\mathbf{r}', t')} \right|^{(0)} \quad \text{and} \\ f_{\text{xc}\sigma\tau}(\mathbf{r}, \mathbf{r}', \omega) &= \lim_{\beta \rightarrow 0} \int dT f_{\text{xc}\sigma\tau}(\mathbf{r}, \mathbf{r}', T) e^{i(\omega + i\beta)T} \end{aligned} \quad (2.14)$$

(where the superscript (0) indicates evaluation in the unperturbed system), and in terms of the GS xc potential and its influence on the KS eigenvalues. The interplay of these two aspects, i. e., the eigenvalue spectrum and the kernel, can be illustrated by the TDDFT response equation [[vL01](#), [SLR<sup>+</sup>12](#)]

$$\chi_{\sigma\tau}(\mathbf{r}_1, \mathbf{r}_2, \omega) = \chi_{s\sigma\tau}(\mathbf{r}_1, \mathbf{r}_2, \omega) + \sum_{\alpha\beta} \int d^3r \int d^3r' \chi_{s\sigma\alpha}(\mathbf{r}_1, \mathbf{r}, \omega) f_{\text{Hxc}\alpha\beta}(\mathbf{r}, \mathbf{r}', \omega) \chi_{\beta\tau}(\mathbf{r}', \mathbf{r}_2, \omega). \quad (2.15)$$

Here,  $\chi_{\sigma\tau}(\mathbf{r}_1, \mathbf{r}_2, \omega)$  is the frequency representation of the (interacting) density-density response function

$$\chi_{\sigma\tau}(\mathbf{r}_1, \mathbf{r}_2, t_1 - t_2) = \left. \frac{\delta n_{\sigma}(\mathbf{r}_1, t_1)}{\delta v_{\tau}(\mathbf{r}_2, t_2)} \right|^{(0)}. \quad (2.16)$$

This is the central quantity of LR TDDFT. It has poles at the excitation energies of the system and yields, e. g., the photoabsorption cross section as [[BG12](#)]

$$\sigma(\omega) \propto \omega \sum_{\sigma\tau} \int \int (\mathbf{r}_1 \cdot \mathbf{r}_2) \chi_{\sigma\tau}(\mathbf{r}_1, \mathbf{r}_2, \omega) d^3r_1 d^3r_2. \quad (2.17)$$

$\chi_{s\sigma\tau}(\mathbf{r}_1, \mathbf{r}_2, \omega)$  is the corresponding quantity in the KS system:

$$\chi_{s\sigma\tau}(\mathbf{r}_1, \mathbf{r}_2, t_1 - t_2) = \left. \frac{\delta n_{\sigma}(\mathbf{r}_1, t_1)}{\delta v_{s\tau}(\mathbf{r}_2, t_2)} \right|^{(0)}, \quad (2.18)$$

and can be expressed directly in terms of the KS orbitals and eigenvalues as [vL01]

$$\chi_{s\sigma\tau}(\mathbf{r}_1, \mathbf{r}_2, \omega) = \delta_{\sigma\tau} \lim_{\beta \rightarrow 0} \sum_{j=1}^{N_\sigma} \sum_{a>N_\sigma} \left[ \frac{\varphi_{j\sigma}^*(\mathbf{r}) \varphi_{a\sigma}(\mathbf{r}) \varphi_{a\sigma}^*(\mathbf{r}') \varphi_{j\sigma}(\mathbf{r}')}{\omega + i\beta - (\varepsilon_{a\sigma} - \varepsilon_{j\sigma})} - \frac{\varphi_{j\sigma}(\mathbf{r}) \varphi_{a\sigma}^*(\mathbf{r}) \varphi_{a\sigma}(\mathbf{r}') \varphi_{j\sigma}^*(\mathbf{r}')}{\omega + i\beta + (\varepsilon_{a\sigma} - \varepsilon_{j\sigma})} \right]. \quad (2.19)$$

Finally,

$$f_{\text{Hxc}\sigma\tau}(\mathbf{r}, \mathbf{r}', \omega) = \frac{e^2}{|\mathbf{r} - \mathbf{r}'|} + f_{\text{xc}\sigma\tau}(\mathbf{r}, \mathbf{r}', \omega) \quad (2.20)$$

is the Hartree-exchange-correlation kernel.

The response equation (2.15) states that the response of the interacting system can be constructed from the response of the KS system, with poles at the differences between occupied and unoccupied KS eigenvalues, through a correction determined by the xc kernel. This correction consists of shifting and mixing the different KS eigenvalue differences, as well as creating additional poles corresponding to double (or higher) excitations [TK14].

While for some types of excitations such as, e. g., Rydberg excitations, the most important feature of a DFA is to provide a realistic KS eigenvalue spectrum [Gör99, KSM99, HHG99], there are also others for which the properties of the kernel become crucial [KG02, KSG03, MZCB04, Mai05, HIG09]. The description of excitonic peaks in the spectrum of periodic systems such as bulk silicon is an example where an accurate representation of both the eigenvalues and the kernel is vitally important [GGG97, RORO02, KG02, DAOR03, KSG03]. The insight that the correct description of the photoabsorption spectrum of silane (SiH<sub>4</sub>) is mostly determined by the GS potential and hardly affected by the choice of DFA used for the xc kernel is one of the results of Pub. 1.

The memory of the TD xc potential as a functional of the density manifests itself in the frequency dependence of the kernel. In the adiabatic approximation, the instantaneous density dependence leads to  $\delta v_{\text{xc}}(t)/\delta n(t') \propto \delta(t - t')$  and, thus, to a frequency-independent xc kernel. This is a serious shortcoming, as the frequency dependence is an important prerequisite for the correct prediction of, e. g., charge-transfer (CT) [Mai05, HIG09] or double excitations [MZCB04, TK14].

## CHAPTER 3

# Orbital Functionals

### 3.1 Beyond Explicit Density Dependence

In this thesis, the terms “standard” or *semi-local* approximation are used to refer either to the class of explicitly density-dependent DFAs for  $E_{xc}$  that are defined as integrals over an approximate xc energy density  $\varepsilon_{xc}[\{n_\sigma\}](\mathbf{r})$ ,

$$E_{xc}[\{n_\sigma\}] = \int \varepsilon_{xc}[\{n_\sigma\}](\mathbf{r}) d^3r, \quad (3.1)$$

which at any point  $\mathbf{r}$  depends only on the local density  $n_\sigma(\mathbf{r})$  or its gradient  $\nabla n_\sigma(\mathbf{r})$ , or to explicitly density-dependent DFAs for  $v_{xc\sigma}$  with a similar local dependence on the density and its derivatives. This class contains the local density approximation (LDA) [HK64] and generalized gradient approximations (GGAs) [PW86] such as the popular Perdew-Burke-Ernzerhof (PBE) [PBE96] functional and occupies the two lowest rungs on Perdew’s famous “Jacob’s Ladder” picture [PS01] of DFAs. In the TD context, these terms are additionally understood to imply the adiabatic approximation.

To go beyond these approximations, one usually allows for another ingredient in the functional construction: The KS orbitals, which, through their implicit density dependence, make DFAs non-local and TD potentials non-adiabatic (cf. Chapter 2). An important example is the EXX defined in Eq. (2.4). Others include various kinds of hybrid functionals based on a mixture of semi-local and exact exchange [Bec93a, Bec93b, SDCF94, PEB96, PSTS08, SKM<sup>+</sup>14, LSWS97, YTH04, SKB09b], as well as different self-interaction correction (SIC) [PZ81] schemes.

The latter aim at correcting for the spurious self-repulsion of electrons included in the Hartree energy, which is not canceled by standard xc functionals, notably leading to a non-vanishing interaction energy for single-particle systems. They usually identify orbitals with electrons and subtract the sum of all single-particle contributions to the interaction energy from a given DFA [PZ81]:

$$E_{xc}^{\text{SIC}} = E_{xc}^{\text{DFA}}[n_\uparrow, n_\downarrow] - \sum_\sigma \sum_{j=1}^{N_\sigma} \left\{ E_{xc}^{\text{DFA}}[|\varphi_{j\sigma}|^2, 0] + E_{\text{H}}[|\varphi_{j\sigma}|^2] \right\}. \quad (3.2)$$

Usually, and throughout this thesis, the correction is applied to the LDA.

As applying a unitary transformation to the set of occupied KS orbitals yields another set of orthonormal orbitals with the same density, all sets of orbitals that result from such a

transformation could be considered to represent single electrons, but lead to different SIC energies. Therefore, specific choices of orbitals used in the correction define different versions of SIC. Typical choices are simply to use the KS orbitals, or to resort to localizing or energy-minimizing transformations [PHL84, KKM08, HKKK12].

EXX-based functionals and SIC both include Coulomb integrals involving the orbitals, which makes their application quite costly. In contrast, meta-GGAs [DFC16] have the positive kinetic energy density of the KS system,

$$\tau_{\sigma}(\mathbf{r}) = \frac{\hbar^2}{2m} \sum_{j=1}^{N_{\sigma}} |\nabla \phi_{j\sigma}(\mathbf{r})|^2, \quad (3.3)$$

at point  $\mathbf{r}$  as an additional ingredient of the xc energy density at  $\mathbf{r}$ . They are numerically cheaper as they only depend on the orbitals in a semi-local fashion, which however still makes them implicitly non-local density functionals.

The types of orbital functionals discussed so far (and in the remainder of this thesis) occupy the third and fourth rung of Perdew's ladder, and only depend on the occupied orbitals. The next higher rung would include functionals that generally depend on unoccupied orbitals and eigenvalues as well, which goes beyond the scope of this thesis.

## 3.2 Problems of Standard Functionals

While going from semilocal to orbital functionals is already important for an accurate description of many GS properties such as bond lengths [SSTP03], it becomes crucial in LR TDDFT. This is because there are various types of electronic excitations for which standard approximations fail drastically, including Rydberg [CJCS98, TH98, HHG99, DG01, DSG02], CT [DWHG03, Toz03, Mai05, HIG09, Küm17] and double excitations [MZCB04, TK14] as well as excitonic excitations at least in bulk materials [GGG97, KG02]. These failures have been traced back to either the unphysical GS potential missing, e. g., the correct  $-e^2/r$  asymptotic [TH98, DG01, HG11], to the lack of frequency dependence [MZCB04, Mai05, HIG09, TK14], divergences [RORO02, KG02, Küm17], a discontinuity [Toz03], dynamic steps [HK12a] and other non-local features in the TD response of the xc potential, or a combination thereof.

The spectrum of any electronic system typically contains various excitations of different types, which are affected quite differently by the shortcomings of semi-local functionals; e. g., local valence excitations can be predicted quite well with an error of the order of 0.1 eV [HHG99], CT excitations are typically drastically underestimated by up to several eV [DHG04, HIG09], and double excitations cannot be predicted at all by the adiabatic approximation [MZCB04, TK14]. Thus, the whole spectrum is not necessarily just shifted by some more or less constant error, but can come out qualitatively wrong, as exemplified by the two different spectra of SiH<sub>4</sub> shown in Fig. 3.1.

While different functionals have been proposed to solve these different issues, what most of them have in common is that they are orbital functionals:

EXX has a more physical GS potential than semilocal DFAs, leading to an improved description of Rydberg excitations [DG01, DSG02, HG11] and band structures [BK95, SMVG97, KSG03]. It yields qualitatively correct CT energies [HIG09, IHG10, HG11] and excitonic peaks [KG02]. The SIC potential also has the correct  $-e^2/r$  asymptotic, more physical eigenvalues [KKMK09, DKK<sup>+</sup>11] than semi-local functionals and TD steps [HK12a], and has been suggested to improve CT excitation energies [HK12b, HKK12]. Range-separated hybrids (RSH) [LSWS97, YTH04, SKB09b] yield accurate CT energies [PHS<sup>+</sup>06, SKB09b, SKB09a, KSBK11, KSRAB12, Küm17] and can improve the description of Rydberg excitations [PHS<sup>+</sup>06]. Finally, meta-GGAs yield improved band gaps, can potentially contain the necessary ultra-nonlocality needed for a correct description of CT [AK19] and have been argued to improve the description of excitonic features in solids [NV11].

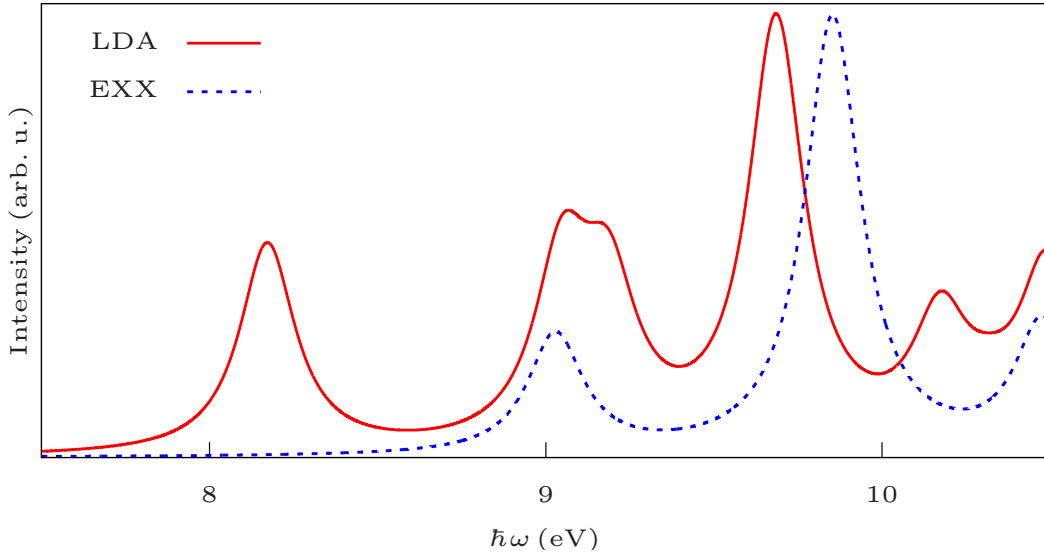


**Figure 3.1:** LDA and EXX predict markedly different photoabsorption spectra for SiH<sub>4</sub>.

### 3.3 The (Time-Dependent) Optimized Effective Potential

Explicitly orbital-dependent approximations to the *xc potential* can in principle be directly transferred to TDDFT by means of the orbital-adiabatic approximation discussed in Sec. 2.3. Constructing the potential associated with an orbital functional for  $E_{xc}$ , however, is nontrivial even in the GS, and becomes even more so in TDDFT. The former is because the density dependence of the KS orbitals is not known explicitly, so the derivative that defines  $v_{xc\sigma}(\mathbf{r})$  cannot be evaluated directly. By rewriting the derivative

$$\frac{\delta}{\delta n_{\sigma}(\mathbf{r})} = \sum_{\alpha\beta} \sum_{j=1}^{N_{\alpha}} \int d^3 r' \int d^3 r'' \frac{\delta v_{s\beta}(\mathbf{r}'')}{\delta n_{\sigma}(\mathbf{r})} \frac{\delta \varphi_{j\alpha}(\mathbf{r}')}{\delta v_{s\beta}(\mathbf{r}'')} \frac{\delta}{\delta \varphi_{j\alpha}(\mathbf{r}')} + \text{c.c.} \quad (3.4)$$

by means of the chain rule, inverting  $\delta v_{s\beta}/\delta n_\sigma$ , and deriving expressions for  $\delta\varphi_{j\alpha}/\delta v_{s\beta}$  and  $\delta n_\sigma/\delta v_{s\beta}$  from first order perturbation theory, one arrives after some algebra at an integral equation for  $v_{xc\sigma}(\mathbf{r})$  that involves all (occupied and unoccupied) orbitals and eigenvalues of the KS system: The optimized effective potential (OEP) equation [SH53, TS76, SGP82, KK08]. This is numerically expensive and hard to solve because it involves unoccupied orbitals and eigenvalues and an inversion of the KS response function. It is usually approximated (cf. Sec. 3.4), but there are ways to solve it both on a numerical grid [KP03b] and in basis set codes [SMVG97, KSG03]. The calculation of the unoccupied KS spectrum can be replaced by introducing the so-called *orbital shifts* [KP03b, KP03a].

As explained in Sec. 2.3, deriving a TD potential from an orbital-dependent DFA for  $E_{xc}$  is not straightforward. One cannot simply apply the adiabatic approximation with respect to the density or the orbitals since  $v_{xc\sigma}$  is only known implicitly as the solution of an integral equation, yet no explicitly density or orbital-dependent expression for  $v_{xc\sigma}$  exists where one could insert the TD density/orbitals.

Thus, orbital functionals have to be treated through the Keldysh formalism. As in the GS, this leads to an integral equation involving all occupied and unoccupied TDKS orbitals, the time-dependent OEP (TDOEP) equation [UGG95, vL98]:

$$\sum_{j=1}^{N_\sigma} \sum_{k=1}^{\infty} \int \int [v_{xc\sigma}(\mathbf{r}', t') - u_{xcj\sigma}(\mathbf{r}', t')] \times \\ \times \varphi_{j\sigma}^*(\mathbf{r}', t') \varphi_{j\sigma}(\mathbf{r}, t) \varphi_{k\sigma}^*(\mathbf{r}, t) \varphi_{k\sigma}(\mathbf{r}', t') \theta(t - t') d^3 r' dt' + c.c. = 0. \quad (3.5)$$

This is not just the GS OEP equation with the GS orbitals replaced by the TD ones, but a generalization which is an integral equation in both space and time. Due to the equation's complexity, so far it has only been solved for small one-dimensional model systems over short periods of propagation time [WU05, WU08, LHRC17, LHRC18].

Both the GS and the TD equation are formulated in terms of the so-called orbital-specific potentials,

$$u_{xci\sigma}(\mathbf{r}) = \frac{1}{\varphi_{i\sigma}^*(\mathbf{r})} \frac{\delta E_{xc}[\{\varphi_{k\alpha}, \varphi_{k\alpha}^*\}]}{\delta \varphi_{i\sigma}(\mathbf{r})} \quad (3.6)$$

and

$$u_{xci\sigma}(\mathbf{r}, t) = u_{xci\sigma}(\mathbf{r})|_{\{\varphi_{k\alpha} = \varphi_{k\alpha}(t)\}}. \quad (3.7)$$

The equations can be interpreted as the condition that the first order change in the density due to a switch from  $v_{xc\sigma}$  to the orbital-specific potentials vanish [KP03a].

As in the GS, the unoccupied orbitals can in principle be replaced by TD orbital shifts [MK06, LHRC17] which then have to be propagated along with the occupied KS orbitals.

To calculate the xc kernel, one would have to take the derivative of the TDOEP with respect to the density. This is even more complicated than the first derivative defining the potential, since the action functional is at least known in terms of the KS orbitals, while no explicit orbital-dependent expression for the potential exists and it is only known as the solution of the TDOEP

equation. However, as this equation is formulated in terms of the occupied and unoccupied orbitals, one can apply the derivative *to the equation* and, using the functional chain-rule again, derive a yet more involved equation for the TDOEP kernel [Gör98a, Gör98b]. As solving this equation is quite tedious, this has so far only been applied to calculate the EXX kernel for a few simple solids and small molecules [KG02, HIGB02, HIBG05, Hir05, SHH06, BSOR06, HvB08, HvB09, HIG09, IHG10, HG11].

### 3.4 Approximations to the Optimized Effective Potential

As solving the OEP equation is far from trivial, it is usually approximated in practice [KK08]. All of the approximations discussed in this thesis lead to explicit, orbital-dependent expressions for the potential. While these approximations can be derived independently in the TD case [UGG95, MK06, Naz13], the resulting TD potentials are just the orbital-adiabatic potentials corresponding to the GS approximations, so the GS and TD case will not be considered separately in this Section.

Minimizing the total energy with an orbital-dependent expression for the xc part without further constraints on the orbitals except for their normalization leads to a set of single particle Schrödinger equations with different potentials for each orbital [Sla51]. These potentials differ by their xc part which is given by the orbital-specific potentials  $u_{xci\sigma}$  introduced in Eq. (3.6) (see also Sec. 3.5). The additional constraint that all orbitals with spin  $\sigma$  solve a Schrödinger equation with the same, multiplicative potential  $v_{s\sigma}$  leads to the OEP equation [SH53, TS76]. Thus, in addition to being the proper xc potential associated with an orbital functional in the KS scheme [SGP82], the OEP can also be seen as the energetically best approximation to the set of potentials  $u_{xci\sigma}$  by a single potential  $v_{xc\sigma}$ . This motivates the oldest and simplest of the approximations to be discussed here: The Slater potential [Sla51, SH53] is the orbital-density weighted average of the  $u_{xci\sigma}$ s, i. e., a simpler, straightforward approximation of the orbital-specific potentials by a single potential:

$$v_{xc\sigma}^{\text{Sla}}(\mathbf{r}) = \sum_{i=1}^{N_{\sigma}} \frac{|\varphi_{i\sigma}(\mathbf{r})|^2}{n_{\sigma}(\mathbf{r})} \text{Re}[u_{xci\sigma}(\mathbf{r})]. \quad (3.8)$$

For EXX and SIC, it already gives the correct  $-e^2/r$  asymptotic, but it lacks many of the important features of the OEP, including step structures [BJ06] and the field-counteracting term [vGSG<sup>+</sup>99], both of which are considered important for the description of CT.

Neglecting the orbital-shift contributions to the OEP using mean-field arguments leads to what is probably the best-known approximation to the OEP, the Krieger-Li-Iafrate (KLI) potential [KLI92]:

$$v_{xc\sigma}^{\text{KLI}}(\mathbf{r}) = v_{xc\sigma}^{\text{Sla}}(\mathbf{r}) + \sum_{i=1}^{N_{\sigma}-1} \frac{|\varphi_{i\sigma}(\mathbf{r})|^2}{n_{\sigma}(\mathbf{r})} \int |\varphi_{i\sigma}(\mathbf{r}')|^2 [v_{xc\sigma}^{\text{KLI}}(\mathbf{r}') - \text{Re}[u_{xci\sigma}(\mathbf{r}')] ] d^3r'. \quad (3.9)$$

While it still significantly reduces the numerical effort compared to an exact OEP calculation, for some functionals like, e. g., EXX, its correction over the Slater potential introduces the missing

step structure, including TD steps [HK12a], and the field-counteracting behavior, leading to an improved description of static CT and (hyper-)polarizabilities [vGSG<sup>+</sup>99, KKP04, AK19]. In the KLI approximation, SIC with energy-minimizing unitary transformations also improves CT excitation energies [HK12b, HKK12].

An alternative derivation of the KLI potential is based on approximating all KS orbital energy differences appearing in the expression for  $\delta\varphi_{j\alpha}/\delta v_{s\beta}$  in the GS OEP equation by a single number, which ultimately drops out of the resulting expression for the potential. Improving on this by only approximating the occupied-unoccupied differences, yet leaving the occupied-occupied differences unchanged, yields the common energy denominator approximation (CEDA) [GB01, DG01, GGB02]:

$$v_{xc\sigma}^{\text{CEDA}}(\mathbf{r}) = v_{xc\sigma}^{\text{sla}}(\mathbf{r}) + \sum'_{i,j=1}^{N_\sigma} \frac{1}{2} \left\{ \frac{\varphi_{i\sigma}(\mathbf{r})\varphi_{j\sigma}^*(\mathbf{r})}{n_\sigma(\mathbf{r})} \int \varphi_{i\sigma}^*(\mathbf{r}') [v_{xc\sigma}^{\text{CEDA}}(\mathbf{r}') - u_{xc\sigma}(\mathbf{r}')] \varphi_{j\sigma}(\mathbf{r}') d^3r' + \text{c.c.} \right\}, \quad (3.10)$$

where the prime indicates that the  $i = j = N_\sigma$  term is missing from the sum. The CEDA potential exhibits a slightly larger field-counteracting effect and better polarizabilities than the KLI approximation [GGB02]. However, it is computationally more involved and, in general, not necessarily yields a sizeable improvement over KLI [KK08].

The exact OEP obeys the *zero-force theorem* [LP85, Vig95, vBDvLS05], which states that the interaction between the electrons of a system does not exert any net force on the system. This is true for the Hartree part of the interaction alone, and thus reduces to a condition on the xc potential:

$$\sum_\sigma \int n_\sigma(\mathbf{r}, t) \nabla v_{xc\sigma}(\mathbf{r}, t) d^3r = 0. \quad (3.11)$$

This condition is generally violated by the approximations to the OEP [MKvLR07, MDRS09, DMRS10, MDRS11, HK12b].

While it is straightforward to evaluate any of these approximations, they are all orbital dependent. Thus, their xc kernel still cannot be constructed directly, as the derivative  $\delta v_{xc\sigma}/\delta n_\tau$  is not accessible. Instead, it would have to be calculated by solving an OEP-like equation, or by applying yet further approximations [PGG96].

### 3.5 The Generalized Kohn-Sham Scheme

The complexity associated with orbital functionals in the KS scheme motivates a different approach which is essentially the standard method in practical calculations: The (TD) generalized Kohn-Sham (gKS) scheme [SGV<sup>+</sup>96, BK18]. Here, the constraint that the auxiliary single-particle Schrödinger equations yielding the orbitals all exhibit the same multiplicative potential is lifted. The resulting equations can be seen as containing either a single potential which, however, is no longer multiplicative, but an integral or differential operator (depending on the specific functional); or different multiplicative potentials for the different orbitals, the

$u_{xci\sigma}$ .

In a nutshell, this amounts to replacing all derivatives with respect to the density by derivatives with respect to the orbitals, which of course can be evaluated directly for an orbital functional.

Note that since the KS and gKS orbitals differ from each other, the same orbital-dependent expression for  $E_{xc}$  thus defines different approximations in the KS and gKS schemes. These differences are usually expected to be small at least for total energies, as they merely stem from an additional constraint in the energy minimization. For other quantities, however, larger differences can occur: While the KS version of EXX yields bound and physically meaningful Rydberg orbitals [DG01, DSG02, KK08, IHG10, HG11], the gKS version, which reduces to Hartree-Fock, typically does not bind unoccupied orbitals and does not exhibit a Rydberg series in the unoccupied eigenvalue spectrum [KK08, IHG10, HG11].

Also, while the energetically highest occupied orbital (HOMO) can be interpreted as an electron removal energy in both schemes, the lowest unoccupied orbital (LUMO) approximates an *excited* electron in the KS and an *additional* electron in the gKS scheme [BGvM13]. This makes gKS the favorable approach for calculating fundamental gaps, defined as the difference between the ionization potential and the electron affinity,  $\Delta = I - A$ , from the eigenvalues. For the calculation of excitation energies, however, this seems to suggest the KS orbitals as the more promising starting point.

Comparisons between the performance of TDKS and TD gKS in predicting excitation energies so far seem to be limited to EXX [HIGB02, HIG09, IHG10, HG11]. In the TD gKS scheme, the use of typical meta-GGAs without current-density dependent modifications yields equations that are not gauge-invariant and violate the continuity equation, and this latter problem even questions the validity of the gKS map for these functionals [Tao05, BF12, BK18]. In the TDKS scheme, the continuity equation of course is always trivially obeyed due to its single, multiplicative potential. This finding suggests that the differences between the TDKS and TD gKS schemes might be more substantial for other functionals than EXX and underscores the need for further development and analysis of the TDKS approach to orbital functionals.



## CHAPTER 4

# Practical Approaches to Computational Spectroscopy within Density Functional Theory

In this Chapter, first the two prevalent methods to calculate excitations within TDDFT are presented in Sec. 4.1. Their properties are reviewed, with special focus on some disadvantages that trigger the search for different approaches. Then, in Sec. 4.2, the alternative scheme that is the main topic of this thesis is briefly discussed. A more in-depth analysis is given in Chapter 5 and in [Pubs. 1-4](#).

### 4.1 Established Methods

#### 4.1.1 Excitation Energies as Eigenvalues: The Casida Scheme

The most popular method for calculating electronic excitations within TDDFT [[SLR<sup>+</sup>12](#)] is the matrix scheme developed by Casida [[Cas95](#)]. Its basic idea is to expand the response into particle-hole pairs, i. e., transitions from an occupied into an unoccupied KS orbital. This leads to the Casida equation from which excitation energies can be calculated as eigenvalues, while oscillator strengths can be deduced from the corresponding eigenvectors. The matrix in this equation has two contributions, mirroring the analysis from Sec. 2.4: a diagonal part containing the KS eigenvalue differences  $\epsilon_{a\sigma} - \epsilon_{i\sigma}$ , and the coupling matrix containing the matrix elements

$$K_{ia\sigma, jb\tau} = \iint \varphi_{i\sigma}^*(\mathbf{r}) \varphi_{a\sigma}(\mathbf{r}) f_{\text{Hxc}\sigma\tau}(\mathbf{r}, \mathbf{r}', \omega) \varphi_{j\tau}^*(\mathbf{r}') \varphi_{b\tau}(\mathbf{r}') d^3r d^3r' \quad (4.1)$$

of the Hartree-xc kernel between different electron-hole pairs. Here,  $i, j$  stand for occupied and  $a, b$  for unoccupied KS orbitals.

An advantage of this method over, e. g., the real-time (RT) approach (cf. Subsec. 4.1.2), is that it gives access to all transitions, including dark ones.<sup>1</sup> It is also very similar to Hartree-Fock based LR methods and can thus easily be implemented in existing quantum chemistry codes. However, it also has several disadvantages:

---

<sup>1</sup>Yet note that in practice, excitations of different spin symmetry, i. e., singlet and triplet transitions, have to be found in two separate calculations.

In principle, all unoccupied KS orbitals and orbital energies are required to set up the Casida matrix, even if the employed DFA only relies on the density or the occupied orbitals. In practice, the number of virtual orbitals needed to converge the excitation energies in a Casida calculation scales unfavorably with the size of the system and the employed basis set, leading to a quickly escalating numerical effort for larger systems.

Diagonalizing a large matrix is costly even for moderate system sizes compared to, e. g., just solving a linear equation [KP03a] (as would be needed in the Sternheimer approach, cf. Sec. 4.2, or for a Crank-Nicholson propagation step [SK18] in the RT approach). Additionally, large, dense matrix diagonalization also scales badly and is not suited for efficient parallelization.

Typically, the eigenvalues are calculated iteratively, starting from the smallest. This means that if one is interested in excitations lying in a specific energy range, or in optically active, bright excitations only, one still has to calculate all the lower lying, possibly dark transitions first. Also, the spectrum is constructed “serially”, i. e., one excitation after another, with no way of distributing the workload for different frequencies over various processors through parallelization.

When non-adiabatic approximations for  $f_{xc}$  are used, the equation becomes nonlinear as the excitation energy appears both as the eigenvalue and as an argument of the Casida matrix, which in general is frequency dependent. Since the frequency dependence can not only modify excitations found in the adiabatic approximation, but also create additional ones [TK14], there is no unique one-to-one mapping from adiabatic to non-adiabatic solutions. Thus, iteratively improving on the solution for a specific transition frequency by, e. g., repeatedly reinserting it into the Casida matrix and then recalculating it, starting from the adiabatic approximation, will not lead to a full solution and, specifically, will not reveal the double excitations created by the kernel’s frequency dependence. This makes systematically solving the non-adiabatic Casida equation quite involved, and existing quantum chemistry codes are typically not adapted for non-adiabatic DFAs.

Finally, an important disadvantage is that the scheme makes explicit use of the xc kernel, which is specifically problematic in combination with orbital functionals in the KS scheme. The kernel, being a function of two coordinates, is generally a more complicated quantity than, e. g., the xc potential. It is more expensive to store and to manipulate and harder to analyze. If one chooses to use an orbital-dependent expression for the xc energy or action functional, the kernel’s construction as the second derivative of that functional with respect to the density becomes extremely complicated, as detailed in Sec. 3.3. Even if one works with an explicit orbital-dependent expression for the potential, the calculation of the kernel would still require to solve an OEP type of equation (cf. Sec. 3.4). Therefore, linear response calculations using orbital functionals are usually performed in the gKS scheme.

#### 4.1.2 Simulating Electron Dynamics in Real Time

Another approach that is becoming increasingly popular [LG11, JSARM<sup>+</sup>15, BLL16, PI16, DGS<sup>+</sup>16, DK16, DWC<sup>+</sup>17, RKP<sup>+</sup>17, SRGGLL<sup>+</sup>18, GLL18, ZH18, SK18, SFG<sup>+</sup>19, JSL19] is

based on propagating the TDKS equations in real time, as pioneered by Yabana and Bertsch [YB96]. Originally proposed for real-space grids, modern applications employ both grids [SRGGLL<sup>+</sup>18, SK18, SFG<sup>+</sup>19, JSL19] and basis sets [BLL16, DWC<sup>+</sup>17, RKP<sup>+</sup>17, ZH18]. Information about excitations is extracted by monitoring observables such as the induced dipole moment during the propagation, so unlike in the Casida scheme, detecting transitions carrying little or no oscillator strengths is not trivial [BLL16, Sch16]. The approach is, however, not strictly limited to “visible”, i. e., dipole singlet excitations; it can, for instance, be used to calculate triplet excitations [OCMR08, IL09] as well.

As the TDKS equations are not explicitly linearized in the RT approach, it can be used to calculate nonlinear effects as well, such as photoionization [DGS<sup>+</sup>16, DK16].

In contrast to the Casida approach, RT calculations can be parallelized efficiently over the orbitals, since the TDKS equations for different orbitals can be propagated independently, and only need to “communicate” for the calculation of  $v_{\text{Hxc}\sigma}(\mathbf{r}, t)$  [SK18]. This fact also ensures a favorable scaling with the system size, as every additional electron basically means only one more orbital has to be propagated [SK18]. In an implementation based on real-space grids, one can additionally exploit the sparsity of the Hamiltonian matrix, allowing for further efficient parallelization over the grid [KMT<sup>+</sup>06, SK18].

Another advantage of the approach is that one avoids having to calculate the kernel, as only the TDKS potential enters the equations.

The usual approach is to initially perturb the system with a  $\delta$ -“kick”, typically modeled by modifying the GS orbitals with a position-dependent initial phase before starting the propagation, and then to let it evolve freely. The system’s dynamic will then be given by a superposition of oscillations with all its resonant frequencies, so from the Fourier transform of the induced dipole moment, one can construct the entire spectrum with just one propagation. This is beneficial when one is interested in calculating the spectrum over a wide frequency range. As the resolution of the spectrum is determined by the propagation time, however, the approach is less suited for high-resolution calculations of only a few excitations in a narrow frequency range.

Finally, RT propagations can suffer from stability issues, specifically in connection with orbital functionals: As detailed in Sec. 3.3, stable propagations of the full TDOEP equation have not yet been reported for realistic three-dimensional systems, while calculations employing the TDOEP kernel in a Casida-like LR approach are demanding, yet possible. Further, due to their violation of the zero-force theorem, the approximations to the TDOEP introduced in Sec. 3.4, as well as direct orbital-dependent approximations to  $v_{\text{xc}}$  such as the Becke-Johnson (BJ) potential, can lead to serious instabilities as well [MKvLR07, MDRS09, HK12b, KAK13].

## 4.2 The Sternheimer Approach as an Efficient Alternative

For a reliable description of different kinds of excitations in large systems such as, e. g., natural light harvesting complexes, one needs a method that scales reasonably with the system size, allows for efficient parallelization, and can be used in combination with orbital dependent

approximations to  $v_{xc}$ . As neither of the standard approaches reviewed in Sec. 4.1 meets these conditions, the main goal of this thesis is to explore the potential of an alternative LR scheme, the Sternheimer equation [Ste51, ABMR07].

In this approach, the TDKS equations are explicitly linearized, but in contrast to the Casida method, the response is *not* expanded into particle-hole pairs, and one does *not* derive an eigenvalue equation for the excitation energies. Instead, one considers a system subject to a monochromatic perturbation with some chosen frequency  $\omega$ ,  $v_{\text{ext}\sigma}(\mathbf{r}, t) = v_{\text{ext}\sigma}^{(+)}(\mathbf{r})e^{-i\omega t} + \text{c.c.}$ <sup>2</sup> Then, one solves the linearized KS equations to construct the system's response to that specific single frequency. This is simplified considerably by the fact that in this case, the involved first-order quantities such as, e. g., the linear response of the density, xc potential, and orbitals, all show the same, analytically known TD behavior (as derived in Pub. 1): They merely oscillate with the frequency of the applied perturbation, e. g.,  $n_{\sigma}^{(1)}(\mathbf{r}, t) = n_{\sigma}^{(+)}(\mathbf{r})e^{-i\omega t} + \text{c.c.}$ , and all one needs to calculate are the corresponding *amplitudes* ( $n_{\sigma}^{(+)}(\mathbf{r})$ ), which are functions of the spatial coordinates but not of time.

Thus, the linearized TDKS equations ultimately can be reduced to differential equations in space only, the frequency dependent Sternheimer equations, which can easily be solved without having to propagate the orbitals numerically:

$$[\hat{h}_{\sigma} - \varepsilon_{j\sigma} \mp \hbar\omega] \varphi_{j\sigma}^{(\pm)}(\mathbf{r}) = - \left[ v_{\text{ext}\sigma}^{(+)}(\mathbf{r}) + v_{\text{Hxc}\sigma}^{(+)}(\mathbf{r}) \right] \varphi_{j\sigma}(\mathbf{r}), \quad (4.2)$$

where  $\hat{h}_{\sigma}$ ,  $\varphi_{j\sigma}(\mathbf{r})$ , and  $\varepsilon_{j\sigma}$  refer to the GS Hamiltonian, orbitals, and orbital energies of the KS system, and the complex-valued TDKS orbitals have independent  $\pm\omega$ -components  $\varphi_{j\sigma}^{(\pm)}(\mathbf{r})$ . From these orbital response amplitudes  $\varphi_{j\sigma}^{(\pm)}(\mathbf{r})$ , one can then calculate the density response amplitude

$$n_{\sigma}^{(+)}(\mathbf{r}) = \sum_{j=1}^{N_{\sigma}} \varphi_{j\sigma}(\mathbf{r}) \left( \varphi_{j\sigma}^{(+)}(\mathbf{r}) + \varphi_{j\sigma}^{(-)}(\mathbf{r}) \right). \quad (4.3)$$

The equations have to be solved self-consistently as the expressions on finds for  $v_{\text{Hxc}\sigma}^{(+)}(\mathbf{r})$  depend on the solutions  $\varphi_{j\sigma}^{(\pm)}(\mathbf{r})$  or  $n_{\sigma}^{(+)}(\mathbf{r})$ .

The solution of these equations allows to calculate the value of spectral response properties, like the dynamic polarizability  $\alpha(\omega)$  or the absorption cross section  $\sigma(\omega)$ , for a single frequency  $\omega$ . This frequency enters the Sternheimer equations simply as a parameter. Thus, in order to construct discretized spectra in any given frequency range, one needs to choose a discrete set of values  $\{\omega_i\}$  for this parameter, and solve the Sternheimer equations for all of these values. From the resulting spectra one can then identify excitation energies.

This has several decisive advantages: First of all, the calculations for different frequencies are completely independent of each other. This allows for massive parallelization, as the whole spectrum can be calculated at once, with all frequencies treated simultaneously on different computer nodes without any communication at all.

---

<sup>2</sup>We here present the scheme in its simplest form, neglecting the switch-on effects and subspace projections discussed in Pubs. 1 and 3.

Also, no diagonalization is involved; instead, one only needs to solve linear equations. Similar to the RT approach, these are simply two equations for each occupied orbital, which can be solved almost independently and are only connected through the calculation of  $v_{\text{Hxc}\sigma}^{(+)}$ , and the matrix of these linear equations (left-hand side of Eq. (4.2)) is basically given by the GS KS Hamiltonian. Thus, the Sternheimer approach shares many of the advantages of the RT method: It has essentially the same scaling with system size, and can be parallelized quite efficiently over the orbitals and, at least in a real-space implementation, also over the grid.

Since the time-dependence, however, is treated analytically in the Sternheimer scheme and no numerical propagations are involved, one can avoid the propagation instabilities from which the RT approach can suffer.

The fact that the equations only need to be solved for the frequencies one is interested in is an additional advantage if one only wants to calculate the spectrum within a specific energy range, or to determine accurate excitation energies for only a few selected transitions. At the same time, however, this makes the method less suited for the calculation of broadband spectra, which is the forte of the RT scheme.

Instead of the kernel, the basic xc functional in the Sternheimer approach is the amplitude  $v_{\text{xc}\sigma}^{(+)}(\mathbf{r})$  of the xc potential's linear response  $v_{\text{xc}\sigma}^{(1)}(\mathbf{r}, t)$  to the perturbation. Like the potential of the GS theory, it is a function of one spatial coordinate  $\mathbf{r}$  only. It can, but need not be explicitly expressed in terms of the kernel. Specifically, as shown in [Pub. 3](#), for an orbital dependent approximation to  $v_{\text{xc}\sigma}(\mathbf{r}, t)$ , the effort of solving an OEP-like equation for the kernel can be avoided, and one can derive simple explicit expressions for the response of, e. g., the KLI or CEDA potential corresponding to any given orbital functional.

Thus, the drawbacks of both methods discussed in Sec. 4.1 related to the use of orbital functionals, i. e., the Casida scheme's dependence on the kernel and the stability issues of RT propagations, are absent in the Sternheimer approach.

This, along with the method's scaling and parallelization properties, makes it an interesting alternative to the established approaches to LR TDDFT that merits further exploration and development.



## CHAPTER 5

# Developing the Sternheimer Method into an Efficient Linear Response Scheme

The Sternheimer formalism is well established in GS DFT [BDDG01], but only few applications to TDDFT have been reported so far [ABMR07, OCMR08, HG14a, HG14b]. Thus, the scheme is not yet as fully developed as, e. g., the Casida approach, both with respect to numerical efficiency and even to basic theory, as it has been missing a full, rigorous derivation within TDDFT: Earlier applications of the scheme have motivated it as an adiabatic extension of the GS Sternheimer theory, or by making educated guesses about the response of the TDKS orbitals to a monochromatic perturbation. The latter typically ignore the switch-on process of the perturbation, or the fact that the TD orbitals evolve from the GS, and that their response should vanish at some initial time.

This lack of a proper derivation has practical consequences: most notably, an imaginary term  $i\eta$  that needs to be added to the frequency on the left-hand side of Eq. (4.2) to regularize the equations and stabilize the convergence is usually introduced *ad hoc* as a positive infinitesimal [ABMR07], while finite values are needed in practice.

More technical questions concern, e. g., the efficient extraction of excitation energies and oscillator strengths from the scheme, and adequate linear algebra algorithms that can deal with the imaginary contribution on the diagonal of the otherwise hermitian, large, sparse matrix of the Sternheimer equations.

Also, applications so far have been mostly restricted to the LDA, and an extension to orbital functionals within the KS scheme has not yet been explored.

To illustrate the progress that has been made on the Sternheimer approach in the course of this thesis, Sec. 5.1 summarizes the basic idea behind the rigorous derivation of the scheme that has been put forward in Pub. 1 and lists several important insights and generalizations that result from this derivation. Section 5.2 then presents some practical improvements (detailed in Pub. 1), including a new and specialized iterative solver for linear equations with a complex, non-hermitian, yet symmetric matrix, as well as novel evaluation strategies for excitation energies. An idea on how to use orbital dependent expressions for the xc potential in Sternheimer LR calculations, which is derived, implemented, and tested in Pub. 3, is explained in Sec. 5.3. The results of Pubs. 2 and 4, which use the Sternheimer approach to study whether selected (meta-)GGAs are capable of improving the description of CT, are summarized in Sec. 5.4. Finally, Sec. 5.5 gives an overview on how the Sternheimer scheme can be used to analyze

properties of different DFAs, as is done throughout Pubs. 1-4.

## 5.1 Formal Insights on the Sternheimer Approach from a New Derivation

To put the Sternheimer scheme on solid formal foundations, Pub. 1 derives it directly from the TDKS equations. To this end, the perturbation is modeled not strictly as a monochromatic perturbation, but is additionally switched on exponentially with a finite rate  $\eta$ , starting at  $t_0 = -\infty$  when the system is in its GS<sup>1</sup>:

$$v_{\text{ext}\sigma}(\mathbf{r}, t) = \left[ v_{\text{ext}\sigma}^{(+)}(\mathbf{r}) e^{-i\omega t} + \text{c.c.} \right] e^{\eta t}. \quad (5.1)$$

Then, the evolution from the GS of a system subject to this perturbation is considered, and expressions for the linear response of the density, orbitals, and potential are rigorously derived through a formal solution (up to first order) of the TD equations: e. g.,

$$n_{\sigma}^{(1)}(\mathbf{r}, t) = \left[ n_{\sigma}^{(+)}(\mathbf{r}) e^{-i\omega t} + \text{c.c.} \right] e^{\eta t}. \quad (5.2)$$

By inserting the corresponding expression for the response of the orbitals back into the linearized TDKS equations, the matrix on the left-hand side of the resulting Sternheimer equations turns out to be  $[\hat{h}_{\sigma} - \varepsilon_{j\sigma} \mp \hbar(\omega + i\eta)]$ , i. e., the switch-on rate automatically appears as an imaginary contribution to the frequency. For this derivation to hold, one does not need to assume that the rate  $\eta$  is infinitesimally small. Based on a formal solution of the scheme, Pub. 1 reveals the effect of this term on the resulting spectra: It turns  $\delta$ -shaped lines positioned at the excitation energies into Lorentzians, with heights related to the oscillator strengths. The width of these Lorentzian lines is given by  $2\hbar\eta$ , but their positions and relative heights, i. e., the experimentally relevant observables, are not affected at all. Efficient ways to extract these observables accurately from the Lorentz spectra are discussed in Sec. 5.2.

Another benefit from the new derivation is that it allows to examine the requirements of a DFA for  $v_{\text{xc}\sigma}(\mathbf{r}, t)$  that are needed for the derivation to hold. This is important in order to be able to compare results from a RT propagation and a Sternheimer calculation based on the same DFA: If a DFA violates some exact condition that is needed in the derivation of the Sternheimer scheme, then one could still insert the corresponding expression for  $v_{\text{xc}\sigma}(\mathbf{r}, t)$  into the Sternheimer equations *a posteriori*, but using these equations would in this case constitute a further approximation and one could not expect the approach to yield the same results as a RT calculation employing the same  $v_{\text{xc}\sigma}(\mathbf{r}, t)$ . Only two rather trivial conditions turn out to be necessary: The KS systems needs to stay in its GS when no perturbation is applied, and the first order change of  $v_{\text{xc}\sigma}(\mathbf{r}, t)$  at time  $t$  due to a change of  $n_{\tau}(\mathbf{r}', t')$  at  $t'$  can only depend on  $\sigma$ ,  $\tau$ ,  $\mathbf{r}$ ,  $\mathbf{r}'$ , and the difference  $t - t'$ .

---

<sup>1</sup>More precisely, the model initially uses an arbitrary, finite switch-on time  $t_0$  that is eventually taken to  $-\infty$ .

Additionally, the derivation in [Pub. 1](#) is given in the spin-dependent formulation of DFT and allows for the perturbation to include couplings between the electron spins and a magnetic field. Thereby, the Sternheimer scheme is extended to the treatment of triplet excitations.

Finally, the derivation allows to clarify the role of phase factors that are separated from the orbitals, and of projectors appearing in the equations. Some further light is shed on this in [Pub. 3](#).

## 5.2 Technical Developments

While Ref. [[ABMR07](#)] already provided some crucial insights on the numerical realization of the Sternheimer scheme, including the importance of the imaginary damping term  $\eta$  for a stable calculation, and of employing mixing techniques to stabilize the self-consistent solution, there are still open problems to tackle.

In principle, the scheme lends itself to a realization on real-space grids as the operator on the left-hand side is basically the KS Hamiltonian, which is represented by a large, but highly sparse matrix on a grid. This leads to efficient algorithms with high potential for parallelization [[KMT<sup>+</sup>06](#), [CAO<sup>+</sup>06](#)]. Large, sparse linear algebra problems are usually tackled by Krylov subspace methods such as the well-known and efficient conjugate gradient algorithm (CG). The latter, however, requires hermitian matrices [[HS52](#), [PTVF07](#)]. Unfortunately, the imaginary contribution  $i\eta$  ruins the hermiticity of the Sternheimer matrix.

More generally applicable algorithms have been proposed, such as the stabilized biconjugate gradient algorithm (BiCGstab) [[ABMR07](#)] and the quasi-minimal residual method (QMR) [[ASD<sup>+</sup>15](#)]. However, none of these methods exploit a property that the Sternheimer operator *does* still have despite the imaginary damping term: Its matrix representation on a cubic grid,

$$A_{kl}^{j\sigma} = (\hat{h}_\sigma)_{kl} - [\epsilon_{j\sigma} \pm \hbar(\omega + i\eta)] \delta_{kl}, \quad (5.3)$$

is not *hermitian*,  $(A_{lk}^{j\sigma})^* \neq A_{kl}^{j\sigma}$ , but *symmetric*,  $A_{lk}^{j\sigma} = A_{kl}^{j\sigma}$ . Based on this premise, [Pub. 1](#) derives a novel algorithm that is similar to the CG, yet adapted to complex, symmetric matrices, dubbed the complex symmetric conjugate gradient algorithm (CGsymm). It is tested and compared to the BiCGstab, and turns out to be considerably more efficient in solving the Sternheimer equations. Thus it is employed in all Sternheimer calculations throughout [Pubs. 1-4](#).

Another issue that the Sternheimer approach shares with RT calculations is the accurate and systematic extraction of excitation energies and oscillator strengths: While these quantities directly result from a Casida calculation, the output of a Sternheimer or RT calculation typically is some response observable, such as the polarizability or the absorption cross section, discretized as a function of the frequency. From the latter one can readily plot a spectrum, but the identification of excitation energies is not always trivial. As mentioned in [Sec. 5.1](#), in a Sternheimer calculation, the linewidth in these discrete spectra is determined by the damping parameter  $\eta$ . This seems to suggest that an accurate identification of excitation energies can only be achieved through expensive calculations: Sharper lines correspond to smaller values of  $\eta$  and, thus, to slower convergence of the calculation. In order to resolve these more narrow lines,

one would then need a finer sampling of the frequency axis, which means that the Sternheimer equations would have to be solved for a larger number of discrete values  $\{\omega_i\}$ .

Two strategies are presented in Pub. 1 that help to avoid this dilemma. The first is based on the knowledge of the exact shape of the spectrum resulting from a Sternheimer calculation: Excitation energies and oscillator strengths can be extracted by simply fitting the positions  $\Omega_I$  and heights  $f_I$  of a superposition of Lorentzians with fixed width  $2\eta$  to the data, e. g.,

$$\text{Im}[\alpha(\omega)] = \sum_I f_I \frac{1}{\pi} \frac{\eta}{\eta^2 + (\omega - \Omega_I)^2}. \quad (5.4)$$

It turns out that the resolution of the fitted excitation energies is typically better by 2-3 orders of magnitude than what one would expect from the linewidths. In fact, as explicitly demonstrated in Pub. 1, even low-intensity transitions that in the raw Sternheimer data are completely buried under a neighboring, stronger peak and are, thus, invisible to the naked eye, can be tracked down; their excitation energies can still be determined roughly 1-2 orders of magnitude more accurately than suggested by the value of  $\eta$ .

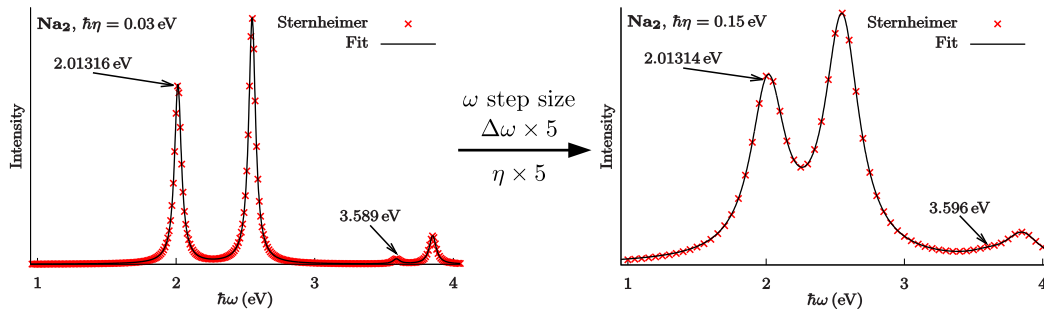


**Figure 5.1:** Stronger damping and fewer sample frequencies hardly affect the fitted excitation energies.

The goal of the second strategy is to compute excitations of as many different types as possible in a single calculation, but evaluate them in a way that separates them into different spectra, each of which contains only a minimal number of overlapping spectral lines, in order to facilitate the accurate identification of the individual transitions. The basic idea to achieve this is to apply a perturbation with *low spatial and spin symmetry*, and then construct spectra by evaluating various *high-symmetry* moments of the resulting density response amplitude  $n_{\sigma}^{(+)}(\mathbf{r}, t)$ . Specifically, one can, e. g., define a perturbation as a sum of different linear and quadratic functions of the coordinates with both even and odd spin-dependence,

$$\mathbf{v}_{\text{ext}\sigma}^{(+)}(\mathbf{r}) \propto (x/a_0 + z/a_0 + xy/a_0^2 + z^2/a_0^2 + \dots) \times \underbrace{(1 + \text{sgn}(\sigma))}_{=2\delta_{\sigma\uparrow}} \quad (5.5)$$

(where  $a_0$  is the Bohr radius). Solving the Sternheimer equations for such a perturbation then results in a density response containing information about different dipole, quadrupole, singlet and triplet excitations. This information is extracted separately by evaluating different components of the dipole and quadrupole operators with the response of both the total density,

$n^{(+)} = n_{\uparrow}^{(+)} + n_{\downarrow}^{(+)}$ , and the spin magnetization density,  $m^{(+)} = -\mu_B (n_{\uparrow}^{(+)} - n_{\downarrow}^{(+)})$ . Similar ideas, yet restricted to dipole singlet and triplet excitations and applied to RT calculations, have been presented in Ref. [OCMR08]. [Publication 1](#) establishes the simultaneous calculation of singlets and triplets in the Sternheimer scheme. It further demonstrates the full potential of this approach by calculating the  $^1\Pi_g$ ,  $^1\Sigma_g^+$ ,  $^3\Sigma_u^+$ ,  $^3\Pi_u$ ,  $^3\Pi_g$ , and  $^3\Sigma_g^+$  transitions of the  $N_2$  molecule using the Sternheimer scheme with only one single perturbation, and then constructing separate spectra, each containing only one type of excitation, from the response of the spin densities.

Additionally, [Pub. 1](#) compares two different mixing strategies and finds Anderson mixing [[And65](#)] to be slightly more efficient than Broyden mixing [[Bro65](#), [Joh88](#)]. It also compares basis-set based Casida calculations to grid-based Sternheimer calculations and studies the convergence of excitation energies with respect to basis set or grid size. The results suggest that the grid based calculations converge more systematically for all excitations, while the accuracy for a given basis set size varies drastically between transitions of different types. [Publications 1](#) and [3](#) further explore the efficiency of different projector schemes.

### 5.3 Orbital Functionals in the Sternheimer Scheme

As discussed in Chapters 3 and 4, harnessing the power of orbital functionals in LR TDDFT is vitally important, yet far from trivial in KS based methods due to propagation instabilities (in RT methods) and the complexity involved in constructing their kernel (in the Casida approach). Providing new and more efficient ways to deal with orbital functionals within the TDKS formalism is one of the promises of the Sternheimer scheme, and [Pub. 3](#) presents a first step in this direction.

Generally, when discussing orbital functionals in TDDFT, one has to differentiate between two levels of complexity regarding the expression for the potential: The first level comprises explicitly orbital dependent expressions for the potential itself, including model potentials as well as the expressions discussed in Sec. 3.4, e. g., the KLI potential, while the second level consists of the exact TD potential corresponding to an orbital dependent DFA for  $E_{xc}$ . The latter is the solution of the TDOEP equation and *not* known explicitly as a functional of the orbitals, cf. Sec. 3.3.

While the ultimate goal would be to find solutions to the TDOEP problem, already the “first-level” orbital dependent potentials challenge the established LR methods. Solving this first problem can both have merits on its own and be seen as a first steps towards an efficient TDOEP scheme, and [Pub. 3](#) essentially provides this solution.

The basic idea behind this is the following: The standard way of constructing the linear response of any quantity  $\mathcal{O}$  (such as the xc potential,  $\mathcal{O} = v_{xc\sigma}(\mathbf{r}, t)$ ) in LR TDKS theory consists of an expansion with respect to the linear response of the density,

$$\mathcal{O}^{(1)} = \sum_{\tau} \int d^3 r' \int dt' \left. \frac{\delta \mathcal{O}}{\delta n_{\tau}(\mathbf{r}', t')} \right|^{(0)} \times n_{\tau}^{(1)}(\mathbf{r}', t'). \quad (5.6)$$

When this is applied to the xc potential, the functional derivative appearing in this expansion introduces the xc kernel, cf. Eq. (2.14) in Sec. 2.4. If the quantity of interest is expressed in terms of the TDKS orbitals, it is still technically a density functional due to the orbitals' implicit density dependence, but the expansion in this case evokes the functional chain rule, leading to OEP-like equations for the kernel. However, one could instead simply expand the quantity with respect to the linear response of the KS orbitals,

$$\mathcal{O}^{(1)} = \sum_{\tau} \sum_{j=1}^{N_{\tau}} \int d^3 r' \int dt' \left[ \frac{\delta \mathcal{O}}{\delta \varphi_{j\tau}(\mathbf{r}', t')} \Big|^{(0)} \times \varphi_{j\tau}^{(1)}(\mathbf{r}', t') + \frac{\delta \mathcal{O}}{\delta \varphi_{j\tau}^*(\mathbf{r}', t')} \Big|^{(0)} \times \varphi_{j\tau}^{(1)*}(\mathbf{r}', t') \right]. \quad (5.7)$$

Thus, the derivatives with respect to the density are then replaced with derivatives with respect to the orbitals, which can be worked out analytically for any orbital dependent expression. The linear response amplitudes  $\varphi_{j\sigma}^{(\pm)}(\mathbf{r})$  of the KS orbitals that  $\varphi_{j\tau}^{(1)}(\mathbf{r}', t')$  is composed of are the basic variables of the Sternheimer approach and are just as available as the density response. Consequently, this approach leads to explicit expressions for the linear response of any orbital dependent quantity (including xc potentials) which can easily be evaluated within a Sternheimer calculation.

The crucial insight is that while this might look like an approximation or a switch from the KS to the gKS scheme (cf. Sec. 3.5), it is actually not: As shown in Pub. 3, the density expansion (Eq. 5.6) involving the kernel can be directly converted into the orbital expansion (5.7) by means of the functional chain rule and some algebraic manipulations. This proves that working with the explicit expressions resulting from this orbital expansion approach is indeed equivalent to solving OEP-like equations for the frequency dependent kernel. The frequency dependence connected with the non-adiabatic density dependence of the orbitals is in this approach “hidden” in the orbital response amplitudes  $\varphi_{j\sigma}^{(\pm)}(\mathbf{r})$ .

Commonly used model potentials such as the ones by Becke and Johnson [BJ06] and Tran and Blaha [TB09] are specifically built to model known features of the GS potential. Therefore, the focus in Pub. 3 is rather on linearizing the standard approximations to the TDOEP. The orbital expansion approach (5.7) is used to derive expressions for the potential response amplitudes  $v_{xc\sigma}^{(+)}(\mathbf{r})$  of the Slater potential (Sl), KLI and CEDA potentials, which are then implemented for EXX and SIC<sup>2</sup>.

The static limit of the frequency-dependent Sternheimer scheme facilitates a comparison to finite-field potential differences constructed from GS calculations in order to verify that the  $v_{xc\sigma}^{(+)}(\mathbf{r})$  constructed this way indeed represents correctly the first order change of the local xc potential. This is done in Pub. 3 for the critical case of a hydrogen chain (H<sub>8</sub>) where the linear response of the EXX potential is known to show a pronounced field-counteracting behavior, which is important for the correct prediction of response properties such as (hyper-)polarizabilities [vGSG<sup>+</sup>99, GGB02, KKP04].

As SiH<sub>4</sub> is known to be an example for a system where RT propagation with the EXX and SIC KLI potential actually *is* stable [MCR01, HK12b], it is used as an additional test case for

<sup>2</sup>without unitary transformations, i. e., based on KS orbitals.

the orbital expansion expressions to show that Sternheimer calculations yield photoabsorption spectra in perfect agreement with RT spectra using the corresponding TD KLI or CEDA potentials.

Finally, it is demonstrated that the new approach allows to circumvent the stability issues associated with the use of orbital functionals in RT methods and to perform numerically robust, stable, converged LR calculations even in the extreme case of the Na<sub>5</sub> cluster, which is a notorious example for propagation instabilities: Using the Sternheimer method, the EXX KLI photoabsorption spectrum of Na<sub>5</sub> is calculated, which is not accessible in the RT approach due to instabilities [MKvLR07].

In Pub. 4, the same method is then used to implement the KLI response of the meta-GGAs TASK and PoC [AK19]. The correctness of the potential is once again checked by comparing the static limit to finite-field potential differences for H<sub>8</sub>, and then the method is used to calculate the absorption spectra of several sample systems. To the best of my knowledge, these are the first ever reported TD LR calculations using meta-GGAs in the KS scheme.

## 5.4 Studying Different Approaches to the Charge-Transfer Problem

Among the different types of transitions that standard functionals fail to predict correctly (cf. Sec. 3.2), the focus in this thesis is on CT excitations. They are hugely underestimated by typical GGAs and global hybrids with a small fraction of exact exchange, and it has been argued that nonlocality and step structures in the xc potential play a crucial role for their correct description [DWHG03, Toz03, DHG04, Mai05, Küm17]. The Casida formulation of LR TDDFT can give some insight on this, following the line of argument of, e. g., Dreuw *et. al.* [DWHG03] and Tozer [Toz03]: For the simple case of a donor-acceptor system and a CT excitation that can be well described as a transition from the HOMO of the donor to the LUMO of the acceptor, the excitation energy from a LR calculation is given by the corresponding orbital energy difference  $\epsilon_H - \epsilon_L$ , corrected by a kernel contribution  $\propto K_{HL,HL}$  from Eq. (4.1). The exact CT energy in this case, on the other hand, approaches the difference between the donor's ionization potential and the acceptor's electron affinity in the limit of large donor-acceptor separation. The orbital energy difference alone cannot give a correct description as even in an exact KS calculation, the LUMO does not describe an electron addition and  $\epsilon_L$  will generally differ from the electron affinity of the acceptor. Thus, a sizeable correction from the kernel is needed. This, however, is not trivial to achieve, as the orbital overlap in  $K_{HL,HL}$  vanishes exponentially for large separation, which the xc kernel must then counteract somehow.

In principle, it is known that this problem can be solved with, e. g., EXX (in KS theory resorting to the TDOEP) or tuned range separated hybrids that use exact long-range and semi-local short-range exchange (in the gKS scheme), cf. Sec. 3.2. However, the Fock integrals that need to be computed for an EXX or hybrid calculation, as well as the single-orbital Hartree integrals needed for SIC, make these DFAs too costly for most systems of relevant

size. Therefore, it would be beneficial to find a second or third-rung DFA, i. e., a GGA or meta-GGA, that can mimic the features of EXX to an extent that would allow for a similarly accurate prediction of CT.

Such a DFA would then have to emulate both the EXX GS potential in order to yield more physical orbital energies, and the response properties of the EXX TD potential that give rise to the kernel corrections discussed above. Solving these two problems with a *single* GGA or meta-GGA, while desirable at least from a formal point of view, would be extremely hard if not impossible. Fortunately, as LR methods such as the Sternheimer scheme allow to approximate the GS potential and the kernel (or potential response amplitude  $v_{xc\sigma}^{(+)}(\mathbf{r})$ ) separately, the two issues can be treated independently, at least as a first step towards a possible future combined solution. Therefore, in this thesis, the response properties of two recently developed DFAs for exchange are studied that were both designed to reproduce EXX properties on two different levels: The Armiento-Kümmel GGA (AK13) [AK13] and the TASK meta-GGA [AK19].

The AK13 construction is inspired by properties of the BJ model and features step structures and mimics discontinuities similar to exact exchange. The fact that it has also been found to diverge on nodal planes of the HOMO [AAK17b, AAK17a] might be beneficial in light of the requirements of the kernel discussed above, i. e., to counteract vanishing orbital overlap, but it hinders the application of AK13 in GS calculations severely. This is not necessarily a problem as within the Sternheimer approach, one can easily apply AK13 only to compute  $v_{xc\sigma}^{(+)}(\mathbf{r})$  and use some “unproblematic” DFA in the GS calculation. Publication 2, therefore, studies, both through numerical calculations and analytical considerations, the behavior of the AK13 potential response in combination with the LDA GS, and compares it with the response of LDA, PBE, and Becke’s B88 GGA [Bec88]. It turns out that while the AK13 response differs strongly and qualitatively from usual GGAs that are incapable of describing CT correctly, strong divergences and instabilities in its asymptotic region prevent it from being used in TDDFT.

The obvious next step then is to use meta-GGAs, as their inherent nonlocality (cf. Sec. 3.1) makes them natural candidates to reproduce EXX features. While the construction of many common meta-GGAs is close in spirit to typical GGAs and, e. g., the SCAN [SRP15] meta-GGA does not improve the prediction of CT significantly [TP18], TASK was specifically constructed with a focus on pronounced nonlocality and EXX-like response properties [AK19]. It has already been shown to demonstrate field-counteracting behavior in hydrogen chains similar to EXX, and to improve qualitatively the description of static response properties (polarizabilities). The remaining question is whether these promising *static* response properties of TASK transfer to TD LR calculations. The application of meta-GGAs in LR calculations is not trivial (cf. Secs. 3.3-3.5), but with the method presented in Pub. 3, KS calculations with meta-GGAs using the KLI approximation to the TDOEP are possible within the Sternheimer scheme. Publication 4 uses this method to study the TD response properties of the TASK functional.

The capability of EXX to yield a qualitatively correct description of CT within the KS scheme has been shown for the exact TDOEP (with, without, or with a partial adiabatic approximation) [HIG09, IHG10, HG11], but not yet for the KLI approximation to the TDOEP, and RSHs are usually employed in the gKS scheme. Therefore, Pub. 4 actually has to answer two questions:

Does TASK perform qualitatively similar to EXX in TD LR calculations within the KLI approximation, and can KLI itself capture the properties of the TDOEP that are relevant for CT?

To answer these questions, [Pub. 4](#) first studies the photoabsorption spectra of several representative systems and compares TASK results to EXX and other functionals, including LDA, PBE and another meta-GGA (PoC [[AK19](#)]), and then computes the energetically lowest CT excitation energy in a donor-acceptor-donor system (*N,N*-diisopropyl-2,6-di(thiophen-2-yl) naphthalene-1,4,5,8-tetracarboxylic acid diimide [[KSBK11](#)] (NDI-1)).

The results suggest a positive answer to the first question: TASK-KLI, e. g., reproduces the EXX-KLI spectrum of H<sub>8</sub> almost perfectly, and its result for the CT energy is also close to the EXX-KLI prediction (closer than with all other approximations studied in [Pub. 4](#) or in Ref. [[KSBK11](#)]). However, both the TASK-KLI and the EXX-KLI calculation seriously underestimate the CT energy as found from tuned RSH calculations or in the experiment [[KSBK11](#)] by more than 0.7 eV. The underestimation is larger than for the global hybrid B3LYP [[KSBK11](#)], and, as also found in [Pub. 4](#), EXX in the gKS scheme (i. e., Hartree-Fock) actually even overestimates the CT energy. At least for EXX, excitation energies calculated in the KS and gKS scheme are expected and have been found to be qualitatively similar as long as the KS calculation is done on the TDOEP level [[HIGB02](#), [HIG09](#), [IHG10](#), [HG11](#)]. The huge discrepancy between EXX-KLI and Hartree-Fock results and the drastic underestimation of the CT energy is therefore suspected to be a failure of the KLI approximation. This suspicion is further corroborated by the finding that the orbital energy contribution to the CT energy, i. e., the gap  $\epsilon_H - \epsilon_L$ , is already roughly 0.4 eV larger in a EXX-OEP than in a EXX-KLI GS calculation.

This indicates a negative answer to the second question and stresses the importance of either extending the approach discussed in [Sec. 5.3](#) to a full TDOEP scheme, or answering the open questions regarding the gKS realization of meta-GGAs (cf. [Sec. 3.5](#)).

## 5.5 The Sternheimer Scheme as a Functional Analysis Tool

Another appealing feature of the Sternheimer approach is that its combination of certain properties of the Casida and the RT method makes it an excellent tool for the analysis of, e. g., different DFAs:

Similar to the Casida approach <sup>3</sup>, in the Sternheimer scheme it is straightforward to treat and approximate GS and LR properties independently through the potential  $v_{xc\sigma}(\mathbf{r})$  used in the GS calculation and the response amplitude  $v_{xc\sigma}^{(+)}(\mathbf{r})$  employed in the subsequent LR calculation. In RT methods, this is technically possible as well [[MCR01](#)] but far less trivial since they work with a single TD potential. At the same time, just like the RT approach, the Sternheimer scheme works with a local potential  $v_{xc\sigma}^{(+)}(\mathbf{r})$  that is intuitively accessible and easy to plot and to analyze, unlike the kernel (depending on two coordinates) or the coupling matrix that the Casida scheme relies upon. [Publications 1-4](#) all make use of these properties in different ways:

<sup>3</sup>Note that common quantum chemistry codes not necessarily allow using different DFAs for the GS potential and the kernel in Casida calculations, although this should in principle be unproblematic.

**Publication 1** analyzes the relevant xc features for a qualitatively correct description of the SiH<sub>4</sub> spectrum, which has been argued to be strongly affected by excitonic effects [RL98, RL00, TC06]. By treating the GS with a SIC scheme based on complex, energy-minimizing unitary transformations, yet merely using the adiabatic LDA for the construction of  $v_{xc\sigma}^{(+)}(\mathbf{r})$ , the GS potential and its corresponding GS orbital energies are found to be the decisive factor.

In **Pub. 2**, the separation of GS and LR approximations is what makes it possible to study the response properties of AK13 without having to perform GS calculations with it. These properties are then studied by plotting the response potential  $v_{xc\sigma}^{(+)}(\mathbf{r})$  in various situations, and by comparing, e. g., its asymptotic behavior with that of other DFAs.

**Publication 3** first relies on the visualization of  $v_{xc\sigma}^{(+)}(\mathbf{r})$  in the static limit to cross-check it against finite-field GS potential differences and to reveal the field-counteracting behavior. Then, in order to prove that the good agreement between these finite-field and LR results, or between the LR and RT spectra of SiH<sub>4</sub>, are actually a result of the correct construction of the KLI (or CEDA)  $v_{xc\sigma}^{(+)}(\mathbf{r})$ , and not merely a result of the correct KLI (or CEDA) GS density and orbitals that are inserted into the expression for  $v_{xc\sigma}^{(+)}(\mathbf{r})$ , additional calculations are performed that combine the LDA GS with the KLI (or CEDA) response, and vice versa.

Finally, after again resorting to the visualization of  $v_{xc\sigma}^{(+)}(\mathbf{r})$  in the static limit for the validation of the meta-GGA  $v_{xc\sigma}^{(+)}(\mathbf{r})$ , **Pub. 4** combines the PoC GS with the adiabatic LDA response to illuminate the origin of a pronounced blueshift (with respect to LDA, EXX, and TASK) of the two energetically lowest excitations in the PoC spectrum for H<sub>8</sub>.

# List of Abbreviations

<b>AK13</b>	Armiento-Kümmel GGA [AK13] . . . . .	4, 32
<b>BiCGstab</b>	stabilized biconjugate gradient algorithm for solving linear equations with large, sparse, non-symmetric matrices . . . . .	27
<b>BJ</b>	Becke-Johnson potential [BJ06] . . . . .	21
<b>CEDA</b>	common energy denominator approximation to the OEP, also known as localized Hartree-Fock (LHF) [GB01, DG01] . . . . .	16
<b>CG</b>	conjugate gradient algorithm for solving linear equations with large, sparse, hermitian matrices . . . . .	27
<b>CGsymm</b>	algorithm for solving linear equations with large, sparse, complex, symmetric matrices . . . . .	27
<b>CT</b>	charge transfer, usually referring to excitations or excited states . . . . .	10
<b>DFA</b>	density functional approximation, typically to $E_{xc}[n]$ or $v_{xc\sigma}[n]$ . . . . .	6
<b>DFT</b>	density functional theory . . . . .	3
<b>EXX</b>	exact-exchange functional as defined in Eq. (2.4) . . . . .	6
<b>GGA</b>	class of semilocal xc functionals that is based on a generalized-gradient approximation [PW86] . . . . .	11
<b>gKS</b>	generalized Kohn-Sham scheme [SGV <sup>+</sup> 96, BK18] . . . . .	16
<b>GS</b>	ground state . . . . .	5
<b>HOMO</b>	energetically highest occupied KS or gKS orbital or eigenvalue . . . . .	17
<b>KLI</b>	approximation to the optimized effective potential equation proposed by Krieger, Li, and Iafrate [KLI92] . . . . .	15
<b>KS</b>	Kohn-Sham, usually referring to the KS scheme, orbitals, eigenvalues, potential, or equation [KS65] . . . . .	5

<b>LDA</b>	local-density approximation xc functional [HK64] . . . . .	11
<b>LR</b>	linear response . . . . .	7
<b>LUMO</b>	energetically lowest unoccupied KS or gKS orbital or eigenvalue . . . . .	17
<b>meta-GGA</b>	meta-generalized gradient approximation, a class of xc functionals that go beyond the GGA by inclusion of the kinetic energy density (or the Laplacian of the density) [DFC16] . . . . .	4
<b>NDI-1</b>	<i>N,N</i> -diisopropyl-2,6-di(thiophen-2-yl) naphthalene-1,4,5,8-tetracarboxylic acid diimide [KSBK11] . . . . .	33
<b>OEP</b>	optimized effective potential [SH53, TS76, SGP82, KK08] . . . . .	14
<b>PARSEC</b>	pseudopotential and real space grid based electronic structure program [KMT+06] in a locally modified version . . . . .	55
<b>PBE</b>	Perdew-Burke-Ernzerhof xc GGA [PBE96] . . . . .	11
<b>PoC</b>	“proof of concept” meta-GGA for exchange [AK19] . . . . .	31
<b>QMR</b>	quasi-minimal residual method, an algorithm for solving linear equations with large, sparse matrices . . . . .	27
<b>RSH</b>	range-separated hybrid functionals . . . . .	13
<b>RT</b>	real-time propagation method [YB96] . . . . .	19
<b>SIC</b>	self-interaction correction [PZ81] . . . . .	11
<b>Sla</b>	Slater or hole potential, defined as the orbital density-weighted average of the orbital-specific potentials [Sla51, SH53] . . . . .	30
<b>TASK</b>	meta-GGA for exchange by Aschebrock and Kümmel [AK19] . . . . .	4
<b>TD</b>	time dependent . . . . .	5
<b>TDDFT</b>	time-dependent density-functional theory . . . . .	3
<b>TDKS</b>	time-dependent Kohn-Sham, usually referring to the TDKS scheme, orbitals, potential, or equation [RG84] . . . . .	7
<b>TDOEP</b>	time-dependent OEP [UGG95, vL98] . . . . .	14
<b>xc</b>	exchange-correlation . . . . .	3

# Bibliography

- [AAK17a] T. Aschebrock, R. Armiento and S. Kümmel, *Challenges for semilocal density functionals with asymptotically nonvanishing potentials*, *Phys. Rev. B* **96**, 075140 (2017).
- [AAK17b] T. Aschebrock, R. Armiento and S. Kümmel, *Orbital nodal surfaces: Topological challenges for density functionals*, *Phys. Rev. B* **95**, 245118 (2017).
- [ABMR07] X. Andrade, S. Botti, M. A. L. Marques and A. Rubio, *Time-dependent density functional theory scheme for efficient calculations of dynamic (hyper)polarizabilities*, *J. Chem. Phys.* **126**, 184106 (2007).
- [AK13] R. Armiento and S. Kümmel, *Orbital Localization, Charge Transfer, and Band Gaps in Semilocal Density-Functional Theory*, *Phys. Rev. Lett.* **111**, 036402 (2013).
- [AK19] T. Aschebrock and S. Kümmel, *Ultranonlocality and accurate band gaps from a meta-generalized gradient approximation*, *Phys. Rev. Res.* **1**, 033082 (2019).
- [And65] D. G. Anderson, *Iterative Procedures for Nonlinear Integral Equations*, *J. ACM* **12**, 547–560 (1965).
- [ASD<sup>+</sup>15] X. Andrade, D. A. Strubbe, U. De Giovannini, A. H. Larsen, M. J. T. Oliveira, J. Alberdi-Rodriguez, A. Varas, I. Theophilou, N. Helbig, M. J. Verstraete, L. Stella, F. Nogueira, A. Aspuru-Guzik, A. Castro, M. A. L. Marques and A. Rubio, *Real-space grids and the Octopus code as tools for the development of new simulation approaches for electronic systems*, *Phys. Chem. Chem. Phys.* **17**, 31371–31396 (2015).
- [Bau97] D. Bauer, *Two-dimensional, two-electron model atom in a laser pulse: Exact treatment, single-active-electron analysis, time-dependent density-functional theory, classical calculations, and nonsequential ionization*, *Phys. Rev. A* **56**, 3028–3039 (1997).
- [BC01] D. Bauer and F. Ceccherini, *Time-dependent density functional theory applied to nonsequential multiple ionization of Ne at 800 nm*, *Opt. Express* **8**, 377–382 (2001).

- [BDDG01] S. Baroni, S. De Gironcoli, A. Dal Corso and P. Giannozzi, *Phonons and related crystal properties from density-functional perturbation theory*, *Rev. Mod. Phys.* **73**, 515–562 (2001).
- [Bec88] A. D. Becke, *Density-functional exchange-energy approximation with correct asymptotic behavior*, *Phys. Rev. A* **38**, 3098–3100 (1988).
- [Bec93a] A. D. Becke, *A new mixing of Hartree–Fock and local density-functional theories*, *J. Chem. Phys.* **98**, 1372–1377 (1993).
- [Bec93b] A. D. Becke, *Density-functional thermochemistry. III. The role of exact exchange*, *J. Chem. Phys.* **98**, 5648–5652 (1993).
- [BF12] J. E. Bates and F. Furche, *Harnessing the meta-generalized gradient approximation for time-dependent density functional theory*, *J. Chem. Phys.* **137**, 164105 (2012).
- [BG12] S. Botti and M. Gatti, *The Microscopic Description of a Macroscopic Experiment*, in *Fundamentals of Time-Dependent Density Functional Theory*, edited by M. A. Marques, N. T. Maitra, F. M. Nogueira, E. Gross and A. Rubio, volume 837 of *Lecture Notes in Physics*, pp. 29–50, Springer Berlin Heidelberg, 2012.
- [BGvM13] E. J. Baerends, O. V. Gritsenko and R. van Meer, *The Kohn-Sham gap, the fundamental gap and the optical gap: the physical meaning of occupied and virtual Kohn-Sham orbital energies*, *Phys. Chem. Chem. Phys.* **15**, 16408–16425 (2013).
- [BJ06] A. D. Becke and E. R. Johnson, *A simple effective potential for exchange*, *J. Chem. Phys.* **124**, 221101 (2006).
- [BK95] D. M. Bylander and L. Kleinman, *Energy Gaps and Cohesive Energy of Ge from the Optimized Effective Potential*, *Phys. Rev. Lett.* **74**, 3660–3663 (1995).
- [BK18] R. Baer and L. Kronik, *Time-dependent generalized Kohn–Sham theory*, *Eur. Phys. J. B* **91**, 170 (2018).
- [BLL16] A. Bruner, D. LaMaster and K. Lopata, *Accelerated Broadband Spectra Using Transition Dipole Decomposition and Padé Approximants*, *J. Chem. Theory Comput.* **12**, 3741–3750 (2016).
- [Bro65] C. Broyden, *A class of methods for solving nonlinear simultaneous equations*, *Math. Comp* **19**, 577–593 (1965).
- [BSOR06] F. Bruneval, F. Sottile, V. Olevano and L. Reining, *Beyond time-dependent exact exchange: The need for long-range correlation*, *J. Chem. Phys.* **124**, 144113 (2006).

- [CAO<sup>+</sup>06] A. Castro, H. Appel, M. J. T. Oliveira, C. A. Rozzi, X. Andrade, F. Lorenzen, M. A. L. Marques, E. K. U. Gross and A. Rubio, *octopus: a tool for the application of time-dependent density functional theory*, *Phys. status solidi* **243**, 2465–2488 (2006).
- [Cas95] M. E. Casida, *Time-Dependent Density Functional Response Theory for Molecules*, pp. 155–192, World Scientific, Singapore, 1995.
- [CJCS98] M. E. Casida, C. Jamorski, K. C. Casida and D. R. Salahub, *Molecular excitation energies to high-lying bound states from time-dependent density-functional response theory: Characterization and correction of the time-dependent local density approximation ionization threshold*, *J. Chem. Phys.* **108**, 4439–4449 (1998).
- [DAOR03] R. Del Sole, G. Adragna, V. Olevano and L. Reining, *Long-range behavior and frequency dependence of exchange-correlation kernels in solids*, *Phys. Rev. B* **67**, 045207 (2003).
- [DFC16] F. Della Sala, E. Fabiano and L. A. Constantin, *Kinetic-energy-density dependent semilocal exchange-correlation functionals*, *Int. J. Quantum Chem.* **116**, 1641–1694 (2016).
- [DG90] R. M. Dreizler and E. K. U. Gross, *Density Functional Theory: An Approach to the Quantum Many-Body Problem*, Springer Berlin Heidelberg, 1990.
- [DG01] F. Della Sala and A. Görling, *Efficient localized Hartree–Fock methods as effective exact-exchange Kohn–Sham methods for molecules*, *J. Chem. Phys.* **115**, 5718–5732 (2001).
- [DGS<sup>+</sup>16] M. Dauth, M. Graus, I. Schelter, M. Wießner, A. Schöll, F. Reinert and S. Kümmel, *Perpendicular Emission, Dichroism, and Energy Dependence in Angle-Resolved Photoemission: The Importance of The Final State*, *Phys. Rev. Lett.* **117**, 183001 (2016).
- [DHG04] A. Dreuw and M. Head-Gordon, *Failure of Time-Dependent Density Functional Theory for Long-Range Charge-Transfer Excited States: The Zinobacteriochlorin-Bacteriochlorin and Bacteriochlorophyll-Spheroidene Complexes*, *J. Am. Chem. Soc.* **126**, 4007–4016 (2004).
- [DK16] M. Dauth and S. Kümmel, *Predicting photoemission intensities and angular distributions with real-time density-functional theory*, *Phys. Rev. A* **93**, 022502 (2016).
- [DKK<sup>+</sup>11] M. Dauth, T. Körzdörfer, S. Kümmel, J. Ziroff, M. Wiessner, A. Schöll, F. Reinert, M. Arita and K. Shimada, *Orbital Density Reconstruction for Molecules*, *Phys. Rev. Lett.* **107**, 193002 (2011).

- [DMRS10] P. M. Dinh, J. Messud, P.-G. Reinhard and E. Suraud, *The self-interaction correction in the time domain*, *J. Phys.: Conf. Ser.* **248**, 012024 (2010).
- [DSG02] F. Della Sala and A. Görling, *The asymptotic region of the Kohn–Sham exchange potential in molecules*, *J. Chem. Phys.* **116**, 5374–5388 (2002).
- [DWC<sup>+</sup>17] G. Donati, A. Wildman, S. Caprasecca, D. B. Lingerfelt, F. Lipparini, B. Menucci and X. Li, *Coupling Real-Time Time-Dependent Density Functional Theory with Polarizable Force Field*, *J. Phys. Chem. Lett.* **8**, 5283–5289 (2017).
- [DWHG03] A. Dreuw, J. L. Weisman and M. Head-Gordon, *Long-range charge-transfer excited states in time-dependent density functional theory require non-local exchange*, *J. Chem. Phys.* **119**, 2943–2946 (2003).
- [ED11] E. Engel and R. M. Dreizler, *Density Functional Theory: An Advanced Course*, Theoretical and Mathematical Physics, Springer Berlin Heidelberg, Berlin, Heidelberg, 2011.
- [FLSM15] J. I. Fuks, K. Luo, E. D. Sandoval and N. T. Maitra, *Time-Resolved Spectroscopy in Time-Dependent Density Functional Theory: An Exact Condition*, *Phys. Rev. Lett.* **114**, 183002 (2015).
- [Fri07] T. L. Friedman, *The power of green*, *The New York Times* (2007).
- [GB01] O. V. Gritsenko and E. J. Baerends, *Orbital structure of the Kohn–Sham exchange potential and exchange kernel and the field-counteracting potential for molecules in an electric field*, *Phys. Rev. A* **64**, 042506 (2001).
- [GGB02] M. Grüning, O. V. Gritsenko and E. J. Baerends, *Exchange potential from the common energy denominator approximation for the Kohn–Sham Green’s function: Application to (hyper)polarizabilities of molecular chains*, *J. Chem. Phys.* **116**, 6435–6442 (2002).
- [GGG97] P. Ghosez, X. Gonze and R. W. Godby, *Long-wavelength behavior of the exchange-correlation kernel in the Kohn–Sham theory of periodic systems*, *Phys. Rev. B* **56**, 12811–12817 (1997).
- [GL93] A. Görling and M. Levy, *Correlation-energy functional and its high-density limit obtained from a coupling-constant perturbation expansion*, *Phys. Rev. B* **47**, 13105–13113 (1993).
- [GL94] A. Görling and M. Levy, *Exact Kohn–Sham scheme based on perturbation theory*, *Phys. Rev. A* **50**, 196–204 (1994).
- [GLL18] J. J. Goings, P. J. Lestrangle and X. Li, *Real-time time-dependent electronic structure theory*, *WIREs Comput. Mol. Sci.* **8**, e1341 (2018).

- [Gör97] A. Görling, *Time-dependent Kohn-Sham formalism*, *Phys. Rev. A* **55**, 2630–2639 (1997).
- [Gör98a] A. Görling, *Exact exchange-correlation kernel for dynamic response properties and excitation energies in density-functional theory*, *Phys. Rev. A* **57**, 3433–3436 (1998).
- [Gör98b] A. Görling, *Exact exchange kernel for time-dependent density-functional theory*, *Int. J. Quantum Chem.* **69**, 265–277 (1998).
- [Gör99] A. Görling, *New KS Method for Molecules Based on an Exchange Charge Density Generating the Exact Local KS Exchange Potential*, *Phys. Rev. Lett.* **83**, 5459–5462 (1999).
- [HG11] A. Heßelmann and A. Görling, *Efficient exact-exchange time-dependent density-functional theory methods and their relation to time-dependent Hartree–Fock*, *J. Chem. Phys.* **134**, 034120 (2011).
- [HG14a] H. Hübener and F. Giustino, *Linear optical response of finite systems using multishift linear system solvers*, *J. Chem. Phys.* **141**, 044117 (2014).
- [HG14b] H. Hübener and F. Giustino, *Time-dependent density functional theory using atomic orbitals and the self-consistent Sternheimer equation*, *Phys. Rev. B* **89**, 085129 (2014).
- [HHG99] S. Hirata and M. Head-Gordon, *Time-dependent density functional theory within the Tamm–Dancoff approximation*, *Chem. Phys. Lett.* **314**, 291–299 (1999).
- [HIBG05] S. Hirata, S. Ivanov, R. J. Bartlett and I. Grabowski, *Exact-exchange time-dependent density-functional theory for static and dynamic polarizabilities*, *Phys. Rev. A* **71**, 032507 (2005).
- [HIG09] A. Heßelmann, A. Ipatov and A. Görling, *Charge-transfer excitation energies with a time-dependent density-functional method suitable for orbital-dependent exchange-correlation kernels*, *Phys. Rev. A* **80**, 012507 (2009).
- [HIGB02] S. Hirata, S. Ivanov, I. Grabowski and R. J. Bartlett, *Time-dependent density functional theory employing optimized effective potentials*, *J. Chem. Phys.* **116**, 6468–6481 (2002).
- [Hir05] S. Hirata, *Time-dependent density-functional theory based on optimized effective potentials for van der Waals forces*, *J. Chem. Phys.* **123**, 026101 (2005).
- [HK64] P. Hohenberg and W. Kohn, *The Inhomogeneous Electron Gas*, *Phys. Rev.* **136**, B864–B871 (1964).

- [HK12a] D. Hofmann and S. Kümmel, *Integer particle preference during charge transfer in Kohn-Sham theory*, *Phys. Rev. B* **86**, 201109 (2012).
- [HK12b] D. Hofmann and S. Kümmel, *Self-interaction correction in a real-time Kohn-Sham scheme: Access to difficult excitations in time-dependent density functional theory*, *J. Chem. Phys.* **137**, 064117 (2012).
- [HKK12] D. Hofmann, T. Körzdörfer and S. Kümmel, *Kohn-Sham Self-Interaction Correction in Real Time*, *Phys. Rev. Lett.* **108**, 146401 (2012).
- [HKKK12] D. Hofmann, S. Klüpfel, P. Klüpfel and S. Kümmel, *Using complex degrees of freedom in the Kohn-Sham self-interaction correction*, *Phys. Rev. A* **85**, 062514 (2012).
- [HS52] M. Hestenes and E. Stiefel, *Methods of Conjugate Gradients for Solving Linear Systems*, *J. Res. Natl. Bur. Stand.* (1934). **49**, 409–436 (1952).
- [HvB08] M. Hellgren and U. von Barth, *Linear density response function within the time-dependent exact-exchange approximation*, *Phys. Rev. B* **78**, 115107 (2008).
- [HvB09] M. Hellgren and U. von Barth, *Exact-exchange kernel of time-dependent density functional theory: Frequency dependence and photoabsorption spectra of atoms*, *J. Chem. Phys.* **131**, 044110 (2009).
- [IHG10] A. Ipatov, A. Heßelmann and A. Görling, *Molecular excitation spectra by TDDFT with the nonadiabatic exact exchange kernel*, *Int. J. Quantum Chem.* **110**, 2202–2220 (2010).
- [IL09] C. M. Isborn and X. Li, *Singlet-triplet transitions in real-time time-dependent Hartree-Fock/density functional theory*, *J. Chem. Theory Comput.* **5**, 2415–2419 (2009).
- [Joh88] D. D. Johnson, *Modified Broydens method for accelerating convergence in self-consistent calculations*, *Phys. Rev. B* **38**, 12807–12813 (1988).
- [JSARM<sup>+</sup>15] J. Jornet-Somoza, J. Alberdi-Rodriguez, B. F. Milne, X. Andrade, M. A. L. Marques, F. Nogueira, M. J. T. Oliveira, J. J. P. Stewart and A. Rubio, *Insights into colour-tuning of chlorophyll optical response in green plants*, *Phys. Chem. Chem. Phys.* **17**, 26599–26606 (2015).
- [JSL19] J. Jornet-Somoza and I. Lebedeva, *Real-Time Propagation TDDFT and Density Analysis for Exciton Coupling Calculations in Large Systems*, *J. Chem. Theory Comput.* **15**, 3743–3754 (2019).

- [KAK13] A. Karolewski, R. Armiento and S. Kümmel, *Electronic excitations and the Becke-Johnson potential: The need for and the problem of transforming model potentials to functional derivatives*, *Phys. Rev. A* **88**, 052519 (2013).
- [KG02] Y.-H. Kim and A. Görling, *Excitonic Optical Spectrum of Semiconductors Obtained by Time-Dependent Density-Functional Theory with the Exact-Exchange Kernel*, *Phys. Rev. Lett.* **89**, 096402 (2002).
- [KK08] S. Kümmel and L. Kronik, *Orbital-dependent density functionals: Theory and applications*, *Rev. Mod. Phys.* **80**, 3–60 (2008).
- [KKM08] T. Körzdörfer, S. Kümmel and M. Mundt, *Self-interaction correction and the optimized effective potential*, *J. Chem. Phys.* **129**, 014110 (2008).
- [KKMK09] T. Körzdörfer, S. Kümmel, N. Marom and L. Kronik, *When to trust photoelectron spectra from Kohn-Sham eigenvalues: The case of organic semiconductors*, *Phys. Rev. B* **79**, 201205 (2009).
- [KKP04] S. Kümmel, L. Kronik and J. P. Perdew, *Electrical Response of Molecular Chains from Density Functional Theory*, *Phys. Rev. Lett.* **93**, 213002 (2004).
- [KLI92] J. B. Krieger, Y. Li and G. J. Iafrate, *Systematic approximations to the optimized effective potential: Application to orbital-density-functional theory*, *Phys. Rev. A* **46**, 5453–5458 (1992).
- [KMT<sup>+</sup>06] L. Kronik, A. Makmal, M. L. Tiago, M. M. G. Alemany, M. Jain, X. Huang, Y. Saad and J. R. Chelikowsky, *PARSEC - The pseudopotential algorithm for real-space electronic structure calculations: Recent advances and novel applications to nano-structures*, *Phys. Status Solidi Basic Res.* **243**, 1063–1079 (2006).
- [KP03a] S. Kümmel and J. P. Perdew, *Optimized effective potential made simple: Orbital functionals, orbital shifts, and the exact Kohn-Sham exchange potential*, *Phys. Rev. B* **68**, 035103 (2003).
- [KP03b] S. Kümmel and J. P. Perdew, *Simple Iterative Construction of the Optimized Effective Potential for Orbital Functionals, Including Exact Exchange*, *Phys. Rev. Lett.* **90**, 043004 (2003).
- [KS65] W. Kohn and L. J. Sham, *Self-consistent equations including exchange and correlation effects*, *Phys. Rev.* **140**, A1133–A1138 (1965).
- [KSBK11] A. Karolewski, T. Stein, R. Baer and S. Kümmel, *Communication: Tailoring the optical gap in light-harvesting molecules*, *J. Chem. Phys.* **134**, 151101 (2011).

- [KSG03] Y.-H. Kim, M. Städele and A. Görling, *Optical Excitations of Si by Time-Dependent Density Functional Theory Based on Exact-Exchange Kohn–Sham Band Structure*, *Int. J. Quantum Chem.* **91**, 257–262 (2003).
- [KSM99] Y.-H. Kim, M. Städele and R. M. Martin, *Density-functional Study of Small Molecules within the Krieger-Li-Iafrate Approximation*, *Phys. Rev. A* **60**, 3633–3640 (1999).
- [KSRAB12] L. Kronik, T. Stein, S. Refaely-Abramson and R. Baer, *Excitation Gaps of Finite-Sized Systems from Optimally Tuned Range-Separated Hybrid Functionals*, *J. Chem. Theo. Comput.* **8**, 1515–1531 (2012).
- [Küm17] S. Kümmel, *Charge-Transfer Excitations: A Challenge for Time-Dependent Density Functional Theory That Has Been Met*, *Adv. Energy Mater.* **1700440**, 1700440 (2017).
- [LFM16] K. Luo, J. I. Fuks and N. T. Maitra, *Studies of spuriously shifting resonances in time-dependent density functional theory*, *J. Chem. Phys.* **145**, 044101 (2016).
- [LG11] K. Lopata and N. Govind, *Modeling Fast Electron Dynamics with Real-Time Time-Dependent Density Functional Theory: Application to Small Molecules and Chromophores*, *J. Chem. Theory Comput.* **7**, 1344–1355 (2011).
- [LHRC17] S.-L. Liao, T.-S. Ho, H. Rabitz and S.-I. Chu, *Time-Local Equation for the Exact Optimized Effective Potential in Time-Dependent Density Functional Theory*, *Phys. Rev. Lett.* **118**, 243001 (2017).
- [LHRC18] S.-L. Liao, T.-S. Ho, H. Rabitz and S.-I. Chu, *Exact-exchange optimized effective potential and memory effect in time-dependent density functional theory*, *Eur. Phys. J. B* **91**, 147 (2018).
- [LK05] M. Lein and S. Kümmel, *Exact Time-Dependent Exchange-Correlation Potentials for Strong-Field Electron Dynamics*, *Phys. Rev. Lett.* **94**, 143003 (2005).
- [LP85] M. Levy and J. P. Perdew, *Hellmann-Feynman, virial, and scaling requisites for the exact universal density functionals. Shape of the correlation potential and diamagnetic susceptibility for atoms*, *Phys. Rev. A* **32**, 2010–2021 (1985).
- [LSWS97] T. Leininger, H. Stoll, H.-J. Werner and A. Savin, *Combining long-range configuration interaction with short-range density functionals*, *Chem. Phys. Lett.* **275**, 151 – 160 (1997).
- [LvL98] D. G. Lappas and R. van Leeuwen, *Electron correlation effects in the double ionization of He*, *J. Phys. B* **31**, L249–L256 (1998).

- [Mai05] N. T. Maitra, *Undoing static correlation: Long-range charge transfer in time-dependent density-functional theory*, *J. Chem. Phys.* **122**, 234104 (2005).
- [MCR01] M. A. L. Marques, A. Castro and A. Rubio, *Assessment of exchange-correlation functionals for the calculation of dynamical properties of small clusters in time-dependent density functional theory*, *J. Chem. Phys.* **115**, 3006–3014 (2001).
- [MDRS09] J. Messud, P. M. Dinh, P.-G. Reinhard and E. Suraud, *Simplification of the time-dependent generalized self-interaction correction method using two sets of orbitals: Application of the optimized effective potential formalism*, *Phys. Rev. A* **80**, 044503 (2009).
- [MDRS11] J. Messud, P. M. Dinh, P.-G. Reinhard and E. Suraud, *The generalized SIC-OEP formalism and the generalized SIC-Slater approximation (stationary and time-dependent cases)*, *Ann. Phys.* **523**, 270–290 (2011).
- [MK06] M. Mundt and S. Kümmel, *Optimized effective potential in real time: Problems and prospects in time-dependent density-functional theory*, *Phys. Rev. A* **74**, 022511 (2006).
- [MKvLR07] M. Mundt, S. Kümmel, R. van Leeuwen and P.-G. Reinhard, *Violation of the zero-force theorem in the time-dependent Krieger-Li-Iafrate approximation*, *Phys. Rev. A* **75**, 050501 (2007).
- [MMN<sup>+</sup>12] M. A. L. Marques, N. T. Maitra, F. Nogueira, E. K. U. Gross and A. Rubio, *Fundamentals of Time-Dependent Density Functional Theory*, volume 837 of *Lecture Notes in Physics*, Springer Berlin Heidelberg, 2012.
- [MZCB04] N. T. Maitra, F. Zhang, R. J. Cave and K. Burke, *Double excitations within time-dependent density functional theory linear response*, *J. Chem. Phys.* **120**, 5932–5937 (2004).
- [Naz13] V. U. Nazarov, *Time-dependent effective potential and exchange kernel of homogeneous electron gas*, *Phys. Rev. B* **87**, 165125 (2013).
- [NV11] V. U. Nazarov and G. Vignale, *Optics of semiconductors from meta-generalized-gradient-approximation-based time-dependent density-functional theory*, *Phys. Rev. Lett.* **107**, 216402 (2011).
- [OCMR08] M. J. T. Oliveira, A. Castro, M. A. L. Marques and A. Rubio, *On the Use of Neumann’s Principle for the Calculation of the Polarizability Tensor of Nanostructures*, *J. Nanosci. Nanotechnol.* **8**, 3392–3398 (2008).
- [PBE96] J. P. Perdew, K. Burke and M. Ernzerhof, *Generalized Gradient Approximation Made Simple*, *Phys. Rev. Lett.* **77**, 3865–3868 (1996).

- [PEB96] J. P. Perdew, M. Ernzerhof and K. Burke, *Rationale for mixing exact exchange with density functional approximations*, *J. Chem. Phys.* **105**, 9982–9985 (1996).
- [PG99] M. Petersilka and E. K. U. Gross, *Strong-field double ionization of helium: A density-functional perspective*, *Laser Phys.* **9**, 105 (1999).
- [PGG96] M. Petersilka, U. J. Gossmann and E. K. U. Gross, *Excitation Energies from Time-Dependent Density-Functional Theory*, *Phys. Rev. Lett.* **76**, 1212–1215 (1996).
- [PHL84] M. R. Pederson, R. A. Heaton and C. C. Lin, *Local-density Hartree–Fock theory of electronic states of molecules with self-interaction correction*, *J. Chem. Phys.* **80**, 1972–1975 (1984).
- [PHS+06] M. J. G. Peach, T. Helgaker, P. Sałek, T. W. Keal, O. B. Lutnæs, D. J. Tozer and N. C. Handy, *Assessment of a Coulomb-attenuated exchange–correlation energy functional*, *Phys. Chem. Chem. Phys.* **8**, 558–562 (2006).
- [PI16] M. R. Provorse and C. M. Isborn, *Electron dynamics with real-time time-dependent density functional theory*, *Int. J. Quantum Chem.* **116**, 739–749 (2016).
- [PK03] J. P. Perdew and S. Kurth, *Density Functionals for Non-relativistic Coulomb Systems in the New Century*, in *A Primer in Density Functional Theory*, edited by C. Fiolhais, F. Nogueira and M. A. Marques, volume 620 of *Lecture Notes in Physics*, pp. 1–55, Springer, 2003.
- [PS01] J. P. Perdew and K. Schmidt, *Jacob’s ladder of density functional approximations for the exchange–correlation energy*, *AIP Conf. Proc.* **577**, 1–20 (2001).
- [PSTS08] J. P. Perdew, V. N. Staroverov, J. M. Tao and G. E. Scuseria, *Density functional with full exact exchange, balanced nonlocality of correlation, and constraint satisfaction*, *Phys. Rev. A* **78**, 052513 (2008).
- [PTVF07] W. H. Press, S. A. Teukolsky, W. T. Vetterling and B. P. Flannery, *Numerical Recipes: The Art of Scientific Computing*, Cambridge University Press, 3 edition, 2007.
- [PW86] J. P. Perdew and Y. Wang, *Accurate and simple density functional for the electronic exchange energy: Generalized gradient approximation*, *Phys. Rev. B* **33**, 8800–8802 (1986).

- [PY89] R. G. Parr and W. Yang, *Density-Functional Theory of Atoms and Molecules*, volume 16 of *International Series of Monographs on Chemistry*, Oxford University Press, New York, 1st edition, 1989.
- [PZ81] J. P. Perdew and A. Zunger, *Self-interaction correction to density-functional approximations for many-electron systems*, *Phys. Rev. B* **23**, 5048–5079 (1981).
- [RG84] E. Runge and E. K. U. Gross, *Density-functional theory for time-dependent systems*, *Phys. Rev. Lett.* **52**, 997–1000 (1984).
- [RKP<sup>+</sup>17] T. P. Rossi, M. Kuisma, M. J. Puska, R. M. Nieminen and P. Erhart, *Kohn–Sham Decomposition in Real-Time Time-Dependent Density-Functional Theory: An Efficient Tool for Analyzing Plasmonic Excitations*, *J. Chem. Theory Comput.* **13**, 4779–4790 (2017).
- [RL98] M. Rohlfing and S. G. Louie, *Excitonic Effects and the Optical Absorption Spectrum of Hydrogenated Si Clusters*, *Phys. Rev. Lett.* **80**, 3320–3323 (1998).
- [RL00] M. Rohlfing and S. G. Louie, *Electron-hole excitations and optical spectra from first principles*, *Phys. Rev. B* **62**, 4927–4944 (2000).
- [RORO02] L. Reining, V. Olevano, A. Rubio and G. Onida, *Excitonic Effects in Solids Described by Time-Dependent Density-Functional Theory*, *Phys. Rev. Lett.* **88**, 066404 (2002).
- [Sch16] I. Schelter, *Excitation dynamics in molecular systems from efficient grid-based real-time density functional theory*, Doctoral thesis, University of Bayreuth, 2016.
- [SDCF94] P. J. Stephens, F. J. Devlin, C. F. Chabalowski and M. J. Frisch, *Ab Initio Calculation of Vibrational Absorption and Circular Dichroism Spectra Using Density Functional Force Fields*, *J. Phys. Chem.* **98**, 11623–11627 (1994).
- [SFG<sup>+</sup>19] I. Schelter, J. M. Foerster, A. T. Gardiner, A. W. Roszak, R. J. Cogdell, G. M. Ullmann, T. B. de Queiroz and S. Kümmel, *Assessing density functional theory in real-time and real-space as a tool for studying bacteriochlorophylls and the light-harvesting complex 2*, *J. Chem. Phys.* **151**, 134114 (2019).
- [SGP82] V. Sahni, J. Gruenebaum and J. P. Perdew, *Study of the density-gradient expansion for the exchange energy*, *Phys. Rev. B* **26**, 4371–4377 (1982).
- [SGV<sup>+</sup>96] A. Seidl, A. Görling, P. Vogl, J. A. Majewski and M. Levy, *Generalized Kohn-Sham schemes and the band-gap problem*, *Phys. Rev. B* **53**, 3764–3774 (1996).

- [SH53] R. T. Sharp and G. K. Horton, *A Variational Approach to the Unipotential Many-Electron Problem*, *Phys. Rev.* **90**, 317 (1953).
- [SHH06] Y. Shigeta, K. Hirao and S. Hirata, *Exact-exchange time-dependent density-functional theory with the frequency-dependent kernel*, *Phys. Rev. A* **73**, 010502 (2006).
- [SK18] I. Schelter and S. Kümmel, *Accurate Evaluation of Real-Time Density Functional Theory Providing Access to Challenging Electron Dynamics*, *J. Chem. Theory Comput.* **14**, 1910–1927 (2018).
- [SKB09a] T. Stein, L. Kronik and R. Baer, *Prediction of charge-transfer excitations in coumarin-based dyes using a range-separated functional tuned from first principles*, *J. Chem. Phys.* **131**, 244119 (2009).
- [SKB09b] T. Stein, L. Kronik and R. Baer, *Reliable Prediction of Charge Transfer Excitations in Molecular Complexes Using Time-Dependent Density Functional Theory*, *J. Am. Chem. Soc.* **131**, 2818–2820 (2009).
- [SKM<sup>+</sup>14] T. Schmidt, E. Kraisler, A. Makmal, L. Kronik and S. Kümmel, *A self-interaction-free local hybrid functional: Accurate binding energies vis-à-vis accurate ionization potentials from Kohn-Sham eigenvalues*, *J. Chem. Phys.* **140**, 18A510 (2014).
- [Sla51] J. C. Slater, *A Simplification of the Hartree-Fock Method*, *Phys. Rev.* **81**, 385–390 (1951).
- [SLR<sup>+</sup>12] D. A. Strubbe, L. Lehtovaara, A. Rubio, M. A. L. Marques and S. G. Louie, *Response Functions in TDDFT: Concepts and Implementation*, in *Fundamentals of Time-Dependent Density Functional Theory*, edited by M. A. Marques, N. T. Maitra, F. M. Nogueira, E. Gross and A. Rubio, volume 837 of *Lecture Notes in Physics*, pp. 139–166, Springer Berlin Heidelberg, 2012.
- [SMVG97] M. Städele, J. A. Majewski, P. Vogl and A. Görling, *Exact Kohn-Sham Exchange Potential in Semiconductors*, *Phys. Rev. Lett.* **79**, 2089–2092 (1997).
- [SRGGLL<sup>+</sup>18] R. Sinha-Roy, P. García-González, X. López Lozano, R. L. Whetten and H.-C. Weissker, *Identifying Electronic Modes by Fourier Transform from  $\delta$ -Kick Time-Evolution TDDFT Calculations*, *J. Chem. Theory Comput.* **14**, 6417–6426 (2018).
- [SRP15] J. Sun, A. Ruzsinszky and J. P. Perdew, *Strongly Constrained and Appropriately Normed Semilocal Density Functional*, *Phys. Rev. Lett.* **115**, 036402 (2015).

- [SSTP03] V. N. Staroverov, G. E. Scuseria, J. Tao and J. P. Perdew, *Comparative assessment of a new nonempirical density functional: Molecules and hydrogen-bonded complexes*, *J. Chem. Phys.* **119**, 12129–12137 (2003).
- [Ste51] R. M. Sternheimer, *On Nuclear Quadrupole Moments*, *Phys. Rev.* **84**, 244–253 (1951).
- [Tao05] J. Tao, *Explicit inclusion of paramagnetic current density in the exchange-correlation functionals of current-density functional theory*, *Phys. Rev. B* **71**, 205107 (2005).
- [TB09] F. Tran and P. Blaha, *Accurate Band Gaps of Semiconductors and Insulators with a Semilocal Exchange–Correlation Potential*, *Phys. Rev. Lett.* **102**, 226401 (2009).
- [TC06] M. L. Tiago and J. R. Chelikowsky, *Optical excitations in organic molecules, clusters, and defects studied by first-principles Green’s function methods*, *Phys. Rev. B* **73**, 205334 (2006).
- [TH98] D. J. Tozer and N. C. Handy, *Improving virtual Kohn–Sham orbitals and eigenvalues: Application to excitation energies and static polarizabilities*, *J. Chem. Phys.* **109**, 10180–10189 (1998).
- [TK14] M. Thiele and S. Kümmel, *Frequency Dependence of the Exact Exchange–Correlation Kernel of Time-Dependent Density-Functional Theory*, *Phys. Rev. Lett.* **112**, 083001 (2014).
- [Toz03] D. J. Tozer, *Relationship between long-range charge-transfer excitation energy error and integer discontinuity in Kohn–Sham theory*, *J. Chem. Phys.* **119**, 12697–12699 (2003).
- [TP18] D. J. Tozer and M. J. G. Peach, *Molecular excited states from the SCAN functional*, *Mol. Phys.* **116**, 1504–1511 (2018).
- [TS76] J. D. Talman and W. F. Shadwick, *Optimized effective atomic central potential*, *Phys. Rev. A* **14**, 36–40 (1976).
- [UGG95] C. A. Ullrich, U. J. Gossmann and E. K. U. Gross, *Time-Dependent Optimized Effective Potential*, *Phys. Rev. Lett.* **74**, 872–875 (1995).
- [vBDvLS05] U. von Barth, N. E. Dahlen, R. van Leeuwen and G. Stefanucci, *Conserving approximations in time-dependent density functional theory*, *Phys. Rev. B* **72**, 235109 (2005).
- [vGSG<sup>+</sup>99] S. J. A. van Gisbergen, P. R. T. Schipper, O. V. Gritsenko, E. J. Baerends, J. G. Snijders, B. Champagne and B. Kirtman, *Electric Field Dependence of the*

- Exchange-Correlation Potential in Molecular Chains*, *Phys. Rev. Lett.* **83**, 694–697 (1999).
- [Vig95] G. Vignale, *Center of Mass and Relative Motion in Time Dependent Density Functional Theory*, *Phys. Rev. Lett.* **74**, 3233–3236 (1995).
- [vL98] R. van Leeuwen, *Causality and Symmetry in Time-Dependent Density-Functional Theory*, *Phys. Rev. Lett.* **80**, 1280–1283 (1998).
- [vL99] R. van Leeuwen, *Mapping from Densities to Potentials in Time-Dependent Density-Functional Theory*, *Phys. Rev. Lett.* **82**, 3863–3866 (1999).
- [vL01] R. van Leeuwen, *Key Concepts in Time-Dependent Density-Functional Theory*, *Int. J. Mod. Phys. B* **15**, 1969 (2001).
- [WU05] H. O. Wijewardane and C. A. Ullrich, *Time-Dependent Kohn-Sham Theory with Memory*, *Phys. Rev. Lett.* **95**, 086401 (2005).
- [WU08] H. O. Wijewardane and C. A. Ullrich, *Real-Time Electron Dynamics with Exact-Exchange Time-Dependent Density-Functional Theory*, *Phys. Rev. Lett.* **100**, 056404 (2008).
- [YB96] K. Yabana and G. F. Bertsch, *Time-dependent local-density approximation in real time*, *Phys. Rev. B* **54**, 4484–4487 (1996).
- [YTH04] T. Yanai, D. P. Tew and N. C. Handy, *A new hybrid exchange–correlation functional using the Coulomb-attenuating method (CAM-B3LYP)*, *Chem. Phys. Lett.* **393**, 51 – 57 (2004).
- [ZH18] Y. Zhu and J. M. Herbert, *Self-consistent predictor/corrector algorithms for stable and efficient integration of the time-dependent Kohn-Sham equation*, *J. Chem. Phys.* **148**, 044117 (2018).

# List of Publications

- Pub. 1**      *Linear response time-dependent density functional theory without unoccupied states: The Kohn-Sham-Sternheimer scheme revisited,*  
Fabian Hofmann, Ingo Schelter, Stephan Kümmel,  
[The Journal of Chemical Physics](#) **149**, 024105 (2018).
- Pub. 2**      *On the challenge to improve the density response with unusual gradient approximations,*  
Julian Garhammer, Fabian Hofmann, Rickard Armiento, Stephan Kümmel,  
[The European Physical Journal B](#) **91**, 159 (2018).
- Pub. 3**      *Efficiently evaluating the Krieger-Li-Iafrate and common-energy-denominator approximations in the frequency-dependent Sternheimer scheme,*  
Fabian Hofmann, Ingo Schelter, Stephan Kümmel,  
[Physical Review A](#) **99**, 022507 (2019).
- Pub. 4**      *Molecular excitations from meta-generalized gradient approximations in the Kohn-Sham scheme,*  
Fabian Hofmann and Stephan Kümmel,  
[The Journal of Chemical Physics](#) **153**, 114106 (2020).



# **Part II**

---

## **Publications**



# Publication 1

Publ. 1

## **Linear response time-dependent density functional theory without unoccupied states: The Kohn-Sham-Sternheimer scheme revisited**

reprinted from  
*The Journal of Chemical Physics* **149**, 024105 (2018),  
with the permission of AIP Publishing.

Fabian Hofmann, Ingo Schelter, Stephan Kümmel

Theoretical Physics IV, University of Bayreuth, 95440 Bayreuth, Germany

---

### **My contribution**

I developed the new derivation of the Sternheimer scheme and its extension to triplet excitations, as well as the symmetry and Lorentzian fit based evaluation techniques. I implemented the relevant routines in PARSEC [KMT<sup>+</sup>06], performed all calculations, prepared all figures, and wrote the first draft of the manuscript.

Publ. 1

# Linear response time-dependent density functional theory without unoccupied states: The Kohn-Sham-Sternheimer scheme revisited

Fabian Hofmann, Ingo Schelter, and Stephan Kümmel

*Theoretical Physics IV, University of Bayreuth, D-95440 Bayreuth, Germany*

(Received 23 March 2018; accepted 20 June 2018; published online 12 July 2018)

The Sternheimer approach to time-dependent density functional theory in the linear response regime is attractive because of its computational efficiency. The latter results from avoiding the explicit calculation of unoccupied orbitals and from the basic structure of the Sternheimer equations, which naturally lend themselves to far-reaching parallelization. In this article, we take a fresh look at the frequency-dependent Sternheimer equations. We first give a complete, self-contained derivation of the equations that complements previous derivations. We then discuss several aspects of an efficient numerical realization. As a worked example, we compute the photoabsorption spectra of small hydrogenated silicon clusters and confirm that for these the quality of the Kohn-Sham eigenvalues is more important than the effects of the exchange-correlation kernel. Finally, we demonstrate how triplet excitations can readily be computed from the Sternheimer approach. *Published by AIP Publishing.*  
<https://doi.org/10.1063/1.5030652>

## I. INTRODUCTION

Time-dependent density functional theory (TDDFT) has become one of the most frequently used approaches for studying excitations of molecules, nanoparticles, and, to some extent, solids. Of particular relevance is the linear response to an external perturbation because it is very frequently used to probe a system's states and electronic structure. Correspondingly, linear response TDDFT has found widespread use. While there is some interest in linear response TDDFT from the fundamental perspective of getting insight into the properties of density functionals,<sup>1–10</sup> the main motivation for the development of TDDFT linear response programs has been the countless applications of TDDFT in physics and chemistry, in which linear response properties are calculated in order to understand and interpret experiments and properties of real-world systems. There is such an extensive body of literature on applications of TDDFT that it is impossible to cite it comprehensively, but the reviews<sup>11–13</sup> provide some overview.

Given the great interest in linear response TDDFT, it does not come as a surprise that it has also been developed to a high degree of maturity on the technical side. In molecular and quantum chemistry applications, the Casida approach<sup>14</sup> has become almost the standard method. It rests on expanding the many-electron excitations in a particle-hole basis. A very different approach is to solve the time-dependent (TD) Kohn-Sham equations in real time,<sup>15–23</sup> i.e., without explicit linearization but with a TD potential that is small enough to be in the linear regime. Both approaches have their advantages and drawbacks. The Casida approach can achieve great efficiency in combination with Gaussian orbital basis sets for moderately sized systems. As excitation energies and oscillator strengths are obtained from the eigenvalues and eigenvectors of a response matrix, it yields information on all transitions, irrespective of whether they

are dark or not. The real-time approach does not offer this advantage in the same way: it typically evaluates the time-dependent dipole moment via a Fourier transform to frequency space, and thus, detecting excitations that carry very little oscillator strength is either impossible or requires special measures.<sup>23,24</sup> One of the major advantages of the real-time approach on the other hand is that it scales favorably with the system size as it involves only occupied orbitals, whereas the Casida approach requires both occupied and unoccupied states. In particular, for larger systems and basis sets, this leads to a rapid escalation of the computational effort in the Casida approach. As the Casida response equations lead to dense matrices, it is non-trivial to compensate for this increasing computational burden by parallelizing Casida computer codes.

There is, however, yet another successful approach to the linear response problem that can combine the strengths of the previously mentioned methods—the Sternheimer equation.<sup>25</sup> The Sternheimer approach has already been used for a long time in the context of density functional perturbation theory,<sup>26</sup> e.g., for calculating phonon spectra. More recently, the Sternheimer equation<sup>27–33</sup> and similar schemes<sup>34</sup> have also been used to compute the frequency-dependent electronic response. In this work, we take a new look specifically at the frequency-dependent Sternheimer equations as pioneered in Ref. 29. Given the above-mentioned wealth of TDDFT methods that already exist, one may wonder whether this is a worthwhile task. However, it certainly is for several reasons: First, in view of the changes in computer hardware development that occurred in recent years, with limiting increases in CPU speeds, whereas parallel architectures are on the advance, larger systems can especially be approached with techniques that parallelize well. The frequency-dependent Sternheimer equation parallelizes naturally as the responses at different frequencies can be computed independently of each other. Second, just as in real-time propagation, the spectrum of

unoccupied orbitals does not need to be computed explicitly. This turns into a major advantage for systems that are large or have a dense spectrum of states. And third, the Sternheimer approach lends itself naturally to applications using real-space grids, which again is advantageous from a parallelization perspective, as grids typically lead to computational steps that involve large but sparse matrices that one usually does not even have to store explicitly.<sup>17,35</sup>

While these conceptual benefits motivate revisiting the frequency-dependent Sternheimer equations, our work here is not about large-scale computational applications, but it is aimed at providing additional insight into the frequency-dependent Sternheimer approach, which will benefit future applications.

To this end, our paper is organized as follows: We first present in Sec. II and the corresponding Appendixes A–C a derivation of the frequency-dependent Sternheimer equation that to some extent differs from previous derivations and complements them. In this course, we extend the scheme to spin-dependent external potentials and investigate the role of approximations to the exchange-correlation potential in the derivation of the scheme. Our numerical implementation of the Sternheimer scheme is discussed in Sec. III. As the first application, we investigate the role of non-local exchange-correlation potentials for the prediction of photoabsorption in small hydrogenated silicon clusters in Sec. IV A, with a particular focus on the self-interaction correction with the generalized optimized effective potential (GSIC). In Sec. IV B and Appendix C 3, we demonstrate how triplet excitations can be computed from the Sternheimer response equations. Section IV B also presents examples for the accuracy and reliability of the method. We offer an outlook and conclusions in Sec. V. Appendixes A–E cover further technical aspects.

## II. DERIVATION OF THE STERNHEIMER SCHEME

In this section, we give an overview of our derivation of the Sternheimer formalism for computing electronic excitations. Complementing details are presented in Appendix A. A discussion of how optical absorption spectra are calculated and how excitation energies for different kinds of transitions are found is given in Appendix C. Our focus here is on a complete, self-contained derivation that closes some gaps that we felt were left open in previous discussions of the approach.

In order to be able to go beyond the description of singlet excitations, we consider the more general case of a system that, apart from a scalar potential  $\phi$ , is also subject to a magnetic field with a fixed axis  $\mathbf{B} = B\mathbf{e}_z$  coupling to the electron spins.  $B$  and  $\phi$  are allowed to vary in both time and space. The potential energy contribution to the many-body Hamiltonian can then be written as

$$\hat{V}(t) = \sum_{\sigma} \int d^3r v_{\sigma}(\mathbf{r}, t) \hat{n}_{\sigma}(\mathbf{r}), \quad (1)$$

where  $\hat{n}_{\sigma}(\mathbf{r})$  is the spin-density operator and  $v_{\sigma}$  is a spin-dependent potential,

$$v_{\sigma}(\mathbf{r}, t) = \phi(\mathbf{r}, t) + \mu_B B(\mathbf{r}, t) \text{sgn}(\sigma), \quad (2)$$

and  $\mu_B$  is the Bohr magneton. While the magnetic field just acts as a time-dependent external perturbation, the scalar potential  $\phi = v_{\text{ion}} + \phi_{\text{ext}}$  describes the electrostatic potential of the nuclei or the ionic cores as well as possibly also an external time-dependent electric field perturbing the system. The total potential in (2) can thus be split into a time- and spin-independent ionic potential and a perturbation,

$$v_{\sigma}(\mathbf{r}, t) = v_{\text{ion}}(\mathbf{r}) + v_{\text{ext},\sigma}(\mathbf{r}, t), \quad (3)$$

$$v_{\text{ext},\sigma}(\mathbf{r}, t) = \phi_{\text{ext}}(\mathbf{r}, t) + \mu_B B(\mathbf{r}, t) \text{sgn}(\sigma). \quad (4)$$

Assuming a magnetization parallel to  $\mathbf{B}$ , the dynamics of the spin densities  $n_{\sigma}$  can be calculated from the spin-generalized, time-dependent Kohn-Sham (TDKS) equations,<sup>36–42</sup>

$$\left[ -\frac{\hbar^2}{2m} \nabla^2 + v_{\sigma}(\mathbf{r}, t) + v_{\text{Hxc}\sigma}[\{n_{\alpha}(\mathbf{r}', t')\}](\mathbf{r}, t) \right] \varphi_{j\sigma}(\mathbf{r}, t) = i\hbar \partial_t \varphi_{j\sigma}(\mathbf{r}, t), \quad (5)$$

where  $\{n_{\alpha}\} = \{n_{\uparrow}, n_{\downarrow}\}$  is the set of spin densities.

For a system that is in its ground state (GS) at some time  $t_0$  and then evolves under the influence of a perturbation of the general form

$$v_{\text{ext},\sigma}(\mathbf{r}, t) = \left[ v_{\text{ext},\sigma}^{(+)}(\mathbf{r}) e^{-i\omega t} + \text{c.c.} \right] e^{\eta t}, \quad (6)$$

the linear response of the density at times  $t \gg t_0$ , i.e., in the limit  $t_0 \rightarrow -\infty$ , is shown in Appendix A to have the form

$$n_{\sigma}^{(1)}(\mathbf{r}, t) = \left[ n_{\sigma}^{(+)}(\mathbf{r}) e^{-i\omega t} + \text{c.c.} \right] e^{\eta t}. \quad (7)$$

From this, the linear response of the Hartree-exchange-correlation potential (both for the exact  $v_{\text{xc}}$  and most approximations) follows as

$$v_{\text{Hxc}\sigma}^{(1)}(\mathbf{r}, t) = \left[ v_{\text{Hxc}\sigma}^{(+)}(\mathbf{r}) e^{-i\omega t} + \text{c.c.} \right] e^{\eta t} \quad (8)$$

with

$$v_{\text{Hxc}\sigma}^{(+)}(\mathbf{r}) = v_{\text{H}}[n^{(+)}](\mathbf{r}) + \sum_{\tau} \int d^3r' n_{\tau}^{(+)}(\mathbf{r}') \times \int d(t-t') \left. \frac{\delta v_{\text{Hxc}\sigma}(\mathbf{r}, t)}{\delta n_{\tau}(\mathbf{r}', t')} \right|_{\{n_{\alpha}^{(0)}\}} e^{i(\omega+i\eta)(t-t')}. \quad (9)$$

We can now expand  $\varphi_{j\sigma}(\mathbf{r}, t)$  into a perturbation series and linearize the TDKS equations, leading to

$$\left[ \hat{h}_{\sigma} - i\hbar \partial_t \right] \varphi_{j\sigma}^{(1)}(\mathbf{r}, t) = -v_{\text{Hxc}\sigma}^{(1)}(\mathbf{r}, t) \varphi_{j\sigma}(\mathbf{r}) e^{-i(\varepsilon_{j\sigma}/\hbar)t}. \quad (10)$$

Here,  $\varphi_{j\sigma}^{(1)}$  is the linear response of the TDKS orbital to the external perturbation;  $v_{\text{Hxc}\sigma}^{(1)}$  is the sum of Eqs. (6) and (8); and  $\hat{h}_{\sigma}$ ,  $\varphi_{j\sigma}(\mathbf{r})$ , and  $\varepsilon_{j\sigma}$  are the unperturbed, time-independent KS Hamiltonian, orbitals, and eigenvalues, respectively, defined by

$$\begin{aligned} \hat{h}_{\sigma} \varphi_{j\sigma}(\mathbf{r}) &:= \left[ -\frac{\hbar^2}{2m} \nabla^2 + v_{\text{ion}}(\mathbf{r}) + v_{\text{Hxc}\sigma}^{(0)}(\mathbf{r}) \right] \varphi_{j\sigma}(\mathbf{r}) \\ &= \varepsilon_{j\sigma} \varphi_{j\sigma}(\mathbf{r}). \end{aligned} \quad (11)$$

We choose the GS orbitals to be real. A formal solution to Eq. (10) can be constructed from an expansion with respect

to the unperturbed orbitals, and at large times, the solution becomes

$$\varphi_{j\sigma}^{(1)}(\mathbf{r}, t) = \left\{ \left[ \varphi_{j\sigma}^{(+)}(\mathbf{r})e^{-i\omega t} + \varphi_{j\sigma}^{(-)*}(\mathbf{r})e^{i\omega t} \right] e^{\eta t} - i\varphi_{j\sigma}(\mathbf{r})\varepsilon_{j\sigma}^{(1)}(t) \right\} e^{-i(\varepsilon_{j\sigma}/\hbar)t}, \quad (12)$$

where

$$\begin{aligned} \varepsilon_{j\sigma}^{(1)}(t) &:= \int d^3r \int_{-\infty}^t \frac{dt'}{\hbar} |\varphi_{j\sigma}(\mathbf{r})|^2 v_{s\sigma}^{(1)}(\mathbf{r}t') \\ &= i \left[ \frac{\int d^3r |\varphi_{j\sigma}(\mathbf{r})|^2 (v_{\text{ext},\sigma}^{(+)}(\mathbf{r}) + v_{\text{Hxc}\sigma}^{(+)}(\mathbf{r}))}{\hbar(\omega + i\eta)} e^{-i\omega t} - \text{c.c.} \right] e^{\eta t} \end{aligned} \quad (13)$$

is real and of first order in the perturbation, and the functions  $\varphi_{j\sigma}^{(\pm)}$  are also of first order and obey

$$\langle \varphi_{j\sigma} | \varphi_{j\sigma}^{(\pm)} \rangle = \int d^3r \varphi_{j\sigma}(\mathbf{r}) \varphi_{j\sigma}^{(\pm)}(\mathbf{r}) = 0. \quad (14)$$

Up to the first order, the TDKS orbitals can thus be written as

$$\begin{aligned} \varphi_{j\sigma}(\mathbf{r}, t) &= e^{-i[(\varepsilon_{j\sigma}/\hbar)t + \varepsilon_{j\sigma}^{(1)}(t)]} \left\{ \varphi_{j\sigma}(\mathbf{r}) \right. \\ &\quad \left. + \left[ \varphi_{j\sigma}^{(+)}(\mathbf{r})e^{-i\omega t} + \varphi_{j\sigma}^{(-)*}(\mathbf{r})e^{i\omega t} \right] e^{\eta t} \right\} + \mathcal{O}(2). \end{aligned} \quad (15)$$

Calculating the TD density from the TDKS orbitals in the form (15) yields a linear density response of the form (7) with

$$n_{\sigma}^{(+)}(\mathbf{r}) = \sum_j^{\text{occ}} \varphi_{j\sigma}(\mathbf{r}) (\varphi_{j\sigma}^{(+)}(\mathbf{r}) + \varphi_{j\sigma}^{(-)}(\mathbf{r})). \quad (16)$$

By inserting (12) and (13) into (10), we arrive at

$$\begin{aligned} &[\hat{h}_{\sigma} - \varepsilon_{j\sigma} \mp \hbar(\omega + i\eta)] \varphi_{j\sigma}^{(\pm)}(\mathbf{r}) \\ &= -\hat{Q}_{j\sigma} [v_{\text{ext},\sigma}^{(+)}(\mathbf{r}) + v_{\text{Hxc}\sigma}^{(+)}(\mathbf{r})] \varphi_{j\sigma}(\mathbf{r}), \end{aligned} \quad (17)$$

where  $\hat{Q}_{j\sigma} := 1 - |\varphi_{j\sigma}\rangle\langle\varphi_{j\sigma}|$  projects onto the subspace orthogonal to  $\varphi_{j\sigma}(\mathbf{r})$ .

Equations (12)–(15) (or similar expressions) are usually proposed as an ansatz for the TD orbitals in perturbation theory,<sup>29,43,44</sup> and inserting them into the TDKS equations and equating only the first-order terms immediately yield the Sternheimer equations. Our main theoretical result is that we have actually proven (Appendix A) that this form of the orbitals is a valid solution of the TDKS equations for the perturbation given by Eq. (6) and that these orbitals meet a reasonable initial condition. To achieve this, we had to model the switch-on of the perturbation by the exponential  $e^{\eta t}$  included in Eq. (6). This leads quite naturally to the regularizing imaginary part  $+i\eta$  in the Sternheimer equations (17), which in earlier presentations of the scheme has been either missing<sup>45</sup> or inserted *a posteriori* and motivated by an exponential decay factor  $e^{-\eta t}$  simulating “artificial lifetime.”<sup>43,44</sup> In our derivation, the only condition on  $\eta$  is that it has to be positive. In other words, it is not required that  $\eta$  be small. This is reassuring, as it shows that one is on safe grounds with using a finite  $\eta$  in the actual calculations and not making an uncontrolled finite approximation to a quantity that should rigorously be a positive infinitesimal.

Furthermore, our derivation includes spin-dependent perturbations and thus allows us to treat triplet excitations in the Sternheimer scheme (cf. Sec. IV B and Appendix C 3). To the best of our knowledge, this has not been done before.

Finally, we did not only consider whether the Sternheimer scheme can be derived within exact TDDFT. In Appendix A, we show that the scheme can still be derived from the TDKS equations when an approximate xc potential is used, as long as this xc approximation fulfills certain conditions.

The Sternheimer equations (17) are the central equations of our work. Together with (14), (16), and (9), they fully determine the density response; i.e., this set of equations constitutes the complete Sternheimer scheme. Because the right-hand side of (17) depends on every occupied solution  $\varphi_{k\tau}^{(\pm)}$  through (9) and (16), the equations have to be solved self-consistently, as discussed in the following.

### III. IMPLEMENTATION

To perform a linear response calculation in the Sternheimer scheme, one first has to perform a self-consistent KS ground-state calculation for the system of interest with some approximation for the ground-state xc potential. This generates occupied eigenvalues and orbitals, the GS density, and the corresponding GS Hamiltonian  $\hat{h}_{\sigma}$ , all of which are needed as ingredients to the Sternheimer equations.

Next, one has to choose  $v_{\text{ext},\sigma}^{(+)}(\mathbf{r})$  (see below and Appendix C for details), a value for the switch-on rate  $\eta$ , and an approximation to the xc potential from which to calculate  $v_{\text{xc}\sigma}^{(+)}(\mathbf{r})$ . A natural choice is to use the same approximation for both  $v_{\text{xc}\sigma}^{(+)}(\mathbf{r})$  and the ground-state xc potential that enters  $\hat{h}_{\sigma}$ . However, the possibility to use different xc approximations for the ground-state xc potential and  $v_{\text{xc}\sigma}^{(+)}(\mathbf{r})$  can also be exploited beneficially in order to obtain insight into which properties of a functional are important for an accurate response. We demonstrate this in Sec. IV A and have employed the same idea in Ref. 46.

Once the xc choice has been made, one has to choose a frequency  $\omega$  and then iteratively solve Eqs. (9), (16), and (17) for this value of  $\omega$ . A typical situation is, e.g., that one is interested in the photoabsorption spectrum within a given energy range. In this case, one solves the equations for a discrete set of values  $\omega_i$  within that range. It is important to note that the calculations for different  $\omega_i$  are completely independent of each other and therefore can be done simultaneously. This allows for massive parallelization.

For each  $\omega_i$ , the equations need to be iterated until self-consistency is reached. In practice, in the first step, we solve the Sternheimer equations (17) with just  $v_{\text{ext},\sigma}^{(+)}$  on the right-hand side, i.e., with  $v_{\text{Hxc}\sigma}^{(+)}$  set to zero. The perturbation is chosen to represent the physical situation of interest; e.g., if one is interested in usual photoabsorption, then

$$v_{\text{ext},\sigma}^{(+)}(\mathbf{r}) = e\mathbf{E} \cdot \mathbf{r}, \quad (18)$$

with  $\mathbf{E}$  being a spatially homogeneous electric field (see Appendix C for details and other perturbations). After having solved for the orbital responses  $\varphi_{j\sigma}^{(+)}$  and  $\varphi_{j\sigma}^{(-)}$ ,

one can calculate  $n_{\sigma}^{(+)}$  and use this to construct  $v_{\text{Hxc}\sigma}^{(+)}$ . Next, one can consequently calculate an updated right-hand side of Eqs. (17) and then again solve for the orbital responses.

When this iteration is converged, one can use the resulting  $n_{\sigma}^{(+)}$  ( $\mathbf{r}$ ) to construct the optical absorption spectrum or alternatively calculate its various moments, plot them as functions of  $\omega$ , and extract excitation energies for different (not necessarily optically active) transitions from fitting superpositions of Lorentzians to these functions (cf. Appendix C).

We have implemented the Sternheimer scheme into the Bayreuth version<sup>18,47</sup> of the PARSEC<sup>35</sup> GS program package employing a real-space grid and norm-conserving Troullier-Martins pseudopotentials.<sup>48,49</sup> The program's multigrid routines<sup>50,51</sup> were used to calculate the response

$$v_{\text{H}}^{(+)}(\mathbf{r}) = v_{\text{H}}[n^{(+)}](\mathbf{r}) = \int \frac{e^2 n^{(+)}(\mathbf{r}')}{|\mathbf{r} - \mathbf{r}'|} d^3 r' \quad (19)$$

of the Hartree potential by solving Poisson's equation. While we used different xc functionals for the GS calculations,  $v_{\text{xc}\sigma}^{(+)}$  ( $\mathbf{r}$ ) was constructed from the adiabatic local (spin-)density approximation (ALDA)<sup>52-54</sup> for all calculations presented in this work.

In Ref. 29, several aspects of the numerical treatment of Sternheimer linear response calculations have already been pointed out: The imaginary shift  $+i\eta$  ruins the hermiticity of the Sternheimer matrix, so the equation cannot be solved with the conjugate gradient<sup>55</sup> (CG) algorithm. Andrade and co-workers<sup>29</sup> suggested to use the stabilized biconjugate gradient (BiCGstab) algorithm<sup>56,57</sup> instead (yet also see Ref. 21 for further comments). They also proposed to use the rather sophisticated Broyden mixing scheme<sup>58,59</sup> in the self-consistency process and noted that a non-zero value for  $\eta$  is necessary for a numerically stable solution of the Sternheimer equations at least near the resonance frequencies. Based on our own experience with the Sternheimer scheme, we comment on these three points in the following.

We have tested both the BiCGstab and a variant of the CG scheme (CGsymm) that we derived for matrices that are complex and symmetric and thus not hermitian. For a discussion of this algorithm, see Appendix D. In our tests, the CGsymm typically reduced the number of matrix-vector multiplications, i.e., the number of applications of the KS Hamiltonian needed for a full self-consistent solution of the Sternheimer equations, by more than one order of magnitude in comparison with the BiCGstab. We therefore used the CGsymm algorithm in all the calculations presented in this work. We further compared the Broyden mixing scheme with the simpler Anderson mixing scheme<sup>60</sup> and did not find the latter to be inferior in any regards to the former. In fact, with Anderson mixing, the self-consistency process typically converges in slightly fewer steps per frequency. We thus use Anderson mixing as our standard method. (Both of the just described tests were done for small sodium and hydrogenated silicon clusters and the CO molecule.)

Concerning the choice of  $\eta$ , we confirm that indeed larger values of  $\eta$  accelerate convergence. However, the linewidths of the computed spectra are also determined by this parameter. Therefore, unless one resorts to the advanced evaluation

described below, its value has to be chosen as a compromise between numerical efficiency and the accuracy of the calculated excitation energies. In our experience, however, there does not seem to be a minimal positive value below which convergence of the scheme becomes impossible. It is important to note, though, that the limitation of the spectral resolution that results from a finite value of  $\eta$  can be circumvented to a large extent: As long as a peak is visible at all and not completely hidden beneath a neighboring line, we can make use of our knowledge of the exact shape and width of the lines and of the different spatial and spin symmetries of different excitations in order to determine the peak position with an accuracy that exceeds the one suggested by the linewidths by roughly two orders of magnitude. We demonstrate this in Sec. IV B. This strategy is similar in spirit to the one recently proposed for the evaluation of real-time signals.<sup>23</sup> Typically, we used values roughly between 0.01 eV and 0.1 eV for  $\hbar\eta$ .

## IV. RESULTS

In the following, we apply the method described in Secs. II and III to calculate photoabsorption spectra as well as the excitation energies of several optically active and inactive singlet and triplet transitions.

### A. Hydrogenated silicon clusters: Photoabsorption

The excitations of silicon clusters such as silane ( $\text{SiH}_4$ ) and disilane ( $\text{Si}_2\text{H}_6$ ) are often described as excitonic and therefore challenging for DFT methods.<sup>50,61-63</sup> This judgement was originally based on a comparison of the qualitatively correct spectra obtained from solving the Bethe-Salpeter equation (BSE) with the substantially blue-shifted spectra calculated directly from GW quasiparticle energies, neglecting the electron-hole interaction kernel.<sup>62,63</sup>

It is well documented that the description of excitonic features at least in extended systems such as bulk silicon by TDDFT requires the xc approximation to yield a non-local response that is capable of correctly describing long-range Coulomb interactions between electrons and holes and that has a divergent long-wavelength behavior.<sup>64-67</sup> These challenges are met by, e.g., the orbital-dependent KS exact exchange (EXX) functional<sup>66</sup> but not by semilocal functionals such as the LDA.<sup>64,65,68</sup> In particular, while the non-local EXX properties are already important for the KS eigenvalue spectrum of molecules<sup>69,70</sup> or the band structure of solids,<sup>68,71,72</sup> combining the improved EXX band structure with the xc response properties (the xc kernel  $f_{\text{xc}}$ ) of the ALDA does not lead to a correct description of the excitonic features in bulk silicon. However, using the EXX for both GS properties and  $f_{\text{xc}}$  does.<sup>66,68</sup>

The notion that excitonic effects might play a role in the spectra of hydrogenated silicon clusters can be supported by the observation that they can be reasonably well described by the EXX but not by semilocal functionals.<sup>3</sup>

In a real-time propagation scheme,<sup>15,18</sup> the self-interaction correction<sup>73</sup> to the LDA with complex energy-minimizing unitary transformations<sup>74</sup> and using the Krieger-Li-Iafrate approximation to the generalized optimized

effective potential<sup>75</sup> (GSIC) has also been shown to yield excitation energies close to the BSE results for SiH<sub>4</sub> and Si<sub>2</sub>H<sub>6</sub>.<sup>50,61</sup> Like the EXX, GSIC is orbital-dependent and contains non-local Coulomb integrals in the form of the self-Hartree correction terms. Thus, it might well be that the response of its potential to an external perturbation has the non-local properties required for the description of excitonic excitations. In the approach of Refs. 50 and 61, one xc approximation is used throughout the whole calculation; i.e., no differentiation is made between ground-state and response properties of  $\nu_{xc\sigma}$ . Thus, these calculations could not distinguish whether the success of GSIC in describing the excitations of silane and disilane is due to its kernel containing non-local response features or whether the improvements seen in the GSIC spectra of silane and disilane are just a consequence of the GSIC GS potential being more physical than the potential of semilocal functionals.

To investigate this question, we perform GS calculations for the two systems using the GSIC functional and then calculate spectra with  $\nu_{xc\sigma}^{(+)}$  constructed with the ALDA (referred to as GSIC + ALDA). For comparison, we also calculate spectra using (A)LDA for both the GS and the response calculation (LDA + ALDA). We use the same coordinates, grid, and pseudopotentials as in Ref. 61 as well as  $\hbar\eta = 0.05$  eV to get similar linewidths.<sup>76</sup> Figure 1 shows our results for the photoabsorption cross section  $\sigma(\omega)$  (cf. Appendix C 1) of SiH<sub>4</sub> and Si<sub>2</sub>H<sub>6</sub>. We have also included the GSIC power spectra of Ref. 61, with the dipole power strength function  $D(\omega)$  defined as the absolute square of the Fourier transformed TD dipole moment  $\mu$  from the real-time propagation,<sup>77</sup>

$$D(\omega) := |\mu_x(\omega)|^2 + |\mu_y(\omega)|^2 + |\mu_z(\omega)|^2. \quad (20)$$

Our first observation is that the fitting procedure works extremely well, with all datapoints lying perfectly on the fitted curves. We estimate our fit errors for the excitation energies to only a few meV. The LDA spectra closely resemble the results from the literature,<sup>3,50,61,78,79</sup> proving the validity of our method and confirming the poor performance of the LDA for these systems. With our GSIC+LDA approach, we can reproduce the full GSIC spectra quite accurately. Most notably, for the position of the first peak, notoriously underestimated by semilocal functionals, GSIC+LDA gives

almost exactly the same value as the propagation using full GSIC for silane and it is off by only  $\approx 0.1$  eV for disilane.

These results suggest that non-local response features play no significant role in the prediction of the spectra of small hydrogenated silicon clusters and that their poor description by semilocal xc approximations can be attributed almost solely to errors in the GS potential. This finding also challenges the description of the excitations as excitonic, at least if the term is understood in a similar way as in bulk solids.

## B. General singlet and triplet excitations

In this section, we demonstrate how our method is capable of predicting and identifying excitations of different spin and spatial symmetries. Excitations with even spin symmetry are interpreted as singlets and odd-spin excitations as triplets. For a further discussion of this classification, we refer to Appendix C 3.

As our test systems we choose N<sub>2</sub>, CO, and C<sub>2</sub>H<sub>4</sub> since for all of them the first singlet and triplet excitations differ by more than 1 eV. This allows for an easy verification of our interpretation of their spin character by comparison with established reference ALDA excitation energies.<sup>80,81</sup> To facilitate this comparison, we use the same molecular geometries as in Ref. 80. Our grids are chosen such that all presented excitation energies are converged to within a few meV.<sup>82</sup> In Appendix E, we compare the numerical accuracy of excitation energies calculated using our numerical grid and pseudopotentials with the one obtained with Gaussian basis sets. We further compare convergence with respect to grid parameters, the pseudopotential cutoff radius or the basis set size, respectively. The (A)LDA is used for both GS and response calculations throughout this section since we want to compare our results with the ALDA reference calculations from the literature.

We first investigate how accurate excitation energies can be extracted from Sternheimer spectra with relatively large linewidths in order to support the corresponding claim made in Sec. III. For this purpose, we consider the first six dipole and quadrupole active singlet and triplet excitations of the nitrogen molecule (some of which are separated by only  $\approx 0.1$  eV) and deliberately choose a large value of  $\hbar\eta = 0.3$  eV

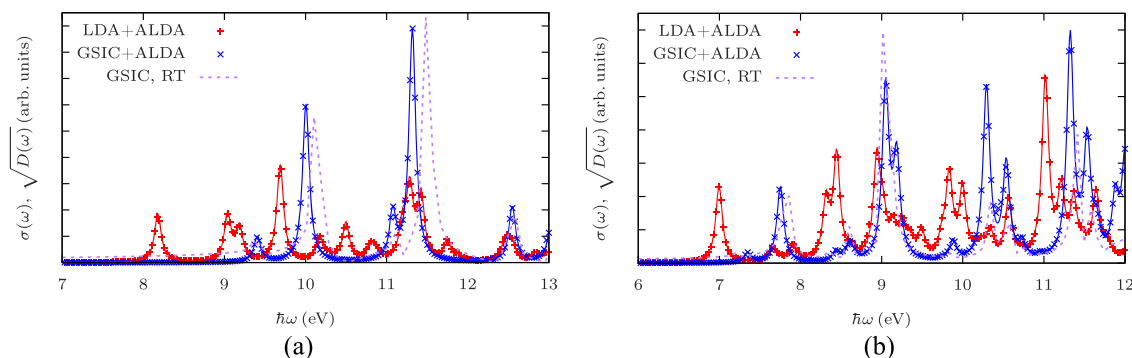


FIG. 1. SiH<sub>4</sub> (a) and Si<sub>2</sub>H<sub>6</sub> (b) spectra from different xc approximations. Points represent solutions of the Sternheimer equations for the absorption cross section  $\sigma(\omega)$  at discrete frequencies  $\omega_j$ . The solid lines result from fitting superpositions of Lorentzians with fixed half-widths of  $\hbar\eta = 0.05$  eV to the data. The purple dashed line is the real-time result for the power spectrum  $\sqrt{D(\omega)}$  from Ref. 61.

(leading to a full linewidth of 0.6 eV) and a frequency step size of  $\hbar\Delta\omega = 0.2$  eV. When the molecule is aligned along the  $x$ -axis, the perturbation

$$v_{\text{ext},\sigma}^{(+)}(\mathbf{r}) \propto \delta_{\sigma\uparrow} \left( x/a_0 + y/a_0 + xy/a_0^2 + z^2/a_0^2 \right) \quad (21)$$

can excite all of these first six transitions. This allows us to find them all from a single linear response calculation, i.e., by finding only one self-consistent solution to the Sternheimer equations for each frequency, instead of having to perform separate calculations for singlets/triplets, dipole/quadrupole excitations, etc. In principle, we can construct a spectrum containing a peak for every transition that can be excited by a certain  $v_{\text{ext},\sigma}^{(+)}(\mathbf{r})$  by plotting the corresponding spin-density moment  $\sum_{\sigma} \int d^3r n_{\sigma}^{(+)}(\mathbf{r}) v_{\text{ext},\sigma}^{(+)}(\mathbf{r})$  as a function of  $\omega$ . The results for the discrete frequencies  $\omega_i$  for which we solved the Sternheimer equations are shown in the top panel of Fig. 2. The strong overlap between the different excitations only allows to

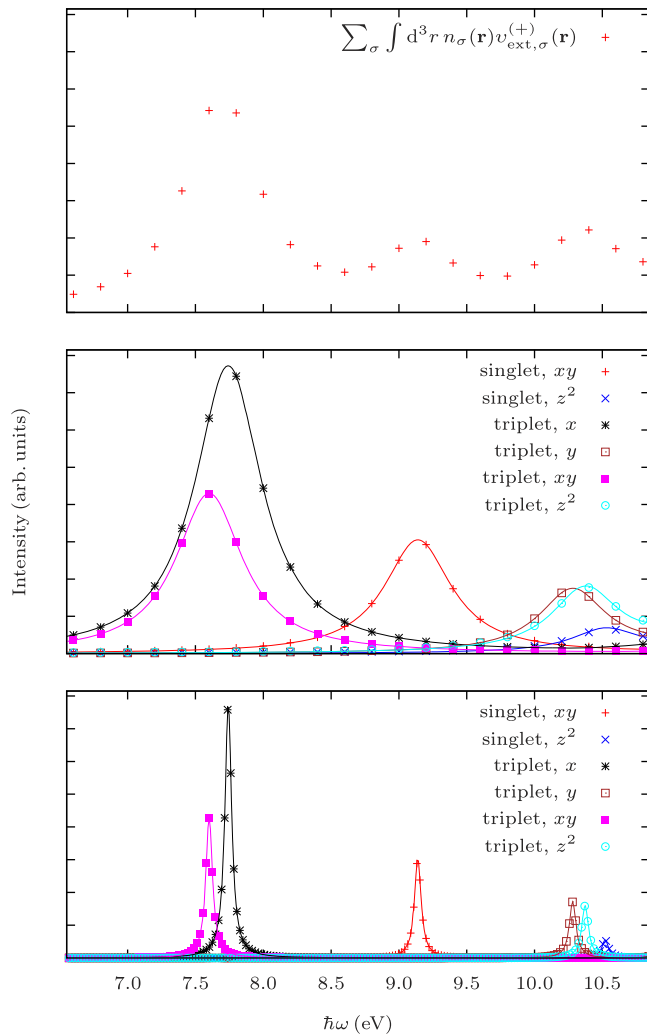


FIG. 2. Different ALDA spectra for  $\text{N}_2$  for the perturbation of Eq. (21). Points represent solutions of the Sternheimer equations at discrete frequencies  $\omega_i$ . The solid lines result from fitting Lorentzians with fixed half-widths  $\eta$  to the data. While the two upper panels show results from a calculation with  $\hbar\eta = 0.3$  eV, the spectra in the bottom panel were calculated with  $\hbar\eta = 0.03$  eV. The top panel shows the full spectrum generated by  $v_{\text{ext},\sigma}^{(+)}(\mathbf{r})$ . In the two lower panels, the spectra are separated by their spin and spatial symmetry (see text) and the Sternheimer results are accompanied by Lorentzian fits.

distinguish between three peaks, the positions of which can only be determined to roughly within 0.1 eV.

However, without having to perform any additional linear response calculation, we can refine our results in two steps: First, instead of plotting the whole spectrum of  $v_{\text{ext},\sigma}^{(+)}(\mathbf{r})$  at once, we separately evaluate and plot the spin-density moments of  $xy$ ,  $z^2$ ,  $\text{sgn}(\sigma) \cdot x$ ,  $\text{sgn}(\sigma) \cdot y$ ,  $\text{sgn}(\sigma) \cdot xy$ , and  $\text{sgn}(\sigma) \cdot z^2$  with the spin-density response  $n_{\sigma}^{(+)}(\mathbf{r})$  resulting from the full perturbation  $v_{\text{ext},\sigma}^{(+)}(\mathbf{r})$  of Eq. (21). Each of these moments, plotted as a function of  $\omega$ , should only contain contributions from one type of excitation (cf. Appendixes C 2 and C 3), namely, the  ${}^1\Pi_g$ ,  ${}^1\Sigma_g^+$ ,  ${}^3\Sigma_u^+$ ,  ${}^3\Pi_u$ ,  ${}^3\Pi_g$ , and  ${}^3\Sigma_g^+$  excitations, respectively. The results are represented by points in the second panel of Fig. 2. In the frequency range displayed in the figure, each of the six separate spectra indeed only contains one peak, so the six different excitations can now be easily distinguished. Next, we make use of our knowledge of the exact form and width of the lines by fitting the positions and heights of Lorentzians to the data. The fitted spectra are also depicted in the middle panel of Fig. 2. They closely match the data, with every point lying almost exactly on the respective fitting curve. This allows us to determine the excitation energies as the positions of the fitted Lorentzians with estimated fit errors of only a few meV. The energies are listed in Table I.

To verify the accuracy of our results, we perform a second linear response calculation with the same choice for  $v_{\text{ext},\sigma}^{(+)}(\mathbf{r})$  [Eq. (21)] but with  $\hbar\eta = 0.03$  eV, i.e., with the linewidth reduced by a factor of 10. With this linewidth, the different peaks could even be identified with a reasonable accuracy if they were simply plotted in a single spectrum and without a fit. However, we evaluate the data the same way as before, by plotting the six different moments listed above and fitting Lorentzians to the datapoints. The results can be seen in the bottom panel of Fig. 2 and in Table I.

For all but the highest ( ${}^1\Sigma_g^+$ ) excitation, the energies calculated with the two different values of  $\eta$  actually differ by less than 1 meV. For  ${}^1\Sigma_g^+$ , the difference is still only about 3 meV, suggesting that the uncertainty of the results from our first calculation is more than two orders of magnitude smaller than the linewidth of 0.6 eV.

To further demonstrate how accurately excitation energies can be extracted from the broad-line calculation, we next focus on the  $\text{sgn}(\sigma) \cdot y$  moment (corresponding to the  ${}^3\Pi_u$  excitations) in the range between 10.2 eV and 11.6 eV, shown in Fig. 3. At first sight, this looks like the area between two peaks, one at 10.28 eV and the other at higher energy ( $\approx 11.96$  eV). However, while a superposition of two Lorentzians at these energies yields a reasonable fit to the data near the maxima,

TABLE I. ALDA results for the six lowest dipole and quadrupole active singlet and triplet excitation energies of  $\text{N}_2$  extracted from Sternheimer linear response calculations with two different values of  $\eta$ . The energies and  $\hbar\eta$  values are given in eV.

$\hbar\eta$	${}^3\Pi_g$	${}^3\Sigma_u^+$	${}^1\Pi_g$	${}^3\Pi_u$	${}^3\Sigma_g^+$	${}^1\Sigma_g^+$
0.3	7.6010	7.7418	9.1397	10.2809	10.3731	10.5244
0.03	7.6010	7.7418	9.1393	10.2812	10.3728	10.5210

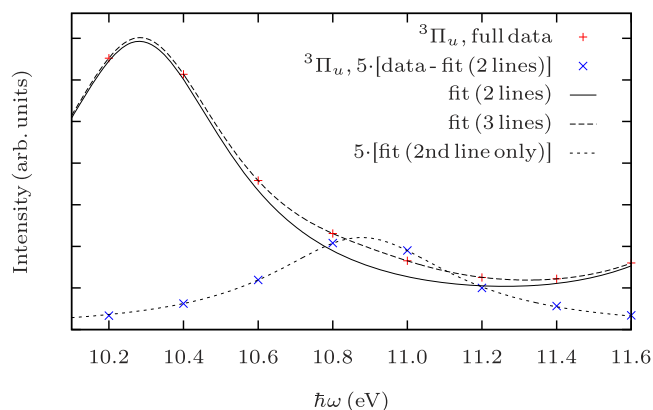


FIG. 3. ALDA  ${}^3\Pi_u$  spectrum of  $\text{N}_2$  for  $\hbar\eta = 0.3$  eV. Red pluses mark the results from a Sternheimer calculation. The black solid line is a superposition of two Lorentzians fitted to these results. Blue crosses and the black short-dashed line denote the difference in the original data and this fitted two-line superposition, as well as a single Lorentzian fit to this difference, both scaled by a factor of 5. The black dashed line is the superposition of all three fitted Lorentzians.

it is too low in the range between 10.6 eV and 11.4 eV. Subtracting this two-line fit from our original data reveals another peak with small intensity (scaled by a factor of 5 in Fig. 3), which is perfectly reproduced by another Lorentzian fit. This fit places the excitation at 10.8775 eV. The resulting superposition of three Lorentzians now yields a good description of our original data over the full frequency range shown in Fig. 3. In the spectrum calculated with  $\hbar\eta = 0.03$  eV (not shown), this line can be readily identified as an almost isolated peak, and a fit yields an excitation energy of 10.8828 eV, which differs by only  $\approx 5$  meV from the result for the bigger linewidth. Thus, by successively fitting and subtracting Lorentzians from spectra, even an excitation that is barely visible from the original data can be determined two orders of magnitude more accurately than one would infer from the linewidth.

Our results for the excitation energies are generally in good agreement with the values found in Refs. 80 and 81, supporting our interpretation of the peaks found at ca. 7.60 eV, 7.74 eV, 10.28 eV, and 10.37 eV as triplet excitations. In particular, the first singlet and triplet excitations (the  $\Pi_g$  excitations) differ from the reference values by only 0.05 eV

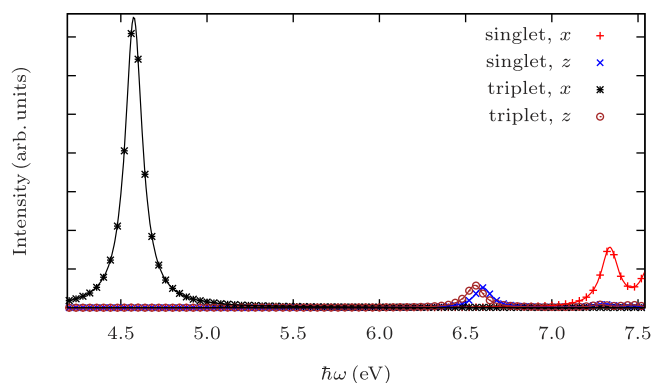


FIG. 4. Singlet and triplet dipole spectra of  $\text{C}_2\text{H}_4$  calculated with the ALDA and  $\hbar\eta = 0.06$  eV. Points represent solutions of the Sternheimer equations at discrete frequencies  $\omega_i$ , and solid lines result from Lorentzian fits to the data.

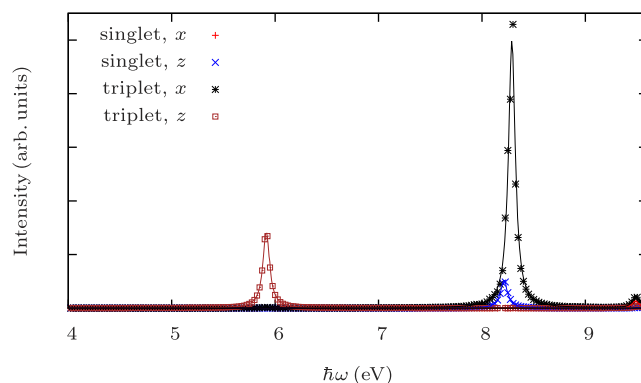


FIG. 5. Singlet and triplet dipole spectra of CO calculated with the ALDA and  $\eta = 0.04$  eV. Points represent solutions of the Sternheimer equations at discrete frequencies  $\omega_i$ , and solid lines result from Lorentzian fits to the data.

and 0.02 eV, respectively, which is negligible compared with their separation of  $\hbar[\Omega({}^1\Pi_g) - \Omega({}^3\Pi_g)] \approx 1.54$  eV. The  $\Sigma_g^+$  singlet-triplet separation is only slightly larger than 0.1 eV, but our result for the triplet  ${}^3\Sigma_g^+$  excitation also deviates by only 0.02 eV from the reference.

As the final test for our method, we calculate the lowest singlet and triplet excitations in  $\text{C}_2\text{H}_4$  and CO. For simplicity, we only consider dipole excitations. We can find them all by applying the single perturbation  $v_{\text{ext},\sigma}^{(+)}(\mathbf{r}) \propto \delta_{\sigma\uparrow}(x+y+z)/a_0$  and then separately plotting the moments of the different coordinates with or without a  $\text{sgn}(\sigma)$ , as demonstrated for  $\text{N}_2$ . The  $x$ -axis is taken to be the CC- and CO-axis, respectively, and the  $\text{C}_2\text{H}_4$  molecule is placed in the  $x$ - $y$ -plane. Figures 4 and 5 show the resulting spectra for  $\text{C}_2\text{H}_4$  and CO, respectively.

The first  ${}^1\text{B}_{1u}$  and  ${}^3\text{B}_{1u}$  excitations of  $\text{C}_2\text{H}_4$  and the first  ${}^1\Pi$  and  ${}^3\Pi$  excitations of CO are separated by roughly 2.8 eV and 2.3 eV, respectively. We find them at  $\hbar\Omega(\text{C}_2\text{H}_4, {}^1\text{B}_{1u}) = 7.34$  eV,  $\hbar\Omega(\text{C}_2\text{H}_4, {}^3\text{B}_{1u}) = 4.58$  eV,  $\hbar\Omega(\text{CO}, {}^1\Pi) = 8.21$  eV, and  $\hbar\Omega(\text{CO}, {}^3\Pi) = 5.91$  eV, differing from the results of Ref. 80 by  $\approx 0.08$  eV for  $\text{C}_2\text{H}_4$  and by only  $\approx 0.03$  eV for CO. We also find a relatively large separation of ca. 1.2 eV between the first  ${}^1\Sigma^+$  and  ${}^3\Sigma^+$  excitation of CO, with our result for the triplet  ${}^3\Sigma^+$  energy of 8.29 eV deviating from the reference value by 0.13 eV. Thus, while this is among the larger deviations between our real-space grid-based results and those calculated using basis functions, it still allows for a clear identification of our peak as the triplet excitation from the reference. The  $\text{B}_{3u}$  excitations of  $\text{C}_2\text{H}_4$  are harder to analyze since in this case the singlet and triplet differ by only 0.05 eV. However, we find these energies at  $\hbar\Omega({}^1\text{B}_{3u}) = 6.60$  eV and  $\hbar\Omega({}^3\text{B}_{3u}) = 6.55$  eV, in almost perfect agreement with Ref. 80. Overall, these very good results strongly support our interpretation of odd-spin excitations as triplet excitations.

## V. CONCLUSION

We have revisited the Sternheimer linear response scheme for calculating electronic excitations and have provided a self-contained, complete derivation of the underlying equations.

We demonstrated how triplet and non-dipole active excitations can easily be calculated in the Sternheimer scheme for finite systems. We discussed important aspects of an efficient numerical implementation and pointed out how a high spectral resolution can be achieved at rather low computational cost by solving only for a sparse set of frequencies but then fitting the analytically known line shapes to these data. High accuracy obtained with a high numerical efficiency and excellent parallelizability makes the Sternheimer scheme attractive for future linear response calculations, in particular, for large systems.

## ACKNOWLEDGMENTS

S.K. is grateful to Xavier Andrade for comments about his Sternheimer calculations. We acknowledge financial support by the program “Biological Physics” of the Elite Network of Bavaria and by the German-Israeli Foundation for Scientific Research and Development. We further acknowledge support through the computational resources provided by the Bavarian Polymer Institute and by the Bavarian State Ministry of Science, Research, and the Arts in the Collaborative Research Network “Solar Technologies go Hybrid”. F.H. acknowledges support by the University of Bayreuth Graduate School.

## APPENDIX A: DETAILS AND DISCUSSION ON THE DERIVATION OF THE STERNHEIMER SCHEME

In general, an external magnetic field not only couples to the spin but also yields additional potential energy contributions such as coupling to the angular momentum. Since the linear response to a sum of perturbations is of course just the sum of the single responses, including these terms in the Hamiltonian could only give rise to additional excitations but not alter the frequencies or amplitudes of the transitions that can be excited by the perturbation of Eq. (4).

The perturbation (6) contains the special case of a harmonic oscillation (for  $\eta = 0$ ), but for  $\eta > 0$ , it has an exponentially increasing amplitude. This is unphysical because any real perturbation will eventually be switched off again. However, the wave function at any finite time  $t > t_0$  only depends on the potential at times between  $t_0$  and  $t$  and not on its future behavior, so we do not have to model how the potential will decrease at a later time.

The linear spin-density response to a perturbation  $v_{\text{ext},\sigma}$  of a system that is in its ground state at  $t_0$  is

$$n_{\sigma}^{(1)}(\mathbf{r}, t) = \sum_{\tau} \int_{t_0}^{\infty} dt' \int d^3r' \chi_{\sigma\tau}(\mathbf{r}, \mathbf{r}', t - t') v_{\text{ext},\tau}(\mathbf{r}', t'). \quad (\text{A1})$$

The time-dependent spin-density response function  $\chi_{\sigma\tau}$  can be written as

$$\chi_{\sigma\tau}(\mathbf{r}, \mathbf{r}', t - t') = \frac{\theta(t - t')}{i\hbar} \sum_{k \neq 0} \left[ \langle \Psi_0 | \hat{n}_{\sigma}(\mathbf{r}) | \Psi_k \rangle \langle \Psi_k | \hat{n}_{\tau}(\mathbf{r}') | \Psi_0 \rangle \times e^{-i(E_k - E_0)/\hbar(t - t')} - \text{c.c.} \right], \quad (\text{A2})$$

where  $\Psi_k$  and  $E_k$  are the eigenstates and eigenvalues of the interacting many-body system, respectively, with  $k = 0$

referring to the ground state. For a perturbation of the form (6), splitting the time integral in Eq. (A1) into

$$\int_{t_0}^{\infty} dt' = \int_{-\infty}^{\infty} dt' - \int_{-\infty}^{t_0} dt' \quad (\text{A3})$$

yields two contributions to the linear response of the spin density,

$$n_{\sigma}^{(1)}(\mathbf{r}, t) = \left[ n_{\sigma}^{(+)}(\mathbf{r}) e^{-i\omega t} + \text{c.c.} \right] e^{\eta t} - \left[ \tilde{n}_{\sigma}^{(+)}(\mathbf{r}, t) e^{-i\omega t_0} + \text{c.c.} \right] e^{\eta t_0} \quad (\text{A4})$$

with

$$n_{\sigma}^{(+)}(\mathbf{r}) = \sum_{k \neq 0} \left[ \frac{\langle \Psi_0 | \hat{V}_{\text{ext}}^{(+)} | \Psi_k \rangle \langle \Psi_k | \hat{n}_{\sigma}(\mathbf{r}) | \Psi_0 \rangle}{E_0 - E_k - \hbar(\omega + i\eta)} - \frac{\langle \Psi_0 | \hat{n}_{\sigma}(\mathbf{r}) | \Psi_k \rangle \langle \Psi_k | \hat{V}_{\text{ext}}^{(+)} | \Psi_0 \rangle}{E_k - E_0 - \hbar(\omega + i\eta)} \right], \quad (\text{A5})$$

$$\tilde{n}_{\sigma}^{(+)}(\mathbf{r}, t) = \sum_{k \neq 0} \left[ \frac{\langle \Psi_0 | \hat{V}_{\text{ext}}^{(+)} | \Psi_k \rangle \langle \Psi_k | \hat{n}_{\sigma}(\mathbf{r}) | \Psi_0 \rangle e^{i \frac{E_k - E_0}{\hbar} (t - t_0)}}{E_0 - E_k - \hbar(\omega + i\eta)} - \frac{\langle \Psi_0 | \hat{n}_{\sigma}(\mathbf{r}) | \Psi_k \rangle \langle \Psi_k | \hat{V}_{\text{ext}}^{(+)} | \Psi_0 \rangle e^{-i \frac{E_k - E_0}{\hbar} (t - t_0)}}{E_k - E_0 - \hbar(\omega + i\eta)} \right], \quad (\text{A6})$$

and

$$\hat{V}_{\text{ext}}^{(+)} = \sum_{\sigma} \int d^3r v_{\text{ext},\sigma}^{(+)}(\mathbf{r}) \hat{n}_{\sigma}(\mathbf{r}). \quad (\text{A7})$$

The first term in Eq. (A4) has the desired simple form of Eq. (7), but the second term has a much more complicated time-dependence containing oscillations at every eigenfrequency of the system that can be excited by  $\hat{V}_{\text{ext}}^{(+)}$ . For a perfectly monochromatic perturbation ( $\eta = 0$ ), all the contributions to (A4) have a constant amplitude, so these additional switch-on terms will never become negligible. For  $\eta > 0$ , however, the ratio between the amplitudes of the switch-on contribution and the desired terms falls off exponentially in time.

This behavior has a simple physical interpretation: The amplitude of the perturbation, as given by Eq. (6), increases exponentially, starting from zero at  $t = -\infty$ . However, if the system is still in its ground state at some finite time  $t_0$  and evolves under the influence of  $v_{\text{ext},\sigma}(\mathbf{r}, t)$  only at times  $t > t_0$ , this corresponds to a sharp finite step in the potential at  $t = t_0$  with a height of  $v_{\text{ext},\sigma}(\mathbf{r}, t_0)$ . This step leads to the switch-on terms in  $n_{\sigma}^{(1)}(\mathbf{r}, t)$ . Since an infinitely sharp step has an infinitely broad spectral representation, it can excite every eigenmode of the system, which explains the time-dependence of  $\tilde{n}_{\sigma}^{(+)}(\mathbf{r}, t)$ . For earlier initial times  $t_0$ , this step is smaller since the amplitude of the perturbation has not yet grown as much and it vanishes exponentially if the initial time is moved toward  $-\infty$ .

We always use (6) with a small positive value of  $\eta$  and only consider the long-time, or  $t \gg t_0$ , asymptotics of the solution, defined by the limit  $t_0 \rightarrow -\infty$ , which leads to (7).

By expanding  $v_{\text{Hxc}\sigma}[\{n_{\alpha}\}]$  around the unperturbed density  $n_{\sigma}^{(0)}$  and inserting the perturbation series of  $n_{\sigma}$ , we can

identify the perturbation series of the Hxc potential,

$$v_{\text{Hxc}\sigma}^{(0)}(\mathbf{r}, t) = v_{\text{Hxc}\sigma} \left[ \{n_{\alpha}^{(0)}\} \right](\mathbf{r}, t), \quad (\text{A8})$$

$$v_{\text{Hxc}\sigma}^{(1)}(\mathbf{r}, t) = \sum_{\tau} \int dt' \int d^3r' \frac{\delta v_{\text{Hxc}\sigma}(\mathbf{r}, t)}{\delta n_{\tau}(\mathbf{r}', t')} \Big|_{\{n_{\alpha}^{(0)}\}} n_{\tau}^{(1)}(\mathbf{r}', t'). \quad (\text{A9})$$

Without the perturbation, the exact ground-state density and KS potential do not change with time, and so we have

$$v_{\text{Hxc}\sigma}^{(0)}(\mathbf{r}, t) = v_{\text{Hxc}\sigma}^{(0)}(\mathbf{r}), \quad n_{\sigma}^{(0)}(\mathbf{r}, t) = n_{\sigma}^{(0)}(\mathbf{r}). \quad (\text{A10})$$

The functional derivative in (A9) can be shown at least for the exact potential to depend on  $t$  and  $t'$  only via  $t - t'$ ,<sup>83</sup> i.e.,

$$\frac{\delta v_{\text{Hxc}\sigma}(\mathbf{r}, t)}{\delta n_{\tau}(\mathbf{r}', t')} \Big|_{\{n_{\alpha}^{(0)}\}} = \frac{e^2 \delta(t - t')}{|\mathbf{r} - \mathbf{r}'|} + f_{\text{xc}\sigma\tau} \left[ \{n_{\alpha}^{(0)}\} \right](\mathbf{r}, \mathbf{r}', t - t'). \quad (\text{A11})$$

Equations (A10) and (A11) are properties of the exact potential which we assume to hold also for the approximations used in this work. We note, however, that numerical real-time propagations employing direct potential approximations that are not defined as a functional derivative have been shown to violate these conditions at least in some systems.<sup>61,84,85</sup> Equations (7), (A9), and (A11) lead to (8) and (9).

For the KS description, we have to solve

$$\left[ \hat{h}_{\sigma} + v_{s\sigma}^{(1)}(\mathbf{r}, t) + \mathcal{O}(2) \right] \varphi_{j\sigma}(\mathbf{r}, t) = i\hbar \partial_t \varphi_{j\sigma}(\mathbf{r}, t) \quad (\text{A12})$$

with the initial condition

$$\varphi_{j\sigma}(\mathbf{r}, t_0) = \varphi_{j\sigma}(\mathbf{r}) e^{-i(\varepsilon_{j\sigma}/\hbar)t_0}. \quad (\text{A13})$$

The  $\mathcal{O}(2)$ -terms stem from the perturbation expansion of  $v_{\text{Hxc}\sigma}$ , and the phase in the initial condition has been chosen such that the limit  $t_0 \rightarrow -\infty$  is well defined not only for observables but also for the resulting TD orbitals. Inserting the perturbation series of  $\varphi_{j\sigma}(\mathbf{r}, t)$  and equating same-order terms yields

$$\hat{h}_{\sigma} \varphi_{j\sigma}^{(0)}(\mathbf{r}, t) = i\hbar \partial_t \varphi_{j\sigma}^{(0)}(\mathbf{r}, t), \quad (\text{A14})$$

$$\varphi_{j\sigma}^{(0)}(\mathbf{r}, t_0) = \varphi_{j\sigma}(\mathbf{r}) e^{-i(\varepsilon_{j\sigma}/\hbar)t_0} \quad (\text{A15})$$

for the zero-order contribution, which is solved by

$$\varphi_{j\sigma}^{(0)}(\mathbf{r}, t) = \varphi_{j\sigma}(\mathbf{r}) e^{-i(\varepsilon_{j\sigma}/\hbar)t}. \quad (\text{A16})$$

To the first order, we get Eq. (10) with the initial condition

$$\varphi_{j\sigma}^{(1)}(\mathbf{r}, t_0) = 0. \quad (\text{A17})$$

Projecting onto the unperturbed eigenstate  $\varphi_{k\sigma}(\mathbf{r})$  leads to the ordinary linear differential equation

$$i\hbar \partial_t \langle \varphi_{k\sigma} | \varphi_{j\sigma}^{(1)}(t) \rangle = \varepsilon_{k\sigma} \langle \varphi_{k\sigma} | \varphi_{j\sigma}^{(1)}(t) \rangle + e^{(\eta - i\varepsilon_{j\sigma}/\hbar)t} \times \langle \varphi_{k\sigma} | \left[ \left( v_{\text{ext},\sigma}^{(+)} + v_{\text{Hxc}\sigma}^{(+)} \right) e^{-i\omega t} + \text{c.c.} \right] | \varphi_{j\sigma} \rangle, \quad (\text{A18})$$

$$\langle \varphi_{k\sigma} | \varphi_{j\sigma}^{(1)}(t_0) \rangle = 0, \quad (\text{A19})$$

which can readily be integrated and used to construct  $\varphi_{j\sigma}^{(1)}(\mathbf{r}, t)$  from an eigenstate expansion, resulting in

$$\varphi_{j\sigma}^{(1)}(\mathbf{r}, t) = \sum_k \varphi_{k\sigma}(\mathbf{r}) e^{-i(\varepsilon_{k\sigma}/\hbar)t} \langle \varphi_{k\sigma} | e^{-i\frac{\varepsilon_{j\sigma} - \varepsilon_{k\sigma}}{\hbar} t'} e^{\eta t'} \times \left[ \frac{\left( v_{\text{ext},\sigma}^{(+)} + v_{\text{Hxc}\sigma}^{(+)} \right) e^{-i\omega t'}}{\varepsilon_{j\sigma} - \varepsilon_{k\sigma} + \hbar(\omega + i\eta)} + \frac{\left( v_{\text{ext},\sigma}^{(+)} + v_{\text{Hxc}\sigma}^{(+)} \right)^* e^{i\omega t'}}{\varepsilon_{j\sigma} - \varepsilon_{k\sigma} - \hbar(\omega + i\eta)^*} \right] \Big|_{t_0}^t | \varphi_{j\sigma} \rangle. \quad (\text{A20})$$

By separating the  $k = j$ - and  $k \neq j$ -terms and taking the limit  $t_0 \rightarrow -\infty$ , we arrive at Eqs. (12)–(14), which, together with (A16), lead to Eqs. (15) and (16).

Note that in our derivation, letting the perturbation (and thereby also the solution) increase exponentially was necessary to meet a reasonable initial condition while having the long-time asymptotics of the solutions free of any unwanted switch-on contributions.

Factoring out the exponential  $e^{-i\varepsilon_{j\sigma}^{(1)}(t)}$  in Eq. (15) has been claimed in Ref. 44 to have two consequences: The possibility of describing the linear response of the remainder of the KS orbital by the two time-independent Fourier components  $\varphi_{j\sigma}^{(\pm)}$  and the orthogonality condition of Eq. (14). The latter is obvious since the  $\varepsilon_{j\sigma}^{(1)}(t)$ -term gives rise to the projector on the rhs of the Sternheimer equations, which ensures that the solutions of these equations obey Eq. (14). Within our derivation, this is just the result of us deliberately separating the contributions orthogonal and proportional to  $\varphi_{j\sigma}$  in Eq. (A20), where the  $k = j$ -term yields the  $\varepsilon_{j\sigma}^{(1)}(t)$ -contribution to Eq. (12), while the  $k \neq j$ -terms are compiled into  $\varphi_{j\sigma}^{(\pm)}$ .

As for the other claim, Eq. (12) shows that the linear response of the full TD orbital (including the phase factor  $e^{-i\varepsilon_{j\sigma}^{(1)}(t)}$ ) contains, apart from the Fourier components  $\varphi_{j\sigma}^{(\pm)}$ , also a TD contribution  $\propto \varepsilon_{j\sigma}^{(1)}(t)$ . If the time-dependence of this term was unknown, then one might fear that it could spoil the Fourier representability of the orbitals. However, from Eq. (13), we see that Eq. (12) can be recast as

$$\varphi_{j\sigma}^{(1)}(\mathbf{r}, t) = \left[ \tilde{\varphi}_{j\sigma}^{(+)}(\mathbf{r}) e^{-i\omega t} + \tilde{\varphi}_{j\sigma}^{(-)*}(\mathbf{r}) e^{i\omega t} \right] e^{(\eta - i\varepsilon_{j\sigma}/\hbar)t}, \quad (\text{A21})$$

where the Fourier component orbitals

$$\tilde{\varphi}_{j\sigma}^{(\pm)}(\mathbf{r}) = \varphi_{j\sigma}^{(\pm)}(\mathbf{r}) \pm \varphi_{j\sigma}(\mathbf{r}) \frac{\langle \varphi_{j\sigma} | v_{\text{ext},\sigma}^{(+)} + v_{\text{Hxc}\sigma}^{(+)} | \varphi_{j\sigma} \rangle}{\hbar(\omega + i\eta)} \quad (\text{A22})$$

no longer obey the orthogonality condition of Eq. (14) but also clearly do not depend on time.

The derivation given above is based on the density response (A4) and (A5) constructed from the exact many-body response function, so it gives the correct time-dependence of the exact density, KS potential, and orbitals. In practical calculations, both the GS properties and the xc potential response  $v_{\text{xc}\sigma}^{(+)}$  have to be constructed from an approximation to  $v_{\text{xc}\sigma}$ . In general, one can even use two different approximations for the ground-state calculation and for the construction of  $v_{\text{xc}\sigma}^{(+)}$ . This corresponds to constructing the KS eigenvalue and the

coupling matrix in the well-known Casida formalism from different functionals. While it is straightforward to just use Eq. (17) as derived for the exact TDDFT and insert approximations *a posteriori*, it is helpful to know whether the resulting approximate linear response scheme is still equivalent to propagating the TDKS equations employing an approximate xc potential, which is what we want to investigate in the following paragraphs.

For the general case of a propagation using different approximations for ground-state and response properties, we use the scheme proposed by Marques *et al.*:<sup>3</sup>

After performing a ground-state calculation with some xc approximation  $\mathcal{A}$ , one evaluates both the xc potentials corresponding to  $\mathcal{A}$  and to some other approximation  $\mathcal{B}$  at the GS density  $n_{\sigma,\mathcal{A}}(\mathbf{r})$ , yielding  $v_{xc\sigma,\mathcal{A}}[n_{\sigma,\mathcal{A}}](\mathbf{r})$  and  $v_{xc\sigma,\mathcal{B}}[n_{\sigma,\mathcal{A}}](\mathbf{r})$ . Then in a propagation starting from the ground state of  $\mathcal{A}$ , the TD potential is constructed as

$$v_{xc\sigma,\mathcal{A}\mathcal{B}}(\mathbf{r}, t) = v_{xc\sigma,\mathcal{B}}(\mathbf{r}, t) - v_{xc\sigma,\mathcal{B}}[n_{\sigma,\mathcal{A}}](\mathbf{r}) + v_{xc\sigma,\mathcal{A}}[n_{\sigma,\mathcal{A}}](\mathbf{r}),$$

replacing the zero-order contributions in the TD potential of functional  $\mathcal{B}$  by those of functional  $\mathcal{A}$ .

This construction obeys the conditions (A10) and (A11) if  $\mathcal{A}$  obeys (A10) and  $\mathcal{B}$  obeys (A11), which we assume to hold in the following.

To work out the time-dependence of the quantities resulting from this propagation, we can no longer rely on the exact TD density. Instead, we try to solve this problem by a self-consistency iteration.

We guess the time-dependence of the density up to first order in the perturbation while letting it have an arbitrary position-dependence. From this guess, we derive the time-dependence of the xc potential, the KS Hamiltonian, and the orbitals up to first order. If the density resulting from these orbitals differs from our guess only in its spatial variation, then further iterations of this self-consistency process will only change the position-dependence of the involved quantities, while their time-dependence is already self-consistent.

Our initial guess for a propagation starting from the ground state of functional  $\mathcal{A}$  is that to order zero, the density is time-independent and thus at all times given by  $n_{\sigma,\mathcal{A}}(\mathbf{r})$ , while its linear response has the exact time-dependence given by Eq. (7) but with an arbitrary  $n_{\sigma}^{(+)}(\mathbf{r})$ .

From Eqs. (A8)–(A11), we then see that the zero-order contribution to the KS Hamiltonian is just the GS Hamiltonian of functional  $\mathcal{A}$  at all times, while its first-order contribution

$$v_{s\sigma,\mathcal{A}\mathcal{B}}^{(1)}(\mathbf{r}, t) = \left[ v_{s\sigma,\mathcal{A}\mathcal{B}}^{(+)}(\mathbf{r}) e^{-i\omega t} + \text{c.c.} \right] e^{i\eta t}$$

has the same time-dependence as for the exact density and an arbitrary position-dependence of  $v_{s\sigma,\mathcal{A}\mathcal{B}}^{(+)}$  corresponding to our arbitrary initial guess for  $n_{\sigma}^{(+)}$ .

Next, the TDKS equations with the initial condition  $\varphi_{j\sigma}(\mathbf{r}, t_0) = \varphi_{j\sigma,\mathcal{A}}(\mathbf{r}) e^{-i(\varepsilon_{j\sigma,\mathcal{A}}/\hbar)t_0}$  (where  $\varphi_{j\sigma,\mathcal{A}}$  and  $\varepsilon_{j\sigma,\mathcal{A}}$  are the GS orbitals and eigenvalues calculated from functional  $\mathcal{A}$ , respectively) can be treated in the same way as was

shown above for the exact case, where the eigenstate expansion is now of course performed with respect to the orbitals  $\varphi_{k\sigma,\mathcal{A}}$ .

The zero-order solutions

$$\varphi_{j\sigma}^{(0)}(\mathbf{r}, t) = \varphi_{j\sigma,\mathcal{A}}(\mathbf{r}) e^{-i(\varepsilon_{j\sigma,\mathcal{A}}/\hbar)t}$$

indeed yield the density  $n_{\sigma,\mathcal{A}}(\mathbf{r})$ , so our initial guess is completely self-consistent to order zero. The linear response of the orbitals for  $t_0 \rightarrow -\infty$  is given by Eqs. (12)–(14) but with the exact GS orbitals and eigenvalues replaced by  $\varphi_{j\sigma,\mathcal{A}}$  and  $\varepsilon_{j\sigma,\mathcal{A}}$ , respectively, and with the position-dependence of  $\varphi_{j\sigma}^{(\pm)}$  resulting from the arbitrary initial  $n_{\sigma}^{(+)}$ .

Thus, the linear response of the density calculated from these orbitals turns out to have the same time-dependence but possibly a different position-dependence as our initial guess.

Since the time-dependence that we have just shown to be self-consistent is the same as for the exact density and since we did not need the detailed position-dependence of  $n_{\sigma}^{(+)}$ ,  $v_{\text{Hxc}\sigma}^{(+)}$ , or  $\varphi_{j\sigma}^{(\pm)}$  to derive Eq. (17), it follows that the Sternheimer equations correctly describe the linear regime of the TDKS equations even when approximate functionals are used as long as these meet the conditions (A10) and (A11).

Contributions to  $\varphi_{j\sigma}^{(\pm)}$  proportional to occupied GS orbitals cancel upon insertion into Eq. (16) (which has been noted earlier for the spin-independent case<sup>29</sup>), so if one is only interested in calculating the spin-density response using an explicitly spin-density-dependent approximation to  $v_{\text{Hxc}\sigma}$ , one can replace the projector  $\hat{Q}_{j\sigma}$  in (17) by  $\hat{Q}_{\sigma} := \prod_j^{\text{occ}} \hat{Q}_{j\sigma}$ . As can be seen from Eq. (A20), the contribution of the  $k$ th GS orbital to  $\varphi_{j\sigma}^{(1)}$  has the denominator  $\varepsilon_{j\sigma} - \varepsilon_{k\sigma} + \hbar(\pm\omega + i\eta)$ . Since the energy differences  $\varepsilon_j - \varepsilon_k$  are usually smaller for two occupied orbitals than for an occupied and an unoccupied orbital, the unnecessary occupied contributions can become large at least for small values of  $\omega$  and  $\eta$ . Therefore, it has been argued that the removal of these contributions might increase numerical stability and efficiency. We have implemented and tested both versions of the projector without noticing any instabilities for the systems considered in this work, so we are using  $\hat{Q}_{j\sigma}$  as in Eq. (17) in the calculations presented here. Note that the cost for applying  $\hat{Q}_{\sigma}$  scales with  $(N_{\uparrow}^2 + N_{\downarrow}^2)N_g$  in contrast to the  $(N_{\uparrow} + N_{\downarrow})N_g$ -scaling of applying only  $\hat{Q}_{j\sigma}$ , where  $N_g$  is the number of grid points and  $N_{\sigma}$  is the number of electrons with spin  $\sigma$ .

## APPENDIX B: COMPLEX GROUND-STATE ORBITALS

In some cases, e.g., when spin-orbit coupling is taken into account, the ground-state orbitals cannot be chosen to be real. As can be seen from the derivation presented in Appendix A, the assumption that the orbitals are real is not yet exploited in Eq. (A20) and only serves to simplify the presentation of the scheme in terms of the Fourier component orbitals  $\varphi_{j\sigma}^{(\pm)}(\mathbf{r})$ . Thus, not much has to be changed when complex orbitals are allowed: The orthogonality constraints (14) have to be replaced by

$$\langle \varphi_{j\sigma} | \varphi_{j\sigma}^{(+)} \rangle = \int d^3r \varphi_{j\sigma}^*(\mathbf{r}) \varphi_{j\sigma}^{(+)}(\mathbf{r}) = 0 \quad (\text{B1})$$

and

$$\langle \varphi_{j\sigma}^* | \varphi_{j\sigma}^{(-)} \rangle = \int d^3r \varphi_{j\sigma}(\mathbf{r}) \varphi_{j\sigma}^{(-)}(\mathbf{r}) = 0 \quad (\text{B2})$$

and the right-hand side of the  $\varphi_{j\sigma}^{(-)}$ -Sternheimer equation (17) has to be changed to

$$-\left[ v_{\text{ext},\sigma}^{(+)}(\mathbf{r}) + v_{\text{Hxc}\sigma}^{(+)}(\mathbf{r}) - \int d^3r' |\varphi_{j\sigma}(\mathbf{r}')|^2 \right. \\ \left. \times \left( v_{\text{ext},\sigma}^{(+)}(\mathbf{r}') + v_{\text{Hxc}\sigma}^{(+)}(\mathbf{r}') \right) \right] \varphi_{j\sigma}^*(\mathbf{r}), \quad (\text{B3})$$

where the subtraction of the integral term in brackets replaces the projector  $\hat{Q}_{j\sigma}$ , while the equation for  $\varphi_{j\sigma}^{(+)}$  does not change.

Finally, Eq. (A22) for  $\tilde{\varphi}_{j\sigma}^{(-)}$  has to be replaced by

$$\tilde{\varphi}_{j\sigma}^{(-)}(\mathbf{r}) = \varphi_{j\sigma}^{(-)}(\mathbf{r}) - \varphi_{j\sigma}^*(\mathbf{r}) \frac{\langle \varphi_{j\sigma} | v_{\text{ext},\sigma}^{(+)} + v_{\text{Hxc}\sigma}^{(+)} | \varphi_{j\sigma} \rangle}{\hbar(\omega + i\eta)}. \quad (\text{B4})$$

Since the response orbitals  $\varphi_{j\sigma}^{(\pm)}(\mathbf{r})$  and potentials  $v_{\text{Hxc}\sigma}^{(\pm)}(\mathbf{r})$  are complex even if the ground-state orbitals are chosen real, the right-hand sides of the Sternheimer equations are complex quantities anyway, and our implementation already uses complex arithmetics. Thus, complex ground-state orbitals do not pose any difficulty at all and only lead to a slightly more complicated appearance of the basic equations.

## APPENDIX C: EVALUATION OF EXCITATION SPECTRA

### 1. Optical absorption spectra

To simulate an optical absorption experiment, we describe the incoming light wave in the dipole approximation by a spin-independent potential

$$v_{\text{ext}}(\mathbf{r}, t) = e\mathbf{E}(t)\mathbf{r} \quad (\text{C1})$$

and calculate the linear response of the electric dipole moment

$$\boldsymbol{\mu}^{(1)}(t) = -e \int d^3r \mathbf{r} n^{(1)}(\mathbf{r}, t). \quad (\text{C2})$$

The dipole moment is connected to the applied homogeneous electric field  $\mathbf{E}(t)$  by the time-dependent linear polarizability tensor  $\underline{\underline{\alpha}}(t)$  according to

$$\boldsymbol{\mu}^{(1)}(t) = \int dt' \underline{\underline{\alpha}}(t-t') \mathbf{E}(t'). \quad (\text{C3})$$

If we approximate a monochromatic wave by choosing the electric field to have a time-dependence of the form of Eq. (6) with a small positive  $\eta$ , we can apply the Sternheimer scheme to calculate the density response and find that

$$\boldsymbol{\mu}^{(+)} := -e \int d^3r \mathbf{r} n^{(+)}(\mathbf{r}) = \underline{\underline{\alpha}}(\omega + i\eta) \mathbf{E}^{(+)}, \quad (\text{C4})$$

where

$$\underline{\underline{\alpha}}(\omega + i\eta) := \int dt \underline{\underline{\alpha}}(t) e^{i(\omega+i\eta)t} \quad (\text{C5})$$

approaches the frequency-dependent polarizability  $\underline{\underline{\alpha}}(\omega)$  for small  $\eta$ . These equations allow to extract the polarizability tensor from the results of Sternheimer calculations: If the applied field points, e.g., in the  $x$ -direction,

$\mathbf{E}^{(+)} = E^{(+)} \hat{\mathbf{e}}_x$ , then evaluating the  $y$ -component of the dipole response  $\mu_y^{(+)} = -e \int d^3r y n^{(+)}(\mathbf{r})$  yields the tensor component

$$\alpha_{yx}(\omega + i\eta) = \mu_y^{(+)} / E^{(+)}. \quad (\text{C6})$$

To construct the full tensor  $\underline{\underline{\alpha}}$  from these equations using the Sternheimer approach, one has to perform three linear response calculations with electric fields pointing in three independent directions.

The quantity of interest is usually the absorption cross section  $\sigma(\omega)$  that is defined in terms of the imaginary part of the polarizability tensor as

$$\sigma(\omega) = \frac{4\pi\omega}{3c} \Im \left[ \text{Tr} \underline{\underline{\alpha}}(\omega) \right]. \quad (\text{C7})$$

### 2. General excitations

The frequency of the applied perturbation enters the Sternheimer equations only as a parameter. Solving Eq. (17) for different frequencies yields  $n_{\sigma}^{(+)}$  as a function of  $\omega$ . From (A5), we see that this function is a sum of terms that depend on the frequency only through their denominators  $\pm\Omega_k - \omega - i\eta$ , where  $\hbar\Omega_k = E_k - E_0 > 0$  are the system's excitation energies. For vanishing  $\eta$ , each of these terms represents a pole of  $n_{\sigma}^{(+)}$  at  $\omega = \pm\Omega_k$  as long as the corresponding matrix element of  $\hat{V}_{\text{ext}}^{(+)}$  in the numerator does not vanish. If  $v_{\text{ext},\sigma}^{(+)}(\mathbf{r})$  as well as the eigenstates  $\Psi_k$  of the interacting many-body Hamiltonian are chosen to be real, then the imaginary parts of these terms become Lorentz-shaped for  $\eta > 0$ , so the imaginary part of the density response  $\Im[n_{\sigma}^{(+)}$ ] becomes a superposition of Lorentzians with the extrema at the  $\hat{V}_{\text{ext}}^{(+)}$ -allowed excitation energies and with the half-widths at half-maximum all given by  $\eta$ .

By plotting the imaginary parts of various moments of the spin-density response for different forms of  $v_{\text{ext},\sigma}^{(+)}$  as functions of  $\omega$  and either directly identifying the extrema (for well-separated lines) or fitting a superposition of Lorentzians with fixed widths to the plotted data, we can thus find excitation energies for different kinds of transitions. By perturbing, e.g., with a quadratic function of the coordinates

$$v_{\text{ext},\sigma}^{(+)}(\mathbf{r}) = \sum_{i,j=1}^3 c_{ij} x_i x_j, \quad (\text{C8})$$

where  $c_{ij}$  are constants, and plotting the second moments of the density, we find the energies of quadrupole excitations.

The numerator of each Lorentzian contributing to an  $l$ th moment of  $n_{\sigma}^{(+)}$  (where an  $l$ th moment is defined as  $\int d^3r x^a y^b z^c n_{\sigma}^{(+)}(\mathbf{r})$  with  $a, b, c \in \mathbb{N}_0$  and  $a + b + c = l$ ) contains the matrix elements of both  $\hat{V}_{\text{ext}}^{(+)}$  and  $\int d^3r x^a y^b z^c \hat{n}_{\sigma}(\mathbf{r})$ . For a spatially constant perturbation  $v_{\text{ext},\sigma}^{(+)}(\mathbf{r}) = c_{\sigma}$  or for  $l = 0$ , these operators reduce to the integrals of the spin-density operators

$$\int d^3r \hat{n}_{\sigma}(\mathbf{r}) = \frac{1}{2} \left[ \hat{N} + \text{sgn}(\sigma) \frac{2}{\hbar} \hat{S}_z \right], \quad (\text{C9})$$

where  $\hat{N}$  is the electron number operator and  $\hat{S}_z$  is the  $z$ -component of the total spin. We are neglecting spin-orbit

coupling, so the eigenstates of the many-body Hamiltonian can be chosen as eigenstates of the  $z$ -component and the square of the total spin  $\hat{S}$ , leading to vanishing matrix elements of  $\hat{N}$  and  $\hat{S}_z$  between  $\Psi_0$  and  $\Psi_k$ .

Therefore, constant contributions to  $v_{\text{ext},\sigma}^{(+)}$  do not affect  $n_{\sigma}^{(+)}$ , and the lowest nontrivial moment to analyze is the dipole moment.

### 3. Singlet vs. triplet excitations

Since the states  $\Psi_k$  can be chosen as eigenstates of  $\hat{S}_z$  and  $\hat{S}^2$  and since a scalar external field  $\phi$ , which does not act on the spin degrees of freedom, does not have non-vanishing matrix elements between different spin eigenstates, we see from Eq. (A5) that it will not lead to transitions between, e.g., the singlet ground state and a triplet excited state. The magnetic field contribution to (4) does act on the spin variables and so it can cause additional excitations, possibly of triplet character.

The  $\phi$  and  $B$  contributions to  $v_{\text{ext},\sigma}$  are an even and an odd function of  $\sigma$ , respectively. For a spin-independent ground state, the response function must have the symmetries  $\chi_{\uparrow\uparrow} = \chi_{\downarrow\downarrow}$  and  $\chi_{\uparrow\downarrow} = \chi_{\downarrow\uparrow}$ ,<sup>38</sup> so the response of the spin densities to each of these contributions must also be even and odd, respectively. But Eq. (A5) shows that the spin-dependence of  $n_{\sigma}^{(+)}$  near an excitation frequency  $\hbar\omega \approx E_k - E_0$  is determined only by the ground state and the target state  $\Psi_k$ , so  $\phi$  and  $B$  must lead to excitations to different target states and there is no transition that can be induced by both a scalar and a magnetic field. Since no singlet transition that can be excited by a scalar potential of any form will thus appear in the spectrum of a magnetic perturbation, we interpret the magnetically active, odd-spin transitions as triplet excitations.

By choosing a perturbation that is neither an even nor an odd function of  $\sigma$  and switching variables from the spin densities to the total density and the magnitude of the magnetization

$$m^{(+)}(\mathbf{r}) = -\mu_B (n_{\uparrow}^{(+)}(\mathbf{r}) - n_{\downarrow}^{(+)}(\mathbf{r})), \quad (\text{C10})$$

we can get separate singlet and triplet spectra out of a single run over frequencies. For instance, a dipole-like perturbation that vanishes for  $\sigma = \downarrow$  (as was proposed for a real-time propagation scheme in Refs. 30 and 86),

$$v_{\text{ext},\sigma}^{(+)}(\mathbf{r}) = \delta_{\sigma\uparrow}(\mathbf{v} \cdot \mathbf{r}), \quad (\text{C11})$$

where  $\mathbf{v}$  is a homogeneous field, has both a scalar and a magnetic contribution. The linear response of the spin densities will be the sum of the responses to both of them, but due to their symmetries the response to the  $\phi$  and the  $B$  contribution will cancel in the magnetization and the total density, respectively. By solving the Sternheimer equation for this potential and different frequencies and plotting the first moments of  $n^{(+)}$  and  $m^{(+)}$  as functions of  $\omega$ , we can construct two separate spectra containing only the dipole-allowed singlet and triplet excitations, respectively.

In Eq. (4), the magnetic field can be spatially inhomogeneous but is assumed to point in the same direction everywhere. A further extension that one may think about is the one to

magnetic fields with a spatially varying orientation. In principle, one may argue that such situations may better be covered by current-density functional theory<sup>87</sup> or spin-current density functional theory.<sup>88</sup> The reasons are that first, the particle density and the three components of the current density naturally correspond to the scalar potential and the three components of a vector potential, and second, spin-current density functional theory provides all the degrees of freedom needed for a complete description of magnetic effects. In practice, one may try to take into account spatially varying orientations of  $\mathbf{B}$  in the Sternheimer scheme by setting up equations for the linear response of the single-particle density matrix, trying to establish an analogy to the equations derived for noncollinear spin-density functional theory.<sup>89</sup> Working out the corresponding equations, however, goes beyond the scope of the present paper.

### APPENDIX D: COMPLEX SYMMETRIC CONJUGATE GRADIENT ALGORITHM

The conjugate gradient algorithm is a well-known, efficient method for solving large, sparse linear systems, but it requires hermitian matrices.<sup>55,90</sup> While the KS Hamiltonian is represented by a real-valued symmetric matrix on our real-space grid and the constant shift by  $-\varepsilon_{j\sigma} \mp (\omega + i\eta)$  only affects the diagonal elements of this matrix, this shift is complex for  $\eta \neq 0$ , resulting in a complex non-hermitian, yet still symmetric matrix  $\underline{\underline{A}}$ . Methods like the biconjugate gradient (BiCG) algorithm<sup>91,92</sup> or its stabilized version can in principle be applied to non-hermitian problems, but they usually need more iteration steps and two matrix-vector multiplications per step (as opposed to just one such multiplication per step in the CG algorithm). The CG can be derived from the BiCG by inserting the hermiticity property  $\underline{\underline{A}}^H = \underline{\underline{A}}$ , which makes one of the two multiplications per step redundant and typically also reduces the number of steps needed to converge.

By inserting the symmetry property  $\underline{\underline{A}}^T = \underline{\underline{A}}$  of our complex matrix into the BiCG, we arrive at an algorithm that differs from the CG only in that the usual inner vector products  $\langle \underline{v}, \underline{w} \rangle = \underline{v}^H \cdot \underline{w}$  are replaced by symmetric products  $\langle \underline{v}, \underline{w} \rangle_s = \underline{v}^T \cdot \underline{w}$  for complex vectors  $\underline{v}$  and  $\underline{w}$ .

This algorithm turns out to be considerably more efficient and stable than the BiCGstab when applied to the Sternheimer equations.

### APPENDIX E: CONVERGENCE AND NUMERICAL ACCURACY OF EXCITATION ENERGIES

This appendix only deals with the numerical errors of excitation energies, not with the performance of approximate functionals or the influence of molecular geometry. Therefore, we only consider ALDA results for CO with a bond length of 1.1283 Å.

In our approach, the accuracy of the results is influenced mostly by three parameters: The radius of our simulation sphere, the spacing of the real-space grid, and the cutoff radius of the pseudopotential. By increasing the sphere radius and decreasing the grid spacing, we can systematically converge

our results with respect to the grid, with the excitation energies decreasing almost monotonically toward their converged results during the process. With a radius of  $23 a_0$  and a spacing of  $0.28 a_0$ , further increasing the grid size changes the excitation energies of CO presented in Sec. IV B by only a few meV.

While decreasing the cutoff radius of the pseudopotential also leads to a roughly monotonic decrease in the energies, it is harder to tell whether this actually improves our results in a systematic fashion. We therefore do not attempt to converge our results with respect to the pseudopotential but merely perform test calculations for several radii to be able to estimate the influence of the potential on the excitation energies. In general, we find that changing the pseudopotential can move the energies by several hundredths of an eV. For instance, decreasing the radii from the ones used in Sec. IV B to  $1.09 a_0$  for both C and O moves the first  $^1\Pi$ ,  $^3\Pi$ , and  $^3\Sigma^+$  excitations from 8.22 eV, 5.92 eV, and 8.28 eV to 8.17 eV, 5.89 eV, and 8.24 eV, respectively.

We note that typically the excitations at lower energies are more sensitive to changes in the grid spacing, while higher excitations are more strongly affected by the sphere radius due to the larger spatial extent of the corresponding excited states. Thus, for the sake of numerical efficiency, one might consider using different grids for different frequency ranges of a spectrum. In this work, however, all spectra were calculated with a single grid for the whole range, which therefore had to be optimized simultaneously for both high- and low-frequency excitations.

To investigate the convergence and accuracy of the reference calculations<sup>80</sup> and, more generally, of the methods employing Gaussian basis sets, we performed several calculations with the TURBOMOLE<sup>93</sup> program package using different basis sets and compared the results with each other and with the values from Ref. 80. The excitation energies are listed in Table II.

Dunning's<sup>94,95</sup> augmented, correlation-consistent basis sets are the largest ones considered here and specifically constructed for correlated post-Hartree-Fock calculations where a large number of virtual orbitals are needed. Therefore, they

can be expected to yield better results for excited states than the Pople<sup>96–98</sup> basis sets 6-31G\*–6-311++G\*\* and are routinely employed in linear response calculations.<sup>99–102</sup> Upon moving from the triple valence aug-cc-pVTZ to the largest aug-cc-pV6Z, some of the excitations (the  $\Sigma^-$ ,  $\Delta$ , the first  $\Pi$ , and the first  $^3\Sigma^+$ ) converge to within 3 meV at the quadruple-zeta level and to within 1 meV for the aug-cc-pV5Z basis, while others still change by more than 0.1 eV from the 5Z to the 6Z basis. Obviously, the convergence of the basis set results has a stronger dependence on the excitation type than the grid methods. The  $^1\Sigma^+$  and  $^1\Pi$  excitations, e.g., are both converged to within a few hundredths of an eV with respect to the grid and pseudopotential with the parameters given above, but while the basis set results for the  $^1\Pi$  energy differ by only 1 meV between the aug-cc-pV5Z and aug-cc-pV6Z basis, the  $^1\Sigma^+$  energies for these two basis sets differ by 0.1 eV. The relatively large influence of the pseudopotential on our Sternheimer results suggests that a proper treatment of core electrons might become important at the level of accuracy considered here; however, replacing the valence-only aug-cc-pV5Z basis by the weighted core-valence aug-cc-pwCV5Z basis set has almost no effect on the excitation energies.

In Ref. 80, only results for excitation energies that can be converged with Dunning's basis sets are given. The converged aug-cc-pV6Z results are lower than the 6-311(2+, 2+)G\*\* reference values by 0.01–0.03 eV for all but the first  $^3\Pi$  excitation, indicating that the latter are not converged to meV accuracy.

Even within the Pople-type basis sets, which include the 6-311(2+, 2+)G\*\* used in Ref. 80, most of the energies do not seem to converge to an accuracy of less than a few tenths of an eV and some of them vary by up to 6 eV. While increasing the number of diffuse functions from the 6-311++G\*\* to the 6-311(2+, 2+)G\*\* basis has little influence on the results (at least for the excitations reported in Ref. 80), going from double to triple valence sets or adding polarization functions changes the results significantly. Furthermore, while all excitation energies decrease monotonically from the aug-cc-pVTZ to the aug-cc-pV6Z basis, even the aug-cc-pVTZ energies are

TABLE II. Vertical excitation energies (in eV) for several low-lying singlet and triplet excited states of CO using the ALDA, the bond length of  $1.1283 \text{ \AA}$ ,<sup>80</sup> and different basis sets. Except for the values in the last row, all energies are calculated with the TURBOMOLE<sup>93</sup> program package.

Basis set	$^1\Sigma^+$	$^1\Sigma^+$	$^1\Sigma^-$	$^1\Pi$	$^1\Pi$	$^1\Delta$	$^3\Sigma^+$	$^3\Sigma^+$	$^3\Sigma^-$	$^3\Pi$	$^3\Pi$	$^3\Delta$
6-31G*	14.616	16.528	10.006	08.401	13.461	10.529	08.490	14.430	10.006	05.979	11.481	09.295
6-311G	14.142	15.996	10.031	08.229	13.357	10.596	08.470	13.505	10.031	05.843	11.095	09.323
6-311G**	14.061	15.696	09.981	08.355	13.387	10.484	08.475	13.613	09.981	06.022	11.466	09.277
6-311G(2df, 2pd)	13.667	15.254	09.978	08.337	13.301	10.461	08.480	13.202	09.978	06.023	11.458	09.262
6-311++G**	10.025	10.075	09.889	08.200	10.835	10.359	08.427	09.603	09.889	05.965	10.724	09.214
def2-QZVP	11.414	12.781	09.881	08.201	12.249	10.338	08.423	11.031	09.881	05.967	11.382	09.188
aug-cc-pVTZ	09.806	10.412	09.875	08.173	10.453	10.326	08.423	09.470	09.875	05.968	10.370	09.189
aug-cc-pVQZ	09.690	10.226	09.870	08.165	10.278	10.320	08.418	09.374	09.870	05.964	10.212	09.182
aug-cc-pV5Z	09.573	10.022	09.868	08.163	10.088	10.317	08.415	09.278	09.868	05.962	10.040	09.180
aug-cc-pwCV5Z	09.573	10.022	09.868	08.163	10.088	10.317	08.415	09.278	09.868	05.962	10.040	09.179
aug-cc-pV6Z	09.476	09.886	09.867	08.162	09.964	10.317	08.415	09.206	09.867	05.962	09.926	09.179
6-311(2+, 2+)G** <sup>a</sup>	...	...	9.89	8.19	...	...	8.42	...	9.89	5.95	...	9.21

<sup>a</sup>Reference 80.

already smaller than every single result from the various Pople basis sets reported here for all excitations except the second  $^1\Sigma^+$  and the first  $^3\Pi$ .

Thus, the small discrepancies between our results presented in Sec. IV B and the reference values can be attributed at roughly equal parts to both our use of pseudopotentials and basis set errors in the reference calculations.

- <sup>1</sup>E. K. U. Gross and W. Kohn, *Phys. Rev. Lett.* **55**, 2850 (1985).
- <sup>2</sup>M. Petersilka, U. J. Gossmann, and E. K. U. Gross, *Phys. Rev. Lett.* **76**, 1212 (1996).
- <sup>3</sup>M. A. L. Marques, A. Castro, and A. Rubio, *J. Chem. Phys.* **115**, 3006 (2001).
- <sup>4</sup>D. Tozer, *J. Chem. Phys.* **119**, 12697 (2003).
- <sup>5</sup>N. T. Maitra, *J. Chem. Phys.* **122**, 234104 (2005).
- <sup>6</sup>N. T. Maitra, F. Zhang, R. J. Cave, and K. Burke, *J. Chem. Phys.* **120**, 5932 (2004).
- <sup>7</sup>C. A. Ullrich and I. V. Tokatly, *Phys. Rev. B* **73**, 235102 (2006).
- <sup>8</sup>G. Vignale, *Phys. Rev. A* **77**, 062511 (2008).
- <sup>9</sup>M. Thiele and S. Kümmel, *Phys. Chem. Chem. Phys.* **11**, 4631 (2009).
- <sup>10</sup>M. Thiele and S. Kümmel, *Phys. Rev. Lett.* **112**, 083001 (2014).
- <sup>11</sup>M. E. Casida and M. Huix-Rotllant, *Annu. Rev. Phys. Chem.* **63**, 287 (2012).
- <sup>12</sup>L. Kronik, T. Stein, S. Refaely-Abramson, and R. Baer, *J. Chem. Theory Comput.* **8**, 1515 (2012).
- <sup>13</sup>A. D. Laurent and D. Jacquemin, *Int. J. Quantum Chem.* **113**, 2019 (2013).
- <sup>14</sup>M. E. Casida, in *Recent Developments and Applications in Density-Functional Theory*, edited by J. M. Seminario (Elsevier Science, Amsterdam, 1996), pp. 391–439.
- <sup>15</sup>K. Yabana and G. F. Bertsch, *Phys. Rev. B* **54**, 4484 (1996).
- <sup>16</sup>M. A. L. Marques, A. Castro, G. F. Bertsch, and A. Rubio, *Comput. Phys. Commun.* **151**, 60 (2003).
- <sup>17</sup>A. Castro, H. Appel, M. Oliveira, C. A. Rozzi, X. Andrade, F. Lorenzen, M. A. L. Marques, E. K. U. Gross, and A. Rubio, *Phys. Status Solidi B* **243**, 2465 (2006).
- <sup>18</sup>M. Mundt and S. Kümmel, *Phys. Rev. B* **76**, 035413 (2007).
- <sup>19</sup>K. Lopata and N. Govind, *J. Chem. Theory Comput.* **7**, 1344 (2011).
- <sup>20</sup>M. Vincendon, P. M. Dinh, P. Romaniello, P.-G. Reinhard, and E. Suraud, *Eur. Phys. J. D* **67**, 97 (2013).
- <sup>21</sup>X. Andrade, D. A. Strubbe, U. De Giovannini, A. H. Larsen, M. J. T. Oliveira, J. Alberdi-Rodriguez, A. Varas, I. Theophilou, N. Helbig, M. J. Verstraete, L. Stella, F. Nogueira, A. Aspuru-Guzik, A. Castro, M. A. L. Marques, and A. Rubio, *Phys. Chem. Chem. Phys.* **17**, 31371 (2015).
- <sup>22</sup>M. R. Provorov and C. M. Isborn, *Int. J. Quantum Chem.* **116**, 739 (2016).
- <sup>23</sup>I. Schelter and S. Kümmel, *J. Chem. Theory Comput.* **14**, 1910 (2018).
- <sup>24</sup>A. Bruner, D. LaMaster, and K. Lopata, *J. Chem. Theory Comput.* **12**, 3741 (2016).
- <sup>25</sup>R. M. Sternheimer, *Phys. Rev.* **84**, 244 (1951).
- <sup>26</sup>S. Baroni, S. De Gironcoli, A. Dal Corso, and P. Giannozzi, *Rev. Mod. Phys.* **73**, 515 (2001).
- <sup>27</sup>S. Y. Savrasov, *Phys. Rev. Lett.* **81**, 2570 (1998).
- <sup>28</sup>J.-I. Iwata, K. Yabana, and G. F. Bertsch, *J. Chem. Phys.* **115**, 8773 (2001).
- <sup>29</sup>X. Andrade, S. Botti, M. A. L. Marques, and A. Rubio, *J. Chem. Phys.* **126**, 184106 (2007).
- <sup>30</sup>M. J. T. Oliveira, A. Castro, M. A. L. Marques, and A. Rubio, *J. Nanosci. Nanotechnol.* **8**, 3392 (2008).
- <sup>31</sup>H. Hübener and F. Giustino, *Phys. Rev. B* **89**, 085129 (2014).
- <sup>32</sup>H. Hübener and F. Giustino, *J. Chem. Phys.* **141**, 044117 (2014).
- <sup>33</sup>K. Cao, H. Lambert, P. G. Radaelli, and F. Giustino, *Phys. Rev. B* **97**, 024420 (2018).
- <sup>34</sup>B. Walker, A. M. Saitta, R. Gebauer, and S. Baroni, *Phys. Rev. Lett.* **96**, 113001 (2006).
- <sup>35</sup>L. Kronik, A. Makmal, M. L. Tiago, M. M. G. Alemany, M. Jain, X. Huang, Y. Saad, and J. R. Chelikowsky, *Phys. Status Solidi Basic Res.* **243**, 1063 (2006).
- <sup>36</sup>P. Hohenberg and W. Kohn, *Phys. Rev.* **136**, B864 (1964).
- <sup>37</sup>W. Kohn and L. J. Sham, *Phys. Rev.* **140**, A1133 (1965).
- <sup>38</sup>U. von Barth and L. Hedin, *J. Phys. C Solid State Phys.* **5**, 1629 (1972).
- <sup>39</sup>M. M. Pant and A. K. Rajagopal, *Solid State Commun.* **10**, 1157 (1972).
- <sup>40</sup>A. K. Rajagopal and J. Callaway, *Phys. Rev. B* **7**, 1912 (1973).
- <sup>41</sup>E. Runge and E. K. U. Gross, *Phys. Rev. Lett.* **52**, 997 (1984).
- <sup>42</sup>K. L. Liu and S. H. Vosko, *Can. J. Phys.* **67**, 1015 (1989).
- <sup>43</sup>L. Lehtovaara and M. A. L. Marques, *J. Chem. Phys.* **135**, 014103 (2011).
- <sup>44</sup>D. A. Strubbe, L. Lehtovaara, A. Rubio, M. A. L. Marques, and S. G. Louie, in *Fundamentals of Time-Dependent Density Functional Theory*, Lecture Notes in Physics, edited by M. A. Marques, N. T. Maitra, F. M. Nogueira, E. Gross, and A. Rubio (Springer Berlin Heidelberg, Berlin, Heidelberg, 2012), Vol. 837, pp. 139–166.
- <sup>45</sup>J. Hutter, *J. Chem. Phys.* **118**, 3928 (2003).
- <sup>46</sup>J. Garhammer, F. Hofmann, R. Armiento, and S. Kümmel, “On the challenge to improve the density response with unusual gradient approximations,” *Eur. Phys. J. B* (to be published).
- <sup>47</sup>M. Mundt, S. Kümmel, B. Huber, and M. Moseler, *Phys. Rev. B* **73**, 205407 (2006).
- <sup>48</sup>N. Troullier and J. L. Martins, *Phys. Rev. B* **43**, 1993 (1991).
- <sup>49</sup>L. Kleinman and D. M. Bylander, *Phys. Rev. Lett.* **48**, 1425 (1982).
- <sup>50</sup>D. Hofmann, T. Körzdörfer, and S. Kümmel, *Phys. Rev. Lett.* **108**, 146401 (2012).
- <sup>51</sup>D. Hofmann, “Charge and excitation-energy transfer in time-dependent density functional theory,” Doctoral thesis, University of Bayreuth, 2012.
- <sup>52</sup>T. Ando, *Z. Phys. B: Condens. Matter Quanta* **26**, 263 (1977).
- <sup>53</sup>M. J. Stott and E. Zaremba, *Phys. Rev. A* **21**, 12 (1980).
- <sup>54</sup>A. Zangwill and P. Soven, *Phys. Rev. A* **21**, 1561 (1980).
- <sup>55</sup>M. Hestenes and E. Stiefel, *J. Res. Natl. Bur. Stand.* **49**, 409 (1952).
- <sup>56</sup>H. A. van der Vorst, *SIAM J. Sci. Stat. Comput.* **13**, 631 (1992).
- <sup>57</sup>M. H. Gutknecht, *SIAM J. Sci. Comput.* **14**, 1020 (1993).
- <sup>58</sup>C. Broyden, *Math. Comput.* **19**, 577 (1965).
- <sup>59</sup>D. D. Johnson, *Phys. Rev. B* **38**, 12807 (1988).
- <sup>60</sup>D. G. Anderson, *J. Assoc. Comput. Mach.* **12**, 547 (1965).
- <sup>61</sup>D. Hofmann and S. Kümmel, *J. Chem. Phys.* **137**, 064117 (2012).
- <sup>62</sup>M. Rohlfing and S. G. Louie, *Phys. Rev. Lett.* **80**, 3320 (1998).
- <sup>63</sup>M. Rohlfing and S. G. Louie, *Phys. Rev. B* **62**, 4927 (2000).
- <sup>64</sup>P. Ghosez, X. Gonze, and R. W. Godby, *Phys. Rev. B* **56**, 12811 (1997).
- <sup>65</sup>L. Reining, V. Olevano, A. Rubio, and G. Onida, *Phys. Rev. Lett.* **88**, 066404 (2002).
- <sup>66</sup>Y.-H. Kim and A. Görling, *Phys. Rev. Lett.* **89**, 096402 (2002).
- <sup>67</sup>R. Del Sole, G. Adragna, V. Olevano, and L. Reining, *Phys. Rev. B* **67**, 045207 (2003).
- <sup>68</sup>Y.-H. Kim, M. Städele, and A. Görling, *Int. J. Quantum Chem.* **91**, 257 (2003).
- <sup>69</sup>A. Görling, *Phys. Rev. Lett.* **83**, 5459 (1999).
- <sup>70</sup>Y.-H. Kim, M. Städele, and R. M. Martin, *Phys. Rev. A* **60**, 3633 (1999).
- <sup>71</sup>D. M. Bylander and L. Kleinman, *Phys. Rev. Lett.* **74**, 3660 (1995).
- <sup>72</sup>M. Städele, J. A. Majewski, P. Vogl, and A. Görling, *Phys. Rev. Lett.* **79**, 2089 (1997).
- <sup>73</sup>J. P. Perdew and A. Zunger, *Phys. Rev. B* **23**, 5048 (1981).
- <sup>74</sup>D. Hofmann, S. Klüpfel, P. Klüpfel, and S. Kümmel, *Phys. Rev. A* **85**, 062514 (2012).
- <sup>75</sup>T. Körzdörfer, S. Kümmel, and M. Mundt, *J. Chem. Phys.* **129**, 014110 (2008).
- <sup>76</sup>In accordance with Ref. 61, we use bond lengths of SiH = 1.474 Å for silane and SiH = 1.48 Å and SiSi = 2.32 Å for disilane; simulation sphere radii of 16  $a_0$  and 18  $a_0$  for silane and disilane, respectively; and a grid spacing of 0.5  $a_0$ . The LDA pseudopotentials with core cutoff radii of  $r_c(\text{H}) = 1.39 a_0$  and  $r_c(\text{Si}) = 1.79 a_0$  were the same as in Ref. 61.
- <sup>77</sup>Note that Ref. 61 erroneously shows  $\sqrt{|\mu_x(\omega)|^2 + 2 \cdot |\mu_y(\omega)|^2}$  instead of the true power spectrum. We recalculated  $D(\omega)$  using the data from the propagations of 61 and show the corrected spectra in this work. This, however, has no visible effects on the SiH<sub>4</sub> spectrum and only minor recognizable consequences for the spectrum of Si<sub>2</sub>H<sub>6</sub>, the most prominent one being the appearance of two weak additional peaks in the GSIC spectrum between 7 eV and 8.5 eV.
- <sup>78</sup>I. Vasiliev, S. Ögüt, and J. R. Chelikowsky, *Phys. Rev. B* **65**, 115416 (2002).
- <sup>79</sup>M. L. Tiago and J. R. Chelikowsky, *Phys. Rev. B* **73**, 205334 (2006).
- <sup>80</sup>S. Hirata and M. Head-Gordon, *Chem. Phys. Lett.* **314**, 291 (1999).
- <sup>81</sup>S. Hirata, S. Ivanov, I. Grabowski, and R. J. Bartlett, *J. Chem. Phys.* **116**, 6468 (2002).
- <sup>82</sup>We use LDA pseudopotentials with core cutoff radii of  $r_c(\text{N}) = 1.50 a_0$ ,  $r_c(\text{C}) = 1.29 a_0$ ,  $r_c(\text{O}) = 1.45 a_0$ , and  $r_c(\text{H}) = 1.39 a_0$ . Our simulation sphere radii  $R$  and grid spacings  $h$  are  $R(\text{N}_2) = 21 a_0$ ,  $h(\text{N}_2) = 0.25 a_0$ ,  $R(\text{CO}) = 23 a_0$ ,  $h(\text{CO}) = 0.28 a_0$ , and  $R(\text{C}_2\text{H}_4) = 28 a_0$ ,  $h(\text{C}_2\text{H}_4) = 0.3 a_0$ .
- <sup>83</sup>R. van Leeuwen, *Int. J. Mod. Phys. B* **15**, 1969 (2001).
- <sup>84</sup>M. Mundt, S. Kümmel, R. Van Leeuwen, and P. G. Reinhard, *Phys. Rev. A* **75**, 050501 (2007).

- <sup>85</sup>A. Karolewski, R. Armiento, and S. Kümmel, *Phys. Rev. A* **88**, 052519 (2013).
- <sup>86</sup>C. M. Isborn and X. Li, *J. Chem. Theory Comput.* **5**, 2415 (2009).
- <sup>87</sup>G. Vignale and M. Rasolt, *Phys. Rev. B* **37**, 10685 (1988).
- <sup>88</sup>S. Rohra and A. Görling, *Phys. Rev. Lett.* **97**, 013005 (2006).
- <sup>89</sup>J. Kübler, K.-H. Höck, J. Sticht, and A. R. Williams, *J. Appl. Phys.* **63**, 3482 (1988).
- <sup>90</sup>W. H. Press, S. A. Teukolsky, W. T. Vetterling, and B. P. Flannery, *Numerical Recipes: The Art of Scientific Computing*, 3rd ed. (Cambridge University Press, 2007).
- <sup>91</sup>D. A. H. Jacobs, *IMA J. Numer. Anal.* **6**, 447 (1986).
- <sup>92</sup>R. W. Freund and N. M. Nachtigal, *Numer. Math.* **60**, 315 (1991).
- <sup>93</sup>R. Ahlrichs, M. Bär, M. Häser, H. Horn, and C. Kölmel, *Chem. Phys. Lett.* **162**, 165 (1989).
- <sup>94</sup>T. H. Dunning, *J. Chem. Phys.* **90**, 1007 (1989).
- <sup>95</sup>R. A. Kendall, T. H. Dunning, and R. J. Harrison, *J. Chem. Phys.* **96**, 6796 (1992).
- <sup>96</sup>R. Ditchfield, W. J. Hehre, and J. A. Pople, *J. Chem. Phys.* **54**, 724 (1971).
- <sup>97</sup>W. J. Hehre, R. Ditchfield, and J. A. Pople, *J. Chem. Phys.* **56**, 2257 (1972).
- <sup>98</sup>R. Krishnan, J. S. Binkley, R. Seeger, and J. A. Pople, *J. Chem. Phys.* **72**, 650 (1980).
- <sup>99</sup>W. Hieringer and A. Görling, *Chem. Phys. Lett.* **419**, 557 (2006).
- <sup>100</sup>A. Heßelmann, A. Ipatov, and A. Görling, *Phys. Rev. A* **80**, 012507 (2009).
- <sup>101</sup>A. Ipatov, A. Heßelmann, and A. Görling, *Int. J. Quantum Chem.* **110**, 2202 (2010).
- <sup>102</sup>A. Görling, A. Ipatov, A. W. Götz, and A. Heßelmann, *Z. Phys. Chem.* **224**, 325 (2010).



## Publication 2

### **On the challenge to improve the density response with unusual gradient approximations**

Reprinted by permission from Springer Nature Customer Service Centre GmbH:

Springer Nature

The European Physical Journal B **91**, 159 (2018)

© 2018.

Julian Garhammer,<sup>1</sup> Fabian Hofmann,<sup>1</sup> Rickard Armiento,<sup>2</sup> Stephan Kümmel<sup>1</sup>

<sup>1</sup>Theoretical Physics IV, University of Bayreuth, 95440 Bayreuth, Germany

<sup>2</sup>Department of Physics, Chemistry and Biology (IFM), Linköping University, SE-581 83 Linköping, Sweden

Publ. 2

---

### **My contribution**

The leading contribution to this publication is from Julian Garhammer. The work is based on my implementation of the Sternheimer linear response scheme, and I helped with the implementation of specific terms of the AK13 response. I participated in the discussion of the results and I contributed to writing the manuscript.

Publ. 2

# On the challenge to improve the density response with unusual gradient approximations<sup>★</sup>

Julian Garhammer<sup>1</sup>, Fabian Hofmann<sup>1</sup>, Rickard Armiento<sup>2</sup>, and Stephan Kümmel<sup>1,a</sup>

<sup>1</sup> Theoretical Physics IV, University of Bayreuth, 95440 Bayreuth, Germany

<sup>2</sup> Department of Physics, Chemistry and Biology (IFM), Linköping University, SE-581 83 Linköping, Sweden

Received 2 March 2018 / Received in final form 25 May 2018

Published online 9 July 2018

© EDP Sciences / Società Italiana di Fisica / Springer-Verlag GmbH Germany, part of Springer Nature, 2018

**Abstract.** Certain excitations, especially ones of long-range charge transfer character, are poorly described by time-dependent density functional theory (TDDFT) when typical (semi-)local functionals are used. A proper description of these excitations would require an exchange–correlation response differing substantially from the usual (semi-)local one. It has recently been shown that functionals of the generalized gradient approximation (GGA) type can yield unusual potentials, mimicking features of the exact exchange derivative discontinuity and showing divergences on orbital nodal surfaces. We here investigate whether these unusual potential properties translate into beneficial response properties. Using the Sternheimer formalism we closely investigate the response obtained with the 2013 exchange approximation by Armiento and Kümmel (AK13) and the 1988 exchange approximation by Becke (B88), both of which show divergences on orbital nodal planes. Numerical calculations for Na<sub>2</sub> as well as analytical and numerical calculations for the hydrogen atom show that the response of AK13 behaves qualitatively different from usual semi-local functionals. However, the AK13 functional leads to fundamental instabilities in the asymptotic region that prevent its practical application in TDDFT. Our findings may help the development of future improved functionals. They also corroborate that the frequency-dependent Sternheimer formalism is excellently suited for running and analyzing TDDFT calculations.

## 1 Introduction

Kohn–Sham (KS) density functional theory (DFT) [1,2] and its time-dependent extension (TDDFT) by Runge and Gross [3] are highly successful and among the most widely used theoretical approaches for describing the electronic structure and dynamics in physical, chemical and biological systems. Many applications of TDDFT are concerned with predicting the linear response. Consequently, the linear response of the exchange–correlation (xc) potential to a time-dependent perturbation, which has been studied in detail by Gross [4–7], to whom this special issue is devoted, plays a prominent role in TDDFT research. Commonly used functionals such as the local-density approximation (LDA), usual generalized gradient corrections (GGAs) such as the one of Perdew et al. [8] (PBE), and hybrid functionals [9] predict many properties reliably. At the same time, however, they are known to systematically fail for certain problems. One such prominent failure of (semi-)local functionals and usual hybrid functionals with moderate fractions of exact exchange is their qualitatively

wrong prediction of long-range charge-transfer phenomena [10–13].

In recent years, semi-local exchange functionals and model-potentials have been developed which yield physically interpretable eigenvalues [14] and show features in their potentials that are very similar to important features of the exact Kohn–Sham exchange (EXX) potential. Prominent examples of this development are the Becke–Johnson model potential [15] with its different modifications [16–21], especially the Tran–Blaha model potential [22–24], and Becke–Johnson inspired new developments such as the AK13 functional [25]. A considerable part of the great interest in these developments stems from the hope that such functionals may allow to obtain information about excited states and the density response accurately at moderate computational cost [26,27]. We review the corresponding arguments in detail in the next section. However, the Becke–Johnson potential cannot be used reliably in TDDFT calculations [27], because it is not a functional derivative [19,28]. As a consequence, TDDFT calculations with the Becke–Johnson model potential in general will be unstable, e.g., due to zero-force theorem violations [29]. Similar conclusions hold for other model potentials.

Hence, the focus of the present work is a careful investigation of the response of the AK13 exchange energy

<sup>★</sup> Contribution to the Topical Issue “Special Issue in honor of Hardy Gross”, edited by C.A. Ullrich, F.M.S. Nogueira, A. Rubio, and M.A.L. Marques.

<sup>a</sup> e-mail: [stephan.kuemmel@uni-bayreuth.de](mailto:stephan.kuemmel@uni-bayreuth.de)

functional, which shares many features with the Becke–Johnson model, yet is a functional derivative. In the present context, the most important feature that the AK13 and Becke–Johnson potential have in common is that for a finite system, the potential asymptotically goes to a value that is determined by the highest occupied eigenvalue. This leads to a discontinuity-like potential step structure similar to exact exchange. As such discontinuities are important for charge-transfer excitations [11], one may hope that a potential with such features may lead to a proper description of those. Therefore, our present study of the TDDFT response of the AK13 functional is, to the best of our knowledge, the first investigation of whether such semi-local step structures have a beneficial impact in TDDFT calculations, and in how far the concept of a “potential with a non-vanishing asymptotic constant” is beneficial in TDDFT.

Summarizing our findings, we have to note that on the one hand, the answer that our study gives is largely negative: the AK13 response yields instabilities in the asymptotic region that prevent its use in TDDFT. On the other hand, the outcome clearly demonstrates that semi-local functionals designed to mimic exact exchange potential features are capable of giving a response that deviates strongly from the one that is observed with usual semi-local functionals. Thus, our results motivate future work on semi-local functionals that achieve an improved response, yet circumvent instabilities. We also expect the methodology and in-depth analysis presented in this work to be useful for future work in the area of designing functionals with improved response properties. Furthermore, our comparison between analytical and numerical results also adds confidence in the ability of the Sternheimer linear response formalism to correctly describe the response of difficult potentials.

The paper is organized as follows. We first review properties of exact and approximate exchange in TDDFT that are of particular relevance for excitations and thus motivate our study of the AK13 response in detail. Next we briefly review the functionals that we test, followed by a recapitulation of the Sternheimer linear response formalism that we use for our TDDFT calculations. After this we present numerical calculations for the sodium dimer as a simple test system. In order to explain the numerical findings that emerge, we then go through the analytically solvable case of the one-electron atom. We close by drawing our conclusions and offering an outlook.

## 2 Exchange response in DFT and TDDFT

Fock exchange is very frequently employed in DFT as a part of hybrid functional constructions and ameliorates deficiencies of usual (semi-)local approximations, e.g., by providing some non-locality to the functional and by reducing self-interaction errors [30]. However, the use of Fock exchange comes at a twofold price. On the practical side, the computational expense of exchange integrals is a burden. On the fundamental side, it has been argued since the beginnings of modern DFT (see, e.g., Ref. [31] for examples) that it may be more consistent with

the intrinsic many-body nature of DFT to approximate exchange and correlation together rather than dividing into single-particle motivated exchange and Coulomb correlation.

While the use of Fock exchange has proven beneficial in ground-state calculations, as testified by the success of hybrid functionals in questions of thermochemistry [32], many of the advantages of using Fock exchange as part of density functional approximations are not related to ground-state observables, but to the use of such functionals in TDDFT. Furthermore, some of the interest in the Becke–Johnson and related approximations has originated from the description of excitations [26,27]. One can readily understand why Fock exchange can be beneficial in TDDFT from arguments based on linear response theory: following, e.g., references [5,33,34] one can interpret the true excitations as resulting from a combination of Kohn–Sham eigenvalue differences and exchange–correlation (xc) kernel corrections via matrix-elements of the type

$$K_{ijkl} = \int \int \varphi_i^*(\mathbf{r}) \varphi_j(\mathbf{r}) \frac{\delta v_{xc}(\mathbf{r}, t)}{\delta n(\mathbf{r}', t')} \varphi_k(\mathbf{r}') \varphi_l^*(\mathbf{r}') d^3r d^3r', \quad (1)$$

where spin indices have been suppressed for clarity of notation. From this perspective, two advantages of using Fock exchange in TDDFT become obvious. First, it typically leads to an eigenvalue spectrum of greater physical interpretability, and this can translate into improved TDDFT excitation energies [5,35–37]. Second, step structures of the EXX potential [38–40] or xc potential [12,41–44] can translate into substantial effects in equation (1), leading to large and important corrections to the single-particle eigenvalue differences.

The latter argument is at the heart of understanding one of the most notorious failures of TDDFT with usual (semi-)local functionals, viz. its massive underestimation of long-range charge transfer excitation energies [10,11]: as argued, e.g., in references [10,12,13], long-range charge-transfer excitations correspond to situations where the orbital overlap in equation (1) is small, vanishing exponentially as a consequence of exponential orbital decay. Thus, the matrix elements of equation (1) vanish unless  $\delta v_{xc}(\mathbf{r}, t)/\delta n(\mathbf{r}', t')$  counters the exponential orbital decay. When Fock exchange is used, the vanishing orbital overlap does not lead to vanishing  $K_{ijkl}$  because EXX (and also an exact calculation including correlation [45]) leads to a non-local kernel, i.e., a kernel that also couples regions of space in which  $\mathbf{r}$  and  $\mathbf{r}'$  are far apart. The kernel of (semi-)local functionals, however, is local, i.e.,  $\propto \delta(\mathbf{r} - \mathbf{r}')$ . Therefore,  $K_{ijkl}$  will vanish for vanishing orbital overlap, erroneously making the TDDFT excitation energy equal to the Kohn–Sham eigenvalue difference, unless the spatial dependence of  $v_{xc}(\mathbf{r})$  is such that  $\delta v_{xc}(\mathbf{r}, t)/\delta n(\mathbf{r}, t')$  itself grows rapidly in regions of space in which the orbital overlap vanishes.

The potentials of the LDA and usual GGAs follow the density closely. Therefore, they do not show a rapid increase or divergence of the kernel in regions of vanishing orbital overlap. Consequently, these approximations fail utterly in the description of long-range charge-transfer excitations [10,11,13,46]. As this physics is decisive in

many highly-relevant questions of material science, with solar-cell development being a prominent example [47–51], (semi-)local functionals to date are of only very limited use in this type of research.

For a long time, it had been believed that closely following the density is an unavoidable feature of (semi-)local approximations. However, it recently has been demonstrated that a functional of the GGA type can have a functional derivative, i.e., a corresponding potential, that resembles exact exchange in several ways [24–26,52,53]. The hope that this functional can be widely used in ground-state material science calculations has been curbed by the yet more recent discovery [54,55] that it, and several other constructions following a related logic [56–58], show divergences in regions of space where the highest occupied molecular orbital (HOMO) has a nodal plane overlapping with a lower occupied orbital. While this feature makes ground-state calculations difficult, it appears attractive from the perspective of TDDFT, where pronounced features of the potential in regions of reduced orbital overlap are required as discussed above.

Therefore, we calculate and analyze the linear response of such semi-local approximations in this manuscript. In order to circumvent issues resulting from the previously reported possible difficulties in ground-state calculations with such functionals, and in order to focus on and bring out the effects of the xc corrections as clearly as possible, we resort to the Sternheimer linear response formalism [37,59]. Thus, we can combine the potential response of unusual semi-local functionals with a plain LDA ground-state calculation to see just the effects of the xc response, and we can analyze and visualize potential responses and densities in real space to obtain a clear understanding of the functionals' properties.

### 3 Functionals studied in this work

The main interest of this work is the investigation of the linear response properties of AK13. However, in order to put the results into perspective, we also take a look at two well established, long-known GGAs: PBE as a paradigm example of a well-tested, usual GGA and the B88 GGA of Becke [56]. The latter is of particular interest for our study because it has recently been pointed out that it shares several unusual features with AK13, such as divergences of the potential on nodal planes of the highest occupied orbital [54,55]. For the sake of completeness, we briefly summarize relevant aspects of these functionals in the following.

Exchange functionals of the GGA type are typically written in the form [60]

$$E_x^{\text{SL}}[n] = A_x \int d^3r n(\mathbf{r})^{\frac{4}{3}} F(s), \quad (2)$$

where  $F(s)$  is the exchange enhancement factor,

$A_x = -\frac{3}{4} \left(\frac{3}{\pi}\right)^{\frac{1}{3}} e^2$  and

$$s = \frac{|\nabla n(\mathbf{r})|}{2(3\pi^2)^{\frac{1}{3}} n(\mathbf{r})^{\frac{4}{3}}} \quad (3)$$

is a dimensionless density gradient. Different GGAs differ by different choices that are made for the enhancement factor.

The PBE functional's construction was guided by the aim to fulfill energetically relevant exact constraints, such as the homogeneous electron gas limit, proper coordinate scaling and the Lieb–Oxford bound. These constraints go along with an enhancement factor that goes to a constant for  $s \rightarrow \infty$ . A property of PBE that makes it a natural functional to compare AK13 to in the linear response context is the fact that PBE's enhancement factor was designed such that the functional recovers the linear response properties of LDA for the homogeneous electron gas. Therefore, the PBE response can be expected to be qualitatively similar to LDA in many cases. In other words, PBE is a GGA from which one expects predictable, unsurprising linear response properties.

The B88 GGA is also considered a standard functional and it is a part of one of the most widely used hybrid functionals [61]. However, the guidelines along which B88 was designed are quite different from the PBE ones. The B88 functional was constructed such that it captures both the exact asymptotic behavior of the exchange energy density and the lowest-order gradient correction to LDA for small density gradients [56]. In order to achieve this, the enhancement factor of B88 diverges for  $s \rightarrow \infty$ , yet in a way that has been called “subcritical” [54], because despite the divergence of  $F(s)$ , the functional derivative of  $E_x^{\text{B88}}[n]$  with respect to  $n$  does not diverge for large distances from a finite's system center.

In contrast to the model potentials by which it was inspired, the AK13 approximation [25] is also based on the general GGA form of equation (2). However, the guiding principles in its construction have not been energetic considerations [62]. Instead, the aim in the design of AK13 was to make its functional derivative, i.e., the AK13 exchange potential, close to the Becke–Johnson model potential [15], which itself is in many respects a good model for the exchange-only Optimized Effective Potential. The most important property of the Becke–Johnson model which AK13 reproduces, is that asymptotically its potential for a finite system goes to a value that is determined by the highest occupied eigenvalue. In the AK13 functional, this is achieved by choosing  $F(s)$  such that it diverges in a specific, “critical” manner [25]. By letting the potential go to a finite, system-dependent value, step-structures are built into the potential which resemble the step-structures in the exchange-only Optimized Effective Potential that are related to the derivative discontinuity [39,41]. As the derivative discontinuity is important for charge-transfer excitations [11], one may hope that a potential with such features may lead to a proper description of those.

### 4 Linear response TDDFT in the Sternheimer approach

The most commonly used form of linear response TDDFT, often going by the name “Casida formalism” [33,34], is

based on expanding the density response into particle–hole excitations. Here, we take a different route and solve the Sternheimer equations [34,59]. So far, the Sternheimer approach is not as widely used as Casida’s formalism, but it has the advantages of parallelizing very efficiently [37] and of not requiring the explicit calculation of unoccupied orbitals. As some of us have recently elsewhere presented the time-dependent Sternheimer approach in detail in the form that we also use here [37], we can restrict ourselves to presenting the basic equations in the following.

In practice, a Sternheimer linear response calculation boils down to self-consistently solving the set of equations

$$[h_{\text{KS},\sigma} - \epsilon_{j\sigma} - \hbar\bar{\omega}] \phi_{j\sigma}^+ = -\hat{Q}_j^\sigma [V_{\text{ext}}^+ + V_{\text{Hxc}}^{+,\sigma}] \varphi_{j\sigma}, \quad (4)$$

$$[h_{\text{KS},\sigma} - \epsilon_{j\sigma} + \hbar\bar{\omega}] \phi_{j\sigma}^- = -\hat{Q}_j^\sigma [V_{\text{ext}}^+ + V_{\text{Hxc}}^{+,\sigma}] \varphi_{j\sigma}, \quad (5)$$

for the orbital response components  $\phi_{j\sigma}^+$ ,  $\phi_{j\sigma}^-$  and excitation energies  $\hbar\bar{\omega}$ . Here,

$$h_{\text{KS},\sigma} = -\frac{\hbar^2}{2m} \nabla^2 + v_{\text{ext}}(\mathbf{r}) + v_{\text{Hxc}}^\sigma(\mathbf{r}) \quad (6)$$

is the usual unperturbed ground-state Kohn–Sham Hamiltonian, with the Hartree and exchange–correlation (xc) contributions  $v_{\text{Hxc}}^\sigma(\mathbf{r}) = v_{\text{H}}(\mathbf{r}) + v_{\text{xc}}^\sigma(\mathbf{r})$ . The Kohn–Sham ground-state orbitals, which have been chosen to be real-valued, and eigenvalues of spin  $\sigma$  are denoted by  $\varphi_{j\sigma}(\mathbf{r})$ ,  $\epsilon_{j\sigma}$ , respectively. A finite  $\eta \ll \omega$  is added [37,59] to the excitation frequencies, i.e.,  $\bar{\omega} := \omega + i\eta$ . This  $\eta$  results from the adiabatic switch-on process, see below and reference [37]. It also improves the numerical stability of equations (4) and (5).  $\hat{Q}_j^\sigma$  denotes the spin-dependent projector

$$\hat{Q}_j^\sigma := 1 - |\varphi_{i\sigma}\rangle\langle\varphi_{i\sigma}|. \quad (7)$$

The Fourier components  $V_{\text{ext}}^+$  of the external potential that appear on the right-hand sides of equations (4) and (5) are defined by the time-dependent, adiabatically applied, quasi-monochromatic external perturbation

$$v_{\text{ext}}(\mathbf{r}, t) = e^{\eta t} [V_{\text{ext}}^+(\mathbf{r})e^{-i\omega t} + V_{\text{ext}}^-(\mathbf{r})e^{i\omega t}], \quad (8)$$

where

$$V_{\text{ext}}^+ = (V_{\text{ext}}^-)^*. \quad (9)$$

The Hartree- and xc-contributions

$$V_{\text{Hxc}}^{+,\sigma} = V_{\text{H}}^+ + V_{\text{xc}}^{+,\sigma}, \quad (10)$$

appearing on the right-hand sides of equations (4) and (5) are obtained by solving the Poisson-like equation

$$\nabla^2 V_{\text{H}}^+ = -4\pi e^2 (n_{\uparrow}^+ + n_{\downarrow}^+), \quad (11)$$

and computing

$$V_{\text{xc}}^{+,\sigma}(\mathbf{r}) = \sum_{\tau=\uparrow,\downarrow} \int n_{\tau}^+(\mathbf{r}') f_{\text{xc}}^{\sigma,\tau}(\mathbf{r}, \mathbf{r}', \bar{\omega}) d^3 r'. \quad (12)$$

Here,

$$f_{\text{xc}}^{\sigma,\tau}(\mathbf{r}, \mathbf{r}', \bar{\omega}) := \int f_{\text{xc}}^{\sigma,\tau}(\mathbf{r}, \mathbf{r}', t - t') e^{i\bar{\omega}(t-t')} d(t - t') \quad (13)$$

is the Fourier transform of the exchange–correlation kernel

$$f_{\text{xc}}^{\sigma,\tau}(\mathbf{r}, \mathbf{r}', t - t') := \left. \frac{\delta v_{\text{xc}}^\sigma[n_{\uparrow}, n_{\downarrow}](\mathbf{r}, t)}{\delta n_{\tau}(\mathbf{r}', t')} \right|_{n_{\uparrow}, n_{\downarrow}}. \quad (14)$$

The density response

$$n_{\sigma}^+ = \sum_{j=1}^{N_{\sigma}} \varphi_{j\sigma} (\phi_{j\sigma}^+ + \phi_{j\sigma}^-) \quad (15)$$

enters into equations (11) and (12), and thus a closed self-consistent cycle is obtained.

The chosen xc approximation enters the Sternheimer equations in two places. First, it is part of the ground-state Hamiltonian of equation (6) and contributes to the eigenvalues and ground-state orbitals that feature in equations (4) and (5). Second, it determines the xc potential response of equation (12). Using the linear response formalism instead of, e.g., a real-time propagation scheme [63–66] is decisive for studying the AK13 approximation’s TDDFT performance, because AK13 ground-state orbitals are difficult to compute for finite, three-dimensional systems due to the previously discussed [54,55] particular features of the AK13 potential. However, in the linear response approach one can combine the ground-state orbitals of one exchange (and correlation) approximation with the kernel of some other approximation. In this way, we can test the kernel resulting from AK13.

In practice, we solve the Sternheimer equations by starting with equations (4) and (5) with merely  $V_{\text{ext}}^+$  on the right-hand side in order to generate initial values for the orbital responses  $\phi_{j\sigma}^+$  and  $\phi_{j\sigma}^-$ , where our external perturbation is

$$V_{\text{ext}}^+(\mathbf{r}) = e(\mathbf{E} \cdot \mathbf{r}), \quad (16)$$

and  $\mathbf{E}$  is a spatially homogeneous electric field. With  $n_{\sigma}^+$  calculated according to equation (15) we obtain a complete set of quantities to start the self-consistency iteration by evaluating  $V_{\text{Hxc}}^{+,\sigma}$  via equations (10)–(12). Thus, we can construct the right-hand sides of equations (4) and (5) via equations (7)–(12) and from there calculate new versions of  $\phi_{j\sigma}^+$  and  $\phi_{j\sigma}^-$  by solving equations (4) and (5) again. These steps are iterated until a self-consistent solution is found.

## 5 Numerical results for Na<sub>2</sub>

Clusters of nearly-free-electron metals are in general reasonably well described by semi-local functionals [67–69]. This is particularly true for sodium-clusters, as sodium (Na) is “the nearly-free-electron metal par excellence” [70]. For this reason, Na-clusters have often served as test systems for density functionals [71–74], and one can argue that a semi-local approximation should at least work for those. If it passes this test, then further tests on more complicated systems are worthwhile, whereas testing it for more complicated systems makes little sense if already the simplest test, Na clusters, fails. In this logic, we here chose the dimer Na<sub>2</sub>, which is known to be reasonably well described by (TD)LDA [73–75], as the primary test system for which we evaluate the AK13 response.

The ground-state calculations were done with the Bayreuth version [76] of the Parsec program [77]. The TDDFT calculations are based on a recently developed Sternheimer program package [37]. We used a Cartesian grid with a spacing of 0.45 Bohr ( $a_0$ ) and sphere radii between 20 and 25  $a_0$ , as indicated in the figure captions. The two Na atoms are located at  $x_1 = -2.9 a_0$  and  $x_2 = +2.9 a_0$  on the  $x$ -axis and are described by a Troullier–Martin [78] pseudopotential ( $r_c = 3.09 a_0$  for  $s$ -,  $p$ -, and  $d$ -shell). These parameters were chosen to ensure that the occupied as well as the first unoccupied eigenvalues of the ground-state calculation were converged to at least  $10^{-4}$  Rydberg (in the following, frequencies and potential responses are given in Rydberg atomic units), and that the obtained TDLDA spectrum is in agreement with the one of reference [74]. The terms “density response”, and “potential response” in the following refer to the “+” Fourier components unless stated otherwise.

For the reasons that have been discussed in detail in reference [55], using the AK13 GGA in self-consistent ground-state calculations is cumbersome and our attempts at converging such calculations have not been successful. Therefore, our interest here is not in using AK13 to set up the left-hand side of equation (4), but in using AK13 for computing the potential response of equation (12). In this way, by combining the AK13 response with a “usual” approximation for  $h_{KS}$ , we can bring out the effects of the AK13  $x$  kernel most clearly. For maximum transparency we chose the LDA for the ground-state Hamiltonian, with which we combine the AK13  $x$  potential response. In order to calculate the latter, the AK13 kernel and potential response, respectively, have to be constructed. These are calculated in Appendix A.

However, we found that we could not converge the self-consistency iteration of the Sternheimer equations with the AK13  $x$  potential response. The lower panel of Figure 1 shows the AK13 exchange potential response during the first five iterations of the Sternheimer equations. In the figures we omitted the last few grid points that lie close to the numerical boundary and are therefore affected by inaccuracies from the real-space finite differences. It is evident that the changes of the AK13 potential response are enormous from one step to the next and the potential response even changes its sign. Oscillations build up at the boundaries of the

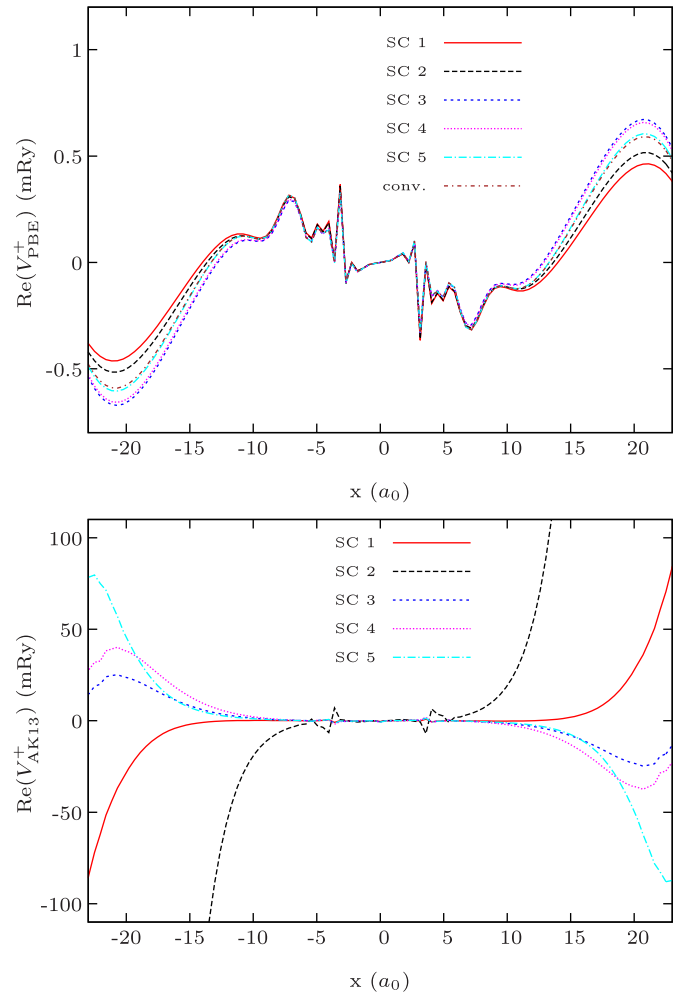


**Fig. 1.** The real part of the  $x(c)$  response for Na<sub>2</sub> according to equation (12) for PBE (upper panel) and AK13 (lower panel) for an external electric field with polarization along the Cartesian (1,1,1) direction and an energy  $\hbar\omega = 0.3$  Ry for the first five self-consistency steps (SC). For PBE, also the converged result is shown. A boundary sphere with radius  $r = 25 a_0$  was used.

simulation sphere and travel to the inside during the self-consistency iteration, impeding convergence. We tried to stabilize the numerical calculations in different ways, e.g., by starting the AK13 Sternheimer self-consistency iteration from a converged self-consistent LDA linear response calculation or using different mixing schemes. However, none of the employed approaches nor combinations of them lead to a self-consistent, converging AK13 linear response calculation, even after several hundred iterations.

As a demonstration of how the  $xc$  response for a “usual” GGA looks like, the upper panel of Figure 1 depicts the  $xc$  response of PBE. The PBE potential response differs relatively little from one self-consistency step to the next, and the Sternheimer iteration converges within nine steps. Thus, there is no problem with the GGA form in the Sternheimer approach per se, but something peculiar is happening in the AK13 calculation.

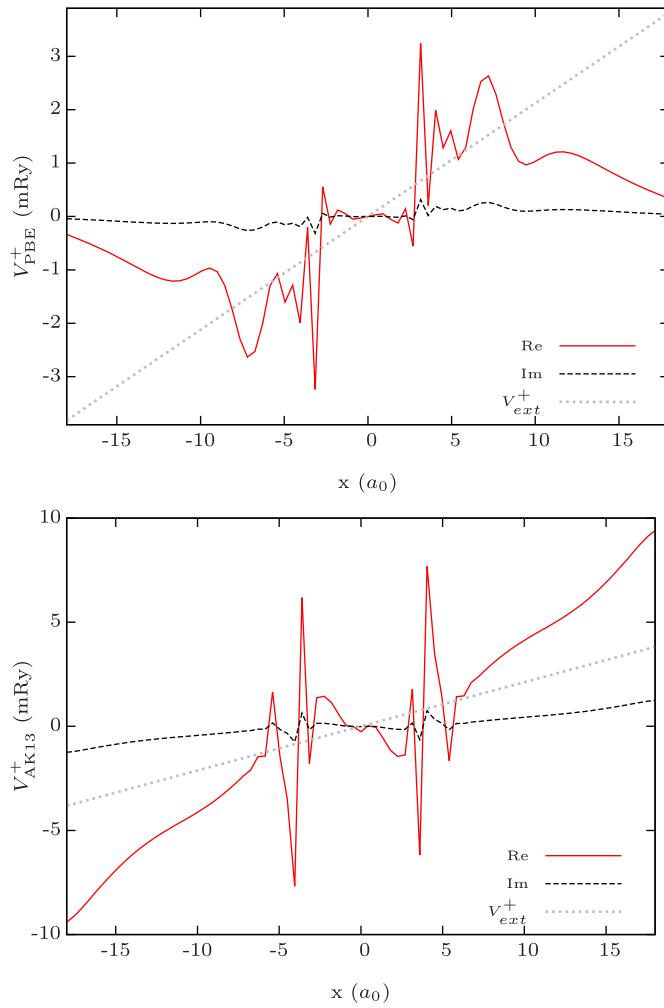


**Fig. 2.** Real and imaginary part of the potential response for  $\text{Na}_2$  of PBE (upper panel) and AK13 (lower panel) along the  $x$ -axis for an external electric field with a polarization direction of  $(1,0,0)$  and energy  $\hbar\omega = 0.11$  Ry. The data is obtained by performing a self-consistent LDA ground-state and linear response calculation and subsequently evaluating the potential response for PBE and AK13, respectively, using the density and density response from the self-consistent LDA calculation. In addition, the potential of the applied external electric field is shown as a reference. A simulation sphere with radius  $r = 20 a_0$  was used.

In order to understand what is going on, we evaluated the potential response again in a different way. Instead of trying to analyze the self-consistent AK13 potential response, we performed a self-consistent LDA ground-state and linear response calculation and subsequently evaluated equation (12) with the density response obtained from LDA (which does not show any spurious features) and the  $x$ - and  $xc$ -kernel of AK13 and PBE, respectively. A striking feature of the AK13 response is revealed in this way. When the external electric field is applied in the  $(1,1,1)$  direction, the AK13 potential response exhibits an overall slope and a rising behavior towards the boundaries of the simulation sphere along all three coordinate axes. When changing the

polarization direction to  $(1,0,0)$ , the rising feature of the AK13 potential response vanishes along the  $y$ - and  $z$ -direction, but remains visible along the  $x$ -axis. The PBE response, on the contrary, always falls off to zero. Figure 2 illustrates these findings, and also displays the potential of the external electric field as a reference. We stress that the observed features are numerically stable and not artifacts of how the potentials and densities are computed numerically.

Summarizing these findings, we note that the direction of the AK13's potential response slope depends on the direction of the external electrical field, and the slope is proportional to the external field's modulus. The real part of the AK13 potential response becomes larger than the potential of the external electric field for large distances, making it the asymptotically leading term. These somewhat surprising findings call for further explanation. To this end, we take a look at the hydrogen atom, for which exact relations for the exchange response can be derived as shown below.

## 6 Analytical analysis of the exchange potential response

In the following section we contrast the exact analytical result for the hydrogen atom response with the one obtained from the different functionals.

### 6.1 Asymptotics of the exact exchange potential response

One may argue that a one-electron system is quite a challenging test for a semi-local functional because of the well-known self-interaction problem, i.e., one might argue that failing the one-electron test may not necessarily imply that a semi-local approximation is useless. E.g., the LDA ground-state energy for the hydrogen (H) atom is not particularly accurate, yet LDA is nonetheless a useful approximation for a lot of many-electron systems. However, for our present purposes the H-atom is a good test case, and a very relevant one, because our aim here is not testing quantitative performance, but understanding qualitative features of the exchange response. For this, the H-atom is ideal because the exact potential response can easily be derived.

For every one-electron system the exact exchange functional just cancels the Hartree contribution [79]. Thus, in this case the exact exchange potential is the negative Hartree potential,

$$v_x^{\text{ex}}(\mathbf{r}, t) = -v_H(\mathbf{r}, t) = -e^2 \int d^3r' \frac{n(\mathbf{r}', t)}{|\mathbf{r} - \mathbf{r}'|}, \quad (17)$$

and consequently the exact  $x$  kernel is also just the negative Hartree kernel, from which the potential response

$$V_{x,\text{ex}}^+(\mathbf{r}) = -V_H^+(\mathbf{r}) = -e^2 \int d^3r' \frac{n^+(\mathbf{r}')}{|\mathbf{r} - \mathbf{r}'|} \quad (18)$$

follows. From equation (18) the asymptotic behavior of the exact  $x$  potential response can be determined via a multipole-expansion

$$\begin{aligned} V_{x,\text{ex}}^+(\mathbf{r}) &= -e^2 \int d^3r' \frac{n^+(\mathbf{r}')}{|\mathbf{r}-\mathbf{r}'|} = -e^2 \frac{\overbrace{\int n^+(\mathbf{r}') d^3r'}^{=0}}{r} \\ &\quad + e \frac{\overbrace{-e \int \mathbf{r}' n^+(\mathbf{r}') d^3r'}^{=: \mathbf{p}^+} \cdot \mathbf{r}}{r^3} + \mathcal{O}\left(\frac{1}{r^3}\right) \\ &= e \frac{\mathbf{p}^+ \cdot \mathbf{e}_r}{r^2} + \mathcal{O}\left(\frac{1}{r^3}\right) \xrightarrow{r \rightarrow \infty} 0, \end{aligned} \quad (19)$$

where the density response integrates to zero due to particle number conservation and  $\mathbf{p}^+ := -e \int \mathbf{r}' n^+(\mathbf{r}') d^3r'$  is the dipole moment of the density response (i.e., the transition dipole). Thus, the exact exchange potential response tends to zero asymptotically proportional to  $\frac{1}{r^2}$  or faster. In directions perpendicular to the dipole moment  $\mathbf{p}^+$  it decays proportionally to at least  $\frac{1}{r^3}$ .

## 6.2 Asymptotics of the potential response of PBE, AK13, and B88

In order to calculate the asymptotic behavior for the exchange–correlation approximations that we want to compare to equation (19), the asymptotics of the density response is required, cf. equation (12). For the transition from the  $1s$  orbital to the  $2p_x$  orbital of a hydrogen atom, it is given by

$$n^+(\mathbf{r}) = \varphi_{1s}(\mathbf{r}) \varphi_{2p_x}(\mathbf{r}), \quad (20)$$

or explicitly,

$$n(\mathbf{r}) = \frac{1}{a_0^3 \pi} e^{-2\frac{r}{a_0}}, \quad (21)$$

and

$$n^+(\mathbf{r}) = \frac{1}{a_0^3 \pi \sqrt{32}} \frac{x}{a_0} e^{-\frac{3}{2}\frac{r}{a_0}}. \quad (22)$$

In Appendix B we derive this relation from the Sternheimer equations.

Based on this density response we can proceed to evaluate the potential response of the PBE, AK13 and B88 approximations. Since all of these originate from the GGA form (2), we calculate the elements required for the evaluation of the potential response asymptotics for the general GGA form in Appendix A. One then just has to insert the enhancement factors  $F(s)$  for PBE, AK13 and B88, respectively, into the resulting equations to obtain the potential response for these functionals.

The important equations are equations (A.16) and (A.17). Together with equations (A.13)–(A.15) they allow expressing the potential response  $V_{x,\text{SL}}^+(\mathbf{r})$ , where

SL stands for PBE, AK13 and B88, in terms of the density, the density response and derivatives of these two. According to equations (21) and (22), in the H-atom calculation the density is spherically symmetric, but the density response only exhibits cylindrical symmetry around the  $x$ -axis. Therefore, we calculate all derivatives in cylindrical coordinates. The gradient and Laplacian of the density for the H-atom case are (cf. Eq. (21))

$$\begin{aligned} \nabla n(\mathbf{r}) &= \frac{2}{a_0} \left( \mathbf{e}_\rho \frac{-\rho}{r} + \mathbf{e}_x \frac{-x}{r} \right) n(\mathbf{r}) \\ &=: -\frac{2}{a_0} \mathbf{e}_r n(\mathbf{r}), \end{aligned} \quad (23)$$

$$\nabla^2 n(\mathbf{r}) = \frac{4}{a_0^2} \left( 1 - \frac{a_0}{r} \right) n(\mathbf{r}), \quad (24)$$

where  $r^2 = x^2 + y^2 + z^2 = x^2 + \rho^2$ ,  $\mathbf{e}_\rho$  and  $\mathbf{e}_x$  are the corresponding unit vectors in cylindrical coordinates and  $\mathbf{e}_r := \mathbf{e}_\rho \frac{\rho}{r} + \mathbf{e}_x \frac{x}{r}$ .

With these two equations, we calculate the reduced density gradients (cf. Eqs. (A.2), (A.3) and (A.4))

$$s = \frac{2}{a_0} \frac{1}{2(3\pi^2)^{\frac{1}{3}}} n(\mathbf{r})^{-\frac{1}{3}} \quad (25)$$

$$u = \frac{8}{a_0^3} \frac{1}{8(3\pi^2)} n(\mathbf{r})^{-1} = s^3 \quad (26)$$

$$\begin{aligned} t &= \frac{4}{a_0^2} \frac{1 - \frac{a_0}{r}}{4(3\pi^2)^{\frac{2}{3}}} n(\mathbf{r})^{-\frac{2}{3}} \\ &= s^2 \left( 1 - \frac{a_0}{r} \right). \end{aligned} \quad (27)$$

The derivatives of the density response are (cf. Eq. (22))

$$\nabla n^+(\mathbf{r}) = \frac{1}{a_0} \left( -\frac{3}{2} \mathbf{e}_r + \frac{a_0}{x} \mathbf{e}_x \right) n^+(\mathbf{r}) \quad (28)$$

$$\nabla^2 n^+(\mathbf{r}) = \frac{1}{a_0^2} \left( \frac{9}{4} - 6 \frac{a_0}{r} \right) n^+(\mathbf{r}), \quad (29)$$

and analogously we obtain (cf. Eqs. (A.13), (A.14) and (A.15))

$$s^+(\mathbf{r}) = -\frac{1}{a_0} \frac{\frac{7}{6} + \frac{a_0}{r}}{2(3\pi^2)^{\frac{1}{3}}} \frac{n^+(\mathbf{r})}{n(\mathbf{r})^{\frac{4}{3}}} \quad (30)$$

$$u^+(\mathbf{r}) = -\frac{1}{a_0^3} \frac{\frac{27}{2} + 10 \frac{a_0}{r}}{8(3\pi^2)} \frac{n^+(\mathbf{r})}{n(\mathbf{r})^2} \quad (31)$$

$$t^+(\mathbf{r}) = -\frac{1}{a_0^2} \frac{\frac{53}{12} - \frac{2}{3} \frac{a_0}{r}}{4(3\pi^2)^{\frac{2}{3}}} \frac{n^+(\mathbf{r})}{n(\mathbf{r})^{\frac{5}{3}}}. \quad (32)$$

Thus, we have derived all quantities that allow to evaluate the general form of the GGA potential response from equations (A.16) and (A.17) for the  $1s \rightarrow 2p_x$  excitation. Inserting the appropriate enhancement factors we find the asymptotic behavior of the PBE potential response as

$$V_{x,\text{PBE}}^+(\mathbf{r}) \xrightarrow{r \rightarrow \infty} (1 + \kappa) V_{x,\text{LDA}}^+(\mathbf{r}), \quad (33)$$

where  $\kappa$  is the parameter fixed in the PBE construction [8] and

$$V_{x,\text{LDA}}^+(\mathbf{r}) \xrightarrow{r \rightarrow \infty} \frac{4}{9} A_x \frac{n^+(\mathbf{r})}{n(\mathbf{r})^{\frac{2}{3}}}. \quad (34)$$

(Formally, LDA corresponds to the general GGA form of Eq. (2) with  $F_{\text{LDA}}(s) \equiv 1$ .) The corresponding asymptotical result (with  $B_1$  being the parameter from the AK13 construction [25]) for the AK13 potential response is

$$V_{x,\text{AK13}}^+(\mathbf{r}) \xrightarrow{r \rightarrow \infty} \frac{91}{144} A_x \frac{B_1}{a_0} \frac{1}{(3\pi^2)^{\frac{1}{3}}} \frac{n^+(\mathbf{r})}{n(\mathbf{r})}, \quad (35)$$

and for B88 we obtain

$$V_{x,\text{B88}}^+(\mathbf{r}) \xrightarrow{r \rightarrow \infty} \frac{313}{96} \frac{a_0 e^2}{r^2} \frac{n^+(\mathbf{r})}{n(\mathbf{r})}. \quad (36)$$

Comparing equations (33)–(36) shows that the PBE response, as expected, is similar to the LDA one, but that the AK13 and B88 responses differ markedly. Inserting equations (21) and (22) we can determine the asymptotics of the potential response for the  $1s \rightarrow 2p_x$  excitation. For PBE, it falls off to zero just like LDA,

$$\lim_{r \rightarrow \infty} V_{x,\text{PBE}}^+(\mathbf{r}) \propto x e^{-\frac{1}{6} \frac{r}{a_0}} \xrightarrow{r \rightarrow \infty} 0, \quad (37)$$

whereas for AK13 we find

$$\lim_{r \rightarrow \infty} V_{x,\text{AK13}}^+(\mathbf{r}) \propto x e^{\frac{1}{2} \frac{r}{a_0}} \xrightarrow{r \rightarrow \infty} \infty, \quad (38)$$

and for B88

$$\lim_{r \rightarrow \infty} V_{x,\text{B88}}^+(\mathbf{r}) \propto \frac{x}{r^2} e^{\frac{1}{2} \frac{r}{a_0}} \xrightarrow{r \rightarrow \infty} \infty. \quad (39)$$

Comparing this to the exact result given in equation (19), we see that for the studied excitation the PBE response, although falling off too rapidly, goes to the correct limiting value (zero). The one of AK13 and B88, however, grows exponentially. We thus find that neither B88 nor AK13 are modeling the exact exchange response well for this one electron transition. The strength of the divergence observed for AK13 is also an important step in understanding the numerical convergence problems.

### 6.3 Numerical confirmation

Finally, in order to really rule out that our non-converging AK13 calculations in Section 5 are a consequence of

numerical issues in our Sternheimer implementation, we check our numerics by reproducing the just derived analytical result with our Sternheimer program. To this end, we do a numerical quasi-exact ground-state calculation of the hydrogen atom with the code used in Section 5, and also do the linear response calculation quasi-exactly for the hydrogen atom. By quasi-exact we mean that numerical convergence parameters were chosen very stringent and only the external perturbation potential in the Sternheimer equations (4) and (5) is taken into account, which is the exact situation for the hydrogen atom. The hydrogen atom was described using a Troullier–Martins [78] pseudopotential ( $r_c = 1.39a_0$ ), and we tested that with this pseudopotential energies and eigenvalues are close to the ones from the true hydrogen potential. With the thus numerically obtained density response we numerically evaluate the AK13 potential response. The result is depicted in Figure 3.

According to equation (35) the AK13 potential response is expected to be proportional to the ratio of the density response and the density. The upper panel of Figure 3 shows the absolute value of these two quantities on a logarithmic scale. Over a wide region of space we find close agreement. In the interior and in the outer region of the displayed simulation volume the two curves slightly deviate from each other. The dotted red line in the lower panel of Figure 3 shows that this is a consequence of the numerical and analytical results for  $\frac{n^+(\mathbf{r})}{n(\mathbf{r})}$  deviating from each other in the center of the grid and close to the boundaries. These deviations are expected and easily understood. The deviation in the interior is expected because of the use of a pseudopotential and the finite discretization, which lead to a numerical ground-state density that lacks the exact cusp at the nuclear position ( $x = 0$ ), as in every pseudopotential calculation. The deviations close to the grid boundary are a consequence of the necessity of enforcing the zero-boundary condition in the calculation of the ground-state orbitals. As the analytical density vanishes asymptotically and thus never becomes zero exactly, the numerical data has to slightly deviate from the correct asymptotic behavior near the boundary.

However, the important observation in Figure 3 is that the numerical evaluation of the AK13 response does show the same behavior as the analytical evaluation in all regions of space where it can be expected to show it (i.e., in those regions of space where the analytical and the numerical density are close to each other). The solid magenta curve in the lower panel of Figure 3 confirms that the ratio  $|V_{\text{AK13}}^+|/|\frac{n^+}{n}|$  tends to a constant for large values of  $x$ , as it should. Therefore, we confirm the reliability of our Sternheimer implementation, and also confirm the conclusion that the non-converging Sternheimer iterations for AK13 are not a result of numerical problems, but are to be attributed to the strongly diverging response of the AK13 approximation.

For the sake of completeness we depict the PBE potential response in Figure 4. The figure is in line with the analytical result for PBE and shows that the PBE response does not show any divergences.

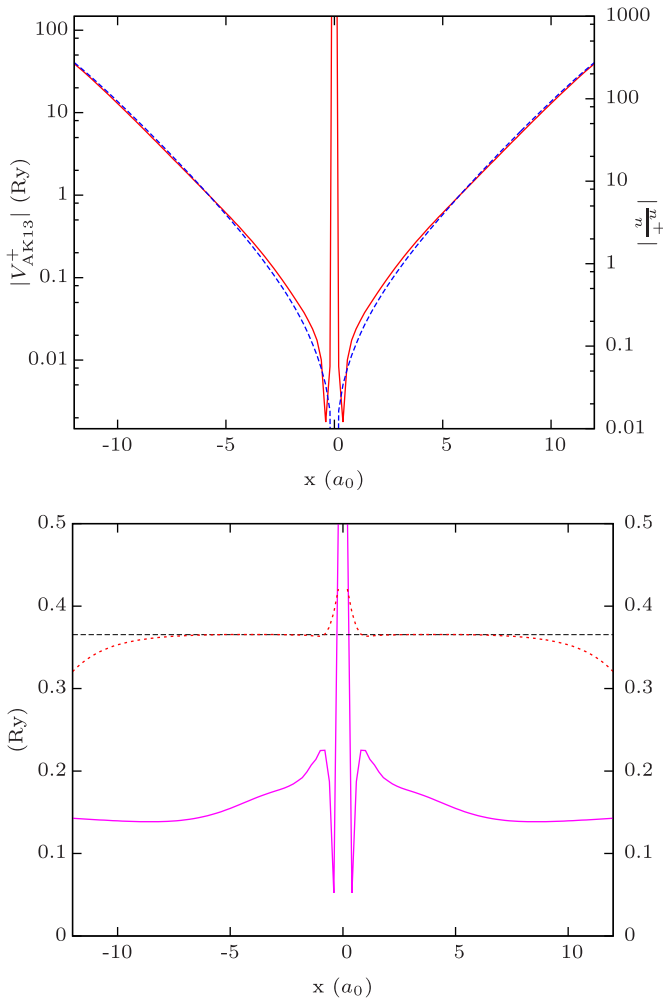


**Fig. 3.** Quasi-exact numerical ground-state and response calculation of the hydrogen atom. A sphere with radius  $r = 15 a_0$  and a grid spacing of  $\Delta r = 0.20 a_0$  was used. Upper panel, red curve, plotted against left ordinate: absolute value of the AK13 potential response  $|V_{AK13}^+|$  evaluated with the ground-state density and density response of the quasi-exact numerical calculation for the hydrogen atom. Dashed blue curve, plotted against right ordinate: ratio of the density response to the density  $|n_{n^+}^+|$ . The plot demonstrates that both functions are proportional to each other. Lower panel, solid magenta curve, plotted against left ordinate: numerical data for  $|V_{AK13}^+|$  divided by the numerical data for  $|n_{n^+}^+|$ . Dotted red curve, plotted against right ordinate: numerical data for  $|n_{n^+}^+|$  divided by the analytical data for  $|n_{n^+}^+|$ . The dashed black line serves as a reference for perfect proportionality between analytical and numerical data.

Finally, we take a look at the B88 response. As explained earlier, one has to keep in mind that B88, like AK13, is built with a diverging enhancement factor, yet the divergence is milder. Figure 5 depicts the potential response for B88, evaluated in the same way on the numerical, quasi-exact density and density response as just described for AK13. The potential response is smooth in regions of space where the density is high. Close to the

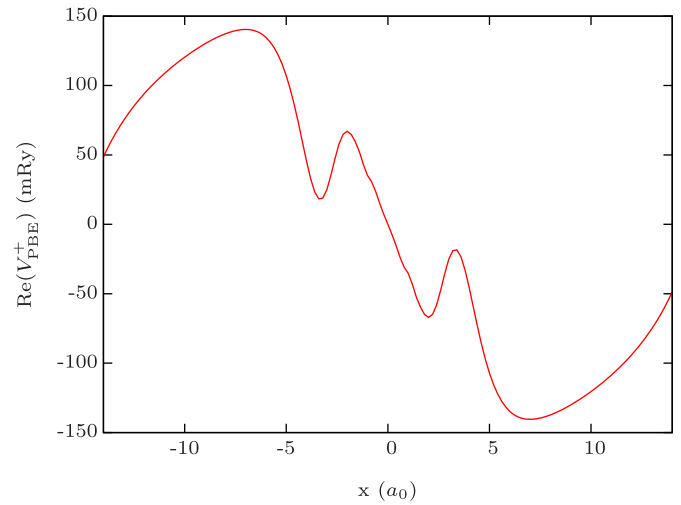


**Fig. 4.** PBE potential response evaluated with the ground-state density and density response of the quasi-exact numerical calculation for the hydrogen atom.

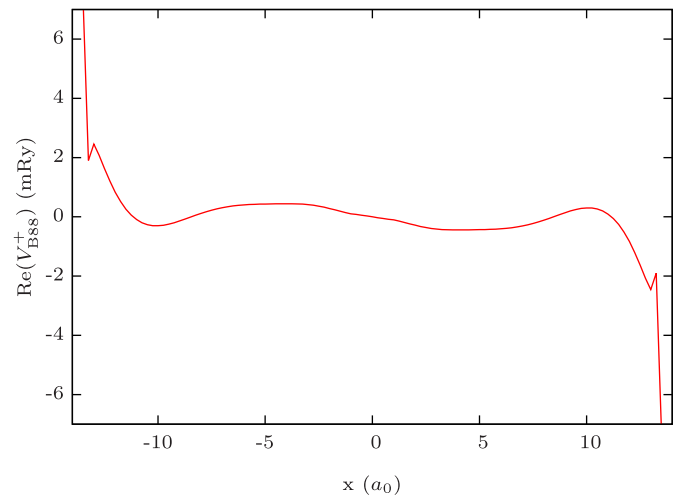


**Fig. 5.** B88 potential response evaluated with the ground-state density and density response of the quasi-exact numerical calculation for the hydrogen atom.

grid boundary we observe a strong rise and see a spike that we attribute to the influence of the grid boundary on the finite differences. However, these features do not hinder convergence of the Sternheimer equations with the B88 approximation. We could obtain fully self-consistent, converged Sternheimer results for the H-atom  $1s \rightarrow 2p_x$  excitation for B88. The excitation energy is not too different to the one found with xLDA or xPBE. On a grid of radius  $r = 15 a_0$  and with a grid spacing of  $\Delta r = 0.20 a_0$ , which leads to a numerical accuracy of a few mRy, we find excitation energies of 542, 572, 575 mRy for xLDA, xPBE and B88, respectively.

Thus, the B88 response calculations show that a diverging enhancement factor and potential response need not necessarily lead to problems in TDDFT calculations. In order to clarify the situation further, we depict in Figure 6 the asymptotics of both functionals, i.e., Figure 6

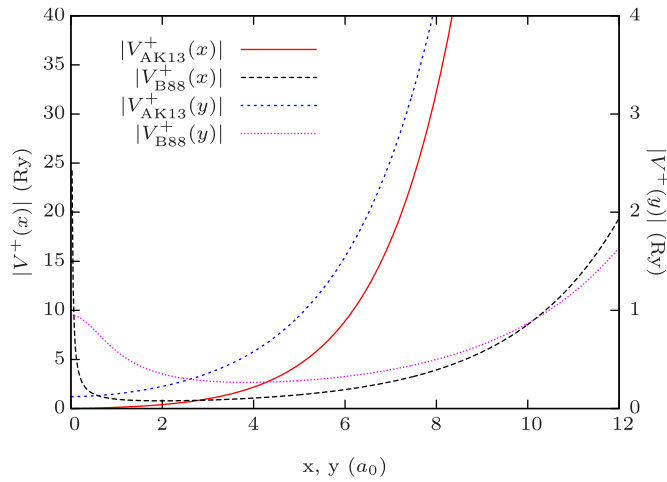


**Fig. 6.** Analytical asymptotic behavior of the AK13 and B88 functional according to equations (35) and (36). The solid red and dashed black curves are plotted against the left ordinate and depict the data along the  $x$ -direction for  $(y, z) = (0, 0) a_0$ . The dashed blue and dashed magenta curves are plotted against the right ordinate and show the data along the  $y$ -direction for  $(x, z) = (1, 0) a_0$ . The offset of  $1 a_0$  in the  $x$ -direction was chosen to avoid the orbital nodal plane.

visualizes equations (35) and (36) evaluated for the exact density and density response. The potential response of both functionals rises with the same exponential rate in the asymptotic limit, but the one of B88 is moderated by  $\frac{1}{r^{1/2}}$ . Figure 6 shows that this leads to a considerably slower rise. This finding is in line with earlier observations for ground-state calculations [54]: although both AK13 and B88 diverge on some orbital nodal planes, it is possible to converge ground-state calculations for B88 but not for AK13. The milder divergence of the B88 ground-state potential can be numerically covered, whereas the pronounced divergence of AK13 leads to serious problems. From our Sternheimer results we conclude that the situation is similar for the potential response.

## 7 Conclusion

We investigated the linear response of the AK13 GGA with the aim of exploring whether the unusual features of its functional derivative can be exploited beneficially in TDDFT calculations. We found that we cannot converge such calculations. Contrasting the AK13 response with the one of the PBE GGA, for which the Sternheimer equations can be solved without any problem, revealed that AK13 leads to an asymptotically increasing exchange response that is absent in PBE. By comparing this to the exact response, which we calculated for the hydrogen atom, we traced this finding back to AK13's diverging enhancement factor and identified the feature as not being in agreement with the proper exchange behavior. Comparison with the B88 exchange GGA, which also has a diverging enhancement factor but leads to a self-consistent solution of the Sternheimer equations, showed that a diverging enhancement factor in itself does not need to ruin the response

properties, but the particular form that is chosen in AK13 is problematic for TDDFT applications.

Our original hope was that the AK13 functional may have been useful for providing “kernel corrections” to the linear response in situations where usual GGAs, which closely follow the density, do not. Long-range charge-transfer excitations would have been a hallmark example. Our study showed that even much simpler excitations cannot be calculated with the adiabatic AK13 functional. The peculiar results found here for AK13 indicate that it is very difficult to develop a semi-local functional that leads to pronounced but beneficial response properties. Whereas it is clear that the GGA potential response would have to be sharply increasing in regions of vanishing orbital overlap in order to provide a non-vanishing correction, our results here showed that too much of a divergence can ruin the response properties altogether. A possible way out of this disaccord may be to try to model the response semi-locally, but not semi-locally in the density, but semi-locally in the orbitals, such as done in meta-GGAs [80]. In this way, it may be possible to obtain finite “kernel corrections” in a different manner, namely not by providing a potential with diverging properties, but by providing a relative potential offset of the donor- and acceptor regions of a charge-transfer system.

S.K. and J.G. acknowledge support by Deutsche Forschungsgemeinschaft Graduiertenkolleg 1640 and by the study program “Biological Physics” of the Elite Network of Bavaria. S.K. further acknowledges support by the German-Israeli Foundation for Scientific Research and Development. J.G. and F.H. acknowledge support by the University of Bayreuth Graduate School. R.A. acknowledges support from the Swedish Research Council (VR) project no. 2016-04810 and the Swedish e-Science Research Centre (SeRC). S.K. thanks E.K.U. Gross for countless discussions at conferences and for infecting him with his enthusiasm for TDDFT.

## Author contribution statement

J.G. did the analytical and numerical calculations including the programming of the AK13 response routines, F.H. developed and programmed the Sternheimer linear response code, S.K. initiated and supervised the project, J.G. and S.K. analyzed the results and structured the discussion, all authors contributed to the discussion, the writing and the proofreading of the manuscript.

## Appendix A: Details of how the GGA kernel enters the Sternheimer equations

We here give some details about how to use functionals of the GGA form in the Sternheimer approach. It is an appealing feature of the Sternheimer equations that they do not require the xc kernel by itself, but only the xc potential response. This is advantageous as the potential response only depends on one three-dimensional spatial coordinate, whereas the xc kernel depends on two. Thus, it is easier to analyze the effects of a particular xc

approximation on the linear response by looking at the xc potential response instead of the xc kernel itself.

The starting point for the derivation of the AK13 potential response is the GGA form of the (semi-local) exchange energy functional from equation (2). The corresponding potential to this is the functional derivative  $\frac{\delta E_x^{\text{SL}}[n]}{\delta n(\mathbf{r})}$ , which can be extracted from reference [60] and rearranged to

$$v_x^{\text{SL}}[n](\mathbf{r}) = \frac{4}{3} A_x n(\mathbf{r})^{\frac{1}{3}} \times \underbrace{\left[ F(s) - \left( \frac{3}{4} \frac{t}{s} - \frac{3}{4} \frac{u}{s^2} + s \right) F'(s) - \left( \frac{3}{4} \frac{u}{s} - s^2 \right) F''(s) \right]}_{=:B(\mathbf{r})}, \quad (\text{A.1})$$

with

$$s = \frac{|\nabla n(\mathbf{r})|}{2(3\pi^2)^{\frac{1}{3}} n(\mathbf{r})^{\frac{4}{3}}} \quad (\text{A.2})$$

$$u = \frac{\nabla n(\mathbf{r}) \cdot \nabla |\nabla n(\mathbf{r})|}{8(3\pi^2) n(\mathbf{r})^3} \quad (\text{A.3})$$

$$t = \frac{\nabla^2 n(\mathbf{r})}{4(3\pi^2)^{\frac{2}{3}} n(\mathbf{r})^{\frac{5}{3}}}. \quad (\text{A.4})$$

According to equation (14) the kernel is the functional derivative of the potential. Thus, it takes the form

$$f_x^{\text{SL}}[n](\mathbf{r}, \mathbf{r}') = \frac{4}{9} A_x n(\mathbf{r})^{-\frac{2}{3}} \delta(\mathbf{r} - \mathbf{r}') B(\mathbf{r}) + \frac{4}{3} A_x n(\mathbf{r})^{\frac{1}{3}} \frac{\delta B(\mathbf{r})}{\delta n(\mathbf{r}')}, \quad (\text{A.5})$$

with

$$B(\mathbf{r}) = F(s) - \left( \frac{3}{4} \frac{t}{s} - \frac{3}{4} \frac{u}{s^2} + s \right) F'(s) - \left( \frac{3}{4} \frac{u}{s} - s^2 \right) F''(s). \quad (\text{A.6})$$

Aside from derivatives of the exchange enhancement factor, the functional derivatives of  $s$ ,  $u$  and  $t$  are needed for  $\frac{\delta B(\mathbf{r})}{\delta n(\mathbf{r})}$ . These are given by:

$$\frac{\delta s(\mathbf{r})}{\delta n(\mathbf{r}')} = \frac{n(\mathbf{r}) \nabla n(\mathbf{r}) \cdot \nabla \delta(\mathbf{r} - \mathbf{r}') - \frac{4}{3} |\nabla n(\mathbf{r})|^2 \delta(\mathbf{r} - \mathbf{r}')}{2(3\pi^2)^{\frac{1}{3}} n(\mathbf{r})^{\frac{7}{3}} |\nabla n(\mathbf{r})|} \quad (\text{A.7})$$

$$\begin{aligned} \frac{\delta u(\mathbf{r})}{\delta n(\mathbf{r}')} &= \frac{n(\mathbf{r}) \nabla |\nabla n(\mathbf{r})| \cdot \nabla \delta(\mathbf{r} - \mathbf{r}')}{8(3\pi^2) n(\mathbf{r})^4} \\ &+ \frac{n(\mathbf{r}) \nabla n(\mathbf{r}) \cdot \nabla \left( \frac{\nabla n(\mathbf{r}) \cdot \nabla \delta(\mathbf{r} - \mathbf{r}')}{|\nabla n(\mathbf{r})|} \right)}{8(3\pi^2) n(\mathbf{r})^4} \\ &- \frac{3 \nabla n(\mathbf{r}) \cdot [\nabla |\nabla n(\mathbf{r})|] \delta(\mathbf{r} - \mathbf{r}')}{8(3\pi^2) n(\mathbf{r})^4} \end{aligned} \quad (\text{A.8})$$

$$\frac{\delta t(\mathbf{r})}{\delta n(\mathbf{r}')} = \frac{n(\mathbf{r}) \nabla^2 \delta(\mathbf{r} - \mathbf{r}') - [\nabla^2 n(\mathbf{r})] \cdot \frac{5}{3} \delta(\mathbf{r} - \mathbf{r}')}{4(3\pi^2)^{\frac{2}{3}} n(\mathbf{r})^{\frac{8}{3}}} \quad (\text{A.9})$$

Altogether these equations yield the functional derivative of  $B(\mathbf{r})$  in terms of the functional derivatives of  $\frac{\delta s(\mathbf{r})}{\delta n(\mathbf{r}'')}$ ,  $\frac{\delta u(\mathbf{r})}{\delta n(\mathbf{r}'')}$  and  $\frac{\delta t(\mathbf{r})}{\delta n(\mathbf{r}'')}$ :

$$\begin{aligned} \frac{\delta B(\mathbf{r})}{\delta n(\mathbf{r}')} &= -F'(s) \left[ \frac{3}{4} \frac{1}{s} \frac{\delta t(\mathbf{r})}{\delta n(\mathbf{r}')} - \frac{3}{4} \frac{t}{s^2} \frac{\delta s(\mathbf{r})}{\delta n(\mathbf{r}')} \right. \\ &\quad \left. - \frac{3}{4} \frac{1}{s^2} \frac{\delta u(\mathbf{r})}{\delta n(\mathbf{r}')} + 2 \cdot \frac{3}{4} \frac{u}{s^3} \frac{\delta s(\mathbf{r})}{\delta n(\mathbf{r}')} \right] \\ &- F''(s) \left[ \frac{3}{4} \frac{t}{s} \frac{\delta s(\mathbf{r})}{\delta n(\mathbf{r}')} - 2 \cdot \frac{3}{4} \frac{u}{s^2} \frac{\delta s(\mathbf{r})}{\delta n(\mathbf{r}')} \right. \\ &\quad \left. + \frac{3}{4} \frac{1}{s} \frac{\delta u(\mathbf{r})}{\delta n(\mathbf{r}')} - s \frac{\delta s(\mathbf{r})}{\delta n(\mathbf{r}')} \right] \\ &- F'''(s) \left[ \frac{3}{4} \frac{u}{s} - s^2 \right] \frac{\delta s(\mathbf{r})}{\delta n(\mathbf{r}')} \end{aligned} \quad (\text{A.10})$$

In none of the Sternheimer equations (4), (5), (11), (12) and (15) the kernel is needed explicitly standalone. The only point where it enters the formalism is by setting up the exchange–correlation potential response via equation (12). As the GGA form (2) is an approximation for the exchange energy and is used in the adiabatic approximation

$$f_x^{\text{SL}}(\mathbf{r}, \mathbf{r}', \bar{\omega}) = f_x^{\text{SL}}(\mathbf{r}, \mathbf{r}'),$$

throughout this manuscript, equation (12) together with equation (A.5) becomes

$$\begin{aligned} V_{x,\text{SL}}^+(\mathbf{r}) &= \int d^3 r' n^+(\mathbf{r}') f_x^{\text{SL}}(\mathbf{r}, \mathbf{r}') \\ &= \frac{4}{9} A_x n(\mathbf{r})^{-\frac{2}{3}} B(\mathbf{r}) n^+(\mathbf{r}) \\ &\quad + \frac{4}{3} A_x n(\mathbf{r})^{\frac{1}{3}} \int d^3 r' n^+(\mathbf{r}') \frac{\delta B(\mathbf{r})}{\delta n(\mathbf{r}')}. \end{aligned} \quad (\text{A.11})$$

In the occurring integral, the integration variable is  $\mathbf{r}'$  and the only dependences on  $\mathbf{r}'$  in  $\frac{\delta B(\mathbf{r})}{\delta n(\mathbf{r}')}$  are buried in the  $\delta$ -functions of  $\frac{\delta s(\mathbf{r})}{\delta n(\mathbf{r}'')}$ ,  $\frac{\delta u(\mathbf{r})}{\delta n(\mathbf{r}'')}$  and  $\frac{\delta t(\mathbf{r})}{\delta n(\mathbf{r}'')}$ . Thus, the  $\mathbf{r}'$  integration in equation (A.11) comes down to integrals of the form

$$\zeta^+(\mathbf{r}) := \int d^3 r' n^+(\mathbf{r}') \frac{\delta \zeta(\mathbf{r})}{\delta n(\mathbf{r}')}, \quad (\text{A.12})$$

where  $\zeta$  is  $s$ ,  $u$  or  $t$ , respectively. These integrals are given by:

$$s^+(\mathbf{r}) = \frac{n(\mathbf{r}) \nabla n(\mathbf{r}) \cdot \nabla n^+(\mathbf{r}) - \frac{4}{3} |\nabla n(\mathbf{r})|^2 n^+(\mathbf{r})}{2(3\pi^2)^{\frac{1}{3}} n(\mathbf{r})^{\frac{7}{3}} |\nabla n(\mathbf{r})|} \quad (\text{A.13})$$

$$\begin{aligned}
u^+(\mathbf{r}) &= \frac{n(\mathbf{r}) \nabla |\nabla n(\mathbf{r})| \cdot \nabla n^+(\mathbf{r})}{8(3\pi^2)n(\mathbf{r})^4} \\
&+ \frac{n(\mathbf{r}) \nabla n(\mathbf{r}) \cdot \nabla \left( \frac{\nabla n(\mathbf{r}) \cdot \nabla n^+(\mathbf{r})}{|\nabla n(\mathbf{r})|} \right)}{8(3\pi^2)n(\mathbf{r})^4} \\
&- \frac{3 \nabla n(\mathbf{r}) \cdot [\nabla |\nabla n(\mathbf{r})|] n^+(\mathbf{r})}{8(3\pi^2)n(\mathbf{r})^4} \quad (\text{A.14})
\end{aligned}$$

$$t^+(\mathbf{r}) = \frac{n(\mathbf{r}) \nabla^2 n^+(\mathbf{r}) - [\nabla^2 n(\mathbf{r})] \cdot \frac{5}{3} n^+(\mathbf{r})}{4(3\pi^2)^{\frac{2}{3}} n(\mathbf{r})^{\frac{8}{3}}} \quad (\text{A.15})$$

At this point the exchange potential response of equation (A.11) is fully determined and can be expressed in terms of  $s^+(\mathbf{r})$ ,  $u^+(\mathbf{r})$  and  $t^+(\mathbf{r})$ , which yields:

$$\begin{aligned}
V_{x,SL}^+(\mathbf{r}) &= \frac{4}{9} A_x n(\mathbf{r})^{-\frac{2}{3}} B(\mathbf{r}) n^+(\mathbf{r}) \\
&+ \frac{4}{3} A_x n(\mathbf{r})^{\frac{1}{3}} \int d^3 r' n^+(\mathbf{r}') \frac{\delta B(\mathbf{r})}{\delta n(\mathbf{r}')} \quad (\text{A.16})
\end{aligned}$$

$$\begin{aligned}
&= \frac{4}{9} A_x n(\mathbf{r})^{-\frac{2}{3}} B(\mathbf{r}) n^+(\mathbf{r}) + \frac{4}{3} A_x n(\mathbf{r})^{\frac{1}{3}} I \quad \text{and} \\
I &= -F'(s) \left[ \frac{3}{4} \frac{1}{s} t^+(\mathbf{r}) - \frac{3}{4} \frac{t}{s^2} s^+(\mathbf{r}) \right. \\
&\quad \left. - \frac{3}{4} \frac{1}{s^2} u^+(\mathbf{r}) + 2 \cdot \frac{3}{4} \frac{u}{s^3} s^+(\mathbf{r}) \right] \\
&- F''(s) \left[ \frac{3}{4} \frac{t}{s} s^+(\mathbf{r}) - 2 \cdot \frac{3}{4} \frac{u}{s^2} s^+(\mathbf{r}) \right. \\
&\quad \left. + \frac{3}{4} \frac{1}{s} u^+(\mathbf{r}) - s s^+(\mathbf{r}) \right] \\
&- F'''(s) \left[ \frac{3}{4} \frac{u}{s} s^+(\mathbf{r}) - s^2 s^+(\mathbf{r}) \right] \quad (\text{A.17})
\end{aligned}$$

This is the potential response for a spin-independent calculation. The spin-scaling relation

$$f_x^{SL,\sigma,\tau}[n_\uparrow, n_\downarrow](\mathbf{r}, \mathbf{r}') = 2 f_x^{SL}[2n_\sigma](\mathbf{r}, \mathbf{r}') \delta_{\sigma\tau}, \quad (\text{A.18})$$

for the x kernel then leads to the spin-dependent potential response

$$\begin{aligned}
V_{x,SL}^{+,\sigma}(\mathbf{r}) &= \sum_{\tau=\uparrow,\downarrow} \int d^3 r' n_\tau^+(\mathbf{r}') f_x^{SL,\sigma,\tau}[n_\uparrow, n_\downarrow](\mathbf{r}, \mathbf{r}') \\
&= 2 \int d^3 r' n_\sigma^+(\mathbf{r}') f_x^{SL}[2n_\sigma](\mathbf{r}, \mathbf{r}'), \quad (\text{A.19})
\end{aligned}$$

in the adiabatic approximation. For implementing a given GGA, it only remains to compute the first, second and third derivatives of the exchange enhancement factor, i.e.,  $F'(s)$ ,  $F''(s)$ ,  $F'''(s)$ .

## Appendix B: Deriving the hydrogen atom density response from the Sternheimer equations

We start from the Sternheimer equations (4) and (5), which for an exact calculation of the hydrogen atom read

$$\begin{aligned}
[h - \epsilon_{1s} - \hbar\bar{\omega}]|\phi^+\rangle &= -\hat{Q} V_{\text{ext}}^+ |\varphi_{1s}\rangle = -V_{\text{ext}}^+ |\varphi_{1s}\rangle \\
[h - \epsilon_{1s} + \hbar\bar{\omega}]|\phi^-\rangle &= -\hat{Q} V_{\text{ext}}^+ |\varphi_{1s}\rangle = -V_{\text{ext}}^+ |\varphi_{1s}\rangle, \quad (\text{B.1})
\end{aligned}$$

where  $|\phi^+\rangle$  and  $|\phi^-\rangle$  are the orbital responses of an orbital starting its propagation in the hydrogen atom 1s ground-state orbital  $|\varphi_{1s}\rangle$ ,  $\epsilon_{1s}$  is the eigenenergy of the hydrogen atom 1s ground-state orbital and  $h$  is the ground-state Hamiltonian of the hydrogen atom.

The projector  $\hat{Q} = 1 - |\varphi_{1s}\rangle\langle\varphi_{1s}|$  is of no effect in this case, as  $\langle\varphi_{1s}|V_{\text{ext}}^+|\varphi_{1s}\rangle = 0$ . This is because  $|\varphi_{1s}\rangle$  is an even function with respect to its spatial coordinates, but  $V_{\text{ext}}^+$  is a linear function with regard to its spatial coordinates according to equation (16) and thus is spatially odd.

The calculation for the hydrogen atom is of course a spin-dependent one. However, as only one spin channel is occupied, and as there is no preference for either of the two possibilities, the spin index is omitted in this section.  $|\phi^+\rangle$  and  $|\phi^-\rangle$  are orthogonal to  $|\varphi_{1s}\rangle$  [37] which can easily be verified by projecting  $\langle\varphi_{1s}|$  onto equations (4) and (5). Hence,  $|\phi^+\rangle$  and  $|\phi^-\rangle$  can be expanded in terms of the unoccupied ground-state orbitals  $|\varphi_j\rangle$  with  $j > 1$  as  $|\varphi_1\rangle := |\varphi_{1s}\rangle$ :

$$\begin{aligned}
|\phi^+\rangle &= \sum_{j=2}^{\infty} c_j^+ |\varphi_j\rangle \\
|\phi^-\rangle &= \sum_{j=2}^{\infty} c_j^- |\varphi_j\rangle \quad (\text{B.2})
\end{aligned}$$

Inserting this into the Sternheimer equations (B.1) and projecting  $\langle\varphi_i|$  onto them yields

$$\begin{aligned}
\langle\varphi_i|[h - \epsilon_{1s} - \hbar\bar{\omega}]|\phi^+\rangle &= \sum_{j=2}^{\infty} (\epsilon_j - \epsilon_{1s} - \hbar\bar{\omega}) c_j^+ \langle\varphi_i|\varphi_j\rangle \\
&= -\langle\varphi_i|V_{\text{ext}}^+|\varphi_{1s}\rangle \quad (\text{B.3})
\end{aligned}$$

$$\begin{aligned}
\langle\varphi_i|[h - \epsilon_{1s} + \hbar\bar{\omega}]|\phi^-\rangle &= \sum_{j=2}^{\infty} (\epsilon_j - \epsilon_{1s} + \hbar\bar{\omega}) c_j^- \langle\varphi_i|\varphi_j\rangle \\
&= -\langle\varphi_i|V_{\text{ext}}^+|\varphi_{1s}\rangle, \quad (\text{B.4})
\end{aligned}$$

where  $\epsilon_j$  is the corresponding hydrogen ground-state energy eigenvalue of  $|\varphi_j\rangle$ . From this the coefficients  $c_i^\pm$  can be determined as

$$c_i^\pm = \frac{-\langle\varphi_i|V_{\text{ext}}^+|\varphi_{1s}\rangle}{\epsilon_i - \epsilon_{1s} \mp \hbar\bar{\omega}}, \quad (\text{B.5})$$

which by inserting these coefficients into equation (B.2) results in

$$|\phi^+\rangle = - \sum_{i=2}^{\infty} \frac{\langle \varphi_i | V_{\text{ext}}^+ | \varphi_{1s} \rangle}{\epsilon_i - \epsilon_{1s} - \hbar\bar{\omega}} |\varphi_i\rangle \quad (\text{B.6})$$

$$|\phi^-\rangle = - \sum_{i=2}^{\infty} \frac{\langle \varphi_i | V_{\text{ext}}^+ | \varphi_{1s} \rangle}{\epsilon_i - \epsilon_{1s} + \hbar\bar{\omega}} |\varphi_i\rangle. \quad (\text{B.7})$$

For the further derivation the matrix element

$$\langle \varphi_i | V_{\text{ext}}^+ | \varphi_{1s} \rangle \stackrel{(16)}{=} eE \langle \varphi_i | x | \varphi_{1s} \rangle,$$

has to be calculated, where the external electric field points in the  $x$ -direction ( $\mathbf{E} = E \mathbf{e}_x$ ). In order to evaluate this, each of the three parts  $\varphi_i$ ,  $x$  and  $\varphi_{1s}$ , respectively, can be expressed by spherical harmonics. Reference [81] calculates such integrals of three spherical harmonics, from which the dipole selection rules can be derived. One finds:

$$\langle \varphi_i | x | \varphi_{1s} \rangle = \langle \varphi_{np_x} | x | \varphi_{1s} \rangle \cdot \delta_{i,np_x} \quad (\text{B.8})$$

With this and equations (B.6) and (B.7) the density response can be expanded in terms of the unoccupied ground-state orbitals according to equation (15). With real-valued ground-state orbitals and the definition  $\hbar\omega_{1i} := \epsilon_i - \epsilon_{1s}$  one arrives at:

$$\begin{aligned} n^+(\mathbf{r}, \bar{\omega}) &= \varphi_{1s}(\mathbf{r}) [\phi^+(\mathbf{r}, \bar{\omega}) + \phi^-(\mathbf{r}, \bar{\omega})] \\ &= - \sum_{n=2}^{\infty} \frac{eE}{\hbar} \langle \varphi_{np_x} | x | \varphi_{1s} \rangle \varphi_{1s}(\mathbf{r}) \varphi_{np_x}(\mathbf{r}) \\ &\quad \times \left[ \underbrace{\frac{1}{\omega_{1n} - \bar{\omega}} + \frac{1}{\omega_{1n} + \bar{\omega}}}_{=: C} \right], \end{aligned} \quad (\text{B.9})$$

with

$$\begin{aligned} \Re(C) &= \frac{2\omega_{1n} [(\omega_{1n}^2 - \omega^2) + \eta^2]}{[(\omega_{1n} - \omega)^2 + \eta^2][(\omega_{1n} + \omega)^2 + \eta^2]} \\ \Im(C) &= \frac{4\omega_{1n}\omega\eta}{[(\omega_{1n} - \omega)^2 + \eta^2][(\omega_{1n} + \omega)^2 + \eta^2]}. \end{aligned} \quad (\text{B.10})$$

As already mentioned in Section 4, the parameter  $\eta$  is introduced to model the switch-on process of the external perturbation. In the adiabatic limit of  $\eta \rightarrow 0$ , the density response for  $\omega \neq \omega_{1n}$  becomes

$$\begin{aligned} n^+(\mathbf{r}, \omega) &= - \sum_{n=2}^{\infty} \frac{eE}{\hbar} \langle \varphi_{np_x} | x | \varphi_{1s} \rangle \varphi_{1s}(\mathbf{r}) \varphi_{np_x}(\mathbf{r}) \\ &\quad \times \frac{2\omega_{1n}}{(\omega_{1n} - \omega)(\omega_{1n} + \omega)}. \end{aligned} \quad (\text{B.11})$$

In line with the objective of Section 6.2 to evaluate the potential response for the  $1s \rightarrow 2p_x$  excitation, equation (B.11) has to be considered in the limit  $\omega \rightarrow \omega_{12}$ .

In this case the term for  $n = 2$  dominates all other contributions. Thus, this yields

$$n^+(\mathbf{r}, \omega \rightarrow \omega_{12}) \propto \varphi_{1s}(\mathbf{r}) \varphi_{2p_x}(\mathbf{r}), \quad (\text{B.12})$$

for the density response of the  $1s \rightarrow 2p_x$  excitation of the hydrogen atom. As the interest in Section 6.2 lies only in the spatial dependence of the investigated quantities, we use

$$n^+(\mathbf{r}) = \varphi_{1s}(\mathbf{r}) \varphi_{2p_x}(\mathbf{r}), \quad (\text{B.13})$$

i.e., drop the proportionality factors. Inserting the explicit, analytic forms of  $\varphi_{1s}(\mathbf{r})$  and  $\varphi_{2p_x}(\mathbf{r})$  [81], equations (21) and (22) follow.

## References

1. P. Hohenberg, W. Kohn, Phys. Rev. **136**, B864 (1964)
2. W. Kohn, L.J. Sham, Phys. Rev. **140**, A1133 (1965)
3. E. Runge, E.K.U. Gross, Phys. Rev. Lett. **52**, 997 (1984)
4. E.K.U. Gross, W. Kohn, Phys. Rev. Lett. **55**, 2850 (1985)
5. M. Petersilka, U.J. Gossmann, E.K.U. Gross, Phys. Rev. Lett. **76**, 1212 (1996)
6. M. Lein, E.K.U. Gross, J.P. Perdew, Phys. Rev. B **61**, 13431 (2000)
7. T. Grabo, T. Kreibich, S. Kurth, E.K.U. Gross, in *Strong Coulomb Correlation in Electronic Structure: Beyond the Local Density Approximation*, edited by V. Anisimov (Gordon & Breach, Tokyo, 2000), pp. 203–311
8. J.P. Perdew, K. Burke, M. Ernzerhof, Phys. Rev. Lett. **77**, 3865 (1996)
9. A.D. Becke, J. Chem. Phys. **98**, 1372 (1993)
10. A. Dreuw, M. Head-Gordon, J. Am. Chem. Soc. **126**, 4007 (2004)
11. D. Tozer, J. Chem. Phys. **119**, 12697 (2003)
12. N. Maitra, J. Chem. Phys. **122**, 234104 (2005)
13. S. Kümmel, Adv. Energy Mater. **7**, 1700440 (2017)
14. J.D. Gledhill, D. Tozer, J. Chem. Phys. **143**, 024104 (2015)
15. A.D. Becke, E.R. Johnson, J. Chem. Phys. **124**, 221101 (2006)
16. A.P. Gaiduk, V.N. Staroverov, J. Chem. Phys. **128**, 204101 (2008)
17. V.N. Staroverov, J. Chem. Phys. **129**, 134103 (2008)
18. R. Armiento, S. Kümmel, T. Körzdörfer, Phys. Rev. B **77**, 165106 (2008)
19. A. Karolewski, R. Armiento, S. Kümmel, J. Chem. Theory Comput. **5**, 712 (2009)
20. E. Räsänen, S. Pittalis, C.R. Proetto, J. Chem. Phys. **132**, 044112 (2010)
21. D. Koller, F. Tran, P. Blaha, Phys. Rev. B **85**, 155109 (2012)
22. F. Tran, P. Blaha, Phys. Rev. Lett. **102**, 226401 (2009)
23. F. Tran, P. Blaha, K. Schwarz, J. Phys.: Condens. Matter **19**, 196208 (2007)
24. F. Tran, P. Blaha, M. Betzinger, S. Blügel, Phys. Rev. B **91**, 165121 (2015)
25. R. Armiento, S. Kümmel, Phys. Rev. Lett. **111**, 036402 (2013)
26. T.F.T. Cerqueira, M.J.T. Oliveira, M.A.L. Marques, J. Chem. Theory Comput. **10**, 5625 (2014)

27. A. Karolewski, R. Armiento, S. Kümmel, Phys. Rev. A **88**, 052519 (2013)
28. A.P. Gaiduk, S.K. Chulkov, V.N. Staroverov, J. Chem. Theory Comput. **5**, 699 (2009)
29. M. Mundt, S. Kümmel, R. van Leeuwen, P.-G. Reinhard, Phys. Rev. A **75**, 050501(R) (2007)
30. T. Körzdörfer, S. Kümmel, Phys. Rev. B **82**, 155206 (2010)
31. A.R. Williams, U. von Barth, in *Theory of the inhomogeneous electron gas*, edited by S. Lundqvist, N.H. March (Springer Science + Business Media, LLC, New York, 1983), p. 200
32. A.D. Becke, J. Chem. Phys. **98**, 5648 (1993)
33. M.E. Casida, in *Recent Developments and Applications in Density-Functional Theory*, edited by J.M. Seminario (Elsevier Science, Amsterdam, 1996), pp. 391–439
34. E.K.U. Gross, K. Burke, in *Time-dependent Density Functional Theory*, edited by M. Marques, C. Ullrich, F. Nogueira, A. Rubio, K. Burke, E. Gross, (Springer, Berlin, 2006), p. 10
35. C. Filippi, C.J. Umrigar, X. Gonze, J. Chem. Phys. **107**, 9994 (1997)
36. R. van Meer, O. Gritsenko, E.J. Baerends, J. Chem. Theory Comput. **10**, 4432 (2014)
37. F. Hofmann, I. Schelter, S. Kümmel, J. Chem. Phys. (submitted)
38. J.B. Krieger, Y. Li, G.J. Iafrate, Phys. Rev. A **46**, 5453 (1992)
39. M. Mundt, S. Kümmel, Phys. Rev. Lett. **95**, 203004 (2005)
40. M. Hellgren, E.K.U. Gross, Phys. Rev. A **85**, 022514 (2012)
41. M. Lein, S. Kümmel, Phys. Rev. Lett. **94**, 143003 (2005)
42. M. Thiele, E.K.U. Gross, S. Kümmel, Phys. Rev. Lett. **100**, 153004 (2008)
43. J.I. Fuks, N.T. Maitra, Phys. Rev. A **89**, 062502 (2014)
44. N. Maitra, J. Chem. Phys. **144**, 220901 (2016)
45. M. Thiele, S. Kümmel, Phys. Rev. Lett. **112**, 083001 (2014)
46. T. Stein, L. Kronik, R. Baer, J. Am. Chem. Soc. **131**, 2818 (2009)
47. A. Karolewski, A. Neubig, M. Thelakkat, S. Kümmel, Phys. Chem. Chem. Phys. **15**, 20016 (2013)
48. T. Körzdörfer, J.-L. Bredas, Acc. Chem. Res. **47**, 3284 (2014)
49. Y. Li, C.A. Ullrich, J. Chem. Theory Comput. **11**, 5838 (2015)
50. Y. Li, C.A. Ullrich, J. Chem. Phys. **145**, 164107 (2016)
51. Y. Li, M. Dhanashree, S. Patil, S. Guha, C.A. Ullrich, Mol. Phys. **114**, 1365 (2016)
52. V. Vlček, G. Steinle-Neumann, L. Leppert, R. Armiento, S. Kümmel, Phys. Rev. B **91**, 035107 (2015)
53. F. Tran, P. Blaha, M. Betzinger, S. Blügel, Phys. Rev. B **94**, 165149 (2016)
54. T. Aschebrock, R. Armiento, S. Kümmel, Phys. Rev. B **95**, 245118 (2017)
55. T. Aschebrock, R. Armiento, S. Kümmel, Phys. Rev. B **96**, 075140 (2017)
56. A.D. Becke, Phys. Rev. A **38**, 3098 (1988)
57. R. van Leeuwen, E.J. Baerends, Phys. Rev. A **49**, 2421 (1994)
58. A. Lembarki, F. Rogemond, H. Chermette, Phys. Rev. A **52**, 3704 (1995)
59. X. Andrade, S. Botti, M.A.L. Marques, A. Rubio, J. Chem. Phys. **126**, 184106 (2007)
60. J.P. Perdew, W. Yue, Phys. Rev. B **33**, 8800 (1986)
61. P.J. Stephens, J.F. Devlin, C.F. Chabalowski, M.J. Frisch, J. Phys. Chem. **98**, 11623 (1994)
62. A. Lindmaa, R. Armiento, Phys. Rev. B **94**, 155143 (2016)
63. X. Andrade, D. Strubbe, U.D. Giovannini, A.H. Larsen, M.J.T. Oliveira, J. Alberdi-Rodriguez, A. Varas, I. Theophilou, N. Helbig, M.J. Verstraete, L. Stella, F. Nogueira, A. Aspuru-Guzik, A. Castro, M.A.L. Marques, A. Rubio, Phys. Chem. Chem. Phys. **17**, 31371 (2015)
64. K. Lopata, N. Govind, J. Chem. Theory Comput. **7**, 1344 (2011)
65. M.R. Provorse, C.M. Isborn, Int. J. Quant. Chem. **116**, 739 (2016)
66. I. Schelter, S. Kümmel, J. Chem. Theory Comput. **14**, 1910 (2018)
67. P.-G. Reinhard, M. Brack, F. Calvayrac, C. Kohl, S. Kümmel, E. Suraud, C.A. Ullrich, Eur. Phys. J. D **9**, 111 (1999)
68. M. Moseler, B. Huber, H. Häkkinen, U. Landman, G. Wrigge, M.A. Hoffmann, B.V. Issendorff, Phys. Rev. B **68**, 165413 (2003)
69. D. Hofmann, S. Kümmel, J. Chem. Phys. **137**, 064117 (2012)
70. S. Kümmel, K. Andrae, P.-G. Reinhard, Appl. Phys. B **73**, 293 (2001)
71. A. Rubio, J.A. Alonso, X. Blase, L. Balbas, S.G. Louie, Phys. Rev. Lett. **77**, 247 (1996)
72. M.A.L. Marques, A. Castro, A. Rubio, J. Chem. Phys. **115**, 3006 (2001)
73. I. Vasiliev, S. Ögüt, J.R. Chelikowsky, Phys. Rev. Lett. **82**, 1919 (1999)
74. I. Vasiliev, S. Ögüt, J.R. Chelikowsky, Phys. Rev. B **65**, 115416 (2002)
75. S. Kümmel, M. Brack, Phys. Rev. A **64**, 022506 (2001)
76. M. Mundt, S. Kümmel, Phys. Rev. B **76**, 035413 (2007)
77. L. Kronik, A. Makmal, M.L. Tiago, M.M.G. Alemany, M. Jain, X. Huang, Y. Saad, J.R. Chelikowsky, Phys. Status Solidi B **243**, 1063 (2006)
78. N. Troullier, J.L. Martins, Phys. Rev. B **43**, 1993 (1991)
79. C. Fiolhas, F. Nogueira, M.A.L. Marques, in *A Primer in Density Functional Theory*, Lecture Notes in Physics (Springer, Berlin, Heidelberg, 2003), Vol. 620
80. V.U. Nazarov, G. Vignale, Phys. Rev. Lett. **107**, 216402 (2011)
81. C. Cohen-Tannoudji, B. Diu, F. Laloë, in *Quantenmechanik* (de Gruyter, Berlin, 2009), Vols. 1 and 2

## Publication 3

### **Efficiently evaluating the Krieger-Li-Iafrate and common-energy-denominator approximations in the frequency-dependent Sternheimer scheme**

Reprinted with permission from  
*Physical Review A* **99**, 022507 (2019)

© 2019 by the American Physical Society.

Fabian Hofmann, Ingo Schelter, Stephan Kümmel

Theoretical Physics IV, University of Bayreuth, 95440 Bayreuth, Germany

Publ. 3

---

### **My contribution**

I performed all analytical derivations, implemented the relevant routines in PARSEC, performed all LR calculations as well as the finite field calculations for  $H_8$ , prepared all figures, and wrote the first draft of the manuscript.

Publ. 3

## Efficiently evaluating the Krieger-Li-Iafrate and common-energy-denominator approximations in the frequency-dependent Sternheimer scheme

Fabian Hofmann, Ingo Schelter, and Stephan Kümmel

*Theoretical Physics IV, University of Bayreuth, 95440 Bayreuth, Germany*



(Received 25 November 2018; revised manuscript received 18 January 2019; published 20 February 2019)

We show that within the Krieger-Li-Iafrate and common-energy-denominator approximations, the linearized time-dependent Kohn-Sham equations for orbital functionals can be solved very efficiently using the frequency-dependent Sternheimer scheme. The Kohn-Sham response can be obtained without the need to explicitly evaluate the exchange-correlation kernel as a functional derivative with respect to the density. Instead, it suffices to compute functional derivatives with respect to the orbitals. The scheme allows for the computationally efficient use of orbital functional potential approximations in Kohn-Sham response theory.

DOI: [10.1103/PhysRevA.99.022507](https://doi.org/10.1103/PhysRevA.99.022507)

### I. INTRODUCTION: TIME-DEPENDENT DENSITY-FUNCTIONAL THEORY AND ORBITAL FUNCTIONALS

Time-dependent density-functional theory (TDDFT) has become one of the most often used approaches to compute optical properties of molecules and nanostructures. The accuracy of TDDFT has greatly increased with the advent of functionals that depend explicitly on the orbitals and are thus implicit density functionals [1,2]. Global hybrid functionals [3–5], local hybrids [6–10], and range-separated hybrids [11–17] exploit the combination of orbital-dependent exact exchange (EXX) with semilocal density functionals in order to achieve a remarkable accuracy. Time-dependent self-interaction corrections (SICs) in different variants [18–21] use the orbital dependence in order to correct for the spurious Hartree self-interaction and are particularly interesting for the description of electron emission [22–26] and charge-transfer processes [27–29].

So far, orbital functionals are mostly used in TDDFT in the generalized Kohn-Sham scheme, with individual potentials for each orbital. First introduced pragmatically as an adiabatic extension of the ground-state generalized Kohn-Sham scheme, the time-dependent (TD) generalized Kohn-Sham approach can also be formally justified [30]. The generalized Kohn-Sham scheme has become the de facto standard for the use of orbital functionals in TDDFT.

Despite the unquestionable successes of the TD generalized Kohn-Sham approach, it would be desirable to be able to use orbital functionals also in TD Kohn-Sham theory, i.e., with equations that use the same global multiplicative potential for all orbitals. From a computational point of view, the use of a single local potential is attractive because it parallelizes nicely and can be used efficiently with many different types of numerical realizations, including numerical grids. From a conceptual point of view, the Kohn-Sham approach is attractive because the Kohn-Sham system is uniquely defined. Furthermore, as the Kohn-Sham potential is the same for occupied and unoccupied orbitals, the unoccupied Kohn-Sham eigenvalue spectrum has attractive features

that are typically not shared by the corresponding generalized Kohn-Sham spectrum, such as a Rydberg series resulting from Fock exchange [1,31]. Also, for the purposes of functional development, the concepts of Kohn-Sham theory serve as an important guideline for learning how to incorporate spatial and temporal nonlocalities [32–34].

The use of orbital functionals in TD Kohn-Sham theory has so far been limited by the difficulties that are associated with solving the TD optimized effective potential (TDOEP) equation [35]. In the linear-response regime, evaluating the exchange-correlation (xc) kernel  $f_{xc}(\mathbf{r}, t, \mathbf{r}', t')$  as a second functional derivative of the xc action functional with respect to the density leads to involved mathematical expressions. The evaluation of the xc kernel for orbital functionals and its numerical realization have been carried out in several important works [36–46]. However, the resulting expressions are challenging to code, not always easy to interpret, and in some of the works the adiabatic approximation has been invoked [36–38]. In the real-time propagation approach to TDDFT [47], one need not evaluate  $f_{xc}(\mathbf{r}, t, \mathbf{r}', t')$ , as only the potential  $v_{xc}(\mathbf{r}, t)$  is required. However, solving the TDOEP equation in the real-time propagation context proved very challenging. Straightforward propagation is fraught with computational difficulties [48–50], and progress made [51] has so far been restricted to one-dimensional model systems. A particularly sobering aspect of the combination of real-time techniques and orbital functionals is the finding that approximations to the OEP such as the Krieger-Li-Iafrate (KLI) approximation [52] and the common-energy-denominator approximation (CEDA) [53] (also termed the localized Hartree-Fock approximation [54]) cannot generally be used. Although these approximations often work quite reliably in ground-state calculations, they, as well as related approximations, frequently become unstable in real-time propagations [29,55,56]. As a consequence, there are only a few systems for which reliable TD Kohn-Sham results using orbital functionals are available.

In this paper we show how approximate Kohn-Sham potentials for orbital functionals such as the KLI approximation and CEDA can be used in TD Kohn-Sham theory without

suffering from instabilities and in a numerically efficient way. The decisive idea is to use the frequency-dependent Sternheimer scheme [57,58]. In this way, one can avoid the explicit evaluation of  $f_{xc}$  for orbital functionals, as well as the accumulation of numerical inaccuracies that hinders real-time propagation with the KLI and CEDA potentials. The power of the Sternheimer approach, which has been brought to bear previously in different areas of electronic structure theory [59–65], can thus be harnessed for TDDFT.

In the following, we first discuss the linearization of orbital-dependent quantities in Kohn-Sham theory in general and then use this concept to set up Sternheimer equations for the linear response following from the KLI and CEDA potentials. After a brief recapitulation of the frequency-dependent Sternheimer scheme, we demonstrate the reliability and accuracy of our method for several paradigm test cases as a proof of concept. We conclude with a summary and an outlook on future work.

## II. LINEARIZATION OF ORBITAL-DEPENDENT QUANTITIES IN THE KOHN-SHAM FRAMEWORK

In TDDFT, the usual way of calculating the linear response of a (spin-)density-dependent quantity  $\mathcal{O}$  to an external perturbation is by means of an expansion with respect to the linear spin-density response  $n_\sigma^{(1)}(\mathbf{r}, t)$  that results from the perturbation [66]:

$$\mathcal{O}^{(1)} = \sum_{\tau=\uparrow,\downarrow} \int dt' \int d^3r' \left[ \frac{\delta \mathcal{O}}{\delta n_\tau(\mathbf{r}', t')} \right]^{(0)} n_\tau^{(1)}(\mathbf{r}', t'). \quad (1)$$

The superscript (0) indicates that the term in square brackets is evaluated in the unperturbed system,  $\sigma$  and  $\tau$  are spin indices,  $\mathbf{r}$  and  $\mathbf{r}'$  are spatial coordinates, and  $t$  and  $t'$  are time variables. Applying Eq. (1) to the exchange-correlation potential  $v_{xc\sigma}(\mathbf{r}, t)$  introduces the xc kernel  $f_{xc\sigma\tau}$  [66,67]:

$$f_{xc\sigma\tau}(\mathbf{r}, \mathbf{r}', t, t') = \left[ \frac{\delta v_{xc\sigma}(\mathbf{r}, t)}{\delta n_\tau(\mathbf{r}', t')} \right]^{(0)}. \quad (2)$$

In this work, we are dealing with quantities [such as approximations to  $v_{xc\sigma}(\mathbf{r}, t)$ ] that are known as functionals of the time-dependent occupied orbitals of the Kohn-Sham system. Consider any occupied-orbital-dependent quantity

$$\mathcal{O} = \mathcal{O} \left[ \left\{ \varphi_{k\alpha}, \varphi_{k\alpha}^* \right\}_{\substack{\alpha=\uparrow,\downarrow \\ k=1,\dots,N_\alpha}} \right] \quad (3)$$

[it can be complex and depend on further variables, e.g.,  $\mathcal{O}_\sigma(\mathbf{r}, t) \in \mathbb{C}$ ]. In the time-dependent Kohn-Sham framework, the orbitals are determined by the density and the initial state [66–68]. For the perturbation theory setting where propagations start in the ground state (GS), the Kohn-Sham orbitals are unique functionals of the density,

$$\varphi_{i\sigma}(\mathbf{r}, t) = \varphi_{i\sigma}[n_\uparrow, n_\downarrow](\mathbf{r}, t). \quad (4)$$

As a consequence,  $\mathcal{O}$  itself is also a functional of the density,

$$\mathcal{O}[\{n_\beta\}] = \mathcal{O}[\{\varphi_{k\alpha}[\{n_\beta\}], \varphi_{k\alpha}^*[\{n_\beta\}]\}]. \quad (5)$$

This means that  $\mathcal{O}$  can be linearized in the perturbation using Eq. (1). However, as it depends on the density via the occupied

orbitals, the functional derivatives in Eqs. (1) and (2) have to be calculated with the help of the chain rule,

$$\begin{aligned} \frac{\delta \mathcal{O}}{\delta n_\tau(\mathbf{r}', t')} &= \sum_{\gamma=\uparrow,\downarrow} \sum_{j=1}^{N_\gamma} \int dt'' \int d^3r'' \\ &\times \left\{ \frac{\delta \mathcal{O}}{\delta \varphi_{j\gamma}(\mathbf{r}'', t'')} \frac{\delta \varphi_{j\gamma}(\mathbf{r}'', t'')}{\delta n_\tau(\mathbf{r}', t')} \right. \\ &\left. + \frac{\delta \mathcal{O}}{\delta \varphi_{j\gamma}^*(\mathbf{r}'', t'')} \frac{\delta \varphi_{j\gamma}^*(\mathbf{r}'', t'')}{\delta n_\tau(\mathbf{r}', t')} \right\}. \quad (6) \end{aligned}$$

The derivatives  $\delta \varphi_{j\gamma}(\mathbf{r}'', t'')/\delta n_\tau(\mathbf{r}', t')$  are not known analytically and have to be calculated from complicated integral equations. This step so far has been a major hurdle in the use of orbital-dependent functionals. A central piece of our work here is to show how the explicit evaluation of these derivatives can be avoided: First, we express the linear response of the TD Kohn-Sham orbitals to an external perturbation in two different ways, namely, as a solution of the Sternheimer equations on the one hand and as a formal density expansion as in Eq. (1) on the other. We can then use the latter to rewrite the chain rule expression for  $\mathcal{O}^{(1)}$  in terms of the response of the orbitals, which we calculate using the former. This procedure is explained in detail in the following.

In the first step, we recall the Sternheimer scheme in the form that we recently discussed in detail in Ref. [58]. We consider perturbations of the form

$$v_{\text{ext},\sigma}(\mathbf{r}, t) = [v_{\text{ext},\sigma}^{(+)}(\mathbf{r})e^{-i\omega t} + \text{c.c.}]e^{\eta t}, \quad \omega, \eta > 0, \quad (7)$$

i.e., the perturbations are exponentially switched on harmonic oscillations. Here  $v_{\text{ext},\sigma}^{(+)}(\mathbf{r})$  denotes the Fourier component and specifies the spatial and spin dependence of the perturbation. The specific forms that we used in the calculations presented in this work are given in Eqs. (54) and (62). For a general discussion of the possible spin and spatial dependences of the perturbation, we refer to Ref. [58].

As shown in Ref. [58], the zeroth- and first-order contributions to the perturbation series of the TD Kohn-Sham orbitals can be written as

$$\varphi_{j\sigma}^{(0)}(\mathbf{r}, t) = \phi_{j\sigma}(\mathbf{r})e^{-i(\varepsilon_{j\sigma}/\hbar)t} \quad (8)$$

and

$$\begin{aligned} \varphi_{j\sigma}^{(1)}(\mathbf{r}, t) &= e^{-i(\varepsilon_{j\sigma}/\hbar)t} \left\{ [\varphi_{j\sigma}^{(+)}(\mathbf{r})e^{-i\omega t} + \varphi_{j\sigma}^{(-)*}(\mathbf{r})e^{i\omega t}]e^{\eta t} \right. \\ &\left. - i\phi_{j\sigma}(\mathbf{r})\varepsilon_{j\sigma}^{(1)}(t) \right\}, \quad (9) \end{aligned}$$

where  $\phi_{j\sigma}(\mathbf{r})$  and  $\varepsilon_{j\sigma}$  are GS orbitals and eigenvalues of the unperturbed Kohn-Sham system, the orbitals  $\phi_{j\sigma}$  are chosen to be real, and

$$\varepsilon_{j\sigma}^{(1)}(t) = [\varepsilon_{j\sigma}^{(+)}e^{-i\omega t} + \text{c.c.}]e^{\eta t} \quad (10)$$

is real as well. The quantities  $\varphi_{j\sigma}^{(\pm)}(\mathbf{r})$  are Fourier components of the first-order response of the orbitals and will be determined by the Sternheimer equations [see Eq. (16) below].

The linear response of the density and of the Hartree-exchange-correlation potential then takes the form

$$n_\sigma^{(1)}(\mathbf{r}, t) = [n_\sigma^{(+)}(\mathbf{r})e^{-i\omega t} + \text{c.c.}]e^{\eta t}, \quad (11)$$

$$n_{\sigma}^{(+)}(\mathbf{r}) = \sum_{i=1}^{N_{\sigma}} \phi_{i\sigma}(\mathbf{r}) [\varphi_{i\sigma}^{(+)}(\mathbf{r}) + \varphi_{i\sigma}^{(-)}(\mathbf{r})], \quad (12)$$

and

$$v_{\text{Hxc},\sigma}^{(1)}(\mathbf{r}, t) = [v_{\text{Hxc},\sigma}^{(+)}(\mathbf{r})e^{-i\omega t} + \text{c.c.}]e^{i\eta t}, \quad (13)$$

where the latter is derived from Eqs. (1) and (11). The Hartree contribution to  $v_{\text{Hxc},\sigma}^{(+)}$  can be calculated from Poisson's equation

$$\nabla^2 v_{\text{H}}^{(+)}(\mathbf{r}) = -4e^2\pi [n_{\uparrow}^{(+)}(\mathbf{r}) + n_{\downarrow}^{(+)}(\mathbf{r})], \quad (14)$$

where  $e$  is the elementary charge. While the energy response components  $\varepsilon_{j\sigma}^{(+)}$  mentioned above eventually drop out of our equations (cf. Sec. III) and thus never need to be computed, they could in principle be calculated from [58]

$$\varepsilon_{j\sigma}^{(+)} = i \int d^3r \frac{\phi_{j\sigma}^2(\mathbf{r}) [v_{\text{ext},\sigma}^{(+)}(\mathbf{r}) + v_{\text{Hxc},\sigma}^{(+)}(\mathbf{r})]}{\hbar(\omega + i\eta)}. \quad (15)$$

Finally, the Sternheimer equations determining the orbital response components  $\varphi_{j\sigma}^{(\pm)}$  read

$$\begin{aligned} & [\hat{h}_{\sigma} - \varepsilon_{j\sigma} \mp \hbar(\omega + i\eta)] \varphi_{j\sigma}^{(\pm)}(\mathbf{r}) \\ &= -\hat{Q}_{j\sigma} [v_{\text{ext},\sigma}^{(+)}(\mathbf{r}) + v_{\text{Hxc},\sigma}^{(+)}(\mathbf{r})] \phi_{j\sigma}(\mathbf{r}), \end{aligned} \quad (16)$$

with the additional condition

$$\langle \phi_{j\sigma} | \varphi_{j\sigma}^{(\pm)} \rangle = \int d^3r \phi_{j\sigma}(\mathbf{r}) \varphi_{j\sigma}^{(\pm)}(\mathbf{r}) = 0. \quad (17)$$

Here

$$\hat{Q}_{j\sigma} := 1 - |\phi_{j\sigma}\rangle\langle\phi_{j\sigma}| \quad (18)$$

projects onto the subspace orthogonal to  $\phi_{j\sigma}$  and  $\hat{h}_{\sigma}$  is the unperturbed (GS) Kohn-Sham Hamiltonian. To perform a linear-response calculation in the Sternheimer scheme, we thus need an expression for  $v_{\text{xc}\sigma}^{(+)}(\mathbf{r})$  in terms of the linear response of the spin density or of the orbitals, so that Eq. (16) can be solved self-consistently.

In the second step we note that due to the orbitals' density dependence (4), an alternative expression for their first-order response can be derived by applying Eq. (1) to them. This leads to

$$\varphi_{j\sigma}^{(1)}(\mathbf{r}, t) = \sum_{\tau=\uparrow,\downarrow} \int dt' \int d^3r' \left[ \frac{\delta\varphi_{j\sigma}(\mathbf{r}, t)}{\delta n_{\tau}(\mathbf{r}', t')} \right]^{(0)} n_{\tau}^{(1)}(\mathbf{r}', t'), \quad (19)$$

as well as a similar relation for the response of the complex conjugate orbitals,  $\varphi_{j\sigma}^{*(1)}(\mathbf{r}, t) = [\varphi_{j\sigma}^{(1)}(\mathbf{r}, t)]^*$ . We can use this to rewrite  $\mathcal{O}^{(1)}$  after applying the chain rule (6) in Eq. (1):

$$\begin{aligned} \mathcal{O}^{(1)} &= \sum_{\tau=\uparrow,\downarrow} \int dt' \int d^3r' \sum_{\gamma=\uparrow,\downarrow} \sum_{j=1}^{N_{\gamma}} \int dt'' \int d^3r'' \left\{ \left[ \frac{\delta\mathcal{O}}{\delta\varphi_{j\gamma}(\mathbf{r}'', t'')} \right]^{(0)} \left[ \frac{\delta\varphi_{j\gamma}(\mathbf{r}'', t'')}{\delta n_{\tau}(\mathbf{r}', t')} \right]^{(0)} \right. \\ &\quad \left. + \left[ \frac{\delta\mathcal{O}}{\delta\varphi_{j\gamma}^*(\mathbf{r}'', t'')} \right]^{(0)} \left[ \frac{\delta\varphi_{j\gamma}^*(\mathbf{r}'', t'')}{\delta n_{\tau}(\mathbf{r}', t')} \right]^{(0)} \right\} n_{\tau}^{(1)}(\mathbf{r}', t') \\ &= \sum_{\gamma=\uparrow,\downarrow} \sum_{j=1}^{N_{\gamma}} \int dt'' \int d^3r'' \left\{ \left[ \frac{\delta\mathcal{O}}{\delta\varphi_{j\gamma}(\mathbf{r}'', t'')} \right]^{(0)} \sum_{\tau=\uparrow,\downarrow} \int dt' \int d^3r' \left[ \frac{\delta\varphi_{j\gamma}(\mathbf{r}'', t'')}{\delta n_{\tau}(\mathbf{r}', t')} \right]^{(0)} n_{\tau}^{(1)}(\mathbf{r}', t') \right. \\ &\quad \left. + \left[ \frac{\delta\mathcal{O}}{\delta\varphi_{j\gamma}^*(\mathbf{r}'', t'')} \right]^{(0)} \sum_{\tau=\uparrow,\downarrow} \int dt' \int d^3r' \left[ \frac{\delta\varphi_{j\gamma}^*(\mathbf{r}'', t'')}{\delta n_{\tau}(\mathbf{r}', t')} \right]^{(0)} n_{\tau}^{(1)}(\mathbf{r}', t') \right\} \\ &\stackrel{(19)}{=} \sum_{\gamma=\uparrow,\downarrow} \sum_{j=1}^{N_{\gamma}} \int dt'' \int d^3r'' \left\{ \left[ \frac{\delta\mathcal{O}}{\delta\varphi_{j\gamma}(\mathbf{r}'', t'')} \right]^{(0)} \varphi_{j\gamma}^{(1)}(\mathbf{r}'', t'') + \left[ \frac{\delta\mathcal{O}}{\delta\varphi_{j\gamma}^*(\mathbf{r}'', t'')} \right]^{(0)} \varphi_{j\gamma}^{(1)*}(\mathbf{r}'', t'') \right\}. \end{aligned}$$

After renaming the summation indices and integration variables, we arrive at

$$\begin{aligned} \mathcal{O}^{(1)} &= \sum_{\tau=\uparrow,\downarrow} \int dt' \int d^3r' \left[ \frac{\delta\mathcal{O}}{\delta n_{\tau}(\mathbf{r}', t')} \right]^{(0)} n_{\tau}^{(1)}(\mathbf{r}', t') \\ &= \sum_{\tau=\uparrow,\downarrow} \sum_{j=1}^{N_{\tau}} \int dt' \int d^3r' \left\{ \left[ \frac{\delta\mathcal{O}}{\delta\varphi_{j\tau}(\mathbf{r}', t')} \right]^{(0)} \varphi_{j\tau}^{(1)}(\mathbf{r}', t') + \left[ \frac{\delta\mathcal{O}}{\delta\varphi_{j\tau}^*(\mathbf{r}', t')} \right]^{(0)} \varphi_{j\tau}^{(1)*}(\mathbf{r}', t') \right\}. \end{aligned} \quad (20)$$

We have thus arrived at an important insight: The expansion with respect to the density response is equivalent to an expansion with respect to the linear response of the Kohn-Sham orbitals.

A special case of particular interest results when we apply Eq. (20) to an orbital-dependent expression for the xc potential,

$$v_{\text{xc}\sigma}^{(1)}(\mathbf{r}, t) = \sum_{\tau=\uparrow,\downarrow} \sum_{j=1}^{N_{\tau}} \int dt' \int d^3r' \left\{ \left[ \frac{\delta v_{\text{xc}\sigma}(\mathbf{r}, t)}{\delta\varphi_{j\tau}(\mathbf{r}', t')} \right]^{(0)} \varphi_{j\tau}^{(1)}(\mathbf{r}', t') + \left[ \frac{\delta v_{\text{xc}\sigma}(\mathbf{r}, t)}{\delta\varphi_{j\tau}^*(\mathbf{r}', t')} \right]^{(0)} \varphi_{j\tau}^{(1)*}(\mathbf{r}', t') \right\}. \quad (21)$$

This shows that one can calculate the linear xc potential response using an orbital expansion instead of a density expansion. Although this expression is still strictly within the Kohn-Sham scheme, the computational effort has basically been reduced to calculating functional derivatives with respect to the orbitals as in the generalized Kohn-Sham scheme.

Note that even an orbital-adiabatic potential, i.e., one that at time  $t$  only depends on the orbitals at time  $t$ , is a nonadiabatic, nonlocal density functional. When the potential is linearized using Eq. (21), the corresponding memory is implicitly contained in the response of the orbitals: If we were to write the response of the potential in terms of a kernel, we would have to reinsert Eq. (19). This would introduce the space and time nonlocality to the kernel in form of the derivatives  $\delta\varphi_{j\sigma}(\mathbf{r}, t)/\delta n_{\tau}(\mathbf{r}', t')$ .

From a practical point of view, Eq. (21) has important and beneficial consequences. First, one is typically interested in using it for  $v_{xc}$  approximations whose dependence on the orbitals is analytically known. The functional derivatives in Eqs. (20) and (21) can thus also be calculated analytically. Second, if one uses the Sternheimer scheme for one's TDDFT calculations, then the linear response of the orbitals is calculated anyway. Therefore, evaluating Eqs. (20) and (21) is equivalent to, but much simpler than, actually calculating the kernel of an orbital-dependent potential. Thus, when one wants to stay on the grounds of Kohn-Sham theory, then the Sternheimer scheme for orbital functionals is much easier to use than the usual Casida [69] linear-response formalism.

### III. LINEARIZATION OF THE ORBITAL-SPECIFIC POTENTIALS OF AN ORBITAL-ADIABATIC FUNCTIONAL

Typically, one is interested in the situation that one knows an orbital-dependent expression  $E_{xc}[\{\varphi_{k\alpha}, \varphi_{k\alpha}^*\}]$  for the xc energy of GS DFT, based on which one can define a TDDFT action functional in an orbital-adiabatic fashion [35,48]. In the following, we demonstrate how the most common approximations to the TDOEP can be evaluated in the Sternheimer scheme.

A key ingredient in the TDOEP (and in its approximations) are the orbital-specific potentials  $u_{xci\sigma}$ , which in the orbital-adiabatic case are given by

$$u_{xci\sigma}(\mathbf{r}, t) = u_{xci\sigma}(\mathbf{r}) \Big|_{\substack{\varphi_{k\alpha} = \varphi_{k\alpha}(t), \\ \varphi_{k\alpha}^* = \varphi_{k\alpha}^*(t)}} \quad (22)$$

where

$$u_{xci\sigma}(\mathbf{r}) = \frac{1}{\varphi_{i\sigma}^*(\mathbf{r})} \frac{\delta E_{xc}[\{\varphi_{k\alpha}, \varphi_{k\alpha}^*\}]}{\delta \varphi_{i\sigma}(\mathbf{r})}. \quad (23)$$

The goal of this section is to derive an expression for their linear response. We will then use this in Sec. IV. Since the  $u_{xci\sigma}$  only depend on the orbitals at time  $t$ , we have

$$\frac{\delta u_{xci\sigma}(\mathbf{r}, t)}{\delta \varphi_{j\tau}(\mathbf{r}', t')} = \delta(t - t') \frac{\delta u_{xci\sigma}[\{\varphi_{k\alpha}, \varphi_{k\alpha}^*\}](\mathbf{r})}{\delta \varphi_{j\tau}(\mathbf{r}')} \Big|_{\substack{\varphi_{k\alpha} = \varphi_{k\alpha}(t), \\ \varphi_{k\alpha}^* = \varphi_{k\alpha}^*(t)}}. \quad (24)$$

The remaining functional derivative, evaluated at the zeroth-order orbitals  $\varphi_{j\sigma}^{(0)}$  [as needed for Eqs. (20) and (21)], is in general neither real nor time independent since Eq. (8) shows that the  $\varphi_{j\sigma}^{(0)}$  are still complex and time-dependent even for our real choice of the GS orbitals  $\phi_{j\sigma}$ . However, we will restrict

our theory to functionals that depend on the orbitals only via products  $\varphi_{j\sigma}^*(\mathbf{r}, t) \cdot \varphi_{j\sigma}(\mathbf{r}', t)$ , which includes functionals containing exact exchange contributions, self-interaction corrections without unitary orbital transformations [70,71], and kinetic-energy-dependent metageneralized gradient approximations. In that case,

$$\begin{aligned} & \left[ \frac{\delta u_{xci\sigma}(\mathbf{r}, t)}{\delta \varphi_{j\tau}(\mathbf{r}', t')} \right]^{(0)} \\ &= \delta(t - t') \frac{\delta u_{xci\sigma}[\{\varphi_{k\alpha}, \varphi_{k\alpha}^*\}](\mathbf{r})}{\delta \varphi_{j\tau}(\mathbf{r}')} \Big|_{\substack{\varphi_{k\alpha} = \phi_{k\alpha} e^{-i\epsilon_{k\alpha} t/\hbar}, \\ \varphi_{k\alpha}^* = \phi_{k\alpha} e^{+i\epsilon_{k\alpha} t/\hbar}}} \\ &= \delta(t - t') e^{+i(\epsilon_{j\tau}/\hbar)t} \frac{\delta u_{xci\sigma}[\{\varphi_{k\alpha}, \varphi_{k\alpha}^*\}](\mathbf{r})}{\delta \varphi_{j\tau}(\mathbf{r}')} \Big|_{\varphi_{k\alpha} = \phi_{k\alpha}^* = \phi_{k\alpha}} \end{aligned} \quad (25)$$

and

$$\begin{aligned} & \left[ \frac{\delta u_{xci\sigma}(\mathbf{r}, t)}{\delta \varphi_{j\tau}^*(\mathbf{r}', t')} \right]^{(0)} \\ &= \delta(t - t') e^{-i(\epsilon_{j\tau}/\hbar)t} \frac{\delta u_{xci\sigma}[\{\varphi_{k\alpha}, \varphi_{k\alpha}^*\}](\mathbf{r})}{\delta \varphi_{j\tau}^*(\mathbf{r}')} \Big|_{\varphi_{k\alpha} = \varphi_{k\alpha}^* = \phi_{k\alpha}}. \end{aligned} \quad (26)$$

Note that during the functional differentiation we still have to treat  $\varphi_{k\alpha}$  and  $\varphi_{k\alpha}^*$  as independent and insert the real-valued GS orbitals  $\phi_{k\alpha}$  only afterward. Also, while  $\varphi_{k\alpha}$  and  $\varphi_{k\alpha}^*$  enter the functional in a symmetric way, Eq. (23) shows that the  $u_{xci\sigma}$  do not depend symmetrically on  $\varphi_{k\alpha}$  and  $\varphi_{k\alpha}^*$ . Thus,

$$\frac{\delta u_{xci\sigma}(\mathbf{r})}{\delta \varphi_{j\tau}(\mathbf{r}')} \Big|_{\varphi_{k\alpha} = \varphi_{k\alpha}^* = \phi_{k\alpha}} \neq \frac{\delta u_{xci\sigma}(\mathbf{r})}{\delta \varphi_{j\tau}^*(\mathbf{r}')} \Big|_{\varphi_{k\alpha} = \varphi_{k\alpha}^* = \phi_{k\alpha}} \quad (27)$$

in general, even though those quantities are real. However,

$$\frac{\delta u_{xci\sigma}(\mathbf{r})}{\delta \varphi_{j\tau}(\mathbf{r}')} \Big|_{\varphi_{k\alpha} = \varphi_{k\alpha}^* = \phi_{k\alpha}} = \frac{\delta u_{xci\sigma}^*(\mathbf{r})}{\delta \varphi_{j\tau}^*(\mathbf{r}')} \Big|_{\varphi_{k\alpha} = \varphi_{k\alpha}^* = \phi_{k\alpha}} \quad (28)$$

and

$$\frac{\delta u_{xci\sigma}(\mathbf{r})}{\delta \varphi_{j\tau}^*(\mathbf{r}')} \Big|_{\varphi_{k\alpha} = \varphi_{k\alpha}^* = \phi_{k\alpha}} = \frac{\delta u_{xci\sigma}(\mathbf{r})}{\delta \varphi_{j\tau}(\mathbf{r}')} \Big|_{\varphi_{k\alpha} = \varphi_{k\alpha}^* = \phi_{k\alpha}} \quad (29)$$

still hold. In principle, we can use these relations and Eqs. (9) and (20) to construct the linear response of  $u_{xci\sigma}^*(\mathbf{r}, t)$  to the perturbation, yielding

$$u_{xci\sigma}^{*(1)}(\mathbf{r}, t) = [u_{xci\sigma}^{(+)}(\mathbf{r}) e^{-i\omega t} + u_{xci\sigma}^{(-)*}(\mathbf{r}) e^{i\omega t}] e^{\eta t}, \quad (30)$$

where we have defined

$$\begin{aligned} u_{xci\sigma}^{(\pm)}(\mathbf{r}) &= \sum_{\tau} \sum_{j=1}^{N_{\tau}} \int d^3 r' \left\{ \frac{\delta u_{xci\sigma}^*(\mathbf{r})}{\delta \varphi_{j\tau}(\mathbf{r}')} \Big|_{\varphi_{k\alpha} = \varphi_{k\alpha}^* = \phi_{k\alpha}} \varphi_{j\tau}^{(\pm)}(\mathbf{r}') \right. \\ &+ \frac{\delta u_{xci\sigma}(\mathbf{r})}{\delta \varphi_{j\tau}(\mathbf{r}')} \Big|_{\varphi_{k\alpha} = \varphi_{k\alpha}^* = \phi_{k\alpha}} \varphi_{j\tau}^{(\mp)}(\mathbf{r}') \\ &\left. \pm i \left[ \frac{\delta u_{xci\sigma}(\mathbf{r})}{\delta \varphi_{j\tau}(\mathbf{r}')} - \frac{\delta u_{xci\sigma}^*(\mathbf{r})}{\delta \varphi_{j\tau}^*(\mathbf{r}')} \right] \Big|_{\varphi_{k\alpha} = \varphi_{k\alpha}^* = \phi_{k\alpha}} \phi_{j\tau}(\mathbf{r}') \varepsilon_{j\tau}^{(+)} \right\}. \end{aligned} \quad (31)$$

However, most approximations to the TDOEP, such as the Slater and KLI potentials, only depend on the real parts of the orbital-specific potentials:

$$w_{xc\sigma}(\mathbf{r}, t) := \text{Re}[u_{xc\sigma}(\mathbf{r}, t)] = \frac{1}{2}[u_{xc\sigma}(\mathbf{r}, t) + u_{xc\sigma}^*(\mathbf{r}, t)]. \quad (32)$$

From the symmetries (28) and (29) it follows that

$$\left. \frac{\delta w_{xc\sigma}(\mathbf{r})}{\delta \varphi_{j\tau}(\mathbf{r}')} \right|_{\varphi_{k\alpha} = \varphi_{k\alpha}^* = \phi_{k\alpha}} = \left. \frac{\delta w_{xc\sigma}(\mathbf{r})}{\delta \varphi_{j\tau}^*(\mathbf{r}')} \right|_{\varphi_{k\alpha} = \varphi_{k\alpha}^* = \phi_{k\alpha}}, \quad (33)$$

and since the derivatives of  $w_{xc\sigma}$  evaluated at the (real) GS orbitals  $\phi_{k\alpha}$  are real, we also have [cf. Eq. (9)]

$$i\varphi_{j\tau}(\mathbf{r}')\varepsilon_{j\tau}^{(1)}(t) \left. \frac{\delta w_{xc\sigma}(\mathbf{r})}{\delta \varphi_{j\tau}(\mathbf{r}')} \right|_{\varphi_{k\alpha} = \varphi_{k\alpha}^* = \phi_{k\alpha}} + \text{c.c.} = 0. \quad (34)$$

That means that if we now use Eq. (20) to calculate the linear response of  $w_{xc\sigma}$ , the  $\varepsilon_{j\tau}^{(1)}(t)$ -dependent contributions to  $\varphi_{j\sigma}^{(1)}(\mathbf{r}, t)$  cancel. Inserting the relations derived above as well as Eq. (9), we arrive at

$$w_{xc\sigma}^{(+)}(\mathbf{r}, t) = [w_{xc\sigma}^{(+)}(\mathbf{r})e^{-i\omega t} + \text{c.c.}]e^{\eta t}, \quad (35)$$

where

$$w_{xc\sigma}^{(+)}(\mathbf{r}) = \sum_{\tau} \sum_{j=1}^{N_{\tau}} \int d^3r' \left. \frac{\delta w_{xc\sigma}(\mathbf{r})}{\delta \varphi_{j\tau}(\mathbf{r}')} \right|_{\varphi_{k\alpha} = \varphi_{k\alpha}^* = \phi_{k\alpha}} \times [\varphi_{j\tau}^{(+)}(\mathbf{r}') + \varphi_{j\tau}^{(-)}(\mathbf{r}')] \quad (36)$$

(which is equal to  $\frac{1}{2}[u_{xc\sigma}^{(+)}(\mathbf{r}) + u_{xc\sigma}^{(-)}(\mathbf{r})]$ ) and

$$\delta w_{xc\sigma}(\mathbf{r})/\delta \varphi_{j\tau}(\mathbf{r}') = \frac{\delta}{\delta \varphi_{j\tau}(\mathbf{r}')} \frac{1}{2} \left[ \frac{\delta E_{xc}[\{\varphi_{k\alpha}, \varphi_{k\alpha}^*\}]}{\varphi_{i\sigma}^*(\mathbf{r})\delta \varphi_{i\sigma}(\mathbf{r})} + \frac{\delta E_{xc}[\{\varphi_{k\alpha}, \varphi_{k\alpha}^*\}]}{\varphi_{i\sigma}(\mathbf{r})\delta \varphi_{i\sigma}^*(\mathbf{r})} \right]. \quad (37)$$

In the following section, we will see that in the linear response of approximations to the TDOEP (including the CEDA),  $w_{xc\sigma}^{(+)}$  plays a role similar to the one that  $u_{xc\sigma}$  plays in the nonlinearized potentials.

#### IV. LINEARIZATION OF COMMON APPROXIMATIONS TO THE TDOEP

One of the most simple and rather crude approximations to the (TD)OEP is the Slater potential. It is the orbital density-weighted average of the orbital-specific potentials [72,73],

$$v_{xc\sigma}^{\text{Sla}}(\mathbf{r}, t) = \sum_{i=1}^{N_{\sigma}} \frac{|\varphi_{i\sigma}(\mathbf{r}, t)|^2}{n_{\sigma}(\mathbf{r}, t)} w_{xc\sigma}(\mathbf{r}, t). \quad (38)$$

A more sophisticated and probably the most commonly known and employed approximation is the KLI potential [35,48,52]

$$v_{xc\sigma}^{\text{KLI}}(\mathbf{r}, t) = v_{xc\sigma}^{\text{Sla}}(\mathbf{r}, t) + \sum_{i=1}^{N_{\sigma}} \frac{|\varphi_{i\sigma}(\mathbf{r}, t)|^2}{n_{\sigma}(\mathbf{r}, t)} \times [v_{ii\sigma}^{\text{KLI}}(t) - w_{ii\sigma}(t)], \quad (39)$$

where

$$v_{ij\sigma}^{\text{KLI}}(t) := \int \varphi_{i\sigma}^*(\mathbf{r}, t) v_{xc\sigma}^{\text{KLI}}(\mathbf{r}, t) \varphi_{j\sigma}(\mathbf{r}, t) d^3r, \quad (40)$$

$$w_{ij\sigma}(t) := \int \varphi_{i\sigma}^*(\mathbf{r}, t) w_{xc\sigma}(\mathbf{r}, t) \varphi_{j\sigma}(\mathbf{r}, t) d^3r \quad (41)$$

are the matrix elements of  $v_{xc\sigma}^{\text{KLI}}$  and  $w_{xc\sigma}$  between the TD Kohn-Sham orbitals. At least for the special case of the exact exchange functional, a further approximation is known. The CEDA potential [53,54,74,75] is defined by

$$v_{xc\sigma}^{\text{CEDA}}(\mathbf{r}, t) = v_{xc\sigma}^{\text{Sla}}(\mathbf{r}, t) + \sum_{i,j=1}^{N_{\sigma}} \frac{1}{2} \left\{ \frac{\varphi_{i\sigma}(\mathbf{r}, t) \varphi_{j\sigma}^*(\mathbf{r}, t)}{n_{\sigma}(\mathbf{r}, t)} \times [v_{ij\sigma}^{\text{CEDA}}(t) - u_{ij\sigma}(t)] + \text{c.c.} \right\}, \quad (42)$$

where  $v_{ij\sigma}^{\text{CEDA}}(t)$  and  $u_{ij\sigma}(t)$  are defined similarly to  $v_{ij\sigma}^{\text{KLI}}(t)$  and  $w_{ij\sigma}(t)$ , but with  $v_{xc\sigma}^{\text{KLI}}(\mathbf{r}, t)$  and  $w_{xc\sigma}(\mathbf{r}, t)$  replaced by  $v_{xc\sigma}^{\text{CEDA}}(\mathbf{r}, t)$  and  $u_{xc\sigma}(\mathbf{r}, t)$ , respectively. If the sums in the KLI and CEDA expressions are allowed to run over all occupied orbitals, then the potentials are defined only up to a TD constant. This constant is usually fixed by the condition

$$v_{N_{\sigma}N_{\sigma}\sigma}^{\text{KLI,CEDA}}(t) - w_{N_{\sigma}N_{\sigma}\sigma}(t) = 0. \quad (43)$$

In practice, realizing the condition amounts to dropping the  $i = N_{\sigma}$  term of the second (primed) sum in the KLI expression and the  $i = j = N_{\sigma}$  term of the primed sum in the CEDA potential. This is indicated by the primes.

The Slater potential is an explicit orbital functional and can thus be linearized by a straightforward application of Eq. (21). With the help of Eqs. (35) and (36) we arrive at

$$v_{xc\sigma}^{\text{Sla}(1)}(\mathbf{r}, t) = [v_{xc\sigma}^{\text{Sla}(+)}(\mathbf{r})e^{-i\omega t} + \text{c.c.}]e^{\eta t}, \quad (44)$$

with

$$v_{xc\sigma}^{\text{Sla}(+)}(\mathbf{r}) = \sum_{i=1}^{N_{\sigma}} \left\{ \frac{\phi_{i\sigma}^2(\mathbf{r})}{n_{\sigma}(\mathbf{r})} w_{xc\sigma}^{(+)}(\mathbf{r}) - \frac{n_{ii\sigma}^{(+)}(\mathbf{r})}{n_{\sigma}(\mathbf{r})} \Delta v_{i\sigma}^{\text{Sla}}(\mathbf{r}) \right\}. \quad (45)$$

Here we have defined

$$n_{ij\sigma}^{(+)}(\mathbf{r}) := \frac{1}{2} \{ \phi_{i\sigma}(\mathbf{r}) [\varphi_{j\sigma}^{(+)}(\mathbf{r}) + \varphi_{j\sigma}^{(-)}(\mathbf{r})] + \phi_{j\sigma}(\mathbf{r}) [\varphi_{i\sigma}^{(+)}(\mathbf{r}) + \varphi_{i\sigma}^{(-)}(\mathbf{r})] \}, \quad (46)$$

and

$$\begin{aligned} \Delta v_{i\sigma}^{\text{Sla}}(\mathbf{r}) &:= [v_{xc\sigma}^{\text{Sla}}(\mathbf{r}) - u_{xc\sigma}(\mathbf{r})]_{\varphi_{k\alpha} = \varphi_{k\alpha}^* = \phi_{k\alpha}} \\ &= [v_{xc\sigma}^{\text{Sla}}(\mathbf{r}) - u_{xc\sigma}^*(\mathbf{r})]_{\varphi_{k\alpha} = \varphi_{k\alpha}^* = \phi_{k\alpha}} \\ &= [v_{xc\sigma}^{\text{Sla}}(\mathbf{r}) - w_{xc\sigma}(\mathbf{r})]_{\varphi_{k\alpha} = \varphi_{k\alpha}^* = \phi_{k\alpha}} \end{aligned} \quad (47)$$

is simply the difference of the real-valued GS Slater and orbital-specific potentials. The diagonals of the symmetric matrix  $n_{ij\sigma}^{(+)}(\mathbf{r}) = n_{ji\sigma}^{(+)}(\mathbf{r})$  reduce to the response components  $n_{ii\sigma}^{(+)}(\mathbf{r}) = \phi_{i\sigma}(\mathbf{r}) [\varphi_{i\sigma}^{(+)}(\mathbf{r}) + \varphi_{i\sigma}^{(-)}(\mathbf{r})]$  of the orbital densities. In addition,  $w_{xc\sigma}^{(+)}$  is the quantity derived in Sec. III and depends on the chosen xc functional through Eq. (37).

The linearization of the KLI and CEDA potentials is slightly more involved since they are only defined semi-explicitly by Eqs. (39) and (42) due to the appearance of their matrix elements on the right-hand sides of these equations. There are two different ways to deal with this problem, which however lead to the same result. The longer way is detailed in Appendix B. For a relatively short derivation one can simply linearize Eqs. (39) and (42) by expanding every input quantity into a perturbation series up to first order. Since these input quantities are known in terms of the Kohn-Sham orbitals, the expansions can be constructed using Eq. (20). Then the only remaining unknown terms are the first- and zeroth-order contributions to the KLI or CEDA potential. Equating only zeroth-order terms simply yields the GS KLI or CEDA equations and equating the first-order terms leads to the equations for the response  $v_{xc\sigma}^{\text{KLI,CEDA}^{(1)}}(\mathbf{r}, t)$  of the KLI or CEDA potential.

The resulting equations are

$$v_{xc\sigma}^{\text{KLI,CEDA}^{(1)}}(\mathbf{r}, t) = [v_{xc\sigma}^{\text{KLI,CEDA}^{(+)}}(\mathbf{r})e^{-i\omega t} + \text{c.c.}]e^{\eta t} \quad (48)$$

[consistent with Eq. (13)], with

$$\begin{aligned} v_{xc\sigma}^{\text{KLI}^{(+)}}(\mathbf{r}) &= \sum_{i=1}^{N_\sigma} \left\{ \frac{\phi_{i\sigma}^2(\mathbf{r})}{n_\sigma(\mathbf{r})} w_{xc\sigma}^{(+)}(\mathbf{r}) - \frac{n_{ii\sigma}^{(+)}(\mathbf{r})}{n_\sigma(\mathbf{r})} \Delta v_{i\sigma}^{\text{KLI}}(\mathbf{r}) \right\} \\ &+ \sum_{i=1}^{N_\sigma'} \left\{ \frac{n_{ii\sigma}^{(+)}(\mathbf{r})}{n_\sigma(\mathbf{r})} \Delta v_{i\sigma}^{\text{KLI}} + \frac{\phi_{i\sigma}^2(\mathbf{r})}{n_\sigma(\mathbf{r})} \right. \\ &\left. \times \left[ v_{ii\sigma}^{\text{KLI}^{(+)}} - w_{ii\sigma}^{(+)} + \int n_{ii\sigma}^{(+)}(\mathbf{r}') \Delta v_{i\sigma}^{\text{KLI}}(\mathbf{r}') d^3 r' \right] \right\} \end{aligned} \quad (49)$$

for the KLI case and

$$\begin{aligned} v_{xc\sigma}^{\text{CEDA}^{(+)}}(\mathbf{r}) &= \sum_{i=1}^{N_\sigma} \left\{ \frac{\phi_{i\sigma}^2(\mathbf{r})}{n_\sigma(\mathbf{r})} w_{xc\sigma}^{(+)}(\mathbf{r}) - \frac{n_{ii\sigma}^{(+)}(\mathbf{r})}{n_\sigma(\mathbf{r})} \Delta v_{i\sigma}^{\text{CEDA}}(\mathbf{r}) \right\} \\ &+ \sum_{i,j=1}^{N_\sigma'} \left\{ \frac{n_{ij\sigma}^{(+)}(\mathbf{r})}{n_\sigma(\mathbf{r})} \Delta v_{ij\sigma}^{\text{CEDA}} + \frac{\phi_{i\sigma}(\mathbf{r})\phi_{j\sigma}(\mathbf{r})}{n_\sigma(\mathbf{r})} \right. \\ &\left. \times \left[ v_{ij\sigma}^{\text{CEDA}^{(+)}} - w_{ij\sigma}^{(+)} + \int n_{ij\sigma}^{(+)}(\mathbf{r}') \Delta v_{i\sigma}^{\text{CEDA}}(\mathbf{r}') d^3 r' \right] \right\} \end{aligned} \quad (50)$$

for the CEDA, where  $\Delta v_{i\sigma}^{\text{KLI,CEDA}}(\mathbf{r})$  are defined equivalently to  $\Delta v_{i\sigma}^{\text{Sla}}(\mathbf{r})$  [Eq. (47)],

$$w_{ij\sigma}^{(+)} := \int \phi_{i\sigma}(\mathbf{r}) w_{xc\sigma}^{(+)}(\mathbf{r}) \phi_{j\sigma}(\mathbf{r}) d^3 r \quad (51)$$

are the matrix elements of  $w_{xc\sigma}^{(+)}(\mathbf{r})$  between the GS orbitals, and  $v_{ij\sigma}^{\text{KLI,CEDA}^{(+)}}$  and  $\Delta v_{ij\sigma}^{\text{KLI,CEDA}}$  are the corresponding matrix elements of  $v_{xc\sigma}^{\text{KLI,CEDA}^{(+)}}(\mathbf{r})$  and  $\Delta v_{i\sigma}^{\text{KLI,CEDA}}(\mathbf{r})$ . As before, primes indicate that the  $i = N_\sigma$  (KLI approximation) or  $i = j = N_\sigma$  (CEDA) terms are missing in the sums, which is a direct result of enforcing the condition (43) in Eqs. (39) and (42). Using Eq. (20) again to expand this condition into a

perturbation series yields, to orders zero and one,

$$\Delta v_{N_\sigma N_\sigma \sigma}^{\text{KLI,CEDA}} = 0 \quad (52)$$

and

$$v_{N_\sigma N_\sigma \sigma}^{\text{KLI,CEDA}^{(+)}} - w_{N_\sigma N_\sigma \sigma}^{(+)} + \int n_{N_\sigma N_\sigma \sigma}^{(+)}(\mathbf{r}) \Delta v_{N_\sigma \sigma}^{\text{KLI,CEDA}}(\mathbf{r}) d^3 r = 0. \quad (53)$$

The left-hand sides in these equations are exactly the terms dropped in the primed sums of Eqs. (49) and (50). The KLI and CEDA response potentials should meet these conditions, which can be used to check or even enhance the numerical accuracy of these potentials.

## V. METHOD

Linear-response calculations in the Sternheimer scheme are performed as described in Ref. [58]. We recapitulate only the main aspects here. The frequency  $\omega$  enters the scheme only as a parameter. By solving the full scheme for a single chosen value of  $\omega$ , we obtain the change in the density to first order in the perturbation. From this we obtain observables, e.g., the frequency-dependent dipole moment, evaluated at our single chosen frequency. From the solutions for various different  $\omega$  values within a frequency range of interest, we can then construct a spectrum. Here  $\eta$  is a real parameter that determines the width of the Lorentzian lines in these spectra. Larger values of  $\eta$  accelerate convergence. Since the potential response  $v_{\text{Hxc}\sigma}^{(+)}$  entering the right-hand side of the Sternheimer equations depends on their solutions, the scheme is solved self-consistently. We use Anderson mixing [76] to stabilize the convergence of this self-consistency loop. In every self-consistency step, Eq. (16) is solved with the complex symmetric conjugate gradient algorithm (CGsymm) introduced in Ref. [58].

To calculate photoabsorption spectra, we use the dipole approximation

$$v_{\text{ext},\sigma}^{(+)}(\mathbf{r}) = e\mathbf{r} \cdot \mathcal{E}^{(+)}, \quad (54)$$

where  $e$  is the elementary charge and  $\mathcal{E}^{(+)}$  is a homogeneous electric field, and evaluate the induced dipole moment

$$\boldsymbol{\mu}^{(+)} = -e \int d^3 r \mathbf{r} n^{(+)}(\mathbf{r}) \quad (55)$$

from which we can deduce the polarizability  $\underline{\alpha}(\omega)$  according to

$$\boldsymbol{\mu}^{(+)} = \underline{\alpha}(\omega) \cdot \mathcal{E}^{(+)}. \quad (56)$$

In general, three calculations with independent field directions are needed to construct the full polarizability tensor. Finally, the absorption cross section  $\sigma(\omega)$  is calculated as

$$\sigma(\omega) = \frac{4\pi\omega}{3c} \text{Im}[\text{Tr}\underline{\alpha}(\omega)], \quad (57)$$

where  $c$  is the speed of light.

During a self-consistent Sternheimer linear-response calculation, after each solution of Eq. (16) we have to update  $v_{xc\sigma}^{(+)}(\mathbf{r})$  for a given set of response orbitals  $\phi_{i\sigma}^{(\pm)}(\mathbf{r})$ . For the Slater potential, this can be done by simply evaluating the

explicit expression (45). The expressions (49) and (50), however, are not explicit due to the matrix elements  $v_{ij\sigma}^{\text{KLI,CEDA}(+)}$  appearing on the right-hand side. This is no major problem, though, as the KLI and CEDA potentials can be evaluated iteratively: For a given approximation to  $v_{xc\sigma}^{\text{KLI,CEDA}(+)}(\mathbf{r})$ , we can calculate approximate matrix elements and use them to construct a new approximation to  $v_{xc\sigma}^{\text{KLI,CEDA}(+)}(\mathbf{r})$  from Eq. (49) or (50). This has to be repeated until self-consistency between the potentials used to calculate the matrix elements and those constructed from these elements is reached. During this procedure, the orbital-specific response potentials  $w_{xcio}^{(+)}(\mathbf{r})$  do not have to be iterated since they do not depend on the matrix elements. This means that they only have to be constructed once per Sternheimer self-consistency step, which is convenient since their construction involves the most time-consuming steps in the calculation of the Slater, KLI, or CEDA potential response: For EXX, they contain  $N_\sigma(N_\sigma + 1)/2$  independent Fock integrals  $\int e^2 n_{ij\sigma}^{(+)}(\mathbf{r}')/|\mathbf{r} - \mathbf{r}'|d^3r'$  per spin channel. This reduces to only  $N_\sigma$  diagonal self-Hartree integrals  $\int e^2 n_{ii\sigma}^{(+)}(\mathbf{r}')/|\mathbf{r} - \mathbf{r}'|d^3r'$  for the self-interaction correction functional [77].

We have added the routines for the construction of the KLI and CEDA potential response to our Sternheimer linear-response code [58] in the Bayreuth version [78,79] of the PARSEC [80] GS program package, which employs a real-space grid and norm-conserving Troullier-Martins pseudopotentials [81,82].

In our implementation, the Coulomb integrals incorporated in  $w_{xcio}^{(+)}(\mathbf{r})$  are evaluated by solving Poisson's equation using multigrid techniques [21,83]. This is also how we calculate the response of the Hartree potential.

In every self-consistency step, the additional iteration that is needed to construct  $v_{xc\sigma}^{\text{KLI,CEDA}(+)}(\mathbf{r})$  is stabilized by Anderson mixing and thus typically converges in roughly three to six (KLI approximation) or five to ten (CEDA) steps. During this iteration, only the numerically cheap one-point integrals for the matrix elements  $v_{ij\sigma}^{\text{KLI,CEDA}(+)}$  have to be evaluated repeatedly, which is of negligible cost compared to solving Poisson's equation. Thus, the cost for constructing the response  $v_{xc\sigma}^{(+)}(\mathbf{r})$  of the Slater, KLI, or CEDA potential once for a given set of response orbitals is roughly the same as for constructing the occupied orbital-specific response potentials  $w_{xcio}^{(+)}(\mathbf{r})$ .

## VI. RESULTS

In this section we present several applications involving the KLI and CEDA potential response, mainly to demonstrate that our method works and to prove that it is a useful addition to other TDDFT approaches like the Casida formalism or real-time propagation. To that purpose, we first consider in Sec. VIA a case that allows us to compare the detailed spatial structure of the xc potential response to reference calculations. We thus confirm that we are able to construct  $v_{xc\sigma}^{(+)}(\mathbf{r})$  with high accuracy throughout the whole simulation sphere and even at large distances from the system.

In Sec. VIB, we then calculate absorption spectra for a system where we can also perform stable real-time propagations with KLI and CEDA potentials. By comparing the resulting spectra we show that our method works well through an

extended frequency range and therefore is a suitable alternative to the real-time method.

Finally, in Sec. VIC, we calculate the absorption spectrum for a system for which real-time propagations with KLI potentials are notoriously unstable. We thus provide a proof of concept that our method allows us to circumvent the stability issues that can arise in real-time calculations employing potentials which are not strictly defined as functional derivatives.

We focus on the KLI and CEDA potential of the exact exchange (XKLI and XCEDA, respectively) functional, defined as the Fock integral evaluated with Kohn-Sham orbitals, and on the KLI potential of the self-interaction-corrected local-density approximation (SICKLI) [29,70].

### A. Hydrogen chain: Comparison to static finite-field results

To test our way of calculating the response of the xc potential, we do not want to rely solely on excitation spectra for two reasons. First, excitation energies are affected by the chosen xc approximation not only through the kernel or the potential response, but also through GS properties such as the Kohn-Sham eigenvalue spectrum or GS potential. It is therefore not straightforward to extract information “purely” on  $v_{xc\sigma}^{(+)}(\mathbf{r})$  from excitation energies. The second problem is that “integrated” quantities such as dipole moments or the absorption cross section contain less information than the potential itself as a function of the spatial coordinates. Even a wrong kernel or potential response can by chance move the energies of some excitations in the right direction on the frequency axis, but potentially makes grave errors for other types of excitations. We would thus have to test our implementation for a large number of excitation energies of as many different excitation types (valence, Rydberg, charge transfer, etc.) as possible to make sure that the potential is calculated correctly.

Therefore, we follow a two-pronged approach. We test our method for excitation energy spectra (see the following sections), but we also directly examine the response potential as a function of the spatial coordinates in this section. For that purpose, we need a test case which should have two properties. The first is that different xc approximations should yield clearly different results for  $v_{xc\sigma}^{(+)}(\mathbf{r})$ . The second is that we should be able to construct the response of the potential for the xc approximations under consideration by some method that is different from and completely independent of our linear-response formalism and can thus serve as a benchmark for our response potential  $v_{xc\sigma}^{(+)}(\mathbf{r})$ .

The static field-counteracting effect in hydrogen chains meets these conditions: Hydrogen chains with alternating H-H distances of  $2a_0$  and  $3a_0$  (where  $a_0$  is the Bohr radius) are frequently used model systems that provide a tough test case for many-body methods [71,84–94]. Local and standard semilocal functionals are known to severely overestimate the static polarizability and hyperpolarizabilities in these systems. This error is not removed but significantly reduced by the EXX, with the CEDA performing better than the KLI approximation and the exact OEP yielding the best results. Due to these pronounced differences, hydrogen chains make for ideal test systems and therefore we study the  $\text{H}_8$  molecule in the following.

The observed differences have been traced back, at least partially, to an ultranlocal feature of the EXX potential which cannot be mimicked by standard semilocal functionals: When a system is placed in a homogeneous external field, the EXX GS potential builds up a field-counteracting term, which makes it harder to move charge and thus lowers the polarizability.

The standard way [74,85,88] to visualize this term is by performing two GS calculations. In the first one, the electrons are merely subjected to the atomic potentials. In the second one, an additional external potential

$$v_{\text{ext}}(\mathbf{r}) = e\mathcal{E}x \quad (58)$$

is applied. This corresponds to a homogeneous electric field of strength  $\mathcal{E}$  along the  $x$  direction. Then one simply plots the difference of the resulting xc potentials

$$\Delta v_{\text{xc}}(\mathbf{r}) := v_{\text{xc}}(\mathbf{r})|_{\mathcal{E} \neq 0} - v_{\text{xc}}(\mathbf{r})|_{\mathcal{E} = 0}. \quad (59)$$

In this way, the position-dependent response of the xc potential to the field can be constructed from two standard GS calculations, without the need for an explicit expression for  $v_{\text{xc}\sigma}^{(+)}(\mathbf{r})$ .

To make the connection to our linear-response scheme, we first treat the potential of the static external field as a small perturbation and expand  $v_{\text{xc}}(\mathbf{r})$  around  $\mathcal{E} = 0$ . For small field strengths, this leads to

$$\Delta v_{\text{xc}}(\mathbf{r}) \xrightarrow{\mathcal{E} \rightarrow 0} v_{\text{xc}}^{(1)}(\mathbf{r}) + O(\mathcal{E}^2), \quad (60)$$

where  $v_{\text{xc}}^{(1)}(\mathbf{r})$  is the static first-order response of the xc potential.

Next we examine the static limit of our TD Sternheimer scheme: For vanishing  $\omega$  and  $\eta$ , the general TD perturbation introduced in Sec. II becomes time independent,

$$v_{\text{ext},\sigma}(\mathbf{r}, t) \xrightarrow{\omega, \eta \rightarrow 0} 2 \text{Re}[v_{\text{ext},\sigma}^{(+)}(\mathbf{r})]. \quad (61)$$

Thus, we can mimic the situation described above in a Sternheimer calculation by setting  $\omega$  and  $\eta$  to zero and choosing the real-valued perturbation

$$v_{\text{ext},\sigma}^{(+)}(\mathbf{r}) = \frac{1}{2} e\mathcal{E}x. \quad (62)$$

Similarly, the TD linear response of the xc potential becomes time independent,

$$v_{\text{xc}\sigma}^{(1)}(\mathbf{r}, t) \xrightarrow{\omega, \eta \rightarrow 0} 2 \text{Re}[v_{\text{xc}\sigma}^{(+)}(\mathbf{r})]. \quad (63)$$

Since in this limit, and for a real perturbation,  $v_{\text{xc}\sigma}^{(+)}$  also becomes real, we can simply evaluate  $\Delta v_{\text{xc}}$  as

$$\Delta v_{\text{xc}}(\mathbf{r}) = 2v_{\text{xc}\sigma}^{(+)}(\mathbf{r}) \quad (64)$$

after performing a self-consistent Sternheimer calculation with the  $v_{\text{ext},\sigma}^{(+)}$  given above and with small or vanishing values for  $\omega$  and  $\eta$ . Comparing the resulting  $\Delta v_{\text{xc}}(\mathbf{r})$  with the one calculated from Eq. (59) after two GS calculations thus allows us to probe directly the full spatial structure of our  $v_{\text{xc}\sigma}^{(+)}(\mathbf{r})$  construction and to compare it to an independent reference. (In this way we check the full spatial structure of the response, whereas the frequency dependence will be checked in the following sections.)

We have performed these tests for the XKLI, XCEDA, and SICKLI potential [95]. To make sure that our static finite-field calculations are well within the linear regime, which is required so that the results from Eqs. (59) and (64) can coincide, we use an extremely small field strength of  $\mathcal{E} = 10^{-6} e/a_0^2$ .

Also, since the frequency  $\omega$  enters the Sternheimer scheme merely as a parameter, it should in principle be sufficient to test our implementation for  $\omega = 0$  in order to verify that our method is correct. However,  $\omega = \eta = 0$  might be a special case numerically. Therefore, we here present results for small but nonvanishing values of  $\hbar\omega = 0.2$  eV and  $\hbar\eta = 0.1$  meV. This should make it easier to conclude that if our method works well for these parameter values, it should in principle also do so for any other value. Additionally, we explicitly checked that doing the calculations for  $\omega = \eta = 0$  poses no problem and yields virtually the same results as for these finite values.

Figure 1 shows our results for the various functionals. For comparison, we also include the LDA potential response. One can clearly see the field-enhancing character of the LDA, the well-known field-counteracting behavior of the EXX, which is slightly more pronounced in the CEDA than in the KLI potential, as well as the lack thereof for the SICKLI potential. (We here once more note that for the SIC energy functional, the details of how the potential is constructed are very important, as discussed previously in Refs. [29,71,94].) More interesting for our purposes is that in all cases, the Sternheimer and finite-field results perfectly coincide not only qualitatively, but also quantitatively. This is true for the whole simulation sphere which extends out to  $\pm 25a_0$ ,  $16.5a_0$  beyond the outermost atom. In Appendix C we verify that the decisive features and the differences between the different functionals observed here do not follow just from differences in the ground-state eigenvalues or orbitals, but are really a consequence of differences in the exchange(-correlation) response.

## B. Silane photoabsorption spectrum: Comparison to propagation results

After having shown in the preceding section that we can construct the response of the KLI and CEDA potentials correctly with its full spatial dependence for a given frequency, we now demonstrate that our approach works for different frequencies, i.e., we verify that our approach allows for calculating absorption spectra using orbital functionals within the Kohn-Sham framework. We thus prove in particular that no unexpected numerical problems arise when solving the Sternheimer scheme with the KLI or CEDA response for a frequency close to a resonance.

For this we need reference Kohn-Sham TDDFT calculations to compare to. As discussed in the Introduction, the number of orbital functional calculations reported in the literature using the Kohn-Sham approach is limited. Furthermore, it makes sense to base the comparison on reference data that are completely independent, but technically and in accuracy comparable to our real-space approach. For these reasons, silane ( $\text{SiH}_4$ ) appears as an ideal test system, because for this molecule, real-space, real-time propagation linear-response calculations using the XKLI and SICKLI potentials

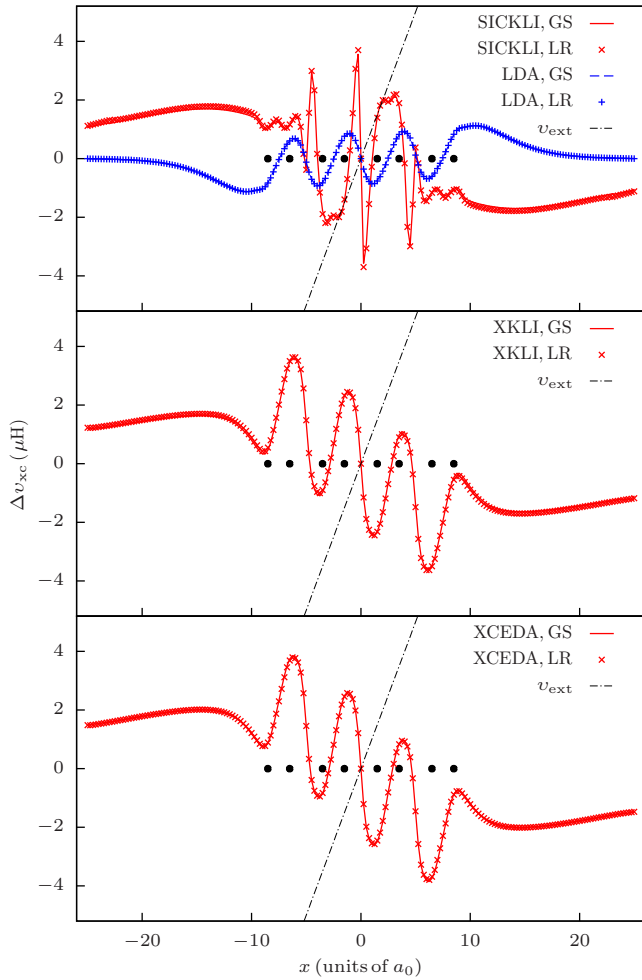


FIG. 1. Static response  $\Delta v_{xc}(\mathbf{r})$  of the xc potential to an external electric field for the  $H_8$  model and  $\mathcal{E} = 10^{-6} e/a_0^2$ . Lines are constructed from GS calculations and Eq. (59), while points are the results from Sternheimer linear-response calculations and Eq. (64). Black circles mark the positions of the H atoms.

have been reported [18,21,29]. In order to have a full set of accurate reference data available for comparison we calculated the photoabsorption spectrum of  $SiH_4$  ourselves once more by real-time propagation for the XKLI, XCEDA, and SICKLI potentials using the BTDFD program package [96].

We compare this reference data to the KLI and CEDA photoabsorption spectra that we calculate with the Sternheimer scheme. In the latter, we use the XKLI approximation (or XCEDA or SICKLI approximation, respectively) throughout the full calculation, i.e., both in the GS calculation and for the construction of  $v_{xc}^{(+)}(\mathbf{r})$ . For the comparison we focus on the energy range in which the most important excitations lie, which is between 8 and 13 eV for the EXX potentials XKLI and XCEDA, and between 7.3 and 11.8 eV for the SICKLI potential. The results for XKLI, XCEDA, and SICKLI potentials are shown in Figs. 2(a), 2(b), and 2(c), respectively [97].

In all three cases, the real-time and Sternheimer spectra with corresponding xc approximations agree perfectly. This confirms our method of linearizing the KLI and CEDA potentials.

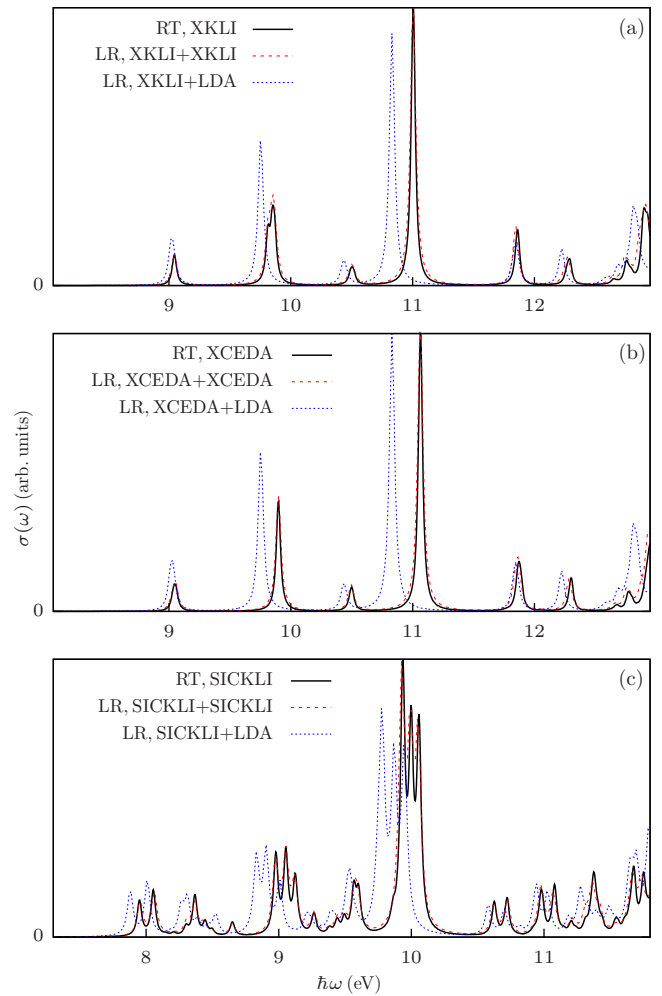


FIG. 2. Photoabsorption spectra of  $SiH_4$  calculated with different xc approximations. Red dashed lines marked LR show results from Sternheimer linear-response calculations in which the same xc approximation has been used for the ground-state calculation and the calculation of the response potential, namely, (a) exact exchange in the KLI approximation, (b) exact exchange in the CEDA, and (c) the SICKLI potential. Black solid lines marked RT denote the results from real-time propagations as a reference. The agreement is excellent. Blue dotted lines show results from Sternheimer linear-response calculations in which the ground-state calculation was done as previously, but the LDA was used for constructing the response potential. This shifts the excitation energies noticeably.

Finally, we perform linear-response calculations where again the KLI or CEDA potentials for the EXX and SIC functionals are used in the GS calculation, but  $v_{xc}^{(+)}(\mathbf{r})$  is constructed from the LDA. In this way, we can check how sensitive the photoabsorption calculation is to the xc approximation that is used for computing the response potential. Using the LDA potential response on top of the orbital functional ground states leads to excitation energies that are shifted by 0.1–0.3 eV, i.e., notable differences. Thus, the response potential does influence the excitation energies and the agreement observed above is not trivial.

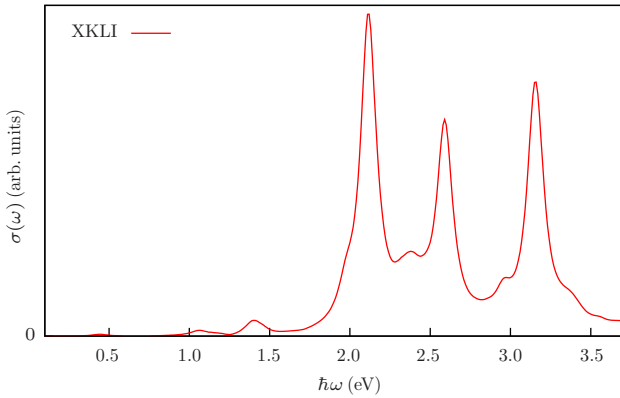


FIG. 3. The XKLI photoabsorption spectrum of  $\text{Na}_5$ .

### C. Photoabsorption in $\text{Na}_5$ : The Sternheimer approach for a system where real-time propagation is unstable

Finally, we demonstrate in the following that the Sternheimer approach allows us to examine cases that cannot be described properly by the real-time approach. When an xc potential approximation is used that is not a functional derivative, the real-time propagation of the Kohn-Sham equations can become unstable. This has been demonstrated explicitly, e.g., for the XKLI potential [55] and other approximations [98]. The violation of the zero-force theorem [99,100] has been suggested as an explanation of this effect [55].

The Sternheimer linear-response approach offers the possibility to avoid such instabilities, as the time dependence of the density, orbitals, and Kohn-Sham potential has been constructed analytically, and one only has to find the Fourier components for various frequencies. These frequencies are independent of each other. Thus, whereas instabilities can build up from time step to time step in a real-time propagation, no instabilities can build up when going from frequency to frequency. Therefore, the Sternheimer formalism can yield stable converged results even for systems where propagations become unstable.

The sodium cluster  $\text{Na}_5$  has become infamous for being a system where propagations with various xc potentials including XKLI and SICKLI have been reported to become unstable and the zero-force violations have been found to be severe [20,29,55,56,98,101]. We therefore focus on this system as a worst-case scenario.

We use the TURBOMOLE [102] program package to optimize the  $\text{Na}_5$  geometry at the B3LYP/def2-QZVPP [3,103,104] level. Then we calculate the XKLI photoabsorption spectrum as described in Sec. V. Figure 3 shows our results [105]. While both the GS and the linear-response self-consistency iterations take more steps to converge than for other sodium clusters of comparable size or for silane, we do not encounter any serious problems in the calculations.

In real-time calculations with a stable propagation, the total propagation time only governs the linewidths. Due to the instabilities arising in the  $\text{Na}_5$  calculations, however, the spectrum changes qualitatively with increasing propagation time: New lines appear, grow in intensity, and move along the frequency axis. This makes it impossible to uniquely identify excitation energies or oscillator strengths.

Therefore, we carefully examine whether our Sternheimer spectrum is unique and robust with respect to numerical parameters. The parameter determining the linewidths in our approach, and in that sense “corresponding” to the total propagation time, is  $\eta$ . Calculations with various different values for  $\eta$  show that it indeed only influences the shape, but not the number, positions, or heights of the lines in the spectrum, as it should.

Additionally, we tested how the atomic coordinates, the numerical grid, and the convergence criteria in the linear-response algorithm influence the calculation. Switching from our coordinates to the MP2/6-31G(d)-optimized coordinates presented in Ref. [106] only leads to an almost rigid redshift of the whole spectrum by approximately 0.1 eV. Using a larger simulation sphere radius, a smaller spacing of the numerical grid, or stricter convergence criteria has almost no noticeable influence on the spectrum. Switching to the unoccupied subspace projection scheme presented in Appendix A also has no effect on the resulting spectrum. Finally, in Appendix D we verify that our XKLI spectrum is physically reasonable by comparing it to reference calculations and to experiment.

All of this leads to the conclusion that the Sternheimer linear-response approach indeed allows us to construct a unique, converged, and robust XKLI photoabsorption spectrum for  $\text{Na}_5$ .

## VII. CONCLUSION

We have derived an approach that enables one to use the KLI approximation and the CEDA in the time-dependent Kohn-Sham scheme in a computationally efficient and numerically stable way. Our approach inherits the computational advantages of the general Sternheimer scheme that have been discussed in previous works [57,58]: No unoccupied orbitals need to be calculated, the approach scales well because adding an electron just adds one more response equation to be solved, and the structure of the equations is such that they can very efficiently be parallelized. In our work, a numerical grid is used for solving the equations, but a basis set implementation is possible as well. Based on the frequency-dependent Sternheimer formalism, we derived a set of transparent equations for the density response in which the frequency of the excitation enters just as a parameter. A linear-response spectrum can thus easily be generated for an orbital functional in the KLI approximation or the CEDA over a wide range of frequencies in a massively parallel computation by solving the equations independently for each frequency. We have demonstrated the stability and accuracy of this orbital-Sternheimer scheme for well-established test cases. In contrast to the real-time propagation approach in which the errors introduced by the KLI or CEDA potential (both being only approximate solutions to the true functional derivative defined by the OEP) can accumulate from time step to time step, no error accumulation can occur in the separate calculations for each frequency.

The derivation of this scheme led to the important insight that the linear response of an orbital functional can be obtained within the Kohn-Sham framework *without* having to compute the xc kernel  $f_{xc}$  explicitly. Instead, the Kohn-Sham response in our scheme is obtained from expressions that involve only functional derivatives with respect to the orbitals.

The latter can straightforwardly be obtained in an analytical calculation for a given density functional. Thus, two notorious limitations that hindered the use of orbital functionals in time-dependent Kohn-Sham theory, the instability of the nonlinearized equations under the KLI approximation and the CEDA, and the construction of  $f_{xc}$ , which is analytically and numerically involved for orbital functionals, have been overcome.

The obvious challenge that remains is to extend the present approach beyond the KLI approximation and the CEDA into a full time-dependent OEP scheme. Despite the progress made in this work, this is still a formidable task. The orbital shift terms that make the difference between, e.g., the KLI potential and the true OEP [48], cannot be taken into account directly within the present scheme. Further work is needed to devise, e.g., an iterative correction scheme similar to the one that can be used for the ground state [107]. Such future work may then also be able to track down signatures of the KLI and CEDA instability in the linear-response signals. The present work thus serves as an important step towards the ultimate goal of being able to use orbital functionals without further approximations efficiently and reliably in the time-dependent Kohn-Sham framework, and it already enables such use within the KLI approximation and the CEDA, which have been demonstrated to be rather accurate in many cases of practical interest.

#### ACKNOWLEDGMENTS

We acknowledge financial support from the German-Israeli Foundation for Scientific Research and Development and the program “Biological Physics” of the Elite Network of Bavaria. We further acknowledge support through the computational resources provided by the Bavarian Polymer Institute and by the Bavarian State Ministry of Science, Research, and the Arts in the Collaborative Research Network “Solar Technologies go Hybrid.” F.H. acknowledges support from the University of Bayreuth Graduate School.

#### APPENDIX A: UNOCCUPIED SUBSPACE PROJECTION

It has been noted earlier that in the construction of the density response, the contributions to  $\varphi_{j\sigma}^{(\pm)}$  proportional to occupied GS orbitals cancel [57,58]. Therefore, if the response of the orbitals is only needed to calculate  $n_{\sigma}^{(+)}$ , one can work with projections of the orbitals onto the unoccupied subspace

$$\tilde{\varphi}_{j\sigma}^{(\pm)}(\mathbf{r}) := \hat{Q}_{\sigma} \varphi_{j\sigma}^{(\pm)}(\mathbf{r}) \quad (\text{A1})$$

with the projector

$$\hat{Q}_{\sigma} := \prod_{j=1}^{N_{\sigma}} \hat{Q}_{j\sigma} = 1 - \sum_{j=1}^{N_{\sigma}} |\phi_{j\sigma}\rangle \langle \phi_{j\sigma}|. \quad (\text{A2})$$

In this work, however, we are dealing with quantities that depend directly on the orbitals instead of only on the density. For these quantities, the occupied contributions do not have to cancel, so we actually need the full orbitals  $\varphi_{j\sigma}^{(\pm)}$ .

If we expand these with respect to the GS orbitals

$$\varphi_{j\sigma}^{(\pm)}(\mathbf{r}) = \sum_{k \neq j} c_{jk\sigma}^{(\pm)} \phi_{k\sigma}(\mathbf{r}) \quad (\text{A3})$$

(where we have already exploited the orthogonality of  $\varphi_{j\sigma}^{(\pm)}$  and  $\phi_{j\sigma}$ ), then the solution to the Sternheimer equations (16) for a fixed right-hand side (i.e., in a single step of the self-consistency iteration) is given by

$$c_{jk\sigma}^{(\pm)} = \frac{\langle \phi_{k\sigma} | v_{\text{ext},\sigma}^{(+)} + v_{\text{Hxc}\sigma}^{(+)} | \phi_{j\sigma} \rangle}{\varepsilon_{j\sigma} - \varepsilon_{k\sigma} \pm \hbar(\omega + i\eta)}. \quad (\text{A4})$$

While in general both occupied and unoccupied GS orbitals and eigenvalues are needed to calculate this expression, we obviously only need the occupied Kohn-Sham spectrum to construct the occupied contributions to  $\varphi_{j\sigma}^{(\pm)}$ . Thus, the full orbital response can be calculated as

$$\varphi_{j\sigma}^{(\pm)}(\mathbf{r}) = \tilde{\varphi}_{j\sigma}^{(\pm)}(\mathbf{r}) + \sum_{\substack{k=1 \\ k \neq j}}^{N_{\sigma}} \frac{\langle \phi_{k\sigma} | v_{\text{ext},\sigma}^{(+)} + v_{\text{Hxc}\sigma}^{(+)} | \phi_{j\sigma} \rangle \phi_{k\sigma}(\mathbf{r})}{\varepsilon_{j\sigma} - \varepsilon_{k\sigma} \pm \hbar(\omega + i\eta)}. \quad (\text{A5})$$

Acting with  $\hat{Q}_{\sigma}$  on Eq. (16) yields

$$\begin{aligned} & [\hat{h}_{\sigma} - \varepsilon_{j\sigma} \mp \hbar(\omega + i\eta)] \tilde{\varphi}_{j\sigma}^{(\pm)}(\mathbf{r}) \\ &= -\hat{Q}_{\sigma} [v_{\text{ext},\sigma}^{(+)}(\mathbf{r}) + v_{\text{Hxc}\sigma}^{(+)}(\mathbf{r})] \phi_{j\sigma}(\mathbf{r}), \end{aligned} \quad (\text{A6})$$

which differs from the original Sternheimer equation only in that  $\hat{Q}_{j\sigma}$  is replaced by  $\hat{Q}_{\sigma}$ . Finally, by construction,

$$\langle \phi_{k\sigma} | \tilde{\varphi}_{j\sigma}^{(\pm)} \rangle = 0 \quad \forall k \in \{1, \dots, N_{\sigma}\}. \quad (\text{A7})$$

These equations fully determine  $\varphi_{j\sigma}^{(\pm)}$ . If we replace the Sternheimer equation (16) by solving the set of equations given above in every self-consistency step, then instead of the full response orbitals, only their unoccupied subspace projections have to be constructed from a conjugate gradient scheme while the occupied contributions are calculated exactly. This can potentially lead to a higher numerical accuracy in the resulting  $\varphi_{j\sigma}^{(\pm)}$ .

The accuracy of the response orbitals can become particularly important when KLI or CEDA potentials are linearized with the method presented in Sec. IV due to the occurrence of terms like  $\frac{n_{ij\sigma}^{(+)}(\mathbf{r})}{n_{\sigma}(\mathbf{r})}$ , where basically the response of the orbitals is divided by the GS density. Since the density falls off exponentially outside the system, inaccuracies in the  $\varphi_{j\sigma}^{(\pm)}$  can easily lead to artificial divergences in the response potential.

We illustrate this for the H<sub>8</sub> system investigated in Sec. VIA: When solving the Sternheimer equation (16) or (A6) with the CGsymm algorithm, we reduce the residual norm by a factor of 10<sup>ρ</sup>. For calculations with the LDA we often find ρ = 6 to be enough to arrive at well-converged, physically meaningful results, but for the KLI and CEDA potentials this convergence criterion turns out to be too weak. Therefore, the calculations in Sec. VIA were done with ρ = 8. When we repeat these calculations with ρ = 6, we find that the LDA results do not change at all. In Fig. 4, however, we show that the XKLI potential response now indeed is erroneously diverging towards the border of our simulation

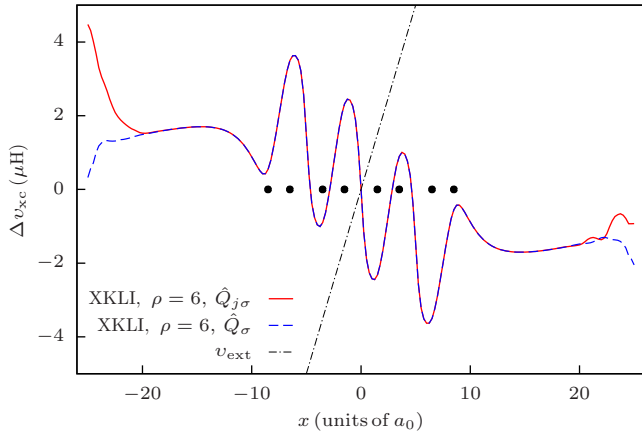


FIG. 4. Linear-response results for  $\Delta v_{xc}(\mathbf{r})$  calculated from Eq. (64) with the XKLI potential and a weak CGSymm convergence criterion of  $\rho = 6$ . The red solid line is based on the Sternheimer equation (16) (designated by the projector  $\hat{Q}_{j\sigma}$  appearing in that equation) and the blue dashed line is based on the projector method (A6) ( $\hat{Q}_\sigma$ ).

sphere, beginning at a distance of approximately  $19a_0$  from the system's center.

The number of self-consistency steps needed for the full calculation is also influenced by these inaccuracies occurring in every single step: With  $\rho = 8$ , we usually need seven to eight steps to converge the self-consistency iteration, independently of whether we are using exactly vanishing or small but finite values for  $\omega$  and  $\eta$  and of whether we are working with the XKLI, XCEDA, or SICKLI potential. With  $\rho = 6$ , however, the XKLI calculation presented in Fig. 4 needed 18 steps to converge.

Both of these deficiencies are affected if we switch from using the “original” Sternheimer equation (16) to the unoccupied subspace projection scheme presented above [i.e., Eq. (A6)]. As can be seen from Fig. 4, the divergent behavior of  $v_{xc}^{(+)}(\mathbf{r})$  is reduced but not eliminated. The potential response still diverges, but less seriously, and it starts doing so only slightly further outside the system, at approximately  $22a_0$ . More interestingly, the self-consistency process is strongly stabilized, with the number of self-consistency iteration steps needed to converge now being reduced again to 8. Thus, in this case of a too-weak CGSymm convergence criterion, the projector method is significantly more effective than the unprojected Sternheimer scheme.

However, since the method cannot completely repair the errors in the response potential that result from an inaccurate solution of the Sternheimer equations in every self-consistency step, we recommend always choosing a sufficiently strong convergence criterion. Additionally, the projector scheme can be applied as a safety net to ensure stability of the self-consistency process. Also, since the results with and without the projector can only differ if the Sternheimer equations are not solved rigorously enough, comparing results from calculations with the two different schemes can be a useful test. We use this to verify that the spectra presented in Secs. VIB and VIC, calculated with  $\rho = 10$  and  $\rho = 12$ , respectively, are indeed accurate.

## APPENDIX B: ALTERNATIVE DERIVATION OF THE LINEARIZATION OF THE KLI AND CEDA POTENTIALS

In this appendix we discuss an alternative derivation of Eqs. (48)–(50). We start by noting that even though Eqs. (39) and (42) are not explicit expressions for the potentials  $v_{xc\sigma}^{\text{KLI,CEDA}}(\mathbf{r}, t)$ , they do allow one to calculate these potentials once the occupied orbitals are known. Therefore,  $v_{xc\sigma}^{\text{KLI,CEDA}}(\mathbf{r}, t)$  can still be seen as implicit orbital functionals and can thus formally be linearized by means of Eq. (21). As the orbital dependence is only implicit, the functional derivatives with respect to the orbitals needed for this approach are not calculated analytically. Instead, one can take the derivative of Eq. (39) or (42). Since all input quantities for these equations except for the potentials themselves are known explicitly in terms of the orbitals, this leads to equations determining the unknown functional derivatives  $\delta v_{xc\sigma}^{\text{KLI,CEDA}}(\mathbf{r}, t)/\delta\varphi_{j\tau}(\mathbf{r}', t')$ . It would be impractical to try to solve these equations directly on a real-space grid since the functional derivatives depend on two spatial variables, i.e., they would be represented by (possibly dense) matrices on the grid. Instead, every operation that has to be performed on the functional derivatives to construct the response potential according to Eq. (21) (i.e., the multiplication with the orbital response, addition of the complex conjugate, summation over the orbitals, and integration) can be applied directly to the equations for the derivatives. Rearranging the resulting equations and inserting Eq. (21) finally leads to equations directly determining the linear response of the potentials  $v_{xc\sigma}^{\text{KLI,CEDA}}(\mathbf{r}, t)$  [cf. Eqs. (48)–(50)], which can be solved on a grid.

## APPENDIX C: CHECKING THE INFLUENCE OF THE GROUND-STATE ELECTRONIC STRUCTURE ON THE $H_8$ CHAIN RESPONSE

With the following test we verify that the large qualitative differences between the  $\Delta v_{xc}(\mathbf{r})$  observed for the different functionals for  $H_8$  are mostly due to the different functionals used to construct  $v_{xc\sigma}^{(+)}(\mathbf{r})$  and not a consequence of differences in the underlying GS calculation. We perform this test because *a priori* one cannot rule out the possibility that at least a highly nonlocal functional such as EXX might be quite sensitive to small differences in the GS density and orbitals that enter the construction of  $v_{xc\sigma}^{(+)}(\mathbf{r})$ .

Thus, one could speculate that the perfect agreement between our GS and Sternheimer results might only partially be due to our correct construction of  $v_{xc\sigma}^{(+)}(\mathbf{r})$  and in another part simply reflect that we are using the correct GS quantities. If that were the case, then our test of the response would not be as stringent as hoped. However, as demonstrated here, this possibility can be ruled out, i.e., the test reported in Fig. 1 is stringent.

As a cross-check we perform two additional linear-response calculations, using different xc approximations in the GS calculation and in the construction of  $v_{xc\sigma}^{(+)}(\mathbf{r})$ : Once we combine the GS of the LDA with the XKLI response (dubbed LDA+XKLI in Fig. 5) and once we use the opposite combination, i.e., the XKLI GS with the potential response of the LDA (XKLI+LDA). Figure 5 unambiguously shows that the LDA+XKLI and XKLI+LDA results are virtually

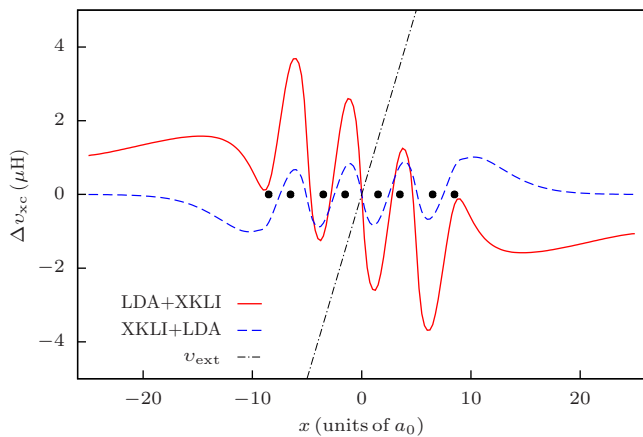


FIG. 5. Linear-response results for  $\Delta v_{xc}(\mathbf{r})$  calculated from Eq. (64) using combinations of two different xc approximations in the GS calculation and the subsequent construction of  $v_{xc}^{(+)}(\mathbf{r})$ .

identical to the XKLI and LDA potentials, respectively. This proves that the functional used to construct  $v_{xc}^{(+)}(\mathbf{r})$  is almost exclusively responsible for its resulting spatial structure, while the functional used in the GS calculation has only very little influence on these results.

#### APPENDIX D: REFERENCE SPECTRA FOR Na<sub>5</sub>

The purpose of the calculations presented in Sec. VIC is only to show that, with our method, stable and robust XKLI calculations can be done even for the extreme case of Na<sub>5</sub>, in spite of this system's known propagation instabilities. However, it is also useful to verify that the resulting XKLI spectrum is physically reasonable. To that purpose, we compare in this section the XKLI spectrum to other calculations and to the experiment [108].

Our calculated spectra using the exchange-only local-density approximation (XLDA), a combination of the XKLI GS with the XLDA response potential (XKLI+XLDA), the Hartree-Fock scheme (HF), and the hybrid functional PBE0 [109,110] in the generalized Kohn-Sham scheme (GKS-PBE0) are depicted in Fig. 6 [111]. The experimental spectrum is rather broad and featureless and only allows to identify the main absorption peak at approximately 2.05 eV. This is well reproduced by the XKLI (approximately 2.11 eV), better than, e.g., with the XLDA.

Comparing the different calculated spectra shows that the XKLI spectrum agrees at least qualitatively rather well with the other results. Somewhat surprisingly, the HF, which is conceptually close to the XKLI in that it is based on the same orbital-dependent energy expression, yields a spectrum that

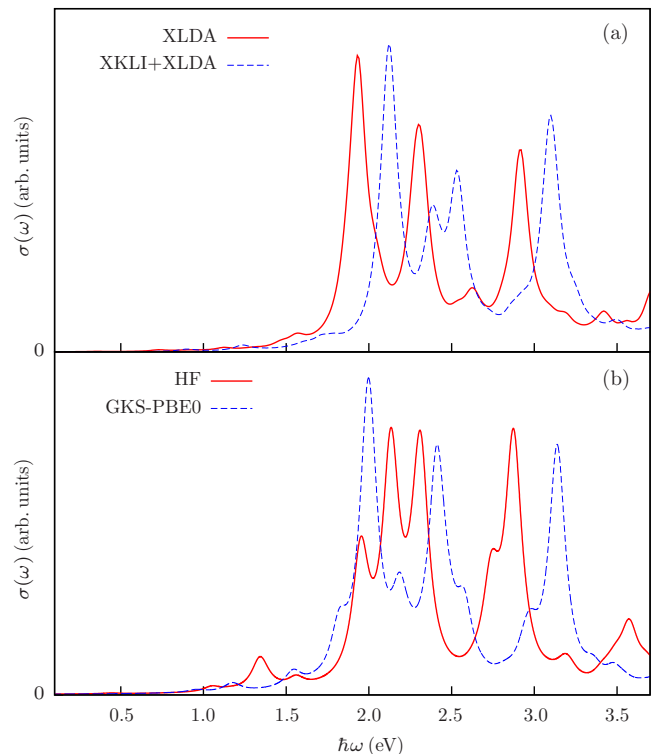


FIG. 6. Photoabsorption spectra of Na<sub>5</sub> calculated with different approximations: (a) exchange-only local density approximation (XLDA) and a combination of the XKLI GS with the XLDA response potential (XKLI+XLDA) and (b) Hartree-Fock (HF) and the hybrid functional PBE0 in the generalized Kohn-Sham scheme (GKS-PBE0).

differs more from the XKLI than any of the other spectra. We carefully tested that this is not merely due to the difference between basis sets and real-space grid-based numerics. All spectra except the HF show three rather-well-defined peaks at about 2.0, 2.5, and 3.0 eV and some smaller peaks in between, with the XLDA spectrum slightly redshifted by approximately 0.2 eV compared to XKLI, XKLI+XLDA, and PBE0. The HF spectrum also has the peak at approximately 3.0 eV but a somewhat different structure between 2.0 and 2.5 eV.

Since the Na<sub>5</sub> spectrum does not contain excitations of, e.g., charge transfer character, it is not surprising that the XKLI and XKLI+XLDA are quite similar. Slightly more unexpected is the good agreement between XKLI and PBE0, as the latter contains only 25% exact exchange and as the generalized Kohn-Sham treatment of this exact exchange is similar to the HF.

- [1] T. Grabo, T. Kreibich, S. Kurth, and E. K. U. Gross, in *Strong Coulomb Correlation in Electronic Structure: Beyond the Local Density Approximation*, edited by V. Anisimov (Gordon & Breach, Tokyo, 2000), pp. 203–311.  
 [2] M. A. L. Marques and E. K. U. Gross, *Annu. Rev. Phys. Chem.* **55**, 427 (2004).

- [3] A. D. Becke, *J. Chem. Phys.* **98**, 5648 (1993).  
 [4] R. E. Stratmann, G. E. Scuseria, and M. J. Frisch, *J. Chem. Phys.* **109**, 8218 (1998).  
 [5] F. Furche and R. Ahlrichs, *J. Chem. Phys.* **117**, 7433 (2002).  
 [6] J. Jaramillo, G. E. Scuseria, and M. Ernzerhof, *J. Chem. Phys.* **118**, 1068 (2003).

- [7] A. V. Arbuznikov, M. Kaupp, and H. Bahmann, *J. Chem. Phys.* **124**, 204102 (2006).
- [8] J. P. Perdew, V. N. Staroverov, J. M. Tao, and G. E. Scuseria, *Phys. Rev. A* **78**, 052513 (2008).
- [9] T. Schmidt, E. Kraisler, A. Makmal, L. Kronik, and S. Kümmel, *J. Chem. Phys.* **140**, 18A510 (2014).
- [10] T. M. Maier, H. Bahmann, A. V. Arbuznikov, and M. Kaupp, *J. Chem. Phys.* **144**, 074106 (2016).
- [11] H. Iikura, T. Tsuneda, T. Yanai, and K. Hirao, *J. Chem. Phys.* **115**, 3540 (2001).
- [12] M. Henderson, B. G. Janesko, and G. E. Scuseria, *J. Chem. Phys.* **128**, 194105 (2008).
- [13] J. Heyd, G. E. Scuseria, and M. Ernzerhof, *J. Chem. Phys.* **118**, 8207 (2003).
- [14] T. Yanai, D. P. Tew, and N. C. Handy, *Chem. Phys. Lett.* **393**, 51 (2004).
- [15] J.-D. Chai and M. Head-Gordon, *J. Chem. Phys.* **128**, 084106 (2008).
- [16] M. A. Rohrdanz, K. M. Martins, and J. M. Herbert, *J. Chem. Phys.* **130**, 054112 (2009).
- [17] L. Kronik, T. Stein, S. Refaely-Abramson, and R. Baer, *J. Chem. Theory Comput.* **8**, 1515 (2012).
- [18] M. A. L. Marques, A. Castro, and A. Rubio, *J. Chem. Phys.* **115**, 3006 (2001).
- [19] C. Legrand, E. Suraud, and P.-G. Reinhard, *J. Phys. B* **35**, 1115 (2002).
- [20] P. M. Dinh, J. Messud, P. G. Reinhard, and E. Suraud, *J. Phys.: Conf. Ser.* **248**, 012024 (2010).
- [21] D. Hofmann, T. Körzdörfer, and S. Kümmel, *Phys. Rev. Lett.* **108**, 146401 (2012).
- [22] X.-M. Tong and S.-I. Chu, *Int. J. Quantum Chem.* **69**, 293 (1998).
- [23] C. A. Ullrich, P.-G. Reinhard, and E. Suraud, *Phys. Rev. A* **62**, 053202 (2000).
- [24] S.-I. Chu, *J. Chem. Phys.* **123**, 062207 (2005).
- [25] M. Dauth and S. Kümmel, *Phys. Rev. A* **93**, 022502 (2016).
- [26] F. Krećinić, P. Wopperer, B. Frusteri, F. Brauße, J.-G. Brisset, U. De Giovannini, A. Rubio, A. Rouzée, and M. J. J. Vrakking, *Phys. Rev. A* **98**, 041401 (2018).
- [27] O. A. Vydrov, G. E. Scuseria, and J. P. Perdew, *J. Chem. Phys.* **126**, 154109 (2007).
- [28] D. Hofmann and S. Kümmel, *Phys. Rev. B* **86**, 201109(R) (2012).
- [29] D. Hofmann and S. Kümmel, *J. Chem. Phys.* **137**, 064117 (2012).
- [30] R. Baer and L. Kronik, *Eur. Phys. J. B* **91**, 170 (2018).
- [31] F. Della Sala and A. Görling, *Int. J. Quantum Chem.* **91**, 131 (2003).
- [32] N. T. Maitra, T. N. Todorov, C. Woodward, and K. Burke, *Phys. Rev. A* **81**, 042525 (2010).
- [33] M. Thiele and S. Kümmel, *Phys. Rev. Lett.* **112**, 083001 (2014).
- [34] Y. Suzuki, L. Lacombe, K. Watanabe, and N. T. Maitra, *Phys. Rev. Lett.* **119**, 263401 (2017).
- [35] C. A. Ullrich, U. J. Gossmann, and E. K. U. Gross, *Phys. Rev. Lett.* **74**, 872 (1995).
- [36] Y.-H. Kim and A. Görling, *Phys. Rev. Lett.* **89**, 096402 (2002).
- [37] S. Hirata, S. Ivanov, I. Grabowski, and R. J. Bartlett, *J. Chem. Phys.* **116**, 6468 (2002).
- [38] S. Hirata, S. Ivanov, R. J. Bartlett, and I. Grabowski, *Phys. Rev. A* **71**, 032507 (2005).
- [39] S. Hirata, *J. Chem. Phys.* **123**, 026101 (2005).
- [40] Y. Shigeta, K. Hirao, and S. Hirata, *Phys. Rev. A* **73**, 010502 (2006).
- [41] F. Bruneval, F. Sottile, V. Olevano, and L. Reining, *J. Chem. Phys.* **124**, 144113 (2006).
- [42] M. Hellgren and U. von Barth, *Phys. Rev. B* **78**, 115107 (2008).
- [43] M. Hellgren and U. von Barth, *J. Chem. Phys.* **131**, 044110 (2009).
- [44] A. Heßelmann, A. Ipatov, and A. Görling, *Phys. Rev. A* **80**, 012507 (2009).
- [45] A. Ipatov, A. Heßelmann, and A. Görling, *Int. J. Quantum Chem.* **110**, 2202 (2010).
- [46] A. Heßelmann and A. Görling, *J. Chem. Phys.* **134**, 034120 (2011).
- [47] K. Yabana and G. F. Bertsch, *Phys. Rev. B* **54**, 4484 (1996).
- [48] M. Mundt and S. Kümmel, *Phys. Rev. A* **74**, 022511 (2006).
- [49] H. O. Wijewardane and C. A. Ullrich, *Phys. Rev. Lett.* **95**, 086401 (2005).
- [50] I. Schelter, Numerische Lösung des Optimized Effective Potential, M.Sc. thesis, University of Bayreuth, 2013.
- [51] S.-L. Liao, T.-S. Ho, H. Rabitz, and S.-I. Chu, *Phys. Rev. Lett.* **118**, 243001 (2017).
- [52] J. B. Krieger, Y. Li, and G. J. Iafrate, *Phys. Rev. A* **46**, 5453 (1992).
- [53] O. V. Gritsenko and E. J. Baerends, *Phys. Rev. A* **64**, 042506 (2001).
- [54] F. Della Sala and A. Görling, *J. Chem. Phys.* **115**, 5718 (2001).
- [55] M. Mundt, S. Kümmel, R. van Leeuwen, and P. G. Reinhard, *Phys. Rev. A* **75**, 050501 (2007).
- [56] J. Messud, P. M. Dinh, P.-G. Reinhard, and E. Suraud, *Phys. Rev. A* **80**, 044503 (2009).
- [57] X. Andrade, S. Botti, M. A. L. Marques, and A. Rubio, *J. Chem. Phys.* **126**, 184106 (2007).
- [58] F. Hofmann, I. Schelter, and S. Kümmel, *J. Chem. Phys.* **149**, 024105 (2018).
- [59] S. Baroni, S. De Gironcoli, A. Dal Corso, and P. Giannozzi, *Rev. Mod. Phys.* **73**, 515 (2001).
- [60] S. Y. Savrasov, *Phys. Rev. Lett.* **81**, 2570 (1998).
- [61] J.-I. Iwata, K. Yabana, and G. F. Bertsch, *J. Chem. Phys.* **115**, 8773 (2001).
- [62] M. J. T. Oliveira, A. Castro, M. A. L. Marques, and A. Rubio, *J. Nanosci. Nanotechnol.* **8**, 3392 (2008).
- [63] H. Hübener and F. Giustino, *Phys. Rev. B* **89**, 085129 (2014).
- [64] H. Hübener and F. Giustino, *J. Chem. Phys.* **141**, 044117 (2014).
- [65] K. Cao, H. Lambert, P. G. Radaelli, and F. Giustino, *Phys. Rev. B* **97**, 024420 (2018).
- [66] *Fundamentals Of Time-Dependent Density Functional Theory*, edited by M. A. L. Marques, N. T. Maitra, F. M. S. Nogueira, E. K. U. Gross, and A. Rubio, Lecture Notes in Physics Vol. 837 (Springer, Heidelberg, 2012).
- [67] R. van Leeuwen, *Int. J. Mod. Phys. B* **15**, 1969 (2001).
- [68] E. Runge and E. K. U. Gross, *Phys. Rev. Lett.* **52**, 997 (1984).
- [69] M. E. Casida, *J. Mol. Struct. THEOCHEM* **914**, 3 (2009).
- [70] J. Chen, J. B. Krieger, Y. Li, and G. J. Iafrate, *Phys. Rev. A* **54**, 3939 (1996).

- [71] T. Körzdörfer, M. Mundt, and S. Kümmel, *Phys. Rev. Lett.* **100**, 133004 (2008).
- [72] J. C. Slater, *Phys. Rev.* **81**, 385 (1951).
- [73] R. T. Sharp and G. K. Horton, *Phys. Rev.* **90**, 317 (1953).
- [74] M. Grüning, O. V. Gritsenko, and E. J. Baerends, *J. Chem. Phys.* **116**, 6435 (2002).
- [75] V. U. Nazarov, *Phys. Rev. B* **87**, 165125 (2013).
- [76] D. G. Anderson, *J. ACM* **12**, 547 (1965).
- [77] J. P. Perdew and A. Zunger, *Phys. Rev. B* **23**, 5048 (1981).
- [78] M. Mundt, S. Kümmel, B. Huber, and M. Moseler, *Phys. Rev. B* **73**, 205407 (2006).
- [79] M. Mundt and S. Kümmel, *Phys. Rev. B* **76**, 035413 (2007).
- [80] L. Kronik, A. Makmal, M. L. Tiago, M. M. G. Alemany, M. Jain, X. Huang, Y. Saad, and J. R. Chelikowsky, *Phys. Status Solidi B* **243**, 1063 (2006).
- [81] N. Troullier and J. L. Martins, *Phys. Rev. B* **43**, 1993 (1991).
- [82] L. Kleinman and D. M. Bylander, *Phys. Rev. Lett.* **48**, 1425 (1982).
- [83] D. Hofmann, Charge and excitation-energy transfer in time-dependent density functional theory, Ph.D. thesis, University of Bayreuth, 2012.
- [84] B. Champagne, D. H. Mosley, M. Vračko, and J.-M. André, *Phys. Rev. A* **52**, 178 (1995).
- [85] S. J. A. van Gisbergen, P. R. T. Schipper, O. V. Gritsenko, E. J. Baerends, J. G. Snijders, B. Champagne, and B. Kirtman, *Phys. Rev. Lett.* **83**, 694 (1999).
- [86] M. van Faassen, P. L. de Boeij, R. van Leeuwen, J. A. Berger, and J. G. Snijders, *Phys. Rev. Lett.* **88**, 186401 (2002).
- [87] M. van Faassen and N. Maitra, *J. Chem. Phys.* **126**, 191106 (2007).
- [88] S. Kümmel, L. Kronik, and J. P. Perdew, *Phys. Rev. Lett.* **93**, 213002 (2004).
- [89] P. Umari, A. J. Williamson, G. Galli, and N. Marzari, *Phys. Rev. Lett.* **95**, 207602 (2005).
- [90] A. Ruzsinszky, J. P. Perdew, G. I. Csonka, G. E. Scuseria, and O. A. Vydrov, *Phys. Rev. A* **77**, 060502(R) (2008).
- [91] A. Ruzsinszky, J. P. Perdew, and G. I. Csonka, *Phys. Rev. A* **78**, 022513 (2008).
- [92] C. D. Pemmaraju, S. Sanvito, and K. Burke, *Phys. Rev. B* **77**, 121204(R) (2008).
- [93] B. Champagne and B. Kirtman, *Int. J. Quantum Chem.* **109**, 3103 (2009).
- [94] T. Körzdörfer and S. Kümmel, in *Theoretical and Computational Developments in Modern Density Functional Theory*, edited by A. K. Roy (Nova Science, New York, 2012), pp. 211–222.
- [95] The eight H atoms are aligned on the  $x$  axis with alternating distances of  $2a_0$  and  $3a_0$ . We use an ellipsoidal simulation sphere with a half axis of  $25a_0$  in the  $x$  direction and  $15a_0$  in the  $y$  and  $z$  directions. The spacing of our cubic grid is  $0.25a_0$  and the cutoff radius of the LDA pseudopotential we use to describe the H atoms is  $1.39a_0$ .
- [96] I. Schelter and S. Kümmel, *J. Chem. Theory Comput.* **14**, 1910 (2018).
- [97] We use a simulation sphere radius of  $16a_0$ , a grid spacing of  $0.5a_0$ , a Si-H bond length of  $1.474 \text{ \AA}$ , and LDA pseudopotentials with cutoff radii of  $1.79a_0$  for Si and  $1.39a_0$  for H. In the linear-response calculations we use  $\hbar\eta = 25 \text{ meV}$  (corresponding to Lorentzian linewidths of  $2\hbar\eta = 0.05 \text{ eV}$ ) and a frequency step size of  $\hbar\Delta\omega = 15 \text{ meV}$ . The real-time propagations are done with a boost strength of  $E_{\text{boost}} = 1 \mu\text{Ry}$ , a time step of  $1 \text{ as}$ , and a fourth-order Taylor propagator. To facilitate the comparison to the Sternheimer spectra, the real-time dipole moment is multiplied with an exponential decay factor prior to the Fourier transform, leading to Lorentzian line shapes.
- [98] A. Karolewski, R. Armiento, and S. Kümmel, *Phys. Rev. A* **88**, 052519 (2013).
- [99] M. Levy and J. P. Perdew, *Phys. Rev. A* **32**, 2010 (1985).
- [100] G. Vignale, *Phys. Rev. Lett.* **74**, 3233 (1995).
- [101] J. Messud, P. M. Dinh, P. G. Reinhard, and E. Suraud, *Ann. Phys. (Berlin)* **523**, 270 (2011).
- [102] R. Ahlrichs, M. Bär, M. Häser, H. Horn, and C. Kölmel, *Chem. Phys. Lett.* **162**, 165 (1989).
- [103] P. J. Stephens, F. J. Devlin, C. F. Chabalowski, and M. J. Frisch, *J. Phys. Chem.* **98**, 11623 (1994).
- [104] F. Weigend and R. Ahlrichs, *Phys. Chem. Chem. Phys.* **7**, 3297 (2005).
- [105] We use a spherical grid with a radius of  $21a_0$  and spacing of  $0.7a_0$ , a LDA pseudopotential with a cutoff radius of  $3.09a_0$ ,  $\hbar\eta = 60 \text{ meV}$ , and a step size of  $\hbar\Delta\omega = 10 \text{ meV}$ . The Na atoms are located in the  $xz$  plane at  $(x, z) = (\pm 3.329a_0, 3.393a_0)$ ,  $(\pm 6.432a_0, -2.219a_0)$ , and  $(0.000a_0, -2.348a_0)$ .
- [106] I. A. Solov'yov, A. V. Solov'yov, and W. Greiner, *Phys. Rev. A* **65**, 053203 (2002).
- [107] S. Kümmel and J. P. Perdew, *Phys. Rev. B* **68**, 035103 (2003).
- [108] C. R. C. Wang, S. Pollack, T. A. Dahlseid, G. M. Koretsky, and M. M. Kappes, *J. Chem. Phys.* **96**, 7931 (1992).
- [109] J. P. Perdew, M. Ernzerhof, and K. Burke, *J. Chem. Phys.* **105**, 9982 (1996).
- [110] J. P. Perdew, K. Burke, and M. Ernzerhof, *Phys. Rev. Lett.* **77**, 3865 (1996).
- [111] The XLDA and XKLI+XLDA calculations are done with the same grid, pseudopotential,  $\eta$  value, and frequency step size as in Sec. VI C. For the HF and GKS-PBE0 calculations, we use TURBOMOLE and the def2-QZVP [104] basis set. To ease comparisons, the “stick spectra” obtained with TURBOMOLE were folded with Lorentzians with a width of  $0.12 \text{ eV}$ .



# Publication 4

## **Molecular excitations from meta-generalized gradient approximations in the Kohn-Sham scheme**

reprinted from

*The Journal of Chemical Physics* **153**, 114106 (2020)

with the permission of AIP Publishing.

Fabian Hofmann and Stephan Kümmel

Theoretical Physics IV, University of Bayreuth, 95440 Bayreuth, Germany

Publ. 4

---

### **My contribution**

I derived and implemented the expressions for the meta-GGA response potential in PARSEC, performed all calculations, prepared all figures, and wrote the first draft of the manuscript.

Publ. 4

# Molecular excitations from meta-generalized gradient approximations in the Kohn–Sham scheme

Cite as: J. Chem. Phys. 153, 114106 (2020); doi: 10.1063/5.0023657

Submitted: 3 August 2020 • Accepted: 19 August 2020 •

Published Online: 16 September 2020



View Online



Export Citation



CrossMark

Fabian Hofmann  and Stephan Kümmel <sup>a)</sup> 

## AFFILIATIONS

Theoretical Physics IV, University of Bayreuth, D-95440 Bayreuth, Germany

<sup>a)</sup> Author to whom correspondence should be addressed: [stephan.kuemmel@uni-bayreuth.de](mailto:stephan.kuemmel@uni-bayreuth.de)

## ABSTRACT

Meta-Generalized Gradient Approximations (meta-GGAs) can, in principle, include spatial and temporal nonlocality in time-dependent density functional theory at a much lower computational cost than functionals that use exact exchange. We here test whether a meta-GGA that has recently been developed with a focus on capturing nonlocal response properties and the particle number discontinuity can realize such features in practice. To this end, we extended the frequency-dependent Sternheimer formalism to the meta-GGA case. Using the Krieger–Li–Iafrate (KLI) approximation, we calculate the optical response for the selected paradigm molecular systems and compare the meta-GGA Kohn–Sham response to the one found with exact exchange and conventional (semi-)local functionals. We find that the new meta-GGA captures important properties of the nonlocal exchange response. The KLI approximation, however, emerges as a limiting factor in the evaluation of charge-transfer excitations.

Published under license by AIP Publishing. <https://doi.org/10.1063/5.0023657>

## I. INTRODUCTION

Time-dependent density functional theory (TDDFT) has become one of the most frequently used approaches for studying excitations of molecules, nanoparticles, and, to some extent, solids. The time-dependent local density approximation (LDA) has been in use for a long time<sup>1–5</sup> and to this day is used with success in simulations of large scale problems.<sup>6–11</sup> However, it suffers from shortcomings among which the inability to correctly predict charge-transfer excitations<sup>12,13</sup> is particularly limiting, e.g., in the area of molecular electronics and light converting processes.<sup>14</sup> The underlying problem is understood and has been traced back to a missing particle number discontinuity<sup>12,15</sup> and missing step-structures and field-counteracting terms in the exchange<sup>16,17</sup> and correlation potential.<sup>18,19</sup> It is thus clear that typical Generalized Gradient Approximations (GGAs), e.g., the well-known Perdew–Burke–Ernzerhof (PBE) approximation,<sup>20</sup> cannot improve over the LDA for the charge-transfer problem. Typical hybrid functionals with  $\approx 20\%$  of exact Fock exchange also do not lead to decisive improvements.<sup>21,22</sup> It takes other functionals, e.g., a self-interaction correction based on the Optimized Effective Potential<sup>23,24</sup> (OEP), or range-separated

hybrids,<sup>25–29</sup> especially with an optimally tuned parameter,<sup>30–34</sup> to cope with the charge-transfer problem within TDDFT.

However, using exact exchange (EXX) substantially increases computational costs. Depending on the size of the problem and the numerical techniques used, the increase can be orders of magnitude. A recent study, e.g., reported that for solid-state, plane-wave calculations, the computational time for using a hybrid functional is about two orders of magnitude larger than for using a regular GGA.<sup>35</sup> Therefore, it would be highly attractive to have functionals that incorporate the qualitative improvements that are achieved with hybrid functionals, especially the particle-number discontinuity and the field-counteracting terms, but at a much lower computational cost.

Exchange–correlation (xc) functionals that depend on the kinetic energy density (meta-GGAs) are natural candidates for such improvements, and their development has led to impressive successes.<sup>36–46</sup> Meta-GGAs explicitly depend on the orbitals, and as the orbitals are nonlocal functionals of the density, meta-GGAs are nonlocal in their density dependence. They can thus feature desired properties such as a derivative discontinuity and step structures in the potential. Furthermore, meta-GGAs can be made

self-correlation free.<sup>37–39</sup> By diligent construction of their exchange parts,<sup>46,47</sup> also their overall self-interaction error can be reduced for many physically relevant situations. At the same time, meta-GGAs do not require the evaluation of nonlocal Fock integrals; thus, their computational cost can be much lower than the one of the hybrid functionals.

However, despite these, in principle, very beneficial properties, meta-GGAs so far have not at all replaced hybrid functionals. There are different reasons for this. On the one hand, nonlocality in many practically available meta-GGAs has been found to be limited (see, e.g., Ref. 48 for examples in a solid-state context and Ref. 49 for a report that the Strongly Constrained and Appropriately Normed (SCAN) meta-GGA does hardly improve charge-transfer characteristics). On the other hand, meta-GGAs can be computationally more demanding than one may naively expect. This is due to the fact that depending on how a meta-GGA's enhancement factor is designed, the higher spatial derivatives that result from the kinetic energy dependence can lead to rapid spatial variations of the meta-GGA xc potential. For standard meta-GGAs, these often require special numerical attention, e.g., finer than usual integration grids.<sup>50</sup>

Progress has been made recently on both of these problems. Aschebrock and Kümmel<sup>47</sup> argued for a new line of meta-GGA construction based on the insight that meta-GGA nonlocality is directly related to the first derivative of the enhancement factor with respect to the kinetic energy density. Following this logic, the TASK meta-GGA has been put forward.<sup>47</sup> The guiding principle of its construction is a pronounced nonlocality that is derived non-empirically and is designed to capture properties that are usually associated with Fock exchange. Its accuracy for the prediction of bandgaps has been demonstrated for a wide range of systems.<sup>35,47</sup> Furthermore, it shows ultranonlocality for the static response of extended molecular systems and increases the accuracy for the prediction of static electric polarizabilities. These properties had so far been thought to be achievable only with Fock exchange. Furthermore, smoothness of the enhancement factor translates into smoothness of the xc potential. This should make TASK a numerically benevolent meta-GGA (and we confirm this hope in this article, see below).

Within ground-state DFT, there are thus clear indications that such meta-GGAs can incorporate nonlocality similar to Fock exchange. Whether their beneficial properties carry over to TDDFT has not yet been explored. This paper takes a first step in this direction. However, using meta-GGAs in TDDFT leads to additional difficulties. The generalized Kohn–Sham scheme, which is typically used for ground-state calculations with orbital functionals,<sup>33,51,52</sup> has pragmatically been used for a considerable time also in TDDFT and recently also has been formally extended to the time domain by Baer and Kronik.<sup>53</sup> They point out, though, that their proof does not apply to the straightforward extension of meta-GGAs to the time-domain because of a violation of the continuity equation. This is in line with the earlier observations by Tao<sup>54</sup> and Bates and Furche.<sup>55</sup> As an alternative to the generalized Kohn–Sham scheme, orbital functionals can also be used in the Optimized Effective Potential (OEP) framework.<sup>56,57</sup> The OEP has also been extended to the time-domain.<sup>58</sup> As the OEP approach stays on the grounds of Kohn–Sham theory, the continuity equation is guaranteed. The practical solution of the TDOEP equation, however, is difficult. Efforts so far

have focused on implementing exact exchange in the OEP scheme. Real-time propagation is prone to instabilities,<sup>59</sup> and solutions have been achieved only for model systems<sup>60,61</sup> that allow for particular numerical treatments. Linear response calculations using the Casida equations lead to a frequency dependent xc kernel and complex sets of equations.<sup>62,63</sup> Applications have thus been restricted to a few explorations of atoms, small molecular systems, and simple solids.<sup>64–74</sup> Several of these studies<sup>65,66</sup> additionally employed the adiabatic approximation, i.e., did not use the full, frequency dependent exchange kernel, or made other modifications to the kernel.<sup>64</sup> Thus, further experience with the use of orbital functionals in Kohn–Sham TDDFT is desirable.

Our work here exploits that the Sternheimer scheme<sup>75,76</sup> has recently been extended to the orbital functionals.<sup>77</sup> This opens a new and efficient route for linear response TD Kohn–Sham calculations with orbital functionals. The Sternheimer scheme avoids the complexity that results from the frequency dependent kernel in the Casida equations and the instability of the real-time OEP propagation. The formalism is, however, so far restricted to the Krieger–Li–Iafrate<sup>78</sup> approximation and the Common-Energy Denominator Approximation (CEDA)<sup>79,80</sup> to the OEP. Furthermore, it has so far been only developed for the exact exchange and self-interaction correction functionals.

In the following, we extend the orbital-functional Sternheimer scheme to meta-GGAs and compute the excitations of several paradigm molecular systems with meta-GGAs in the Kohn–Sham approach to TDDFT. We thus avoid the above-mentioned conceptual questions connected to the generalized Kohn–Sham TDDFT realization of meta-GGAs. We specifically focus on meta-GGAs that were designed to incorporate exact exchange-like nonlocality. In our study, we explore whether the frequency dependent electrical response obtained with these meta-GGAs is similar to the one obtained from exact exchange.

Our paper is structured as follows: In Sec. II, we first shortly review the theory that our work relies on by recapitulating the fundamental properties of the two meta-GGAs that we study and by presenting the essential equations of the Sternheimer approach. We also address some relevant analytical and computational steps in this section. Section III presents photoabsorption spectra for several molecular systems that represent different physical situations. In each case, we compare the response that we obtain with the meta-GGAs to the one that we find with semilocal functionals such as TDLDA or TDPBE and with nonlocal exact exchange. We summarize the results and offer conclusions in Sec. IV.

## II. METHOD

### A. Meta-GGA approximations studied in this work

The specific focus of this work is to explore the response properties of two recently developed meta-GGAs<sup>47</sup> that are designated by PoC (proof of concept) and TASK (author initials) in the following. This choice is motivated by the functionals' construction principle: They were designed to be similar to exact exchange in ground-state and static response calculations. The functionals are written in the general meta-GGA form

$$E_x^{\text{mGGA}}[n] = A_x \int n^{4/3} F_x(s, \alpha) d^3r, \quad (1)$$

where  $A_x = -(3e^2/4)(3/\pi)^{1/3}$ , and the enhancement factor  $F_x(s, \alpha)$  is parameterized by the dimensionless variables

$$s = \frac{|\nabla n|}{2(3\pi^2)^{1/3}n^{4/3}} \quad (2)$$

and

$$\alpha = (\tau - \tau^W)/\tau^{\text{unif}}. \quad (3)$$

Here,

$$n = \sum_{j=1}^{N_{\text{occ}}} 2|\varphi_j|^2 \quad (4)$$

is the density,

$$\tau = \frac{\hbar^2}{2m} \sum_{j=1}^{N_{\text{occ}}} 2|\nabla\varphi_j|^2 \quad (5)$$

is the positive definite kinetic energy density of the Kohn–Sham system,  $N_{\text{occ}} = \frac{1}{2}N_{e^-}$  is the number of occupied orbitals in a closed-shell system of  $N_{e^-}$  electrons,

$$\tau^W = \frac{\hbar^2}{8m} \frac{|\nabla n|^2}{n} \quad (6)$$

is the von Weizsäcker kinetic energy density, and  $\tau^{\text{unif}} = A_s n^{5/3}$  with  $A_s = (3\hbar^2/10m)(3\pi^2)^{2/3}$  being the uniform-density limit.  $e$  and  $m$  are the elementary charge and the electron mass, respectively. A decisive property of the PoC and TASK functionals that distinguishes them from many other meta-GGAs is a substantial negative derivative of the enhancement factor with respect to  $\alpha$ , i.e., their construction ensures

$$\partial F_x/\partial\alpha < 0. \quad (7)$$

Both functionals are thus endowed with a substantial positive derivative discontinuity.

The important conceptual difference between the PoC and the TASK functional is that the PoC construction focuses on capturing field-counteracting terms in a very simple analytical form without attempting to create a generally useful and broadly applicable functional. TASK, on the other hand, is a general meta-GGA approximation for exchange that has been carefully designed from non-empirical principles and respects most of the known exact constraints. We do not explicitly write down the enhancement factors but refer the reader to Ref. 47 for the sake of brevity.

## B. The Sternheimer scheme

The Sternheimer approach to TDDFT has been developed in previous works.<sup>75,81</sup> It is still less commonly used than the earlier developed Casida-equations<sup>82</sup> or real-time techniques,<sup>2,3</sup> but a rigorous derivation of how the Sternheimer scheme connects to Kohn–Sham TDDFT has been given.<sup>76</sup> From a practical point of view, the Sternheimer scheme is highly attractive because of its natural and excellent parallelization, which makes it ideal for modern computer systems. In the following, we recapitulate the main aspects of how the scheme is used for calculating the linear response for orbital functionals. We here focus on singlet excitations in closed-shell systems and, therefore, restrict ourselves to the spin independent formalism. For the spin dependent formulation of Sternheimer linear

response theory, the calculation of triplets, and a detailed derivation and explanation of the computational procedures, we refer to Ref. 76.

For any given frequency  $\omega$ , we solve the Sternheimer equations

$$\left[\hat{h} - \varepsilon_j \mp \hbar(\omega + i\eta)\right]\tilde{\varphi}_j^{(\pm)}(\mathbf{r}) = -\hat{Q}\left[v_{\text{ext}}^{(+)}(\mathbf{r}) + v_{\text{Hxc}}^{(+)}(\mathbf{r})\right]\phi_j(\mathbf{r}), \quad (8)$$

subject to the condition

$$\langle\phi_i|\tilde{\varphi}_j^{(\pm)}\rangle = 0 \quad \forall i, j \in \{1, \dots, N_{\text{occ}}\}, \quad (9)$$

for the  $j$ th occupied (projected) response orbitals  $\tilde{\varphi}_j^{(\pm)}(\mathbf{r})$  from which the density response amplitude  $n^{(+)}(\mathbf{r})$  can be constructed as

$$n^{(+)}(\mathbf{r}) = \sum_{j=1}^{N_{\text{occ}}} 2\phi_j(\mathbf{r})\left[\tilde{\varphi}_j^{(+)}(\mathbf{r}) + \tilde{\varphi}_j^{(-)}(\mathbf{r})\right]. \quad (10)$$

Here,

$$\hat{h} = -\frac{\hbar^2}{2m}\nabla^2 + v_{\text{ion}}(\mathbf{r}) + v_{\text{Hxc}}(\mathbf{r}) \quad (11)$$

is the ground-state (GS) Kohn–Sham Hamiltonian containing the electrostatic potential of the nuclei and the GS Hartree-exchange–correlation potential,  $\varepsilon_j$  and  $\phi_j(\mathbf{r})$  are the corresponding occupied GS orbital energies and (real-valued) orbitals, respectively, and

$$\hat{Q} = 1 - \sum_{j=1}^{N_{\text{occ}}} |\phi_j\rangle\langle\phi_j| \quad (12)$$

projects onto the unoccupied subspace. On the right-hand side of Eq. (8),  $v_{\text{ext}}^{(+)}(\mathbf{r})$  defines a perturbation and  $v_{\text{Hxc}}^{(+)}(\mathbf{r})$  describes the response of the Hartree-exchange–correlation potential to the perturbation. In this work, we are only calculating dipole excitations and (static) dipole polarizabilities, and so we always use

$$v_{\text{ext}}^{(+)}(\mathbf{r}) = e\mathbf{E} \cdot \mathbf{r}, \quad (13)$$

where  $\mathbf{E}$  is a homogeneous electric field.  $v_{\text{Hxc}}^{(+)}(\mathbf{r})$  is expressed in terms of the density and orbital response amplitudes  $n^{(+)}(\mathbf{r})$  and  $\tilde{\varphi}_j^{(\pm)}(\mathbf{r})$  (see Subsection II C for explicit expressions), respectively, and so the Sternheimer equations have to be solved self-consistently. We do this by initially setting  $v_{\text{Hxc}}^{(+)}(\mathbf{r})$  to zero. This leaves only the external perturbation on the rhs of the Sternheimer equations. From the resulting solutions of Eq. (8), we can evaluate  $v_{\text{Hxc}}^{(+)}(\mathbf{r})$ , insert it into the rhs of the Sternheimer equations, and solve them again. This is repeated until  $v_{\text{Hxc}}^{(+)}(\mathbf{r})$  is converged.

Finally, the real-valued parameters  $\omega$  and  $\eta$  are the frequency and the damping parameter, respectively.  $\eta$  is formally introduced as an exponential switch-on rate of the perturbation, regularizes the Sternheimer equations, and leads to Lorentzian line shapes with half-width  $\eta$  in the resulting spectra. Larger values of  $\eta$  speed up the convergence of the calculations.

From  $n^{(+)}(\mathbf{r})$ , one can calculate spectral response quantities, evaluated at the frequency  $\omega$ . By choosing the field  $\mathbf{E}$  to point, e.g., in the  $x$ -direction,

$$\mathbf{E} = \mathcal{E}\hat{e}_x, \quad (14)$$

the  $yx$ -component of the dynamic polarizability can be evaluated as

$$\alpha_{yx}(\omega) = \int d^3r (-e) y n^{(+)}(\mathbf{r}) / \mathcal{E}. \quad (15)$$

Static polarizabilities can be calculated this way by choosing small or vanishing values for  $\omega$  and  $\eta$ . To construct spectra discretized over any chosen frequency range, the Sternheimer equations have to be solved for a discrete set of values  $\{\omega_i\}$  and a suitable damping parameter  $\eta$ . As discussed in Ref. 76, we evaluate the spectra by fitting the positions and heights of a superposition of Lorentzians with the fixed width  $2\eta$  to the resulting discrete values of the polarizability. This allows us to extract accurate excitation energies and oscillator strengths from calculations using only relatively few sample frequencies and a large damping parameter  $\eta$ . All spectra shown in this work are constructed in this way.

We represent optical absorption spectra by the absorption cross section  $\sigma(\omega)$ , which is defined by the imaginary part of the polarizability tensor as

$$\sigma(\omega) = \frac{4\pi\omega}{3c} \text{Im}[\text{Tr}\underline{\alpha}(\omega)], \quad (16)$$

where  $\text{Tr}$  denotes the trace and  $c$  is the speed of light. In general, three calculations per frequency with fields pointing in linearly independent directions are needed to construct the trace (see remarks about possible shortcuts in Sec. II D).

### C. The response potential

The Hartree part of  $v_{\text{Hxc}}^{(+)}(\mathbf{r})$  is the Coulomb potential of the density response amplitude and solves Poisson's equation,

$$\nabla^2 v_{\text{H}}^{(+)}(\mathbf{r}) = -4\pi e^2 n^{(+)}(\mathbf{r}). \quad (17)$$

In principle, the exchange–correlation part can be expressed in terms of the (damped) exchange–correlation kernel,<sup>76</sup>

$$f_{\text{xc}}(\mathbf{r}, \mathbf{r}', \omega + i\eta) = \int d(t-t') \left. \frac{\delta v_{\text{xc}}(\mathbf{r}, t)}{\delta n(\mathbf{r}', t')} \right|_{n_{\text{GS}}} e^{i(\omega+i\eta)(t-t')} \quad (18)$$

as

$$v_{\text{xc}}^{(+)}(\mathbf{r}) = \int f_{\text{xc}}(\mathbf{r}, \mathbf{r}', \omega + i\eta) n^{(+)}(\mathbf{r}') d^3r'. \quad (19)$$

This corresponds to an expansion of the exchange–correlation potential with respect to the density response. For LDA and GGAs, this leads to simple, explicit, local or semi-local expressions for  $v_{\text{xc}}^{(+)}(\mathbf{r})$ , e.g.,

$$v_{\text{xc}}^{\text{LDA}(+)}(\mathbf{r}) = \left. \frac{\partial^2 \epsilon_{\text{xc}}^{\text{HEG}}}{\partial n^2} \right|_{n_{\text{GS}}(\mathbf{r})} n^{(+)}(\mathbf{r}), \quad (20)$$

where  $\epsilon_{\text{xc}}^{\text{HEG}}$  is the exchange–correlation energy density per unit volume of the homogeneous electron gas and  $n_{\text{GS}}(\mathbf{r})$  is the GS density at point  $\mathbf{r}$ .

For the orbital functionals employed in this work, i.e., EXX and meta-GGAs, we stay within the Kohn–Sham scheme using the KLI approximation to the TDOEP. As shown in Ref. 77, for orbital dependent potentials, the density expansion underlying Eq. (19) can be rewritten into an expansion with respect to the response orbitals without any further approximation and without switching to a generalized Kohn–Sham formalism. This leads to an explicit expression

for the response of the KLI potential that can be readily evaluated without having to solve an OEP-like equation for its kernel,

$$\begin{aligned} v_{\text{xc}}^{\text{KLI}(+)}(\mathbf{r}) = & 2 \sum_{i=1}^{N_{\text{occ}}} \left\{ \frac{\phi_i^2(\mathbf{r})}{n_{\text{GS}}(\mathbf{r})} w_{\text{xc}i}^{(+)}(\mathbf{r}) - \frac{n_i^{(+)}(\mathbf{r})}{n_{\text{GS}}(\mathbf{r})} \Delta v_i(\mathbf{r}) \right\} \\ & + 2 \sum_{i=1}^{N_{\text{occ}}-1} \left\{ \frac{n_i^{(+)}(\mathbf{r})}{n_{\text{GS}}(\mathbf{r})} \int \phi_i^2(\mathbf{r}') \Delta v_i(\mathbf{r}') d^3r' \right. \\ & + \frac{\phi_i^2(\mathbf{r})}{n_{\text{GS}}(\mathbf{r})} \int \phi_i^2(\mathbf{r}') [v_{\text{xc}}^{\text{KLI}(+)}(\mathbf{r}') - w_{\text{xc}i}^{(+)}(\mathbf{r}')] d^3r' \\ & \left. + \frac{\phi_i^2(\mathbf{r})}{n_{\text{GS}}(\mathbf{r})} \int n_i^{(+)}(\mathbf{r}') \Delta v_i(\mathbf{r}') d^3r' \right\} \quad (21) \end{aligned}$$

with

$$\begin{aligned} w_{\text{xc}i}^{(+)}(\mathbf{r}) = & \sum_{j=1}^{N_{\text{occ}}} \int d^3r' [\varphi_j^{(+)}(\mathbf{r}') + \varphi_j^{(-)}(\mathbf{r}')] \\ & \times \frac{\delta}{\delta \varphi_j(\mathbf{r}')} \left[ \frac{\delta E_{\text{xc}}[\{\varphi_k, \varphi_k^*\}]}{4\varphi_i^*(\mathbf{r}) \delta \varphi_i(\mathbf{r})} + \frac{\delta E_{\text{xc}}[\{\varphi_k, \varphi_k^*\}]}{4\varphi_i(\mathbf{r}) \delta \varphi_i^*(\mathbf{r})} \right] \Big|_{\varphi_k = \varphi_k^* = \phi_k} \quad (22) \end{aligned}$$

Here,

$$\varphi_i^{(\pm)}(\mathbf{r}) = \tilde{\varphi}_i^{(\pm)}(\mathbf{r}) + \sum_{\substack{j=1 \\ j \neq i}}^{N_{\text{occ}}} \frac{\langle \phi_j | v_{\text{ext}}^{(+)} + v_{\text{Hxc}}^{(+)} | \phi_i \rangle \phi_j(\mathbf{r})}{\varepsilon_i - \varepsilon_j \pm \hbar(\omega + i\eta)} \quad (23)$$

are the unprojected response orbitals including occupied contributions,  $E_{\text{xc}}[\{\varphi_k, \varphi_k^*\}]$  is the orbital dependent approximation to the exchange–correlation energy with general complex arguments  $\{\varphi_k, \varphi_k^*\}$ ,

$$n_i^{(+)}(\mathbf{r}) = \phi_i(\mathbf{r}) (\varphi_i^{(+)}(\mathbf{r}) + \varphi_i^{(-)}(\mathbf{r})) \quad (24)$$

is the  $i$ th orbital density response amplitude, and

$$\Delta v_i(\mathbf{r}) = [v_{\text{xc}}^{\text{KLI}}(\mathbf{r}) - u_{\text{xc}i}(\mathbf{r})]_{\varphi_k = \varphi_k^* = \phi_k} \quad (25)$$

is the difference of the GS KLI and orbital-specific potentials,

$$u_{\text{xc}i}(\mathbf{r}) = \frac{1}{\varphi_i^*(\mathbf{r})} \frac{\delta E_{\text{xc}}[\{\varphi_k, \varphi_k^*\}]}{\delta \varphi_i(\mathbf{r})}. \quad (26)$$

Note that a Sternheimer calculation using these expressions is completely equivalent to a Casida calculation using the frequency-dependent kernel of the TD KLI potential, which is non-adiabatic due to the nonlocal density dependence (with respect to both space and time) of the Kohn–Sham orbitals.

These expressions have already been successfully employed in calculations using EXX-KLI and self-interaction corrected<sup>83</sup> LDA-KLI.<sup>77</sup> The numerics involved in applying them to meta-GGAs require some care, specifically regarding the order of terms and the numerical evaluation of derivatives in the meta-GGA expressions for  $w_{\text{xc}i}^{(+)}(\mathbf{r})$ . We will report on these technical issues in separate, future work. Here, we focus on the results for the linear response properties of the TASK and PoC meta-GGAs.

### D. Computational details

We have added the routines for the evaluation of the meta-GGA expressions for  $w_{\text{xc}i}^{(+)}(\mathbf{r})$  to our Sternheimer linear response

code,<sup>76,77</sup> which is part of the Bayreuth version<sup>84,85</sup> of the PARSEC<sup>86</sup> GS program package. It employs a real-space grid and norm-conserving Troullier–Martins pseudopotentials.<sup>87,88</sup> In all the following calculations, the TASK-KLI and PoC-KLI exchange functionals were used without adding a correlation expression, as our focus is mostly on the comparison to the EXX-KLI results.

The Coulomb integrals needed for the Hartree and EXX-KLI response potential are evaluated by solving Poisson’s equation using multigrid techniques.<sup>23,89</sup> For further details on the evaluation of the KLI response potential expression (21), see Ref. 77. We use LIBXC<sup>90</sup> in the construction of the PBE<sup>20</sup> response potential.

Anderson mixing<sup>91</sup> is our preferred way to stabilize the self-consistent solution of the Sternheimer equations. In each self-consistency step, the equations are solved with the complex symmetric conjugate gradient algorithm presented in Ref. 76.

We use different simulation sphere radii or half axes, grid spacings, discrete frequency step sizes  $\Delta\omega$ , and damping parameter values  $\eta$  for the different systems considered in this work. Those parameters, along with the cutoff radii of the pseudopotentials we employ in this work, are listed in the Appendix.

In some calculations, the symmetries of the system can be exploited to avoid doing the three separate calculations that were mentioned at the end of Sec. II B. For example, for the Na<sub>4</sub> cluster, we align the axes of symmetry with the coordinate axes and choose the electric field to point along the (1, 1, 1)-direction. We can thus extract the response from just one calculation per frequency.

In Sec. III C, we study an organic semiconductor molecule and are only interested in the energetic position of one specific transition of charge-transfer character. Thus, we first calculate optical absorption spectra with the TDLDA, once using our implementation of the Sternheimer scheme and, for comparison, also using Casida calculations with TURBOMOLE<sup>92</sup> and the def2-TZVP and def2-QZVP basis sets.<sup>93</sup> From these, we consistently identify the charge-transfer excitation and the direction  $\hat{e}_{\text{CT}}$  of the corresponding transition dipole. We then use this in our subsequent calculations with various different functionals to calculate the spectra that specifically highlight the charge-transfer excitation: Choosing the perturbing field to point along  $\hat{e}_{\text{CT}}$ , we evaluate

$$\text{Im}[\alpha_{\text{CT}}(\omega)] = \int d^3r (-e) (\mathbf{r} \cdot \hat{e}_{\text{CT}}) \text{Im}[n^{(+)}(\mathbf{r})] / \mathcal{E}. \quad (27)$$

### III. RESULTS

In this section, we present several examples of what one can expect from the PoC and TASK meta-GGA KLI response potential. First, in Sec. III A, we study the zero-frequency limit of the response of a hydrogen chain. This serves to demonstrate the correctness of our technical implementation and allows us to probe the response potential directly. We then discuss the results for the photoabsorption spectra of several small molecules and clusters in Sec. III B. Finally, in Subsection III C, we study a charge transfer excitation energy in a larger organic semiconductor molecule.

#### A. The zero-frequency limit of the response potential for a hydrogen chain

The response properties of an exchange–correlation functional, which are represented by the kernel in conventional Kohn–Sham

linear response theory based on the Casida approach, enter the Sternheimer scheme through the response potential  $v_{\text{xc}}^{(+)}(\mathbf{r})$ . Since the evaluation of this quantity for meta-GGAs in the KLI approximation is the main new feature in this work, which enables us to employ meta-GGAs in Kohn–Sham based linear response calculations, we first analyze the response potential itself before proceeding to studying its effects in the calculation of absorption spectra.

As discussed in detail in Ref. 77, the static response of a hydrogen chain to an external electric field lends itself for such a test for several reasons. First, the response potentials of different functionals show huge qualitative differences for this case, ranging from the pronounced field-counteracting behavior of EXX to the slightly field-enhancing potential of the LDA. The missing field-counteracting features lead to a severe overestimation of linear and nonlinear polarizabilities by many functionals, especially LDA, GGAs, and conventional hybrids that use  $\approx 20\%$  of Fock exchange. EXX leads to a much improved (with respect to the exact results) response. These pronounced differences are the main reason why hydrogen chains with alternating H–H distances of 2 and  $3a_0$  are frequently used model systems that provide a tough test case for many-body methods.<sup>15,16,94–103</sup>

Second, the static response can be used as a test because as shown in Ref. 77, the static limit of the change  $\Delta v_{\text{xc}}(\mathbf{r})$  of the exchange–correlation potential due to a static external field can be calculated in two ways: It can be either computed in a finite field approach as the difference  $\Delta v_{\text{xc}}(\mathbf{r}) := v_{\text{xc}}(\mathbf{r})|_{\mathcal{E} \neq 0} - v_{\text{xc}}(\mathbf{r})|_{\mathcal{E} = 0}$  between the potentials of two GS calculations with and without an external field added to the Coulomb potential of the hydrogen cores or obtained as twice the response potential  $\Delta v_{\text{xc}}(\mathbf{r}) = 2v_{\text{xc}}^{(+)}(\mathbf{r})$  from a frequency dependent Sternheimer linear response calculation in the zero-frequency limit  $\omega, \eta \rightarrow 0$ . This allows us to cross-check our implementation of  $v_{\text{xc}}^{(+)}(\mathbf{r})$  against an independent reference based on GS calculations.

In the context of the two meta-GGAs studied in this work, this test case has yet another appeal. The PoC functional was specifically designed to reproduce the field-counteracting effect of EXX in hydrogen chains. One of the central ideas of the TASK functional<sup>47</sup> is to incorporate a realistic derivative discontinuity, and the latter is closely related to the field-counteracting term.<sup>15,47</sup> Therefore, it is a natural and relevant test to check whether the Sternheimer implementation reproduces the field-counteracting features.

We compare the finite field and linear response results for  $\Delta v_{\text{xc}}(\mathbf{r})$  in a chain consisting of eight hydrogen atoms. As some meta-GGAs have been shown to require rather fine grids,<sup>50</sup> we performed our TASK-KLI calculations with two different grid spacings of  $h = 0.14a_0$  and  $h = 0.28a_0$ , respectively, while for the calculations with the relatively smooth PoC functional, we only used the coarser grid with  $h = 0.28a_0$ .

Figure 1 shows our results for PoC-KLI (upper panel) and TASK-KLI (lower panel,  $h = 0.14a_0$ ). For comparison, we have included the linear response results for EXX-KLI in the upper panel.

For the PoC functional, the finite field and the linear response results are in almost perfect agreement. They also match the EXX-KLI result quite well, confirming the results of Ref. 47.

Also for TASK-KLI, the linear response curve follows the general trend of the finite field result and reproduces it accurately in

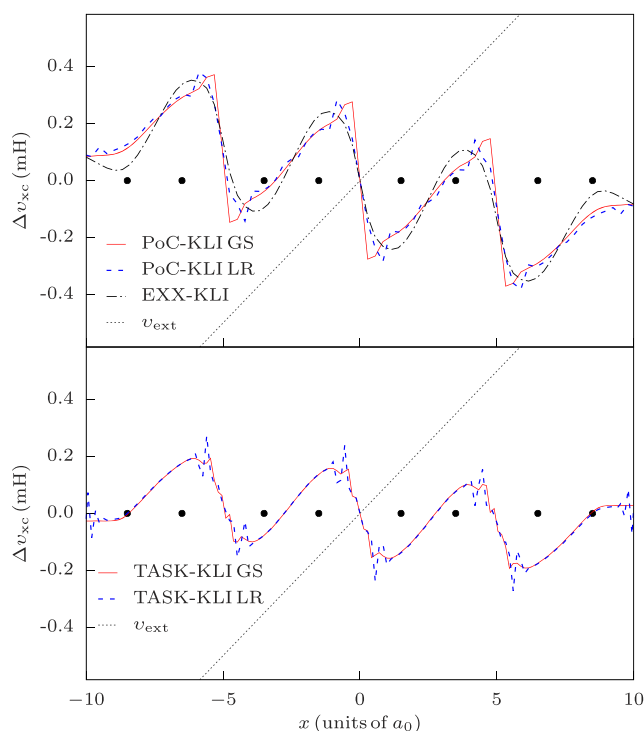


**FIG. 1.** Static response  $\Delta v_{xc}(\mathbf{r})$  to an external field for the  $H_8$  model molecular chain. Red solid lines are constructed from GS calculations, and dashed lines result from Sternheimer linear response calculations. The KLI approximation is used in all calculations. The dotted line indicates the perturbing external field, and the black disks mark the positions of the H atoms.

most regions of space. We note, however, that there are also regions in which the linear response potential shows spatial variations that are not seen as pronouncedly in the finite-field result. We have checked that these differences increase when doubling the grid spacing from  $0.14a_0$  to  $0.28a_0$ , i.e., they are of numerical origin and reflect the demands of accurately representing the high derivatives that appear in the meta-GGA response potential. A very reassuring finding is, though, that the photoabsorption spectra computed from the Sternheimer approach are very insensitive to these features (cf. Subsection III B).

As an additional test to check whether physical observables are sensitive to these numerical features, we compared the static linear polarizability along the chain,  $\alpha_{xx}$ , as obtained in the finite field and linear response approach within the KLI approximation.<sup>104</sup> The finite field and linear response KLI results (with identical settings and the coarser grid,  $h = 0.28a_0$ ) differ only marginally [ $\approx 0.01\%$  for PoC ( $80.92 a_0^3$  vs  $80.91 a_0^3$ ) and  $\approx 0.58\%$  for TASK ( $98.59 a_0^3$  vs  $98.02 a_0^3$ )]. These differences are minute compared to the substantial differences that one finds with different xc approximations.<sup>15,103</sup>

## B. Photoabsorption spectra

With the technical correctness and accuracy of our meta-GGA KLI-Sternheimer implementation established, we proceed to study optical spectra for different prototypical small systems.

We first compute the photoabsorption spectrum of the hydrogen chain for which we already discussed the static response in Sec. III A. It is shown in Fig. 2. As in Subsection III A, we compare two different grid spacings for TASK-KLI while performing all other calculations only for the coarse grid with  $h = 0.28a_0$ . The top panel of Fig. 2 shows the spectrum that we find with exchange-only LDA (XLDA) and EXX-KLI. The relative appearance of the peaks in both spectra is similar, but the XLDA spectrum is redshifted by  $\sim 0.4$  eV: The first transitions appear at 5.89 eV, 7.52 eV, and 8.36 eV for XLDA and at 6.32 eV, 7.93 eV, and 8.91 eV with EXX-KLI. The excitation energies being too low is in line with the static polarizability being too high in XLDA.

The middle panel shows the photoabsorption spectrum that we obtain with the TASK-KLI functional. It is in striking similarity to the EXX-KLI spectrum. The three brightest excitations are found at 6.35 eV, 7.86 eV, and 8.82 eV, all deviating by less than 0.1 eV from the EXX-KLI excitation energies. The peak heights,

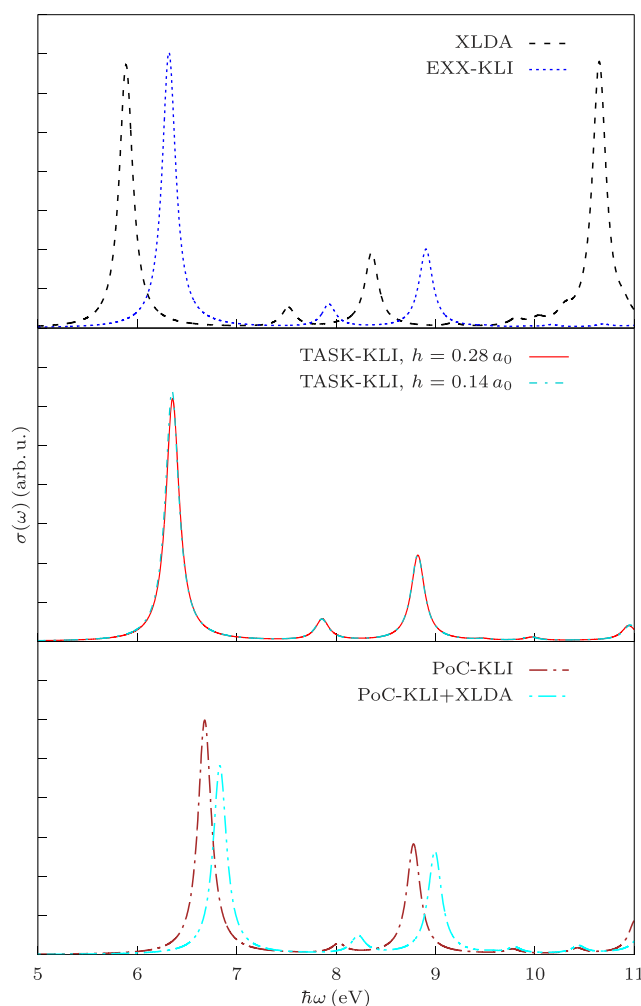


**FIG. 2.** Photoabsorption cross section for  $H_8$  calculated with different exchange-correlation functionals (orbital functionals in the KLI approximation).

i.e., oscillator strengths, are also very similar. This is an important result as it confirms that the TASK meta-GGA KLI calculation captures similar effects as the EXX-KLI calculation. Additionally, the spectra corresponding to the two different grid spacings coincide almost perfectly: On a grid with a spacing twice as large as the one on which Fig. 1 is based, the excitation energies change by less than 0.01 eV, confirming that the relevant observables are not significantly affected by the numerical features mentioned in Subsection III A.

The brown dashed-dotted line in the bottom panel shows the spectrum that results from the PoC-KLI functional. It also shows three main peaks, but the first two are blueshifted (6.68 eV and 8.03 eV) and the third one is redshifted (8.78 eV) with respect to the corresponding EXX-KLI peaks. To examine this further, we perform another calculation where we use the PoC-KLI functional only in the GS calculation and construct  $v_{xc}^{(+)}$  within the XLDA (PoC-KLI+XLDA). The resulting line (cyan dashed-dotted-dotted line in the bottom panel of Fig. 2) reveals that this leads to yet higher excitation energies at 6.83 eV, 8.22 eV, and 8.99 eV. Thus, we conclude that the higher excitation energies obtained with the PoC-KLI functional are not a result of the field-counteracting term included in its response potential but follow from its GS properties.

As our next test, we discuss  $\text{Na}_4$  as a paradigm example of a small metallic cluster (Fig. 3). The spectra of sodium clusters, which come close to the idealized picture of free-electron metals,<sup>105</sup> are known to be well described by the (TD)LDA.<sup>5,106</sup> The upper panel of Fig. 3 shows that EXX-KLI yields quite similar results. We find

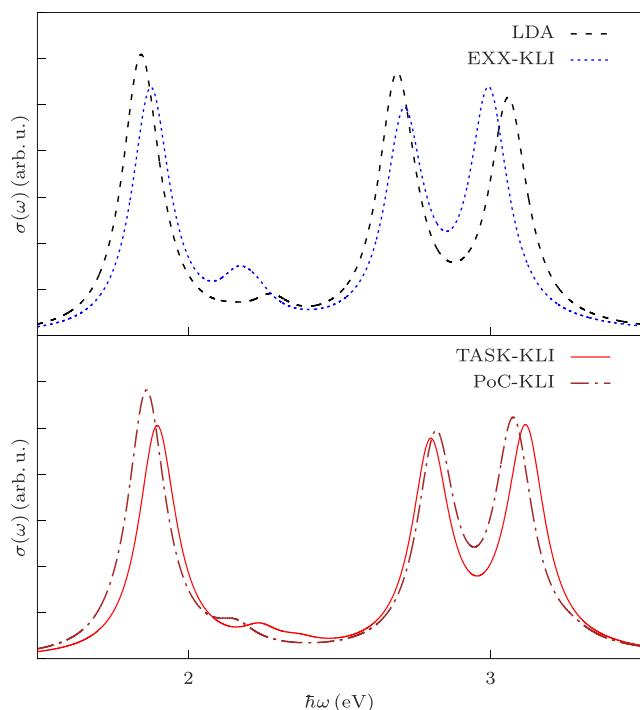


**FIG. 3.** Photoabsorption cross section for  $\text{Na}_4$  calculated with different exchange–correlation functionals (orbital functionals in the KLI approximation).

three pronounced peaks at 1.84 eV, 2.69 eV, and 3.06 eV with LDA and at 1.87 eV, 2.71 eV, and 2.99 eV with EXX-KLI, i.e., shifted by less than 0.1 eV.

Both PoC-KLI and TASK-KLI yield similar spectra as LDA and EXX-KLI, with the three strongest excitations at 1.90 eV, 2.80 eV, and 3.12 eV (TASK) and at 1.86 eV, 2.82 eV, and 3.07 eV (PoC). We, therefore, conclude that the meta-GGA-KLI response for  $\text{Na}_4$  falls within the range of accuracy that one expects from TDDFT without revealing striking features.

We next turn to the CO molecule (Fig. 4) for an example of typical valence excitations in a small molecule. Our LDA result of 8.24 eV for the  $^1\Pi$  valence excitation is in good agreement with the basis set result from Ref. 107 (8.19 eV), underestimating the experimental value (8.51 eV<sup>108</sup>) by  $\approx 0.3$  eV. This underestimation is slightly larger for EXX-KLI (8.16 eV). Note that adding the van Leeuwen–Baerends 1994 correction<sup>109</sup> to the LDA GS potential, thus restoring the proper  $-e^2/r$  asymptotic, leads to a similar, yet even larger increase in the underestimation of the  $^1\Pi$  excitation energy for CO.<sup>107</sup>

TASK-KLI leads to a larger energy of 8.37 eV and, thus, to a better agreement with the experiment, halving the error of LDA from 3.2% to 1.6%. Hirata and Head-Gordon<sup>107</sup> reported a less pronounced improvement for the BLYP<sup>110,111</sup> GGA. As TASK obeys several constraints typical for the construction of semi-local functionals,<sup>47</sup> we test if PBE as a prototypical constraint-based GGA leads to a similar improvement. However, our LDA and PBE results are nearly identical (8.25 eV). Overall, the spectra between 7 eV and

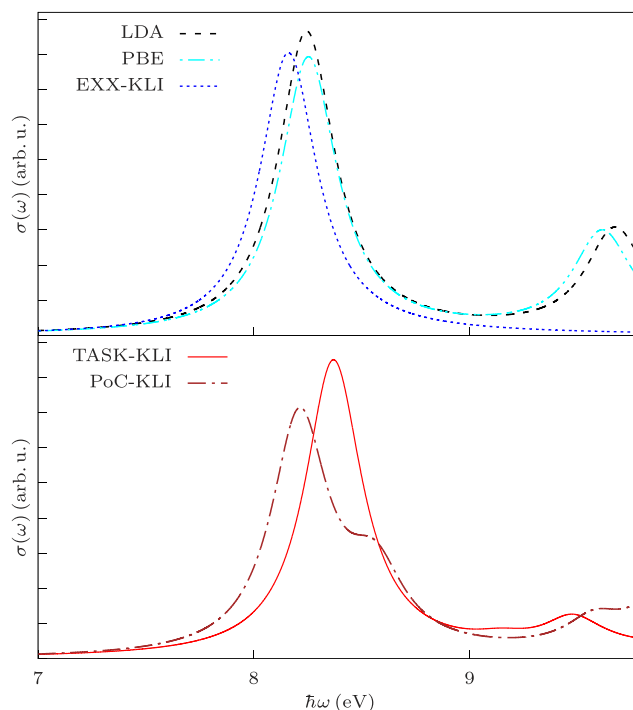


**FIG. 4.** Photoabsorption cross section for CO calculated with different exchange–correlation functionals (orbital functionals in the KLI approximation).

11 eV are qualitatively similar for all functionals, except for PoC-KLI that displays a pronounced “shoulder” at 8.56 eV above its main peak (at 8.21 eV).

With SiH<sub>4</sub> (Fig. 5), we turn to a system for which the construction principles underlying the TASK and PoC meta-GGAs are not expected to lead to any improvement over usual semilocal functionals. This expectation emerges from a review of earlier findings for SiH<sub>4</sub>, which we recapitulate in the following.

Response calculations for SiH<sub>4</sub> that are based on the LDA or usual GGAs lead to spectra that are qualitatively wrong, have a distorted structure, and underestimate the onset of absorption by up to  $\approx 1$  eV.<sup>24</sup> Within TDDFT, it was found that EXX-KLI<sup>112</sup> and the time-dependent OEP-based self-interaction correction to the LDA<sup>23,24</sup> substantially improve over LDA. Works that found a substantial improvement over LDA based on solving the Bethe–Salpeter equation<sup>113–115</sup> argued that the improvement is due to a correct description of excitonic effects. In the TDDFT context, the latter would be associated with the xc kernel.<sup>116</sup> However, recent work clarified that for a correct spectrum of SiH<sub>4</sub> from TDDFT, it is not the xc kernel that is decisive, but the GS eigenvalues.<sup>76</sup> Thus, reproducing the response of the EXX and self-interaction correction functionals is not important for SiH<sub>4</sub>. Reproducing the eigenvalues would be. The TASK and PoC functionals, however, were designed to mimic the features of the EXX response. They cannot mimic the full EXX eigenvalue spectrum because being semilocal, they cannot yield a  $-e^2/r$  decay of the xc potential.

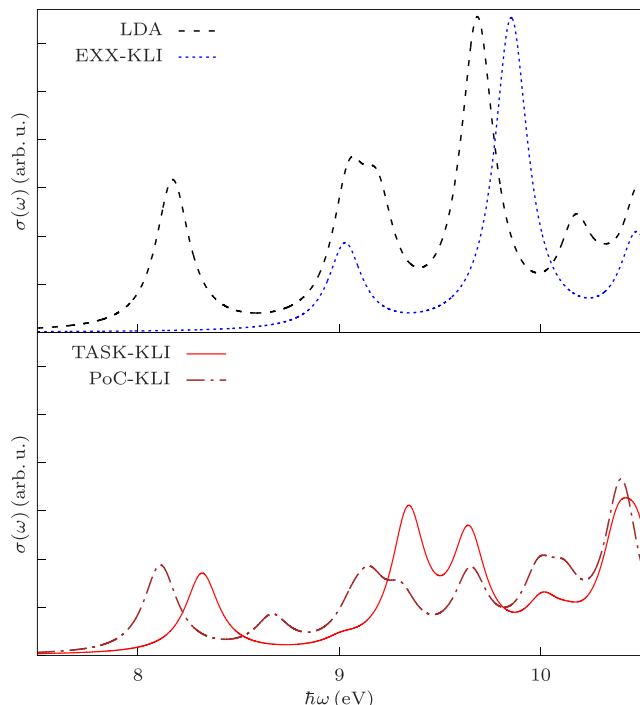


**FIG. 5.** Photoabsorption cross section for SiH<sub>4</sub> calculated with different exchange–correlation functionals (orbital functionals in the KLI approximation).

Our results from the Sternheimer scheme confirm this expectation and the previous findings. In the upper panel of Fig. 5, one sees the substantial differences between EXX-KLI and LDA. The two spectra clearly have a different structure, and the lowest excitation energies of 9.03 eV (EXX-KLI) and 8.17 eV (LDA) differ by almost 1 eV. In the lower panel, we see that the TASK-KLI spectrum to some extent improves over the LDA result, e.g., the onset of absorption is shifted to somewhat higher energies. However, very noticeable differences to the EXX-KLI spectrum remain. The spectrum from the PoC-KLI functional is not similar to any of the other results. We see this as another confirmation that PoC, as pointed out in its design, is not a generally useful functional.

### C. Charge transfer in an organic semiconductor molecule

We finally turn to the most challenging test. As discussed in the Introduction, charge-transfer excitations have been a long-standing challenge to TDDFT. The use of range-separated hybrids with a tuned-range separation parameter<sup>117</sup> has become the standard approach for obtaining them accurately. This has led to impressive successes. It is not a panacea, though, as tuned range-separated hybrids come at an increased computational cost, violate size consistency,<sup>118,119</sup> and lead to a parameter dilemma (as discussed, e.g., in Ref. 120): The typical values for the range-separation parameter that emerge from the tuning as being optimal for TDDFT are quite different from the values that lead to good ground-state binding. One can hope that meta-GGAs could be able to describe charge-transfer excitations without a parameter dilemma.

We, therefore, look at an organic semiconductor system with naphthalene diimide (NDI) as an acceptor and one thiophene each attached to the left and to the right as a donor. We denote this system as NDI-1, following the notation of a previous study<sup>32</sup> that showed that the lowest excitation in this system has charge-transfer character and can be well described by a tuned range-separated hybrid. We focus on this excitation (cf. Sec. II D). Our choice of the NDI-1 molecule, and not some of the other molecules that have been put forward in the literature as charge-transfer test systems,<sup>13,73</sup> is motivated by the following observation. Many of the previously used charge-transfer test systems feature charge-transfer excitations of vanishing oscillator strength. Excitations of vanishing oscillator strength, however, are difficult to observe in the Sternheimer scheme. NDI-1 with its charge-transfer excitation that carries some oscillator strength is thus ideal for tests within the Sternheimer scheme.

Figure 6 shows the results from the Sternheimer calculations. EXX-KLI shows the first line at 1.76 eV. The corresponding LDA line is at 1.69 eV, i.e., we see an underestimation of the excitation energy. The first excitation energy with the TASK-KLI functional appears at 1.80 eV. This is a shift in the right direction, and TASK-KLI again seems to capture the physics similar to EXX-KLI. The PoC-KLI functional shifts the first excitation to substantially higher energies.

Karolewski *et al.*<sup>32</sup> reported that the charge-transfer excitation in this case is well described as a transition from the highest occupied (HOMO) to the lowest unoccupied orbital (LUMO), which we can confirm. Inspection of the orbital energies reveals that for our

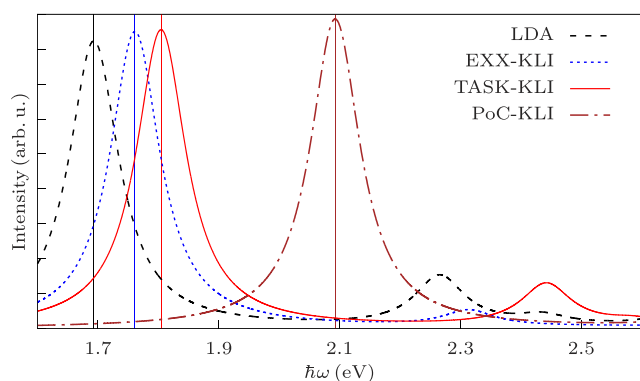


**FIG. 6.**  $\hat{\epsilon}_{CT}$ -component of the dynamic polarizability [cf. Eq. (27)] for NDI-1. Vertical lines indicate the position of the charge-transfer excitation for LDA, EXX-KLI, TASK-KLI, and PoC-KLI.

calculations, the differences in the excitation energies from LDA, EXX-KLI, TASK-KLI, and PoC-KLI mostly reflect the corresponding differences in the HOMO–LUMO gaps.<sup>121</sup>

Comparing to the experimental and tuned range-separated hybrid results from Ref. 32, we are confronted with a puzzle, though. The lowest excitation energy for NDI-1 is found around 2.52 eV with the tuned range-separated hybrid and at  $\sim 2.6$  eV experimentally, i.e., substantially higher than our EXX-KLI and TASK-KLI results. To shed further light on the situation, we calculated the excitation spectrum of NDI-1 also with TD Hartree–Fock using TURBOMOLE with the def2-TZVP basis set. The latter calculation yields the lowest excitation energy at 3.45 eV, i.e., also at a substantially higher energy than our TDDFT calculation using EXX-KLI, and actually even higher than the experimental and range-separated hybrid results by almost 1 eV. Therefore, it seems that the KLI approximation is leading to a severe underestimation of the excitation energy.

To test the influence of the KLI approximation on the results, we have calculated the ground-state of the NDI-1 molecule with EXX using the full OEP instead of the KLI approximation, employing the method of Ref. 122. While hardly affecting the occupied orbital energies, EXX-OEP leads to higher energies for the unoccupied orbitals compared to EXX-KLI, thus shifting the HOMO–LUMO gap by roughly 0.4 eV from 1.52 eV to 1.93 eV. It is to be expected that the excitation energy will be upshifted by at least the same amount when one would go from the TD-KLI calculation to a TD-OEP calculation. Unfortunately, however, the explicit calculation cannot be done as there presently is no TD-OEP scheme that can handle a molecule of the complexity of NDI-1.

#### IV. SUMMARY AND CONCLUSION

We have calculated the optical response of several paradigm molecular systems with the Kohn–Sham Sternheimer approach, comparing the recently developed TASK and PoC meta-GGAs to EXX, in each case using the KLI approximation to construct the (approximate) Kohn–Sham potential. Our study was motivated by the new construction principle that underlies these meta-GGAs: They were designed to capture the nonlocal response properties and a particle number discontinuity similar to EXX in ground-state DFT.

We here check whether these beneficial properties carry over to TDDFT.

We have carefully tested the numerics of our meta-GGA response calculations and found that reliable results for the observables can be obtained without requiring unusually fine grid settings. This confirms that the TASK and PoC functionals are numerically benevolent and do not seem to share the issues that have been reported for some other meta-GGAs.

Our calculations showed that the physics contained in the PoC functional is not very systematic. This is in line with its simplistic construction that did not aim at obtaining a general xc approximation. Thus, we do not recommend PoC for further general use. Another caveat about both PoC and TASK emerged from studying the spectrum of SiH<sub>4</sub>. TASK and PoC were designed to yield a nonlocal response similar to EXX, but being semilocal meta-GGAs, they cannot achieve a  $\propto -e^2/r$  potential. Thus, when the eigenvalues are the most important ingredient for the absorption spectrum and the xc response is of little importance, as in SiH<sub>4</sub>, then functionals such as PoC and TASK offer little improvement over usual GGAs.

However, for other systems in which the xc response plays a more important role, the results obtained with the TASK functional nourish hope: TASK-KLI captures the ultranlocal response in hydrogen chains, yields realistic results for the excitations of the here studied molecule and metal cluster, and also improves the description of the charge-transfer excitation in an organic semiconductor molecule similar to EXX-KLI.

It turned out, however, that the KLI approximation itself can be a serious limitation. Therefore, it is a worthwhile aim of future work to extend the frequency-dependent Sternheimer scheme to the full TD-OEP. This might then allow us to explore whether the conceptual caveats that have been pointed out in the literature about the generalized Kohn–Sham use of meta-GGAs in TDDFT<sup>53,55</sup> are restrictive in practice.

#### ACKNOWLEDGMENTS

We acknowledge financial support from the program “Biological Physics” of the Elite Network of Bavaria and from the Bavarian State Ministry of Science, Research, and the Arts in the Collaborative Research Network “Solar Technologies go Hybrid.” We further acknowledge support through the computational resources provided by the Bavarian Polymer Institute. F.H. acknowledges support from the University of Bayreuth Graduate School. F.H. is grateful to Thilo Aschebrock for discussions about meta-GGAs, in general, and the TASK and PoC functionals, in particular.

#### APPENDIX: NUMERICAL PARAMETERS

We used LDA pseudopotentials throughout this work.

For the H<sub>8</sub> calculations, we used a pseudopotential with a core cutoff radius of  $r_c(\text{H}) = 1.39a_0$  (where  $a_0$  is the Bohr radius). The molecule was aligned along the  $x$  axis, and we used a simulation ellipsoid with a half-axis of  $R_x = 18a_0$  in the  $x$  direction and  $R_y = R_z = 10a_0$  in the  $y$  and  $z$  directions, as well as a spacing  $h$  of the cubic grid of  $h = 0.28a_0$ . With TASK, we also performed additional calculations using  $h = 0.14a_0$  for comparison. For the finite field calculations, we used a field strength of  $\mathcal{E} = 10^{-4} e/a_0^2$ . The quasi-static

linear response calculations were done with  $\hbar\omega = \hbar\eta = 1$  meV. The spectra were calculated with a frequency step size of  $\hbar\Delta\omega = 4$  mRy and a damping of  $\hbar\eta = 6$  mRy.

In the  $\text{Na}_4$  calculations, we employed a pseudopotential with  $r_c(\text{Na}) = 3.09a_0$ , a simulation sphere radius of  $R = 18a_0$ , a grid spacing of  $h = 0.35a_0$ ,  $\hbar\Delta\omega = 50$  meV, and  $\hbar\eta = 75$  meV.

We used  $r_c(\text{Si}) = 1.79a_0$ ,  $r_c(\text{H}) = 1.39a_0$ ,  $R = 16a_0$ ,  $h = 0.35a_0$ ,  $\hbar\Delta\omega = 60$  meV, and  $\hbar\eta = 0.1$  eV for  $\text{SiH}_4$  and  $r_c(\text{C}) = 1.60a_0$ ,  $r_c(\text{O}) = 1.45a_0$ ,  $R = 18a_0$ ,  $h = 0.3a_0$ ,  $\hbar\Delta\omega = 80$  meV, and  $\hbar\eta = 0.16$  eV for CO.

Finally, for the NDI-1 calculations, we used  $r_c(\text{C}) = 1.29a_0$ ,  $r_c(\text{H}) = 1.39a_0$ ,  $r_c(\text{N}) = 1.50a_0$ ,  $r_c(\text{O}) = 1.45a_0$ ,  $r_c(\text{S}) = 1.39a_0$ ,  $R_x = 20a_0$ ,  $R_y = 13a_0$ ,  $R_z = 17a_0$ ,  $h = 0.35a_0$ ,  $\hbar\Delta\omega = 25$  meV, and  $\hbar\eta = 50$  meV.

## DATA AVAILABILITY

The data that support the findings of this study are available from the corresponding author upon reasonable request.

## REFERENCES

- 1 A. Zangwill and P. Soven, *Phys. Rev. A* **21**, 1561 (1980).
- 2 U. Saalmann and R. Schmidt, *Z. Phys. D* **38**, 153–163 (1996).
- 3 K. Yabana and G. F. Bertsch, *Phys. Rev. B* **54**, 4484 (1996).
- 4 F. Calvayrac, P. G. Reinhard, and E. Suraud, *Ann. Phys.* **255**, 125 (1997).
- 5 I. Vasiliev, S. Ögüt, and J. R. Chelikowsky, *Phys. Rev. Lett.* **82**, 1919 (1999).
- 6 C. A. Rozzi, S. M. Falke, N. Spallanzani, A. Rubio, E. Molinari, D. Brida, M. Maiuri, G. Cerullo, H. Schramm, J. Christoffers, and C. Lienau, *Nat. Commun.* **4**, 1602 (2013).
- 7 H. Hübener and F. Giustino, *J. Chem. Phys.* **141**, 044117 (2014).
- 8 X. Andrade, D. Strubbe, U. De Giovannini, A. H. Larsen, M. J. T. Oliveira, J. Alberdi-Rodriguez, A. Varas, I. Theophilou, N. Helbig, M. J. Verstraete, L. Stella, F. Nogueira, A. Aspuru-Guzik, A. Castro, M. A. L. Marques, and A. Rubio, *Phys. Chem. Chem. Phys.* **17**, 31371 (2015).
- 9 M. Dauth, M. Graus, I. Schelter, M. Wiefner, A. Schöll, F. Reinert, and S. Kümmel, *Phys. Rev. Lett.* **117**, 183001 (2016).
- 10 J. Jorner-Somoza and I. Lebedeva, *J. Chem. Theory Comput.* **15**, 3743 (2019).
- 11 I. Schelter, J. M. Foerster, A. T. Gardiner, A. W. Roszak, R. J. Cogdell, G. M. Ullmann, T. B. de Queiroz, and S. Kümmel, *J. Chem. Phys.* **151**, 134114 (2019).
- 12 D. J. Tozer, *J. Chem. Phys.* **119**, 12697 (2003).
- 13 A. Dreuw and M. Head-Gordon, *J. Am. Chem. Soc.* **126**, 4007 (2004).
- 14 S. Kümmel, *Adv. Energy Mater.* **7**, 1700440 (2017).
- 15 S. Kümmel, L. Kronik, and J. P. Perdew, *Phys. Rev. Lett.* **93**, 213002 (2004).
- 16 S. J. A. van Gisbergen, P. R. T. Schipper, O. V. Gritsenko, E. J. Baerends, J. G. Snijders, B. Champagne, and B. Kirtman, *Phys. Rev. Lett.* **83**, 694 (1999).
- 17 M. Hellgren and E. K. U. Gross, *Phys. Rev. A* **85**, 022514 (2012).
- 18 N. T. Maitra, *J. Chem. Phys.* **122**, 234104 (2005).
- 19 A. Kaiser and S. Kümmel, *Phys. Rev. A* **98**, 052505 (2018).
- 20 J. P. Perdew, K. Burke, and M. Ernzerhof, *Phys. Rev. Lett.* **77**, 3865 (1996).
- 21 M. J. G. Peach, T. Helgaker, P. Salek, T. W. Keal, O. B. Lutnæs, D. J. Tozer, and N. C. Handy, *Phys. Chem. Chem. Phys.* **8**, 558 (2006).
- 22 S.-H. Ke, H. U. Baranger, and W. Yang, *J. Chem. Phys.* **126**, 201102 (2007).
- 23 D. Hofmann, T. Körzdörfer, and S. Kümmel, *Phys. Rev. Lett.* **108**, 146401 (2012).
- 24 D. Hofmann and S. Kümmel, *J. Chem. Phys.* **137**, 064117 (2012).
- 25 H. Iikura, T. Tsuneda, T. Yanai, and K. Hirao, *J. Chem. Phys.* **115**, 3540 (2001).
- 26 H. Sekino, Y. Maeda, M. Kamiya, and K. Hirao, *J. Chem. Phys.* **126**, 014107 (2007).
- 27 Y. Tawada, T. Tsuneda, S. Yanagisawa, T. Yanai, and K. Hirao, *J. Chem. Phys.* **120**, 8425 (2004).
- 28 R. Baer and D. Neuhauser, *Phys. Rev. Lett.* **94**, 043002 (2005).
- 29 T. Yanai, D. P. Tew, and N. C. Handy, *Chem. Phys. Lett.* **393**, 51 (2004).
- 30 T. Stein, L. Kronik, and R. Baer, *J. Am. Chem. Soc.* **131**, 2818 (2009).
- 31 J. Autschbach, *ChemPhysChem* **10**, 1757 (2009).
- 32 A. Karolewski, T. Stein, R. Baer, and S. Kümmel, *J. Chem. Phys.* **134**, 151101 (2011).
- 33 L. Kronik, T. Stein, S. Refaely-Abramson, and R. Baer, *J. Chem. Theory Comput.* **8**, 1515 (2012).
- 34 L. Kronik and S. Kümmel, *Adv. Mater.* **30**, 1706560 (2018).
- 35 P. Borlido, J. Schmidt, A. Huran, F. Tran, M. Marques, and S. Botti, *npj Comput. Mater.* **6**, 96 (2020).
- 36 A. D. Becke, *Int. J. Quantum Chem.* **27**, 585 (1985).
- 37 A. D. Becke, *J. Chem. Phys.* **109**, 2092 (1998).
- 38 T. Van Voorhis and G. E. Scuseria, *J. Chem. Phys.* **109**, 400 (1998).
- 39 J. P. Perdew, S. Kurth, A. Zupan, and P. Blaha, *Phys. Rev. Lett.* **82**, 2544 (1999).
- 40 A. D. Boese and N. C. Handy, *J. Chem. Phys.* **116**, 9559 (2002).
- 41 J. Tao, J. P. Perdew, V. N. Staroverov, and G. E. Scuseria, *Phys. Rev. Lett.* **91**, 146401 (2003).
- 42 Y. Zhao and D. G. Truhlar, *J. Chem. Phys.* **125**, 194101 (2006).
- 43 R. Peverati and D. G. Truhlar, *Phys. Chem. Chem. Phys.* **14**, 13171 (2012).
- 44 H. S. Yu, X. He, and D. G. Truhlar, *J. Chem. Theory Comput.* **12**, 1280 (2016).
- 45 J. Sun, B. Xiao, Y. Fang, R. Haunschild, P. Hao, A. Ruzsinszky, G. I. Csonka, G. E. Scuseria, and J. P. Perdew, *Phys. Rev. Lett.* **111**, 106401 (2013).
- 46 J. Sun, A. Ruzsinszky, and J. P. Perdew, *Phys. Rev. Lett.* **115**, 036402 (2015).
- 47 T. Aschebroek and S. Kümmel, *Phys. Rev. Res.* **1**, 033082 (2019).
- 48 V. U. Nazarov and G. Vignale, *Phys. Rev. Lett.* **107**, 216402 (2011).
- 49 D. J. Tozer and M. J. G. Peach, *Mol. Phys.* **116**, 1504 (2018).
- 50 Z.-h. Yang, H. Peng, J. Sun, and J. P. Perdew, *Phys. Rev. B* **93**, 205205 (2016).
- 51 R. Neumann, R. H. Nobes, and N. C. Handy, *Mol. Phys.* **87**, 1 (1996).
- 52 A. Seidl, A. Görling, P. Vogl, J. A. Majewski, and M. Levy, *Phys. Rev. B* **53**, 3764 (1996).
- 53 R. Baer and L. Kronik, *Eur. Phys. J. B* **91**, 170 (2018).
- 54 J. Tao, *Phys. Rev. B* **71**, 205107 (2005).
- 55 J. E. Bates and F. Furche, *J. Chem. Phys.* **137**, 164105 (2012).
- 56 S. Kümmel and L. Kronik, *Rev. Mod. Phys.* **80**, 3 (2008).
- 57 E. Engel and R. M. Dreizler, *Density Functional Theory: An Advanced Course, Theoretical and Mathematical Physics* (Springer Berlin Heidelberg, Berlin, Heidelberg, 2011).
- 58 C. A. Ullrich, U. J. Gossmann, and E. K. U. Gross, *Phys. Rev. Lett.* **74**, 872 (1995).
- 59 M. Mundt and S. Kümmel, *Phys. Rev. A* **74**, 022511 (2006).
- 60 H. O. Wijewardane and C. A. Ullrich, *Phys. Rev. Lett.* **95**, 086401 (2005).
- 61 S.-L. Liao, T.-S. Ho, H. Rabitz, and S.-I. Chu, *Phys. Rev. Lett.* **118**, 243001 (2017).
- 62 A. Görling, *Phys. Rev. A* **57**, 3433 (1998).
- 63 A. Görling, *Int. J. Quantum Chem.* **69**, 265 (1998).
- 64 Y.-H. Kim and A. Görling, *Phys. Rev. Lett.* **89**, 096402 (2002).
- 65 S. Hirata, S. Ivanov, I. Grabowski, and R. J. Bartlett, *J. Chem. Phys.* **116**, 6468 (2002).
- 66 S. Hirata, S. Ivanov, R. J. Bartlett, and I. Grabowski, *Phys. Rev. A* **71**, 032507 (2005).
- 67 S. Hirata, *J. Chem. Phys.* **123**, 026101 (2005).
- 68 Y. Shigeta, K. Hirao, and S. Hirata, *Phys. Rev. A* **73**, 010502 (2006).
- 69 F. Bruneval, F. Sottile, V. Olevano, and L. Reining, *J. Chem. Phys.* **124**, 144113 (2006).
- 70 M. Hellgren and U. von Barth, *Phys. Rev. B* **78**, 115107 (2008).
- 71 M. Hellgren and U. von Barth, *J. Chem. Phys.* **131**, 044110 (2009).
- 72 A. Heßelmann, A. Ipatov, and A. Görling, *Phys. Rev. A* **80**, 012507 (2009).
- 73 A. Ipatov, A. Heßelmann, and A. Görling, *Int. J. Quantum Chem.* **110**, 2202 (2010).
- 74 A. Heßelmann and A. Görling, *J. Chem. Phys.* **134**, 034120 (2011).
- 75 X. Andrade, S. Botti, M. A. L. Marques, and A. Rubio, *J. Chem. Phys.* **126**, 184106 (2007).
- 76 F. Hofmann, I. Schelter, and S. Kümmel, *J. Chem. Phys.* **149**, 024105 (2018).

- <sup>77</sup>F. Hofmann, I. Schelter, and S. Kümmel, *Phys. Rev. A* **99**, 022507 (2019).
- <sup>78</sup>J. B. Krieger, Y. Li, and G. J. Iafrate, *Phys. Rev. A* **46**, 5453 (1992).
- <sup>79</sup>M. Grüning, O. V. Gritsenko, and E. J. Baerends, *J. Chem. Phys.* **116**, 6435 (2002).
- <sup>80</sup>F. Della Sala and A. Görling, *J. Chem. Phys.* **115**, 5718 (2001).
- <sup>81</sup>D. A. Strubbe, L. Lehtovaara, A. Rubio, M. A. L. Marques, and S. G. Louie, in *Fundamentals of Time-Dependent Density Functional Theory*, Lecture Notes in Physics Vol. 837, edited by M. A. Marques, N. T. Maitra, F. M. Nogueira, E. Gross, and A. Rubio (Springer Berlin Heidelberg, 2012), pp. 139–166.
- <sup>82</sup>M. E. Casida, “Time-dependent density functional response theory for molecules,” in *Recent Advances in Density Functional Methods*, edited by D. P. Chong (World Scientific, Singapore, 1995), pp. 155–192.
- <sup>83</sup>J. P. Perdew and A. Zunger, *Phys. Rev. B* **23**, 5048 (1981).
- <sup>84</sup>M. Mundt, S. Kümmel, B. Huber, and M. Moseler, *Phys. Rev. B* **73**, 205407 (2006).
- <sup>85</sup>M. Mundt and S. Kümmel, *Phys. Rev. B* **76**, 035413 (2007).
- <sup>86</sup>L. Kronik, A. Makmal, M. L. Tiago, M. M. G. Alemany, M. Jain, X. Huang, Y. Saad, and J. R. Chelikowsky, *Phys. Status Solidi (B)* **243**, 1063 (2006).
- <sup>87</sup>N. Troullier and J. L. Martins, *Phys. Rev. B* **43**, 1993 (1991).
- <sup>88</sup>L. Kleinman and D. M. Bylander, *Phys. Rev. Lett.* **48**, 1425 (1982).
- <sup>89</sup>D. Hofmann, “Charge and excitation-energy transfer in time-dependent density functional theory,” Ph.D. thesis, University of Bayreuth, 2012.
- <sup>90</sup>S. Lehtola, C. Steigemann, M. J. T. Oliveira, and M. A. L. Marques, *SoftwareX* **7**, 1 (2018).
- <sup>91</sup>D. G. Anderson, *J. ACM* **12**, 547 (1965).
- <sup>92</sup>R. Ahlrichs, M. Bär, M. Häser, H. Horn, and C. Kölmel, *Chem. Phys. Lett.* **162**, 165 (1989).
- <sup>93</sup>F. Weigend and R. Ahlrichs, *Phys. Chem. Chem. Phys.* **7**, 3297 (2005).
- <sup>94</sup>B. Champagne, D. H. Mosley, M. Vračko, and J.-M. André, *Phys. Rev. A* **52**, 178 (1995).
- <sup>95</sup>M. van Faassen, P. L. de Boeij, R. van Leeuwen, J. A. Berger, and J. G. Snijders, *Phys. Rev. Lett.* **88**, 186401 (2002).
- <sup>96</sup>M. van Faassen and N. Maitra, *J. Chem. Phys.* **126**, 191106 (2007).
- <sup>97</sup>P. Umari, A. J. Williamson, G. Galli, and N. Marzari, *Phys. Rev. Lett.* **95**, 207602 (2005).
- <sup>98</sup>T. Körzdörfer, M. Mundt, and S. Kümmel, *Phys. Rev. Lett.* **100**, 133004 (2008).
- <sup>99</sup>A. Ruzsinszky, J. P. Perdew, G. I. Csonka, G. E. Scuseria, and O. A. Vydrov, *Phys. Rev. A* **77**, 060502(R) (2008).
- <sup>100</sup>A. Ruzsinszky, J. P. Perdew, and G. I. Csonka, *Phys. Rev. A* **78**, 022513 (2008).
- <sup>101</sup>C. D. Pemmaraju, S. Sanvito, and K. Burke, *Phys. Rev. B* **77**, 121204(R) (2008).
- <sup>102</sup>B. Champagne and B. Kirtman, *Int. J. Quantum Chem.* **109**, 3103 (2009).
- <sup>103</sup>T. Körzdörfer and S. Kümmel, “Self-interaction correction in the Kohn-Sham framework,” in *Theoretical and Computational Developments in Modern Density Functional Theory*, edited by A. K. Roy (Nova Science Publishers, New York, 2012), pp. 211–222.
- <sup>104</sup>Note that in our Sternheimer approach, both the static polarizability and photoabsorption spectra are based on the evaluation of the same quantity, i.e., the induced dipole moment  $\int(-er)n^{(+)}(\mathbf{r})d^3r$  (cf. Subsection II B), and thus should be affected in a similar fashion.
- <sup>105</sup>S. Kümmel, K. Andrae, and P.-G. Reinhard, *Appl. Phys. B* **73**, 293 (2001).
- <sup>106</sup>I. Vasiliev, S. Ögüt, and J. R. Chelikowsky, *Phys. Rev. B* **65**, 115416 (2002).
- <sup>107</sup>S. Hirata and M. Head-Gordon, *Chem. Phys. Lett.* **314**, 291 (1999).
- <sup>108</sup>E. S. Nielsen, P. Jørgensen, and J. Oddershede, *J. Chem. Phys.* **73**, 6238 (1980).
- <sup>109</sup>R. van Leeuwen and E. J. Baerends, *Phys. Rev. A* **49**, 2421 (1994).
- <sup>110</sup>A. D. Becke, *Phys. Rev. A* **38**, 3098 (1988).
- <sup>111</sup>C. Lee, W. Yang, and R. G. Parr, *Phys. Rev. B* **37**, 785 (1988).
- <sup>112</sup>M. A. L. Marques, A. Castro, and A. Rubio, *J. Chem. Phys.* **115**, 3006 (2001).
- <sup>113</sup>M. Rohlfing and S. G. Louie, *Phys. Rev. Lett.* **80**, 3320 (1998).
- <sup>114</sup>M. Rohlfing and S. G. Louie, *Phys. Rev. B* **62**, 4927 (2000).
- <sup>115</sup>M. L. Tiago and J. R. Chelikowsky, *Phys. Rev. B* **73**, 205334 (2006).
- <sup>116</sup>G. Onida, L. Reining, and A. Rubio, *Rev. Mod. Phys.* **74**, 601 (2002).
- <sup>117</sup>T. Stein, L. Kronik, and R. Baer, *J. Chem. Phys.* **131**, 244119 (2009).
- <sup>118</sup>E. Livshits and R. Baer, *Phys. Chem. Chem. Phys.* **9**, 2932 (2007).
- <sup>119</sup>A. Karolewski, L. Kronik, and S. Kümmel, *J. Chem. Phys.* **138**, 204115 (2013).
- <sup>120</sup>T. Schmidt, E. Krausler, A. Makmal, L. Kronik, and S. Kümmel, *J. Chem. Phys.* **140**, 18A510 (2014).
- <sup>121</sup>Note that the orbital energies of PoC generally appear to be rather unphysical for this system, yielding no bound virtual orbitals and a HOMO energy that is higher than our EXX results by roughly 7 eV. Thus, we refrain from interpreting the higher excitation energy found with PoC as a systematic improvement.
- <sup>122</sup>S. Kümmel and J. P. Perdew, *Phys. Rev. B* **68**, 035103 (2003).



# Acknowledgments

During the past five years I was accompanied and supported by a number of people without whom the preparation of this thesis certainly would not have been possible. I am deeply grateful, in particular to:

- **Stephan Kümmel**, not least because he always found the right balance between letting me go where I wanted to with my work and tightening the reins whenever I was in danger of going astray. Always a deep well of ideas, advice and inspiration, I couldn't imagine a better supervisor (although admittedly I never had any other supervisor I could compare him to...).
- **Monika Birkelbach**, **Susanne Süss**, and **Markus Hilt** for their administrative and technical assistance.
- **Julian Garhammer** and **Thilo Aschebrock**, not only for carefully proofreading this manuscript, but also for being great traveling companions during three truly memorable weeks in China, and my long-time office mate Julian for always being open for discussions about just everything, including DFT problems, Scotch, numerical problems, Bourbon, whatever work-unrelated mathematical question I somehow had stumbled upon, or nosing-glasses.
- My two-time paper collaborator **Ingo Schelter** for his unlimited patience while finding the sources for every last tiny discrepancy between his real-time and my Sternheimer results, and for a history of supporting and advising me that goes back all the way to my Bachelor thesis.
- **All other former and current members of the Theoretical Physics IV group** for their collaborative spirit, the always friendly atmosphere, a lot of great discussions, and for all those Stammtisch sessions (and a few game nights), not to mention Jana's surprisingly long series of "Thank you parties".
- My parents **Sabine** and **Elmar** as well as my sister **Verena** for always having my back and supporting me in every conceivable way.

I further acknowledge financial support from the German-Israeli Foundation for Scientific Research and Development, and from the University of Bayreuth Graduate School.



# Eidesstattliche Versicherung

Hiermit versichere ich an Eides statt, dass ich die vorliegende Arbeit selbstständig verfasst und keine anderen als die von mir angegebenen Quellen und Hilfsmittel verwendet habe.

Weiterhin erkläre ich, dass ich die Hilfe von gewerblichen Promotionsberatern bzw. -vermittlern oder ähnlichen Dienstleistern weder bisher in Anspruch genommen habe, noch künftig in Anspruch nehmen werde.

Zusätzlich erkläre ich hiermit, dass ich keinerlei frühere Promotionsversuche unternommen habe.

Bayreuth, den 9. Dezember 2020

Fabian Hofmann